

การสังเคราะห์และสมบัติการจับของตัวรับไดทอปิกประเภทเฮกซาโซโมไตรเอชาคาลิกซ์[3]เอรีน

และเดนไดรเมอร์ที่ว่องไวทางเคมีไฟฟ้า



นายชาติไทย แก้วทอง

สถาบันวิทยบริการ

วิทยานิพนธ์นี้เป็นส่วนหนึ่งของการศึกษาตามหลักสูตรปริญญาวิทยาศาสตรดุษฎีบัณฑิต

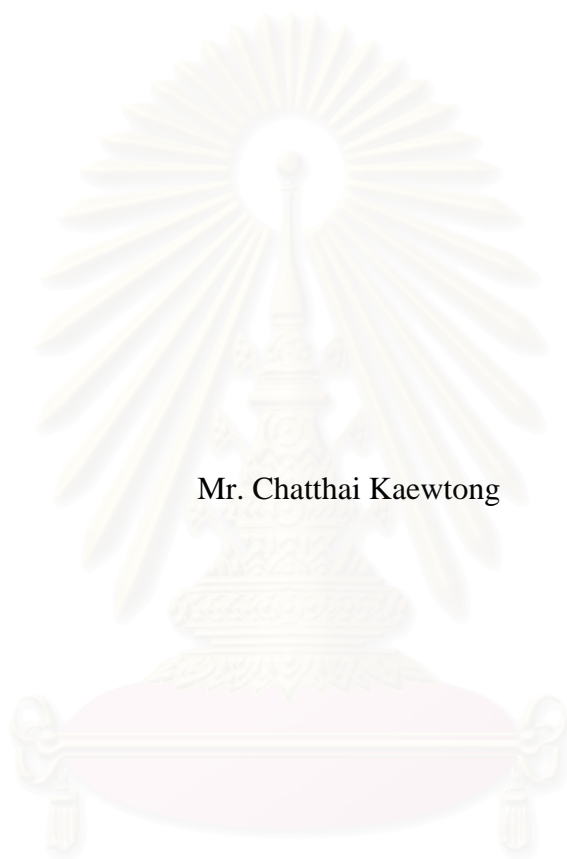
สาขาวิชาเคมี ภาควิชาเคมี

คณะวิทยาศาสตร์ จุฬาลงกรณ์มหาวิทยาลัย

ปีการศึกษา 2550

ลิขสิทธิ์ของจุฬาลงกรณ์มหาวิทยาลัย

SYNTHESIS AND BINDING PROPERTIES OF DITOPIC RECEPTORS BASED
ON HEXAHOMOTRIAZACALIX[3]ARENE AND ELECTROCHEMICALLY
ACTIVE DENDRIMERS



Mr. Chatthai Kaewtong

สถาบันวิทยบริการ
จุฬาลงกรณ์มหาวิทยาลัย

A Dissertation Submitted in Partial Fulfillment of the Requirements
for the Degree of Doctor of Philosophy Program in Chemistry

Department of Chemistry

Faculty of Science

Chulalongkorn University

Academic Year 2007

Copyright of Chulalongkorn University


Thesis title SYNTHESIS AND BINDING PROPERTIES OF
DITOPIC RECEPTORS BASED ON
HEXAHOMOTRIAZACALIX[3]ARENE AND
ELECTROCHEMICALLY ACTIVE DENDRIMERS

By Mr. Chatthai Kaewtong

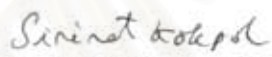
Field of Study Chemistry


Thesis Advisor Associate Professor Buncha Pulpoka, Ph.D.

Accepted by the Faculty of Science, Chulalongkorn University in Partial
Fulfillment of the Requirements for the Doctoral Degree



.....Dean of the Faculty of Science
(Professor Supot Hannongbua, Ph.D.)

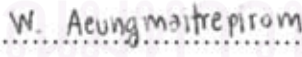
DISSERTATION COMMITTEE


.....Chairman
(Associate Professor Sirirat Kokpol, Ph.D.)


.....Thesis Advisor
(Associate Professor Buncha Pulpoka, Ph.D.)


.....External member
(Professor Pramuan Tangboriboonrat, Ph.D.)


.....Member
(Associate Professor Nongnuj Muangsin, Ph.D.)


.....Member
(Assistant Professor Wanlapa Aeungmaitrepirom, Ph.D.)


.....Member
(Assistant Professor Yongsak Sritana-anant, Ph.D.)

ชาติไทย แก้วทอง : การสังเคราะห์และสมบัติการจับของตัวรับไดทอปิกประเภทเฮกซาไฮโดรเอ
 ซาคาลิกซ์[3]เอรีนและเดนไดรเมอร์ที่ว่องไวทางเคมีไฟฟ้า. (SYNTHESIS AND BINDING
 PROPERTIES OF DITOPIC RECEPTORS BASED ON
 HEXAHOMOTRIAZACALIX[3]ARENE AND ELECTROCHEMICALLY ACTIVE
 DENDRIMERS) อ. ที่ปรึกษา: รศ. ดร. บัญชา พูลโกทา, 196 หน้า.

งานวิจัยนี้ได้ทำการสังเคราะห์เฮกซาไฮโดรเอซา-พราว-กลอโรคาลิกซ์[3]เอรีน (L1) และทำการ
 ให้เกิดหมู่ฟังก์ชันเพื่อสร้างเป็นเซนเซอร์ไดทอปิกชนิดใหม่ 2 ชนิด จากการศึกษาสารประกอบเชิงซ้อน
 พบว่าเฮกซาไฮโดรเอซา-พราว-กลอโรคาลิกซ์[3]เอรีนสามารถใช้เป็นโครโมเจนิกเซนเซอร์สำหรับ F^-
 และ $H_2PO_4^-$ ได้ สำหรับเฮกซาไฮโดรเอซา-พราว-กลอโรคาลิกซ์[3]-ไดรเนฟทิลาไมด์ (L2) ที่มีรูปร่าง
 แบบพาร์เซียล-โคนยังแสดงความสามารถเป็นฟลูออเรสเซนซ์เซนเซอร์ที่จำเพาะกับ Cd^{2+} , Pb^{2+} และ F^- ส่วน
 เฮกซาไฮโดรเอซา-พราว-กลอโรคาลิกซ์[3]-คริปแตนด์ (L3) ซึ่งอยู่ในรูปแบบโคนและมีโพรงแบบปิด
 สามารถใช้เป็นตัวรับที่จำเพาะสำหรับไอออนคลอไรด์ซึ่งสามารถเปลี่ยนไปจับกับไอออนโบรไมด์เมื่ออยู่ใน
 รูปสารประกอบเชิงซ้อนของไอออนสังกะสี จากนั้นได้ทำการสังเคราะห์ฟิล์มบางโดยทำการเชื่อมโยง
 โมเลกุล L4 ซึ่งประกอบด้วยวงเฮกซาคาลิกซ์[3]เอรีนเป็นรีเซปเตอร์และคาร์บาโซลเข้าด้วยกันโดยใช้เทคนิค
 ทางเคมีเชิงไฟฟ้า จากการทดลองแสดงให้เห็นความไวและความจำเพาะเจาะจงต่อการตอบสนองกับ Zn^{2+}

ได้ทำการสังเคราะห์และศึกษาการเกิดกระบวนการเคลฟ-แอสเซมบลีระหว่างโพลีอะมิโคอิมิน
 (PAMAM) เดนไดรเมอร์และเดนดรอน (G_0COOH , G_1COOH และ G_2COOH) โดยใช้อันตรกิริยาทางเคมี
 ชูปราโมเลกุล จากการศึกษาสมบัติการรวมตัวกันโดยไฟฟ้าของสารประกอบเชิงซ้อนเดนไดรเมอร์ พบว่าใน
 กรณีที่เป็น PAMAM- G_1COOH จะเกิดโครงสร้างคล้ายแหวนหรือโดมที่ประกอบด้วย PAMAM เป็น
 แกนและคาร์บาโซลเดนดรอนเป็นเปลือกนอก จากนั้นได้ทำการต่อ PAMAM กับเทอร์ไทโอฟีน (PT) และ
 คาร์บาโซล (PC) เพื่อใช้เป็นตัวปกป้องความเสถียรของอนุภาคนาโนของทอง โดยการผ่านกระบวนการเกิด
 ริดจ์ชั้นของ $AuCl_3$ ด้วยเดนไดรเมอร์ PAMAM ที่มีหน่วย PT หรือ PC อยู่ด้านนอก

ภาควิชา.....เคมี..... ลายมือชื่อนิสิต.....ชาติไทย แก้วทอง.....
 สาขาวิชา.....เคมี..... ลายมือชื่ออาจารย์ที่ปรึกษา.....
 ปีการศึกษา ...2550.....

4673807923 : MAJOR CHEMISTRY

KEY WORDS: AZACALIX[3]ARENE / HETERODITOPIC SENSORS / HOST-GUEST INTERACTIONS / SELF-ASSEMBLY/ GOLD NANOPARTICLE

CHATTHAI KAEWTONG: SYNTHESIS AND BINDING PROPERTIES OF DITOPIC RECEPTORS BASED ON HEXAHOMOTRIAZACALIX[3]ARENE AND ELECTROCHEMICALLY ACTIVE DENDRIMERS.

THESIS ADVISOR: ASSOC. PROF. BUNCHA PULPOKA, Ph.D., 196 pp.

Hexahomotriaza-*p*-chlorocalix[3]arene (**L1**) was successfully synthesized and functionalized to provide two novel heteroditopic sensors. From complexation studies, the hexahomotriaza-*p*-chlorocalix[3]arene could be used as a selective chromogenic sensor for F⁻ and H₂PO₄⁻. The partial-cone hexahomotriaza-*p*-chlorocalix[3]-trinaphthylamide (**L2**) synthesized from both cone and partial cone triester derivatives exhibited a selective fluorescent sensor for Cd²⁺, Pb²⁺ and F⁻. Hexahomotriaza-*p*-chlorocalix[3]-cryptand (**L3**) which is fixed in cone conformation and possesses a close well-defined cavity showed a high selectivity for Cl⁻ ion. Tuning this ligand by complexing with Zn²⁺ on hexahomotriaza-*p*-chlorocalix[3]arene framework, its anion binding selectivity changed to Br⁻ ion. Moreover, a new class of chemosensor recognition elements based on conjugated polymer network ultra-thin films from electrochemical cross-linking of hexahomotriaza-*p*-chlorocalix[3]arene-carbazole (**L4**) was successfully realized. Its demonstrated high selectivity and sensitivity towards Zn²⁺ was observed.

A self-assembly between polyamidoamine (PAMAM) dendrimer and dendron surfmers (G₀COOH, G₁COOH and G₁COOH) was prepared through an efficient supramolecular interaction. The electrochemical cross-linking of dendrimer complexes (PAMAM-G₁COOH) provided thin films which have a ring-like or donut structure most likely composed of the PAMAM-core and dendron-carbazole shell. In addition, π -conjugated dendrimer-protected gold nanoparticles in a stable colloidal form have been successfully prepared via simultaneous reduction of AuCl₃ with terthiophene (PT) and carbazole (PC) peripheral functionalized PAMAM dendrimers.

Department:.....Chemistry.....Student's signature:.....Chatthai Kaewtong.....
 Field of study:.....Chemistry.....Advisor's signature:.....Buncha Pulpoka.....
 Academic year:.....2007.....

ACKNOWLEDGEMENTS

First of all, I would like to express my deepest gratitude to Associate Professor Dr. Buncha Pulpoka who gave me a chance by accepting me to be a PhD student under the Royal Golden Jubilee (RGJ) program scholar even though he didn't know who I was which has changed my life forever. He always supervises and guides me during my graduate study at Department of Chemistry, Chulalongkorn University. His profound insight and optimistic attitude always provide a strong support for my research, especially when it's getting very tough. I am honored to have him as my advisor. Particular thanks belong to Professor Rigoberto Advincula for offering me an opportunity to participate in the interesting and challenging project at University of Houston.

I would like to express my appreciation to Associate Professor Dr. Thawatchai Tuntulani for being my special co-advisor. As an excellent teacher and scientist, I have learned a lot from him, making me more confident and comfortable in the realm of supramolecular chemistry. In addition, I would like to thank Associate Professor Dr. Sirirat Kokpol, Professor Dr. Pramuan Tangboriboonrat, Assistant Professor Dr. Wanlapa Aeungmaitrepirom, Associate Professor Dr. Nongnuj Muangsin and Assistant Professor Dr. Yongsak Sritana-anant for their input, interest, valuable suggestions, comments and acceptance as thesis examiners. I would like to acknowledge the grant and funding supports provided by RGJ grant from The Thailand Research Fund (PHD/0137/2546).

The bulk of my thanks goes to all the past and present members of the Supramolecular Chemistry Research Unit and RCA group with whom I have spent many hours in the lab over the past half-decade. Like a big family, I can always get wholehearted help and valuable advices from them whenever I need. I also thank Mr. Guoqian Jiang for his trainings, expert guidance and assistance in all instruments in RCA group.

Especially, I would also like to thank my parents and my family for their love, kindness, encouragement, and financial support throughout my life. I love you all. I know I have been here a long time but it would not be much longer. Note, what can I say but thank you! Thank you for being there for me during my ups and downs. Thank you for those talks that I really needed even if I didn't want to hear it at the time. You continue to support and encourage me to be the best that I can be. Love you!

CONTENTS

	Page
ABSTRACT (THAI)	iv
ABSTRACT (ENGLISH)	v
ACKNOWLEDGEMENTS	vi
CONTENTS	vii
LIST OF FIGURES	xv
LIST OF TABLES	xxiv
LIST OF SCHEMES	xxv
LIST OF ABBREVIATIONS AND SIGNS	xxvi
CHAPTER I INTRODUCTION AND BACKGROUND	1
1.1 Introduction of calixarene and azacalixarene.....	1
1.1.1 Calixarenes.....	1
1.1.1.1 History of calixarenes	1
1.1.1.2 Nomenclature of calixarenes.....	1
1.1.1.3 Conformations of calix[4]arenes	2
1.1.1.4 Complexation of metal ions by calix[4]arenes.....	3
1.1.2 Heteroatom-bridged calixarenes.....	4
1.1.3 Hexahomotriazacalix[3]arenes or azacalix[3]arenes	5
1.1.3.1 One-pot synthesis of azacalix[3]arenes.....	5
1.1.3.2 Stepwise synthesis of azacalix[3]arenes	8
1.1.4 Complexation of metal ions by azacalix[3]arenes.....	9
1.2 Introduction of carbazole, thiophene, oligothiophenes, dendrimers, and their applications.....	11
1.2.1 General aspects of conducting polymers.....	11
1.2.2 Polycarbazole.....	13
1.2.3 Polythiophenes.....	15
1.2.4 Oligothiophenes.....	16
1.2.5 Synthesis of oligothiophenes.....	17
1.2.5.1 Copper(II)-mediated oxidative coupling.....	18

	Page
1.2.5.2 Nickel-catalyzed Kumada cross coupling reactions.....	18
1.2.5.3 “Stille coupling” reactions.....	19
1.2.5.4 Suzuki coupling reactions.....	19
1.2.6 Dendrimers.....	20
1.2.7 Synthesis of dendrimers.....	21
1.2.7.1 Divergent approach.....	21
1.2.7.2 Convergent approach.....	22
1.2.8 Functional dendrimers and their applications.....	23
1.2.8.1 Transition metal catalysis using functional dendrimers.....	23
a) Functional dendrimers with a catalytic core.....	24
b) Functional dendrimers with peripheral catalytic sites.....	27
c) Transition metal nanocomposites in the dendrimer interior.....	27
1.2.8.2 Functional dendrimers for light-harvesting applications.....	28
1.2.8.3 Functional dendrimers in supramolecular chemistry.....	29
1.3 Objectives and outline of this dissertation.....	30

CHAPTER II DITOPIC RECEPTORS BASED ON HEXAHOMOTRIAZACALIX[3]ARENE	32
2.1 Synthesis and binding properties of ditopic receptors based on hexahomotriazacalix[3]arene.....	32
2.1.1 Introduction.....	32
2.1.2 Objectives of this research	33
2.1.3 Experimental section.....	34
2.1.3.1 Synthesis of heteroditopic receptors based on azacalix[3]arene.....	34

	Page
a) General procedure.....	34
a1) Materials.....	34
a2) Instrumentations.....	35
b) Synthesis.....	35
b1) Synthesis of <i>N</i> -chlorobenzylhexahomotriazacalix[3]-arene (L1)....	35
b2) Synthesis of <i>N</i> -benzylhexahomotriaza- <i>p</i> -chloro-calix-[3]-trinaphthylamide (L2).....	37
b3) Synthesis of <i>N</i> ₇ -hexahomotriaza- <i>p</i> -chlorocalix-[3]cryptand (L3).....	40
2.1.3.2 Complexation studies	43
a) Complexation studies of ligand L1 , L2 and L3 by using ¹ H-NMR spectroscopy.....	43
b) Complexation studies by using UV-vis spectroscopy.....	43
b1) Complexation studies of L2 and L3 with metal ions by using the UV-vis titration...	43
b2) Complexation studies of L2 and L3 with anion by using the UV-vis titration.....	43
c) Complexation studies by using fluorescent spectroscopy.....	44
c1) Complexation studies between L2 with cation by using the fluorescent spectroscopy.....	44
c2) Complexation studies between L1 and L2 with anion by using the fluorescent spectroscopy.....	45
2.1.4 Results and discussion	46
2.1.4.1 Synthesis and characterization of sensor L1 , L2 and L3	46
2.1.4.2 Investigation of binding ability.....	49

	Page
a) Complexation studies of ligand L1 with various anions by using ¹ H-NMR, UV-vis and fluorescent spectroscopies.....	50
b) Fluorogenic properties of ligand L2	55
c) Complexation studies of ligand L2 with various anions by using ¹ H-NMR, UV-vis and fluorescent spectroscopies.....	56
d) Complexation studies of ligand L3 with various anions by using ¹ H-NMR and UV-vis spectroscopies	62
2.2 Ultrathin films of azacalixarene-carbazole conjugated polymer networks (CPN) for specific cation sensing	67
2.2.1 Introduction.....	67
2.2.2 Objectives of this research	68
2.2.3 Experimental section.....	69
2.2.3.1 Synthesis of sensor based on azacalix[3]arene.....	69
a) General procedure.....	69
a1) Materials.....	69
a2) Instrumentations.....	70
b) Synthesis.....	72
b1) Synthesis of <i>p</i> -chloro- <i>N</i> -benzylhexahomotri-azacalix[3]-tri(butyl carbazole) (L4).....	72
b2) Synthesis of 11-(9 <i>H</i> -carbazol-9-yl)-undecane-1-thiol (2.8).....	74
b3) Synthesis of 9-(4-(9 <i>H</i> -carbazol-9-yl)butyl)-9 <i>H</i> -carbazole (2.9).....	78
2.2.3.2 Electrochemical synthesis of cross-linked polymers (P-L4).....	79
2.2.3.3 Sensitivity and selectivity studies of P-L4 by using potentiometry.....	79

	Page
2.2.3.4 Sensitivity and selectivity studies of P-L4 by using EC-QCM and QCM.....	79
2.2.3.5 Sensitivity and selectivity studies of P-L4 by using EC-SPR and SPR.....	80
2.2.4 Results and discussion	81
2.2.4.1 Synthesis of macrocyclic receptor monomer (L4)....	81
2.2.4.2 Electropolymerization of L4	82
2.2.4.3 Morphological studies.....	84
2.2.4.4 Spectroelectrochemistry studies.....	87
2.2.4.5 Selectivity and sensitivity studies by using potentiometric measurements	88
2.2.4.6 Selectivity and sensitivity studies by using spectroelectrochemical measurements.....	94
2.2.4.7 Selectivity and sensitivity studies by using electrochemistry and quartz crystal microbalance method (EC-QCM).....	95
2.2.4.8 Selectivity and sensitivity studies by using electrochemistry and surface plasmon spectroscopy method (EC-SPR).....	97
CHAPTER III ELECTROCHEMICALLY ACTIVE DENDRIMERS	99
3.1 Lord of the nano-rings: self-assembly and electropolymerization of PAMAM-carbazole dendron surfmer complexes.....	99
3.1.1 Introduction.....	99
3.1.2 Objectives of this research	101
3.1.3 Experimental section.....	102
3.1.3.1 Synthesis of carbazole dendrons to complex with dendrimer.....	102
a) General procedure.....	102
a1) Materials.....	102
a2) Instrumentations.....	103

	Page
b) Synthesis.....	104
b1) Synthesis of carbazole dendrons ($G_0\text{COOH}$, 3.2).....	104
b2) Synthesis of carbazole dendrons ($G_1\text{COOH}$, 3.4).....	106
b3) Synthesis of carbazole dendrons ($G_2\text{COOH}$, 3.7).....	108
3.1.3.2 Electrochemical synthesis of cross-linked dendron complexations.....	111
3.1.3.3 Complex preparation.....	111
3.1.4 Results and discussion	112
3.1.4.1 Formation of the spherical assemblies of the $G_0\text{COOH}$, $G_1\text{COOH}$ and $G_2\text{COOH}$ with G4- PAMAM.....	112
3.1.4.2 Formation of the spherical assemblies of the $G_0\text{COOH}$, $G_1\text{COOH}$ and $G_2\text{COOH}$ with G4- PAMAM.....	118
3.1.4.3 Electrochemical studies of dendron surfmer complexes	120
3.1.4.4 Spectro-electrochemical studies of dendron surfmer complexes.....	125
3.1.4.5 Morphological studies.....	126
3.2 Redox nanoreactor dendrimer boxes: <i>in-situ</i> hybrid gold nanoparticles via terthiophene and carbazole-PAMAM dendrimer oxidation.....	136
3.2.1 Introduction.....	136
3.2.2 Objectives of this research	138
3.2.3 Experimental section.....	138
3.2.3.1 Synthesis of carbazole and terthiophene dendrons to modify dendrimer.....	138
a) General procedure.....	138
a1) Materials.....	138

	Page
a2) Instrumentations.....	139
b) Synthesis.....	140
b1) Synthesis of (3,5-bis(4-(9H-carbazol-9-yl)butoxy)-benzoyl-functionalized dendrimer (PC, 3.13).....	140
b2) Synthesis of 2-(2,5-di-(thiophen-2-yl)thiophen-3-yl) acetoxy-functionalized dendrimer (PC, 3.14).....	142
3.2.4 Results and discussion	147
3.2.4.1 Synthesis of derivative of PAMAM dendrimers.....	147
3.2.4.2 Preparation of Au DENs.....	148
3.2.4.3 Formation of DENs by UV-vis, FT-IR and fluorescent spectrometry.....	149
3.2.4.4 Characterization of DENs by XPS, and AFM.....	152
CHAPTER IV CONCLUSIONS.....	157
4.1 Ditopic receptors based on hexahomotriazacalix[3]arene.....	157
4.1.1 Synthesis and binding properties of ditopic receptors based on hexahomotriazacalix[3]arene.....	157
4.1.2 Ultrathin films of azacalixarene-carbazole conjugated polymer networks (CPN) for specific cation sensing.....	158
4.2 Electrochemically reactive dendrimers.....	159
4.2.1 Lord of the nano-rings: self-assembly and electropolymerization of PAMAM-carbazole dendron surfmer complexes.....	159
4.2.2 Redox nanoreactor dendrimer boxes: <i>in-situ</i> hybrid gold nanoparticles via terthiophene and carbazole-PAMAM dendrimer oxidation.....	160
4.3 Suggestion for future works.....	160

	Page
REFERENCES	161
APPENDICES	184
VITA	196



สถาบันวิทยบริการ
จุฬาลงกรณ์มหาวิทยาลัย

LIST OF FIGURES

Figure		Page
1.1	General structure of calixarene.....	2
1.2	Four interchangeable conformations of <i>p-tert</i> -butylcalix[4]arene...	3
1.3	Complexation of calix[4]arene with metal lead to double calix[4]arene in the present of NaH as base.....	4
1.4	Structures of heteroatom-bridged calixarene.....	5
1.5	View of the complex molecule in <i>p</i> -chloro- <i>N</i> -benzylhexahomotriazacalix[3]arene with (a) Nd ³⁺ , and (b) UO ₂ ²⁺ which are shown hydrogen bonds in dashed lines, protons of the ammonium groups represented as small spheres of arbitrary radii.....	9
1.6	Chemical structures of (1.16) <i>trans</i> -polyacetylene (PA); (1.17) poly(<i>p</i> -phenylene) (PPP); (1.18) poly(<i>p</i> -phenylene vinylene) (PPV); (1.19) polythiophene (PT); (1.20) polypyrrole (PPy); (1.21) polyfluorene (PF); (1.22) polycarbazole (PCbz); (1.23) polyaniline (PANI).....	12
1.7	Resonance structures of PA , PPP , and PT that show the difference in the two mesomeric forms (aromatic and quinoid) that define the lowest energy states.....	16
1.8	Dendrimers are generally synthesized by two complementary approaches (a) Divergent approach, and (b) Convergent approach..	22
1.9	Catalytically active transition metal complexes can be attached to (a) the periphery or (b) the core.....	24
1.10	Carbosilane dendrimers synthesized by Oosterom and coworkers...	25
1.11	Nanoparticle-core dendrimers (NCDs) synthesized by Fox and coworkers.....	25
1.12	The carbosilane dendrimers 1.25 synthesized by Van Koten and coworkers.....	26
1.13	Synthesis of dendrimer-encapsulated metal nanoparticles and their application in catalysis	28
1.14	Cartoon of dendrimers for light harvesting	29

Figure	Page
1.15 Gallic acid dendrons self-assembling to supramolecular dendrimers, which again organize themselves in thermotropic, liquid-crystalline phases.....	30
2.1 ORTEP drawing of <i>N</i> -benzylhexahomotriaza- <i>p</i> -chlorocalix[3]-tri(ethyl acetate) (2.3a) (a) and <i>N</i> -benzylhexahomotriaza- <i>p</i> -chlorocalix[3]-trinaphthylamide (L2) (b). The displacement ellipsoids are drawn at the 50% probability level.....	48
2.2 Formation of solid structure L3 stabilized by intermolecular CH/Cl hydrogen bond interactions.....	49
2.3 ORTEP drawing of <i>N</i> ₇ -azacalix[3]cryptand (L3). The displacement ellipsoids are drawn at the 50% probability level.....	49
2.4 ¹ H-NMR spectra (400 MHz, DMSO- <i>d</i> ₆) (a) azacalix[3]arene (L1), (b) L1 ⊃F ⁻ , (c) L1 ⊃H ₂ PO ₄ ⁻ , (d) L1 ⊃CH ₃ COO ⁻ , (e) L1 ⊃PhCOO ⁻ , and (f) L1 ⊃Cl ⁻ complexes obtained upon addition of a CDCl ₃ solution of L1 into NBu ₄ ⁺ X ⁻ salts (10 equivalent).....	50
2.5 Spectral change in the UV absorption of L1 (C _L = 5×10 ⁻⁵ M) upon addition of NBu ₄ ⁺ F ⁻ (C _A = 0.04 M) in DMSO (0 ≤ C _A /C _L ≤ 6).....	51
2.6 Color changes of L1 in DMSO after addition of 30 equivalent of anions.....	51
2.7 Absorption spectra of ligand L1 ([L] = 1×10 ⁻⁴ M) upon addition excess of anions (30 equivalent).....	52
2.8 Emission spectra of ligand L1 ([L] = 1 × 10 ⁻⁴ M) upon addition excess of anions (30 equivalent).	53
2.9 Intensity of emission spectra of L1 (1 × 10 ⁻⁵ M) enhanced by addition of F ⁻ (λ _{ex} = 295 nm) in DMSO.....	54
2.10 Plot of the ratio of excimer to monomer emission versus concentration of ligand L2	56
2.11 Fluorescence changes (<i>I</i> - <i>I</i> ₀) of L2 upon addition of various metal ions. Conditions: L2 (1 μM) in DMSO, excitation at 285 nm, metal nitrate and chloride (300 equivalent) in DMSO. <i>I</i> : fluorescence emission intensity of complexes L2 . <i>I</i> ₀ : fluorescence emission intensity of free L2	57

Figure	Page
2.13 Spectral change in the UV-vis absorption of L2 ($C_L = 3 \times 10^{-5}$ M) upon addition of Pb^{2+} ($C_C = 1.2 \times 10^{-3}$ M) in DMSO ($0 \leq C_A/C_L \leq 30$).....	59
2.14 Fluorescence changes of L2 upon addition of various anions. Conditions: L3 (0.1 μ M) in DMSO, excitation at 285 nm, TBAX (300 equivalent) in DMSO.	59
2.15 1H -NMR spectra of L2 with 10 equivalent of TBAX in $CDCl_3$	60
2.16 1H -NMR spectra (400 MHz, $CDCl_3$) (a) N_7 -azacalix[3]-cryptand (L3), (b) $L3 \supset F^-$, (c) $L3 \supset Cl^-$, (d) $L3 \supset Br^-$, and (e) $L3 \supset I^-$ complexes obtained upon addition of $NBu_4^+X^-$ (10 equivalent) into a $CDCl_3$ solution of L3 . \blacktriangledown : signals of $L3 \supset X^-$; *: signals of NBu_4^+ . Residual solvents and partially protonated water are labeled as “S” and “W respectively.....	63
2.17 Spectral changes in the UV absorption of (a) L3 ($C_L = 6 \times 10^{-5}$ M) upon addition of $NBu_4^+Br^-$ ($C_A = 8 \times 10^{-4}$ M) in DMSO ($0 \leq C_A/C_L \leq 10.3$), and (b) $L3.Zn^{2+}$ ($C_L = 3.429 \times 10^{-5}$ M) upon addition of $NBu_4^+Br^-$ ($C_A = 8 \times 10^{-4}$ M) in DMSO ($0 \leq C_A/C_L \leq 18$).....	64
2.18 Percentage of free anions by each ligand studied as a function of ligand L3 concentration ($C_L = 1 \times 10^{-3}$ M).....	65
2.19 Electrochemical polymerization (cross-linking) of <i>p</i> -chloro- <i>N</i> -benzylhexahomotriazacalix[3]-tri(buthyl carbazole) or monomer L4	69
2.20 Sensor diagram studies by using QCM	80
2.21 Sensor setup for <i>in situ</i> EC-SPR/SPR measurement.....	81
2.22 Cyclic voltammograms of the electrochemical cross-linking/deposition of L4 at a scan rate of 50 mV/s, 8 cycles: (a) deposited material on 2.8 coated gold substrates(0-1.0 V), (b) on ITO substrates (0-1.3 V), (c) on gold-coated slides (0-1.0 V), and (d) on ITO substrates (0-1.5 V).....	83

Figure	Page	
2.23	AFM images, the topological or height images (left) and three-dimensional topographic images (right): (a) bare gold, (b) poly hexahomotriazacalix[3]arene-carbazole (PL4) electropolymerized at 50 mV/s (0 to 1.0), 8 cycles in TBAPF ₆ /CH ₂ Cl ₂ electrolyte (WE, gold-coated slides; CE, Pt wire; RE, Ag/AgCl wire), and (c) after electropolymerization of PL4 at 50 mV/s (0 to 1.0), 8 cycles in TBAPF ₆ /CH ₂ Cl ₂ electrolyte (WE, 2.8 coated gold substrates; CE, Pt wire; RE, Ag/AgCl wire).....	85
2.24	AFM images, the topological or height images (left) and three-dimensional topographic image (right): (a) bare ITO, (b) after electropolymerization of L4 at 50 mV/s (0 to 1.3), 8 cycles in TBAPF ₆ /CH ₂ Cl ₂ electrolyte (WE, ITO; CE, Pt wire; RE, Ag/AgCl wire), and (c) after electropolymerization of L4 at 50 mV/s (0 to 1.5), 8 cycles in TBAPF ₆ /CH ₂ Cl ₂ electrolyte (WE, ITO; CE, Pt wire; RE, Ag/AgCl wire).....	86
2.25	(a) Spectroelectrochemical analysis performed in 0.1 M TBAPF ₆ /CH ₂ Cl ₂ of L4 , growth of the 445 and 950 nm peaks during electrodeposition of PL4 , spectra taken in situ at 0 V during each CV cycle, and (b) Fluorescence spectra before and after electropolymerization of L4 which are taken at the excitation wavelength $\lambda = 320$ nm.....	87
2.26	Potentiometric profiles of PL4 on ITO in 10 mM TBACl aqueous solution: (a) various cation analytes, and (b) various concentrations of Zn ²⁺ . Plotted data are within 5% deviation from several measurements.....	89
2.27	Potentiometric profiles of PL4 on ITO in aqueous solution in different concentration of cations at 0 V: (a) H ⁺ , (b) Co ²⁺ , (c) Ni ²⁺ , (d) Cu ²⁺ , (e) Cd ²⁺ , and (f) Hg ²⁺	91

Figure	Page
2.28 (a) Cyclic voltammograms electrochemical cross-linking/deposition of 2.9 polymerization at a scan rate of 50 mV/s, 8 cycle deposited material on ITO substrates., (b) The UV-Vis absorption spectrum of 2.9 films before and after addition of Zn^{2+} cations 10^{-3} M on ITO substrates, and (c) Potentiometric profiles of 2.9 on ITO in aqueous solution in different concentration of Zn^{2+} at 0 V.....	93
2.29 The UV-vis absorption spectrum of PL4 films upon the addition of different cations with the concentration 10^{-3} M on ITO substrates.....	95
2.30 Electrochemical quartz crystal microbalance studies: (a) ΔF , frequency change and ΔR , resistance change during the CV cycling., (b) Changes in the viscoelastic behavior in the polymers., and (c) ΔF , frequency change as a function of different cations concentration.....	96
2.31 EC-SPR and SPR studies of PL4 on 2.8 coated gold substrates: (a) kinetic measurement during deposited film, (b) kinetic sensorogram at different concentrations of Zn^{2+} , and (c) angular sensorogram at different concentrations of Zn^{2+}	98
3.1 PAMAM dendrimer generation 4 with carboxylic acid terminal dendrons containing peripheral electroactive carbazole groups of different generations (G_0COOH , G_1COOH and G_2COOH) and possibility to form nano-ring structures.....	101
3.2 1H -NMR spectra (300 MHz, 298 K) in $CDCl_3$ of 2 mM solutions (based on the concentration of PAMAM) (a) G_1COOH , and (b) complex of PAMAM- G_1COOH	113
3.3 1H -NMR spectra (300 MHz, 298 K, DMSO) of a 2 mM solution (based on the concentration of PAMAM) of (a) G_0COOH , and (b) complex of PAMAM+ G_0COOH	114
3.4 Optimized structures of G_2COOH built from the Gaussian 98 B3LYP/STO-3G output using the “Molekel” software (a) side view, and (b) top view.	114

Figure	Page
3.5 (a) UV-vis absorption spectra of G ₁ COOH solutions in MeOH and CHCl ₃ before and after complexation with PAMAM, and (b) fluorescence emission spectra of G ₁ COOH before and after complexation with PAMAM, $\lambda_{\text{ex}} = 293 \text{ nm}$, $\lambda_{\text{em}} = 360 \text{ nm}$	115
3.6 (a) UV-vis absorption spectra of G ₀ COOH before and after complexation with PAMAM, and (b) fluorescence emission spectra of G ₀ COOH before and after complexation with PAMAM, $\lambda_{\text{ex}} = 293 \text{ nm}$, $\lambda_{\text{em}} = 360 \text{ nm}$	116
3.7 FT-IR spectra of (a) PAMAM, G ₁ COOH and G ₁ COOH-PAMAM complex., (b) G ₀ COOH and G ₀ COOH-PAMAM complex. Resolution is at 4 cm^{-1} for each spectrum.....	116
3.8 WCA measurement for: (a) PAMAM (0°), (b) complex PAMAM-G ₁ COOH (55.7°), and (c) complex PAMAM-G ₀ COOH (80.3°).....	118
3.9 AFM images complex on a mica substrate of (a) PAMAM G ₄ (b) PAMAM-G ₁ COOH complex in CHCl ₃ , and (c) PAMAM-G ₁ COOH complex in MeOH.....	119
3.10 Optimized structures built from the Gaussian 98 B3LYP/STO-3G output file using the “Molekel” software.....	119
3.11 AFM images on a mica substrate of (a) PAMAM G ₄ , and (b) PAMAM+G ₀ COOH complex in MeOH.....	120
3.12 Cyclic voltammograms of the electrochemical cross-linking/deposition of PAMAM-G ₁ COOH complex at a scan rate of 50 mV/s , 10 cycles: (a) concentration of 10^{-6} M , potential window from $0\text{-}1.3 \text{ V}$, (b) concentration of 10^{-6} M , potential window from $0\text{-}1.5 \text{ V}$, (c) concentration of 10^{-5} M , potential window from $0\text{-}1.3 \text{ V}$, and (d) concentration of 10^{-5} M , potential window from $0\text{-}1.5 \text{ V}$	122

Figure	Page
3.13 Cyclic voltammograms of the electrochemical cross-linking/deposition of PAMAM-G ₀ COOH complexes at a scan rate of 50 mV/s, 10 cycles: (a) concentration of 10 ⁻⁶ M, potential window from 0-1.3 V, (b) concentration of 10 ⁻⁶ M, potential window from 0-1.5 V, (c) concentration of 10 ⁻⁵ M, potential window from 0-1.3 V, and (d) concentration of 10 ⁻⁵ M, potential window from 0-1.5 V.....	124
3.14 Cyclic voltammograms of the electrochemical cross-linking/deposition of PAMAM-G ₁ COOH complexes at a scan rate of 50 mV/s, 10 cycles: concentration 10 ⁻⁶ M, potential window from 0-1.1 V.....	125
3.15 Absorption spectra analysis performed in 0.1 M TBAPF ₆ /CHCl ₃ on ITO substrate in the present of different concentrations and potential windows. (a) PAMAM-G ₁ COOH, and (b) PAMAM-G ₀ COOH.....	126
3.16 AFM images of PAMAM-G ₁ COOH complex after electropolymerization on ITO at a scan rate of 50 mV/s, 10 cycles: (a) concentration of 10 ⁻⁶ M, potential window from 0-1.3 V, (b) concentration of 10 ⁻⁶ M, potential window from 0-1.5 V, (c) concentration of 10 ⁻⁵ M, potential window from 0-1.3 V, and (d) concentration of 10 ⁻⁵ M, potential window from 0-1.5 V.....	128
3.17 (a) Absorption spectra of Nile red in a solution of 70 μM G ₁ COOH, and (b) Emission intensity of different saturated solutions of Nile red at 640 nm (λ _{ex} =570 nm) versus concentration of G ₁ COOH in 0.1 M TBAPF ₆	129
3.18 Cyclic voltammograms of the electrochemical cross-linking/deposition of G ₁ COOH at a scan rate of 50 mV/s, 10 cycles: (a) concentration of 10 ⁻⁶ M, potential window from 0-1.3 V, (b) concentration of 10 ⁻⁶ M, potential window from 0-1.5 V, (c) concentration of 10 ⁻⁵ M, potential window from 0-1.3 V, and (d) concentration of 10 ⁻⁵ M, potential window from 0-1.5 V.....	130

Figure	Page
3.19 AFM images of G ₁ COOH after electropolymerization on ITO at a scan rate of 50 mV/s, 10 cycles: (a) concentration of 10 ⁻⁶ M, potential window from 0-1.3 V, (b) concentration of 10 ⁻⁶ M, potential window from 0-1.5 V. (c) concentration of 10 ⁻⁵ M, potential window from 0-1.3 V, and (d) concentration of 10 ⁻⁵ M, potential window from 0-1.5 V.....	132
3.20 High-resolution XPS spectra of the cross-linked polymer: (a) C 1s, and (b) N 1s.....	133
3.21 Spectroelectrochemical analysis performed in 0.1 M TBAPF ₆ /CHCl ₃ on ITO substrate in the present of different concentrations and potential windows of PC	133
3.22 Cyclic voltammograms of the electrochemical cross-linking/deposition of (3,5-Bis(4-(9H-carbazol-9-yl)butoxy)-benzoyl-Functionalized Dendrimer PAMAM (PC) at a scan rate of 50 mV/s, 10 cycles: (a) concentration of 10 ⁻⁶ M, potential window from 0-1.3 V, (b) concentration of 10 ⁻⁶ M, potential window from 0-1.5 V, (c) concentration of 10 ⁻⁵ M, potential window from 0-1.3 V, and (d) concentration of 10 ⁻⁵ M, potential window from 0-1.5 V.....	134
3.23 AFM topography images of PC after electropolymerization on ITO at a scan rate of 50 mV/s, 10 cycles: (a) concentration of 10 ⁻⁶ M, potential window from 0-1.3 V, and (b) concentration of 10 ⁻⁵ M, potential window from 0-1.3 V.....	135
3.24 UV-vis absorption spectra of PAMAM dendrimers functionalized with terthiophene (PT) and carbazole (PC) dendrons 10 ⁻⁶ M before and after adding with AuCl ₃ in toluene. (a) PT at different time (0-30 mins), and (b) PC after adding AuCl ₃ 30 mins. Dendrimer PT and PC show their characteristic absorption bands at 345, 333 and 346 nm, respectively.....	149

Figure	Page
3.25 Steady-state fluorescent spectra of PAMAM dendrimers functionalized with terthiophene (PT) and carbazole (PC) dendrons 10^{-6} M before and after treated with AuCl_3 in toluene by using excitation wavelengths at 345 and 333 nm, respectively. ET mechanism was proved by quenching phenomena and new peaks of AuNPs.....	151
3.26 FT-IR spectra of films (drop-cast on ITO substrate, from top to bottom) of PAMAM dendrimers functionalized with 10^{-6} M of PC (a) and PT (b) dendrons before and after treated with AuCl_3 in toluene.	152
3.27 High-resolution XPS of the informative elements for the structure determination of (a) PPT-AuNPs, and (b) PPC-AuNPs.....	153
3.28 AFM image ($2 \times 2 \mu\text{M}$) of PT (a) and PPT-AuNPs (b) on mica substrate.....	154
3.29 AFM image ($2 \times 2 \mu\text{M}$) of PC (a) and PPC-AuNPs (b) on mica substrate.....	154
3.30 Cyclic voltammograms of the electrochemical cross-linking/deposition of PC at a scan rate of 50 mV/s, 10 cycles: (a) concentration of 10^{-6} M, potential window from 0-1.3 V, (b) concentration of 10^{-6} M, potential window from 0-1.5 V, (c) concentration of 10^{-5} M, potential window from 0-1.3 V, and (d) concentration of 10^{-5} M, potential window from 0-1.5 V.....	155
3.31 Spectroelectrochemical analysis performed in 0.1 M $\text{TBAPF}_6/\text{CHCl}_3$ on ITO substrate in the present of different concentrations and potential windows of PC.....	156
4.1 The derivative receptors based on hexahomotriazacalix[3]arene ...	157
4.2 Molecular device based on hexahomotriazacalix[3]arene	158
4.3 Self-assembly of PAMAM-carbazole dendron surfmer complexes.	159
4.4 The possibility to form hybrid gold nanoparticles via terthiophene and carbazole-PAMAM dendrimer oxidation	160

LIST OF TABLES

Table	Page
2.1 Concentration of anions ($X^- = F^-, H_2PO_4^-, CH_3COO^-$ and $PhCOO^-$) used in anion complexation studies with ligand L1 and the final ratios of guest : host.....	45
2.2 Stability constant ($\log \beta$) ^a of hexahomotriazacalix[3]arene (L1) complexes with anion in DMSO by UV-vis titration method ($T = 25\text{ }^\circ\text{C}$, $I = 0.01\text{ M Bu}_4\text{NPF}_6$).....	54
2.3 Stability constants ($\log \beta$) ^a of 1:1 complexes of L2 with cations in DMSO by UV-vis titration method ($T = 25\text{ }^\circ\text{C}$, $I = 0.01\text{ M Bu}_4\text{NPF}_6$).....	58
2.4 Variation in absorbances of compounds L2 in the absence or presence of various anions ^a ($\lambda=293\text{ nm}$).....	60
2.5 Stability constants ($\log \beta$) ^a of complexes of L2 with anions in DMSO by UV-vis titration method ($T = 25\text{ }^\circ\text{C}$, $I = 0.01\text{ M Bu}_4\text{NPF}_6$).....	61
2.6 Relative affinities of the halide salts toward host L3 and ¹ H-NMR chemical Induced downfield shifts (CIS) observed through their endo-complexation in $CDCl_3$	62
2.7 Stability constant ($\log \beta$) ^a of <i>N</i> ₇ -azacalix[3]-cryptand (L3) complexes with anion in DMSO by UV-vis titration method ($T = 25\text{ }^\circ\text{C}$, $I = 0.01\text{ M Bu}_4\text{NPF}_6$).....	65
2.8 Stability constant ($\log \beta'$) ^a of L3 • Zn^{2+} complexes with anion in DMSO by UV-vis titration method ($T = 25\text{ }^\circ\text{C}$, $I = 0.01\text{ M Bu}_4\text{NPF}_6$).....	66
3.1 Anodic and cathodic currents/potentials of precursor polymers and their corresponding onsets of oxidation potential.....	123

LIST OF SCHEMES

Scheme	Page
1.1 Reaction of hydroxyphenol derivatives with amines.....	6
2.1 Synthesis pathway of L2 (a) ethylbromoacetate, NaH, THF, DMF, reflux, 72 hours; (b) 1-aminomethylnaphthalene, toluene:MeOH (1:1), RT, 3 days, L2a (41%); and (c) 1-aminomethyl-naphthalene, toluene:MeOH(1:1), RT, 7 days, L2b (42%).....	47
2.2 Synthesis pathway of <i>N</i> ₇ -Azacalix[3]cryptand (L3).....	48
2.3 The two explanations for the potential changes after the addition of different cations (a) cations can be protected electron transfer to the conjugated polymer backbone, and (b) cations complexation can be a hole to improve the hole transport pathways in-between chains.....	92
3.1 Electroactive groups (terthiophene, T and carbazole, C) of modified PAMAM dendrimer were used in this study.....	147

LIST OF ABBREVIATIONS AND SIGNS

$^{\circ}\text{C}$	Degree celsius
$^{13}\text{C-NMR}$	Carbon-13-Nuclear Magnetic Resonance Spectroscopy
$^1\text{H-NMR}$	Proton-1-Nuclear Magnetic Resonance Spectroscopy
α	Alpha
δ	Chemical shift
\supset	Encapsulation
λ_{ex}	Excitation wavelenght
λ_{em}	Emission wavelenght
\AA	Angstrom
μA	Microampere
μL	Microliter
μM	Micromolar
ΔE	Change in potential
E_0	Observed potential
E_i	Initial potential
E_{pa}	Anodic potential
E_{pc}	Cathodic potential
I_{pa}	Anodic currents
I_{pc}	Cathodic currents
ΔF	Frequency change
ΔR	Resistance change
AFM	Atomic Force Microscopy
ATR	Attenuated Total Reflection
BD	Butterworth-van Dyke
cmc	Critical Micelle Concentration
cm^{-1}	Wave number

CCA	2-cyano-4-hydroxycinnamic acid
COSY	Correlation Spectroscopy
CPNs	Conjugated polymer networks
CT	Charge Transfer
CV	Cyclic Voltammetry
d	Doublet
DCM	Dichloromethane
DEMNs	Dendrimer-Encapsulated Metal Nanoparticles
DENs	Dendrimer-Encapsulated Nanoparticles
DHB	2,5-dihydroxy-benzoic acid
DMF	Dimethylformamide
DMSO	Dimethylsulfoxide
EC-QCM	Electrochemical Quartz Crystal Microbalance
EC-SPR	Electrochemical Surface Plasmon Resonance Spectroscopy
EDTA	Ethylenediamine tetraacetic acid
EL	Electroluminescence
EtOAc	Ethylacetate
EtOH	Ethanol
FT-IR	Fourier Transform Infrared Spectroscopy
g	Gram
HLB	Hydrophilic-lipophilic balance
HMBC	Heteronuclear Multiple Bond Correlation
HMQC	Heteronuclear Multiple-Quantum Coherence
HOMO	Highest Occupied Molecular Orbital
HSAB	Hard soft acid and base principle
Hz	Hertz
ITO	Indium Tin Oxide
IR	Infrared Spectroscopy

J	Coupling Constant
K	Kelvin
K_{asso}	Association Constant
kJ	Kilojule
LB	Layer by layer
LEDs	Light-Emitting Diodes
LUMO	Lowest Unoccupied Molecular Orbital
m	Multiplet
m/z	Mass per charge ratio
mg	Milligram
mL	Milliliter
mmol	Millimol
mV	Millivolt
mV/s	Millivolt per second
M	Molar
MALDI-TOF	Matrix Assisted Laser Desorption Ionization Time-of-flight
MLCT	Metal-to-Ligand Charge Transfer
MHz	Mega Hertz
nm	Nanometer
NCDs	Nanoparticle-core dendrimers
NEt ₃	Triethylamine
NMR	Nuclear Magnetic Resonance Spectroscopy
MS	Mass Spectroscopy
PAMAM	Poly(amidoamine)
PA	Polyacetylene
PANI	Polyaniline
PCBz	Polycarbazole
PEDOT	Poly(3,4-ethylenedioxythiophene)

PET	Photo-induced electron transfer
PF	Polyfluorene
PLEDs	Polymer light-emitting diodes
PPP	Poly (<i>p</i> -phenylene)
PPV	Poly(<i>p</i> -phenylenevinylene)
PPy	Polypyrrole
PSS	Polystyrene sulfonate
PT	Polythiophene
PVK	Poly(<i>N</i> -vinylcarbazole)
PVP	Poly(vinyl pyrrolidone)
QCM	Quartz Crystal Microbalance
RQCM	Research Quartz Crystal Microbalance
s	Singlet
SAM	Self-assembled monolayer
SPR	Surface Plasmon Resonance Spectroscopy
t	Triplet
T	Temperature
TBA	Tetrabutylammonium cation
TEM	Transmission Electron Microscopy
THF	Tetrahydrofuran
TLC	Thin Layer Chromatography
TNF	2,4,7-trinitrofluorenone
UV-vis	Ultraviolet-Visible Spectroscopy
V	Volt or Volume
WCA	Water Contact Angle

CHAPTER I

INTRODUCTION AND BACKGROUND

1.1 Introduction of calixarene and azacalixarene

In supramolecular chemistry, a wide variety of macrocyclic receptors are able to recognize or selectively interact with neutral, anionic and cationic species to form host-guest complexes which are extremely important in chemistry. Recognition is related to selective host-guest receptors and is strongly dependent on the host-guest intermolecular interactions. The one family of model systems in supramolecular host-guest chemistry is calix[n]arenes [1,2,3].

1.1.1 Calixarenes

1.1.1.1 History of calixarenes

The calixarenes, generally having the structure shown in Figure 1.1, were discovered by Zinke in the 1940s [4] and fully interpreted by Gutsche in the 1970s [5]. Gutsche was also the first person who drew an attention to the potential use of these cyclic oligomers as the molecular receptors or the enzyme mimics. In 1978, Gutsche proposed that these cyclic oligomers were known collectively as “calixarenes” [4]. Derived from the Greek word *calix* meaning vase, and *arene* indicating the presence of aromatic rings, calixarenes have been synthesized in a number of sizes. A bracketed number positions between *calix* and *arene* indicates the number of phenolic units linked to each other by the methylene bridges to form the cavity of the molecule. A substitution on the aromatic rings is specified by the appropriate prefixes. The naming scheme is illustrated in Figure 1.1.

1.1.1.2 Nomenclature of calixarenes

The calixarene descriptor is taken to designate only the basic macrocyclic framework. A bracketed number specifies the number of aromatic rings. The substituents

on the upper (wider, usually located on the top) and lower (narrower) rims (see Figure 1.1) are designated as prefixes along with an appropriate numbering [6].

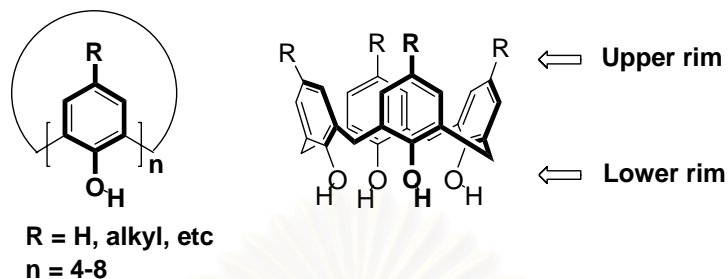


Figure 1.1 General structure of calixarene.

The cyclic tetramer derived from *p-tert*-butylphenol and formaldehyde is named *p-tert*-butylcalix[4]-arene, or 5,11,17,23-tetrakis(1,1-dimethylethyl)-25,26,27,28-tetrahydroxycalix[4]arene. According to the IUPAC system of nomenclature, the name is pentacyclo-[19.3.1.1^{3,7}.1^{9,13}.1^{15,19}]octacos-1(25),3,5,7(28),9,11,13(27),15,17,19(26),21,23-dodecaene-25,26,27,28-tetrol-5,11,17,23-tetrakis(1,1-dimethylethyl).

1.1.1.3 Conformations of calix[4]arenes

The solid-state structure of *p-tert*-butylcalix[4]arene adopts a vase-like arrangement called the “cone” conformation. In this conformation, all four phenolic groups point to the same direction. As shown in Figure 1.2, the region where the *p-tert*-butyl groups locate is called the “upper rim” or “wide rim” and the region where the four hydroxyl groups lie is called the “lower rim” or “narrow rim”. A rotation of the *p-tert*-butyl groups passing through the upper rim is prohibited in calix[4]arenes, but it is possible in the calixarenes with larger rings. However, a rotation of the hydroxyl group through the lower rim is permitted, which results in three other conformations: partial-cone, 1,2-alternate and 1,3-alternate. In the solid state, the cone conformer is the only form, stabilized by intramolecular hydrogen bonding. In a solution, however, the four conformations are interchangeable. The interconversion is slow at low temperatures and rapid at high temperatures, as evidenced by NMR spectroscopy. The different conformations of calix[4]arenes originate from lower rim rotation. When the size of the OR group becomes larger, such rotation becomes impossible, giving four conformationally rigid isomers. The attachments of the groups with different sizes to the

hydroxyl groups were performed and the mobility of the calix[4]arenes was studied. It was found that the tetramethyl [7,8], tetraethyl [8] and tetrakis(cyanomethyl) ethers [9] of calix[4]arene are all conformationally mobile, while the tetrapropyl ether [8] is conformationally rigid even at elevated temperatures. Therefore, *O*-substituted groups larger than the ethyl group will lock the conformation of a calix[4]arenes into four stereoisomers. Another interesting phenomenon is that partially etherified calix[4]arenes are less flexible than the corresponding fully etherified calix[4]arenes. This is attributed to the existence of intramolecular hydrogen bonding, which stabilizes the cone conformation.

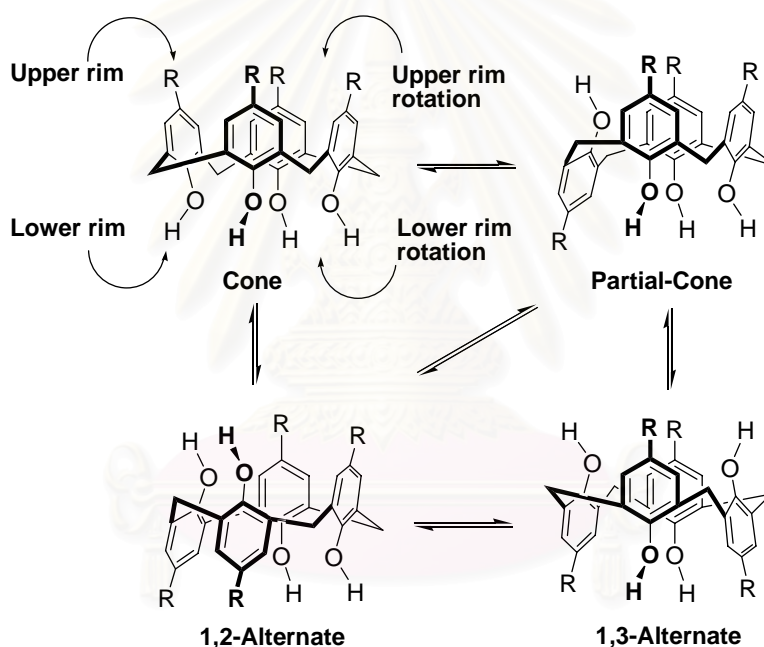


Figure 1.2 Four interchangeable conformations of *p*-*tert*-butylcalix[4]arene.

1.1.1.4 Complexation of metal ions by calix[4]arenes

Early studies showed that *p*-*tert*-butylcalix[4]arene exhibited no metal ion transport ability in a neutral solution. In a solution of the metal hydroxide, however, the transport behavior was greatly enhanced [10]. Among all the cations investigated, the calix[4]arene preferably transported Cs^+ . During the complexation process, the calix[4]arene is deprotonated first, followed by the complexation with a cation to form a

neutral complex that remains in the organic phase. It can be confirmed by a dimer formation in reaction of calix[4]arene with SiCl_4 [11] and TiCl_4 [12] in the NaH in THF as demonstrated in Figure 1.3. To further understand the limited properties of calixarene, the researchers try to increase the interaction between calixarene and cation by incorporated heteroatom instant methylene bridges. As we know in the name of “heteroatom-bridged calixarenes”.

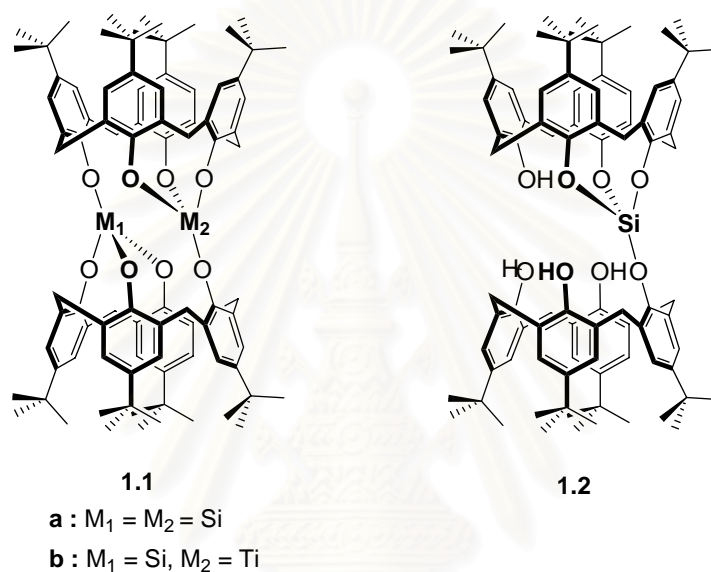


Figure 1.3 Complexation of calix[4]arene with metal lead to double calix[4]arene in the present of NaH as base.

1.1.2 Heteroatom-bridged calixarenes

The names of “heteroatom-bridged calixarenes” are currently used to indicate in a specific manner. The calixarene analogues in which CH_2 groups are completely replaced by a heteroatom such as oxygen, sulfur and nitrogen are called hexahomotrioxacalixarenes or oxacalixarenes (**1.3**) [13], hexahomotrithiacalixarenes or thiacalixarenes (**1.4**) [14] and hexahomotriazacalixarenes or azacalixarenes (**1.5**) [15], respectively. In recent years, these calixarene analogues have been synthesized as part of a class of compounds called expanded calixarenes. From the structural point of view, hexahomooxacalix[3]arene and hexahomothiocalix[3]arene have similar size to that of

the 18-crown-6 but, for the topological one, they provide 3-D cavity, which can better envelop the substrates.

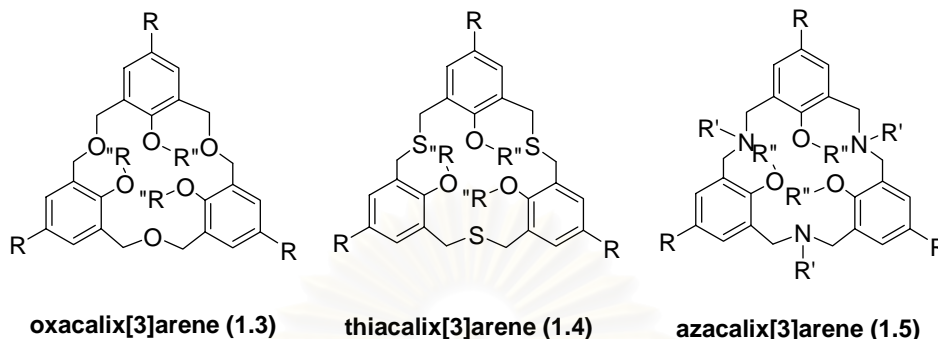


Figure 1.4 Structures of heteroatom-bridged calixarene.

It is well known that more coordinating sites give more complexation stability. Therefore, scientists replace oxygen and sulfur atoms on **1.3** and **1.4** by nitrogen atoms to attach more binding sites affording hexahomoazacalix[3]arenes (**1.5**). Furthermore, the structure of azacalix[3]arenes (**1.5**) can be modified at not only the upper-rim (R) and lower-rim (R''), but also within the macrocycle cup at the inner-rim (R'). So, this molecular platform is interesting to be developed for a selective sensor for anions, cations and/or organic molecules.

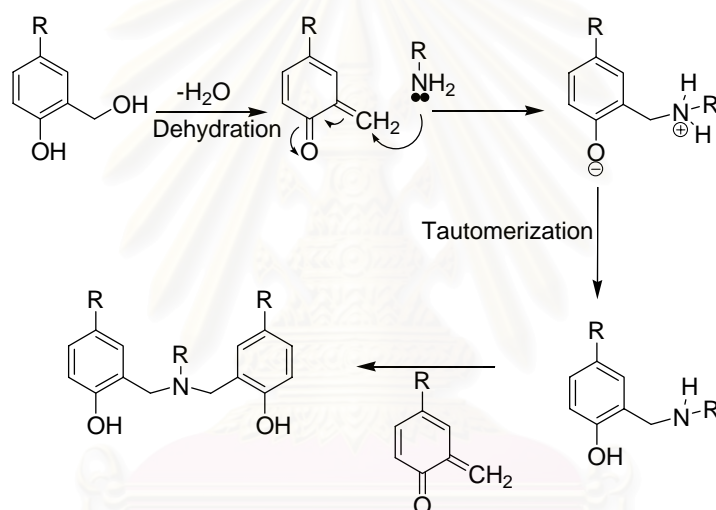
1.1.3 Hexahomotriazacalix[3]arenes or azacalix[3]arenes

Although the literature on azacalix[3]arenes is sparser than that on oxacalix[3]arenes, their chemistry is in principle even richer. Both the reactivity of the amino groups and the interaction of the substituents on the side arms with those on the upper and on the lower rim should be considered. The azacalix[3]arene can be synthesized by one-pot and stepwise methods.

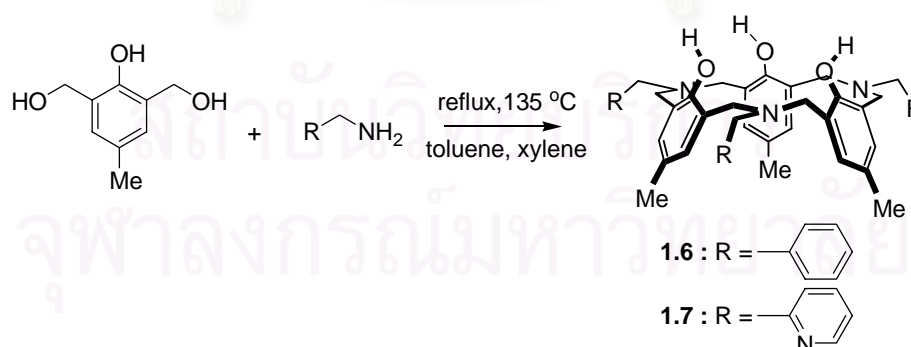
1.1.3.1 One-pot synthesis of azacalix[3]arenes

Azacalix[3]arenes can be easily synthesized by heating bis(hydroxymethyl)phenol derivatives and benzylamine in refluxing toluene or xylene for 3 days [16]. The desired cyclic compounds are obtained selectively in moderate to high yields. The choice of non-polar solvents is essential in this reaction because the template effect by $\text{OH} \cdots \text{OH}$ and

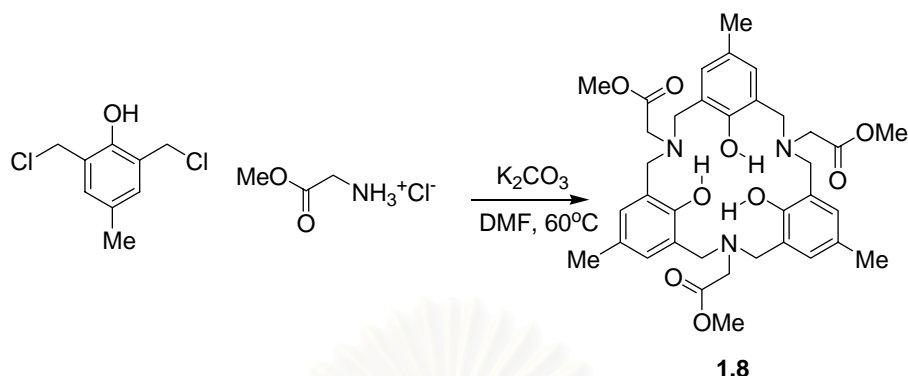
OH...N hydrogen bonds play an important role in the cyclization [16a]. Thus, the high dilution technique is not required in this reaction. Several reports support this phenomenon; i.e., a phenol cyclic trimer was observed in supersonic jets [17]. Generally, condensation reaction between alcohol and amine require drastic reaction conditions and catalysts [18]. However, in the case of hydroxymethylphenols, C–N bond formation occurs under a relatively mild condition. The reaction is not a simple dehydration reaction but seems to be a kind of Mannich reaction via quinonemethides as shown in Scheme 1.1. This is because of that an absence of the phenolic OH group allows no reaction; i.e., 1,3-bis(hydroxymethyl)-5-*tert*-butylbenzene and benzylamine do not react at all under similar conditions.



Scheme 1.1 Reaction of hydroxyphenol derivatives with amines.

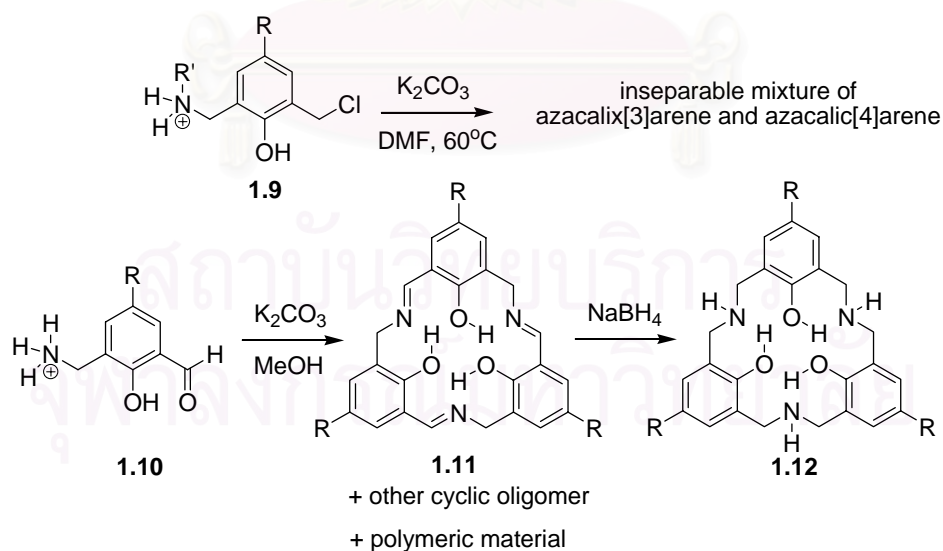


For example, Takemura and coworkers [19,16b] first reported the divergent synthesis of azacalix[3]arene (**1.6** and **1.7**) by azeotropic refluxing of 2,6-bis(hydroxymethyl)phenol in the presence of a primary amine in toluene.



Several years later, Hampton and coworkers [20] developed an alternative approach to the azacalix[3]arenes (**1.8**) which is compatible with volatile amines that involves a cyclooligomerization reaction between 2,6-bis(chloromethyl)-4-methylphenol and glycine methyl ester hydrochloride in dimethylformamide (DMF) under high-dilution condition in the presence of potassium carbonate.

The receptor **1.8** exhibits a cone-shape in the solid state with all three of its ester functional groups surrounding the cavity of the macrocycle. Although the macrocycle possesses a well defined pocket for inclusion chemistry, it does not extract alkali metal picrates because of the intramolecular hydrogen bonding which prevents both the phenolic oxygens and amines from participation in molecular recognition processes.

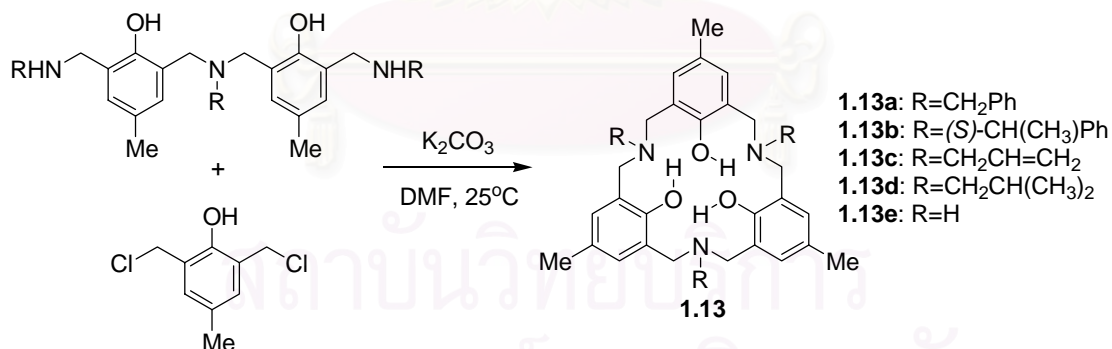


Moreover, the condensation of aminomethyl-chloromethyl monomer **1.9** and cyclization of the aminomethyl-salicylaldehyde **1.10** were used as starting materials to

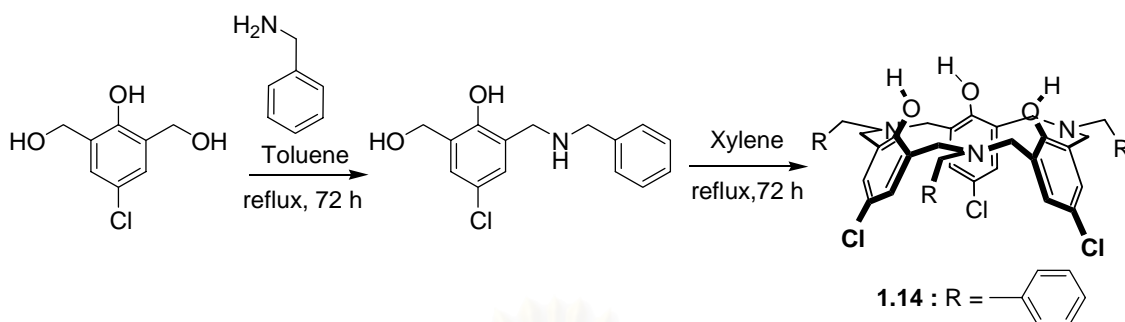
synthesize azacalix[3]arene [21]. Both of them have demonstrated a separation problem. The inseparable mixtures of azacalix[3]arene and azacalix[4]arene macrocycles were observed when monomer **1.9** was used. Similar results were obtained with a cyclization of **1.10**. Separation of the imine-linked macrocycles was not possible due to the ability of the azacalix[n]arenes (n=3, 4) exhibited too similar of chromatographic property to separate the mixture.

1.1.3.2 Stepwise synthesis of azacalix[3]arenes

In 2000, Hampton and coworkers [22] described a new selective convergent synthesis of azacalix[3]arenes (**1.13a-e**). The key transformation in this synthesis involves the coupling of the triamines with 2,6-bis-(chloromethyl)-4-methylphenol. This condensation proceeds in an exceptionally high yield (~95%) and without the formation of other macrocyclic products, i.e. the azacalix[4]arene. The desired **1.13a-e** were obtained in overall yield ~57%. Deprotection of azacalix[3]arene **1.13c** to from the *N*-unsubstituted azacalix[3]arene **1.13e** has been accomplished under palladium catalyzed conditions.



Moreover, the azacalix[3]arene **1.14** [23a] can be synthesized by using this method instead of the previous one. The acyclic intermediate was synthesized first, after that it was cyclized by refluxing in xylene for 72 hours to get the azacalix[3]arene.



1.1.4 Complexation of metal ions by azacalix[3]arenes

The azacalix[3]arene macrocycles have the potential of binding trivalent metal ions as neutral (H_3L) and trianionic (L^{3-}) ligands; complexes of both types have been observed depending on the reaction conditions. The reaction of macrocycle **1.8** with a stoichiometric amount of MX_3 ($M=Sc, Y, La$; $X=Cl, OTf$) resulted in the formation of $M(H_3L)X_3$ complexes. The metal bound to the three phenolic oxygen atoms and the three ring nitrogen atoms were protonated resulting in a metal complex of an overall neutral ligand (H_3L) [20]. This was supported by 1H -NMR spectrum of complex which indicated an N-H signal coupling with the adjacent methylene protons.

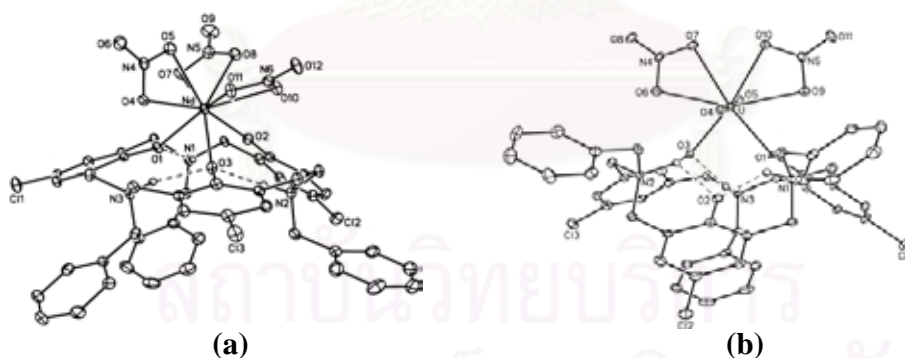
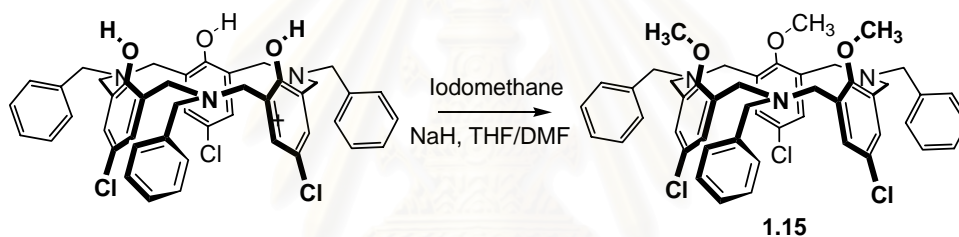


Figure 1.5 View of the complex molecule in *p*-chloro-*N*-benzylhexahomotriazacalix[3]arene with (a) Nd^{3+} , and (b) UO_2^{2+} which are shown hydrogen bonds in dashed lines, protons of the ammonium groups represented as small spheres of arbitrary radii [23].

Thuéry and coworkers [23] prepared Nd^{3+} , UO_2^{2+} and Yb^{3+} complexes of azacalixarenes (**1.14**) without using any bases and succeeded in obtaining complexes

suitable for crystallographic analyses (Figure 1.5). Interestingly, in the crystal structures, OH protons are not located on the oxygen atoms but are transferred to nitrogen atoms and form intramolecular zwitter-ionic structures. The metal ions are placed out of the plane of the $O \cdots NH^+ \cdots O \cdots$ linkage: this is ascribed to the $NH^+ \cdots M^+$ repulsion. A review by Thuéry and coworkers [2] described the complexes of *f*-element ions of oxa- and azacalixarenes. Furthermore, alkali and alkyl ammonium ions can be extracted by these macrocycles. Macrocycle **1.15** was prepared by *O*-methylation of **1.14**. Picrate extraction studies indicated no detectable extraction of alkaline metal ion, NH_4^+ , or $PrNH_3^+$ picrates by azacalix[3]arene **1.14**. Under identical condition, the *O*-methylated **1.15** exhibits a greater extraction ability than **1.14** does which is likely due to the removal of intramolecular hydrogen bonding and the enhanced donor ability of the ether groups.



The inner rim was modified by Takemura and coworkers [16] and it extracted UO_2^+ efficiently even in the presence of a high concentration of NaCl. This ligand proved to be a weak complexant with a remarkable K^+ selectivity while the analogue with 2-picolyl substitution (**1.7**) in the side arm was much more effective in alkali metal ion complexation but the selectivity was very poor because of the flexibility of the picolyl side arms [16b].

1.2 Introduction of carbazole, thiophene, oligothiophenes, dendrimers, and their applications

1.2.1 General aspects of conducting polymers

Most polymers, either natural or synthetic, are traditionally associated with insulating properties. Therefore, they have been widely used as insulators of metallic conductors, packaging materials, and photoresists in the electronics industry. Since the unexpected discovery in 1977 that doping of polyacetylene resulted in increased conductivity by 11 orders of magnitude [24,25], conjugated polymers have been proclaimed as futuristic new materials that will lead to the next generation of electronic and optical devices. This “conducting polymer” field is deemed especially exciting because it evolves at the boundary between chemistry and condensed matter physics. It also creates a number of opportunities to address questions in quantum chemistry and the fundamental understanding of π -bonded macromolecules. Although the initial emphasis was on the conduction properties of these “synthetic metals” obtained through doping of conjugated polymers, the past two decades have focused on the study of soluble and intrinsically semiconducting polymers. During the past 29 years, many novel materials have been designed, synthesized, and developed for their specific physical or chemical properties. Some have even been implemented in working devices in the marketplace.

The discovery of highly conducting polyacetylene in 1977 prompts the synthesis of other polymers with conjugated π -systems such as poly (*p*-phenylene) (**PPP**), poly(*p*-phenylenevinylene) (**PPV**), polythiophene (**PT**), polycarbazole (**PCBz**), polypyrrole (**PPy**), and polyaniline (**PANI**). Their chemical structures are shown in Figure 1.6. The major drawback to these materials is that they are intractable because of their limited solubility. However, there is still great interest in these materials from a theoretical perspective and scientists would eventually overcome the solubility problem through molecular design. Two major approaches involved are direct functionalization of the polymer backbone with solubilizing alkyl groups and the creation of a “doped complex” with other soluble polymers. Using the “complex” strategy, the Bayer Corporation developed the first commercially successful conducting polymer, Baytron P, in 1988. It consists of a complex of poly(3,4-ethylenedioxythiophene) (PEDOT) and polystyrene

sulfonate (PSS) and has found applications in antistatic coatings, batteries, and “smart” windows [26].

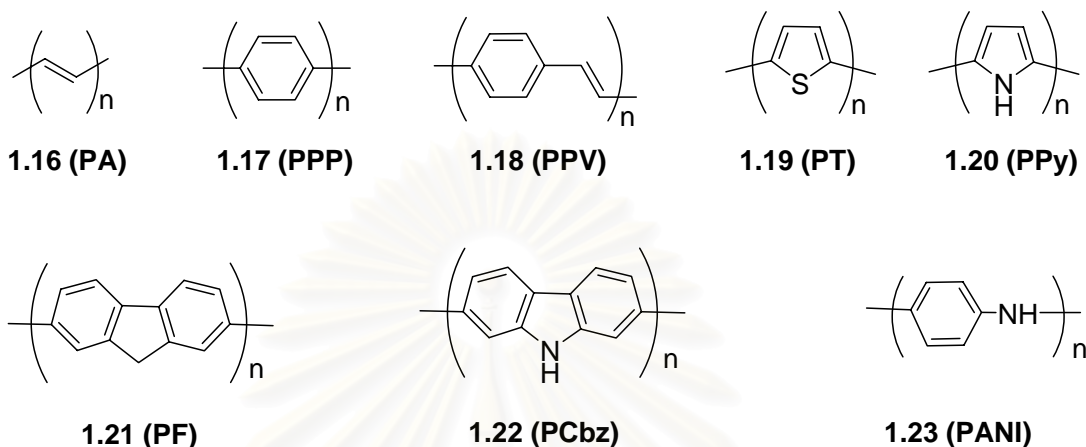


Figure 1.6 Chemical structures of (1.16) *trans*-polyacetylene (**PA**); (1.17) poly(*p*-phenylene) (**PPP**); (1.18) poly(*p*-phenylene vinylene) (**PPV**); (1.19) polythiophene (**PT**); (1.20) polypyrrole (**PPy**); (1.21) polyfluorene (**PF**); (1.22) polycarbazole (**PCbz**); (1.23) polyaniline (**PANI**).

In the undoped, or pristine state, the bandgap of conjugated polymers, which is defined by the energy difference between the highest occupied molecular orbital (HOMO) and the lowest unoccupied molecular orbital (LUMO), falls in the semiconductor regime. They become conductive in their doped state, which can be achieved either chemically or electrochemically. Upon doping, the electrochemical potential (Fermi level) is moved either by a redox reaction or by an acid-base reaction into a region of energy where there is a high density of electronic states. Charge neutrality in the material is maintained by the addition of counterions. In this sense, metallic polymers can be considered as salts. Their electrical conductivity results from the existence of charge carriers through doping and from the ability of the charge carriers to move freely along the π -system. Since every monomeric repeat unit is a potential redox site, conjugated polymers can be doped to charge carriers of high density [27].

About the time that the scientific community began to accept the concept of organic conductors, the Cambridge group, in 1990, reported emission of light from a plastic sandwich that was connected to a battery [28]. The discovery of electroluminescence (EL), i.e., the emission of light upon excitation by flow of electric current in conjugated polymers, has provided a new incentive for the development of polymer light-emitting diodes (PLEDs) for display technologies. Other applications, such as field-effect transistors and organic solar cells were soon to follow. This discovery provided a stimulus for a major push into a new, emerging field called “organic electronics”. This field has become extremely popular in the scientific community, involving hundreds of research groups and millions of dollars in funding by governmental and industrial sources.

1.2.2 Polycarbazole

The beginning of the first wave dates back to the sixth decade of the last century. A lot of interest in these polymers was caused by the discovery of photoconductivity in poly(*N*-vinylcarbazole) (PVK) by H. Hoegl [29]. In 1957, he has established that PVK sensitized with suitable electron acceptors showed high enough levels of photoconductivity to be useful in practical applications like electrophotography. As a result of the following activities, IBM introduced its Copier I series in 1970, in which an organic photoconductor, the charge transfer complex of PVK with 2,4,7-trinitrofluorenone (TNF), was used for the first time [30]. The photoconductor was a 13 μm single-layer device. It was prepared by casting a tetrahydrofuran solution containing PVK and TNF onto an aluminium substrate [31]. Since then numerous carbazole-containing polymers have been described in scientific literature and especially as patents. The ongoing peak of interest in carbazole-containing polymers is connected mostly with the discovery of polymeric light emitting diodes [28] and organic photorefractive materials [32]. In the recent investigations of organic electroluminescent devices and photorefractive materials an important role belongs to the carbazole-containing polymers. Apart from electrophotographic photoreceptors [33], light-emitting diodes, and

photorefractive materials carbazole-containing polymers are studied as the components of photovoltaic devices [34]. These fields of the present and potential application of carbazole-containing polymers can be named smart material. In all these fields of application photoconductive properties of carbazole-containing polymers or their ability to transport positive charges (holes) are exploited.

Carbazole-based compounds are attractive as photoconductors or charge-transporting materials from the following reasons:

- (1) Carbazolyl groups easily forms relatively stable radical cations (holes);
- (2) Some carbazole-containing compounds exhibit relatively high charge carrier mobility;
- (3) Different substituents can be easily introduced into the carbazole ring;
- (4) Carbazole-containing compounds exhibit high thermal and photochemical stability;
- (5) Carbazole is a cheap raw material readily available from coal–tar distillation.

Few reviews only have been published exclusively on carbazole-containing polymers. Synthesis and properties of PVK and some other carbazole-containing polymers are described in previous work [35]. Vinylcarbazole polymers have been reviewed by Pearson [36]. Different classes of carbazole-based polymers are described in a review article of Biswas and Das [37]. Since carbazole-containing polymers constitute an important part of photoconductive polymers much attention is paid to the carbazole-based compounds in the studies reviewing photoconductive polymers and organic photoreceptors [38]. Most of the above mentioned books and the review articles were published ten or more years ago. During this time a lot of developments have been observed in the field of carbazole-containing polymers which is a new class of amorphous, film-forming photoconductive and charge-transporting materials.

1.2.3 Polythiophenes

Among conducting polymers, polythiophenes have become the most frequently investigated because their conductivity is mostly unaffected by substituents [39]. In addition, polythiophenes are some of the most environmentally and thermally stable materials. As an important representative class of conjugated polymers, polythiophenes can be used as electrical conductors, non-linear optical devices, polymer LEDs, transistors, electrochromic windows, photoresists, antistatic coatings, sensors, batteries, electromagnetic shielding materials, artificial noses and muscles, solar cell, electrodes, microwave absorbing materials, new types of memory devices, batteries, nanoswitches, nanoelectronics, and optical devices [40,41].

Polythiophenes (**PT**) can be generally viewed as conjugated chains consisting of sp^2p_x -carbon atoms that have the analogous structure to a *cis*-poly(acetylene) (PA) chain stabilized by the bridging sulfur atom. The ability of a conjugated system to transduce electronic effects depends on the amount of delocalization of charge carriers, which are created along the molecular chain due to optical or electronic excitation. This charge delocalization can be represented by resonance structures. In the case of conjugated systems, an aromatic and a quinoid structure can be drawn as shown in Figure 1.7.

Among the conjugated chains, resonance is most pronounced for polyenes due to the energetic equivalency of the resonance forms. Polyenes have a degenerate ground state. Because of the reduced conjugation between moieties, this is not the case for other aromatic or heteroaromatic π -systems. The reduced conjugation is either caused by decreased aromaticity and/or the reduced planarity due to the steric hindrance of *o*-hydrogen atoms and/or substituents. Therefore, in the case of aromatic systems, the quinoidal resonance form is only of minor consequence and leads to a non-degenerate ground state [42]. In comparison to PA, polythiophenes provide several interesting features, such as (a) higher environmental stability, (b) structural versatility that allows for the modulation of electronic and solubility properties by attaching appropriate side groups to the thiophene monomers, and (c) a non-degenerate ground state related to the non-energetic equivalence of the two limiting mesomeric forms (aromatic and quinoid) of PT.

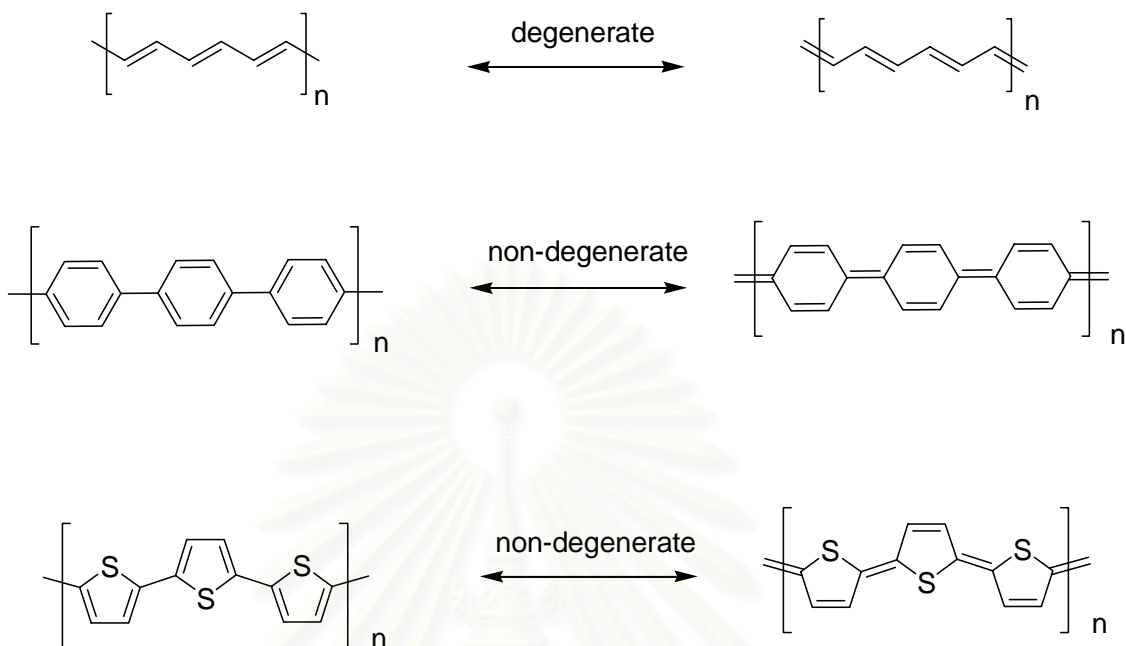


Figure 1.7 Resonance structures of **PA**, **PPP**, and **PT** that show the difference in the two mesomeric forms (aromatic and quinoid) that define the lowest energy states.

1.2.4 Oligothiophenes

Although the optical and electronic properties of polythiophenes can be tuned by the substituents on the backbone to a certain extent, precise predictions about indisputable structure/property relationships are not possible. The physical properties of polythiophenes cannot be correlated directly to the structural parameters. Due to statistical chain length distribution and interruption of the conjugated chain by mislinkages and other defects (such as sp^3 defects), polythiophenes lack a rigidly defined structural principle.

The study of well-defined oligothiophenes is therefore useful to gain insight into structural and electronic peculiarities of the corresponding polythiophenes. Oligothiophenes serve as excellent models for polydispersed polythiophenes. They often provide specific information concerning the solution, electronic, photonic, thermal, and morphological properties of their higher homologues: polythiophenes. Moreover, they

serve as useful models for interpreting structural and conformational properties of polythiophenes.

The study of defined oligomers also provides useful information to improve strategies for the development of novel materials. Some of their physical properties even surpass those of the polythiophenes. For example, an all- α -linked sexithiophene has been successfully used for organic field-effect transistor [43]. The mobility of the charge carriers and the transistor characteristics are superior to those of an analogous polythiophene transistor and even approach those of silicon transistors. Oligothiophenes are now widely considered as a valuable route towards understanding the intrinsic properties of polythiophenes from both experimental and theoretical perspectives [44].

The oligomer approach to the investigation of properties of conjugated polythiophenes offers several key advantages:

- (1) The starting material has a well-defined molecular composition;
- (2) It can be purified by high vacuum sublimation and/or (if solubility permits) by recrystallization;
- (3) It can be processed as a thin film by sublimation in ultra high-vacuum in the absence of both solvents and contaminants;
- (4) These films, if made with exceptional purity, allow for a comparison of film and single-crystal properties, which is useful for determining the correlation between molecular ordering and intrinsic response;
- (5) The ability to grow large single crystals from the vapor phase have allowed the preparation of single crystal devices that allow for the study of intrinsic properties of conjugated materials, such as conductivity or polarized emission along different crystal planes.

1.2.5 Synthesis of oligothiophenes

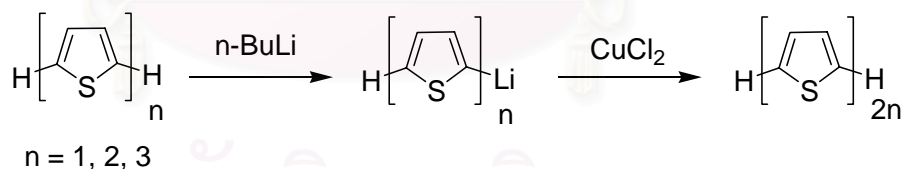
It is interesting to note that the initial driving force for the synthesis of oligothiophenes was their potential use as biologically active compounds. Many bi- and terthiophene derivatives exhibit biological activities such as phototoxicity against microorganisms [45,46], or antibiotic and antiviral properties in the presence of UV light

[47,48]. The second and major motivation is related to their use as materials for electronic device applications. As early as 1974, Kuhn and co-work [49] described photocurrent measurements on **LB** films of α -quintathiophene (α -5T). But the discovery in 1988 of the charge- transport properties of α -sexithiophene (α -6T) is the true starting point for this second generation of oligothiophenes [50,51].

For the synthesis of oligothiophenes, one of the most useful procedures in the formation of C-C σ -bonds is the metal-promoted coupling reaction of organic halides. The reactions of active organometallic agents, such as organolithium or organomagnesium reagents with salts of transition metals, are briefly described below. These reactions have a great disadvantage in that they require at least stoichiometric amounts of transition metals, and have been replaced by more effective, purely catalytic low-valent transition metal-catalyzed methods. A brief description of some of the most relevant methods is given below.

1.2.5.1 Copper(II)-mediated oxidative coupling

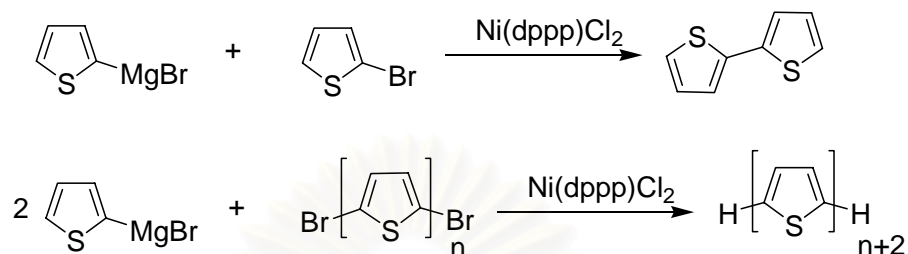
The oxidative coupling reaction was done by using organolithium compounds coupling with cupric chloride [52] that the reaction yields were drastically improved, reaching ~85% for bithiophene.



1.2.5.2 Nickel-catalyzed Kumada cross coupling reactions

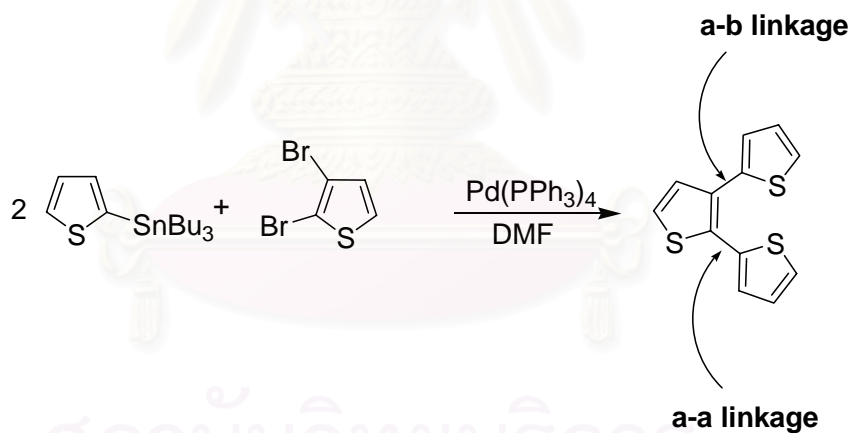
Kumada published an extensive report in 1982 describing the Grignard cross-coupling reactions with heterocyclic compounds, including thiophene and pyridine derivatives [53]. By adding a Grignard solution to a mixture of the organic halide and catalytic amounts of nickel-complexes (0.1 – 1 mol %) in ether solution, the reaction proceeds under mild conditions and gives a coupling product in high yield. Since then,

the “Kumada coupling” has become the most frequently used method in the synthesis of various types of oligothiophenes.



1.2.5.3 “Stille coupling” reactions

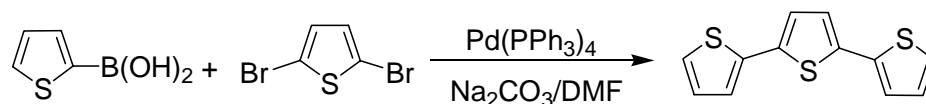
The palladium-catalyzed coupling of organotin compounds has become one of the two most general and selective cross-coupling reactions in organic chemistry [54]. A general mechanistic representation is involving three major steps: (1) oxidative addition, (2) transmetalation, and (3) reductive elimination.



1.2.5.4 Suzuki coupling reactions

The second of the two most general selective cross-coupling reactions in organic chemistry is the palladium-catalyzed cross-coupling of an aromatic diboron derivative with a vinyl- or aryl-dihalide (or triflate) in the presence of base. It is the so-called Suzuki (or Suzuki-Miyaura) cross coupling reaction [55]. One advantage of this reaction

over Stille coupling is that it uses boronic acids or esters, which are much safer than the aforementioned stannates.



1.2.6 Dendrimers

Dendrimer is derived from the Greek words *dendron* (tree) and *meros* (part). Dendrimers are highly branched, perfect monodispersed, three-dimensional (3D), tree-like macromolecules. They are synthesized by an iterative sequence of reaction steps, in which each additional iteration, leads to a higher generation material. Vögtle [56] first reported an iterative synthetic procedure toward well-defined branched structures. However, it was Tomalia's PAMAM dendrimers [57,58] and Newkome's "arborol" systems [59] that made dendrimers receive world-wide attention. Besides these two dendrimers, poly(propylene imine) [60,61], Fréchet type polybenzylether [62] and Moore's phenylacetylene dendrimers [63,64] are the five classes of most well-studied and well-known dendrimers. Additionally, many other types of interesting, valuable, and aesthetically appealing dendritic systems have been developed [65], and thus, various dendritic scaffolds have been accessible with defined nanoscopic dimensions and discrete numbers of functional end- groups.

Compared with classical linear polymers, dendrimers have three distinguishing architecture components, namely (a) an initiator or connecting core, (b) interior layers called "generations" (denoted by the letter G) consist of repeating units radially attached to the initiator core, and (c) a layer of terminal groups attached to the outermost branching units.

Due to these three architectural components, dendrimers have at least three characteristic features in sharp contrast to those of classical linear polymers:

- (1) A dendrimer can be isolated as an essentially monodispersed compound;

- (2) As their molecular weight increases, the physicochemical properties are dominated by the nature of the end groups;
- (3) Dendritic growth is mathematically limited. Dendrimer size increases linearly and the number of surface functional groups increases exponentially with generation number. Therefore, dendrimers adopt a more globular conformation as generation increases. At a certain generation a steric limit to regular growth, known as the De Gennes dense packing [66] is reached.

1.2.7 Synthesis of dendrimers

Dendrimers are generally synthesized by two complementary approaches, the divergent [67] and the convergent [67,68]. Figure 1.8 shows the basic concept of these two approaches [69]. Both approaches have advantages and disadvantages.

1.2.7.1 Divergent approach

The divergent approach starts growth of the dendrimer at the core and continues outward by the repetition of coupling and activation steps. The number of reactions at the periphery increases exponentially as the dendrimer grows from one generation to the next higher generation. Therefore, an excess of reagent is required to drive both reactions to completion. This approach is ideal for the preparation of large quantities of higher-generation dendrimers, but the dendrimers thus produced always have defects because of the difficulties in driving exponentially increased numbers of reactions to completion.

1.2.7.2 Convergent approach

The convergent method initiates growth from the exterior of the dendron and continues inward by the repetition of coupling and activation steps. Although it also uses an iterative synthesis, the convergent approach is different from its divergent counterpart in that it involves only a small number of reactions per molecule during the coupling and activation steps. The convergent approach will generate fewer defects in dendrimers, but

it is typically limited to lower generations of dendrimers. The convergent synthesis, however, has the advantage of allowing precise control of functionality at specific locations of the dendrimer. It also can produce various novel architectures through attachment of dendritic branches to other molecules. The final step is the coupling of these dendrons to a central core.

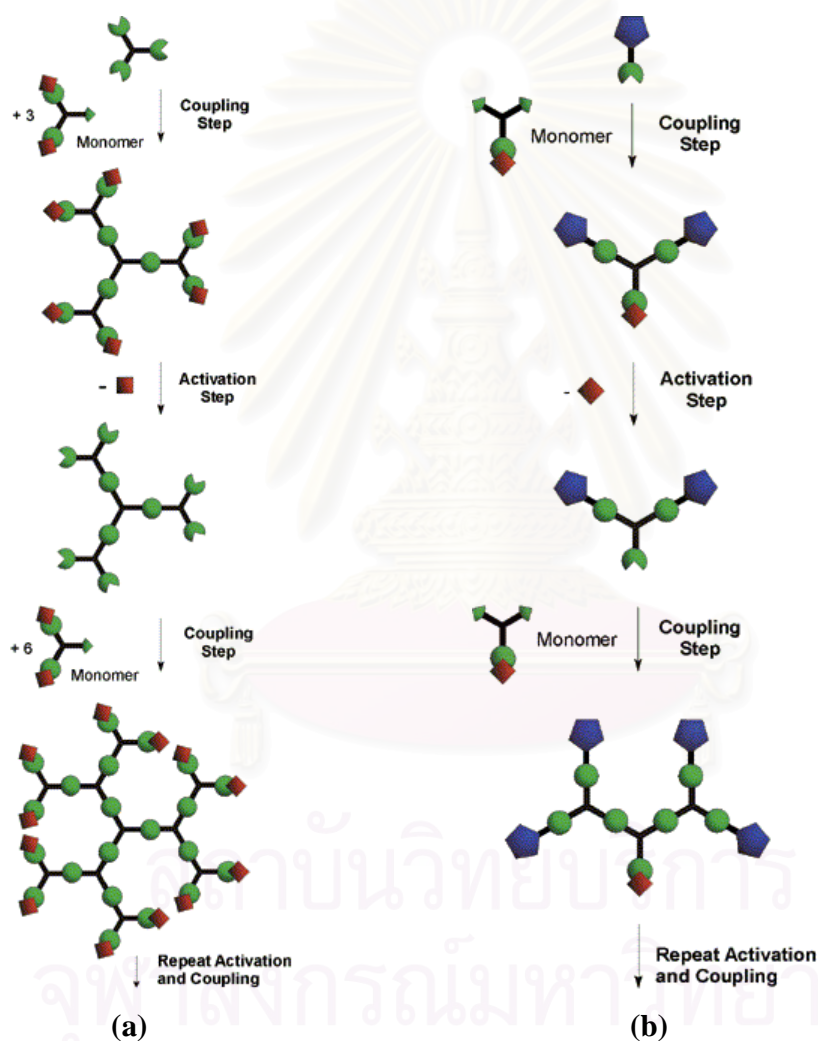


Figure 1.8 Dendrimers are generally synthesized by two complementary approaches (a) Divergent approach, and (b) Convergent approach [69].

1.2.8 Functional dendrimers and their applications

Since the Tomalia [57] and Newkome [59] reported on dendrimers, research on dendrimers has mainly focused on the preparation and characterization of fundamentally new dendrimer skeletons. Due to the wealth of already well-established dendrimers, the interest in this field of chemistry has gradually shifted to research in specific functions and particular applications for dendrimers. The high density of terminal functional groups in higher generation dendrimers offers a larger number of reactive sites for potential applications in the field of catalysis, light-harvesting systems, supramolecular chemistry, and medicinal chemistry. Since this dissertation involves dendrimers with potential applications in catalysis, light-harvesting, and supramolecular assembly, the next section provides a brief review in these three areas and related theories.

1.2.8.1 Transition metal catalysis using functional dendrimers

Transition metal catalysis based on functional dendrimers is one of the promising applications of dendrimers [70]. The ideal catalyst should be highly active and selective under mild conditions. It should be stable and can be separated from the product using a relatively simple process. Right from the start, the regular monodispersed structure and tree-like topology of dendrimers inspired chemists to design dendrimers with peripheral catalytic sites as soluble supported catalysts. Dendrimers have nanoscopic dimensions and can be molecularly dissolved. These features make dendrimers suitable to close the gap between homo- and heterogeneous catalysis. Since heterogeneous systems generally contain at least 10^{12} active sites per conglomerated particle, it is fair to say that the class of dendritic catalysts containing at most 1000 active sites is closer to the monomeric homogeneous systems. Therefore, functional dendrimers potentially can combine the advantages of both homogeneous and heterogeneous catalytic systems. Moreover, their globular architecture makes them more suitable for recycling than soluble polymer-supported catalysis. In principle, catalytically active transition metals can be attached to either the periphery or the core (Figure 1.9).

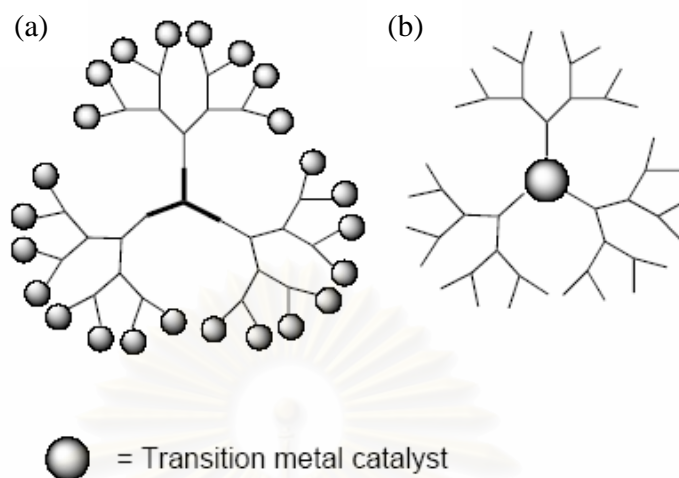


Figure 1.9 Catalytically active transition metal complexes can be attached to (a) the periphery or (b) the core [70].

a) Functional dendrimers with a catalytic core

By virtue of the dendritic architecture, transition metal cored-dendrimers can enclose large void spaces near the core. Thus, most of the metal core is available for catalysis. In addition, the placement of the catalytic active site at the core can result in beneficial interactions between the substrate and the catalyst because the dendritic layer exhibit container/scaffolding properties, helping to bring the reactants to the metal core. Placing the catalytic group at the core of the dendrimer allows spatial control of functionalities so that steric, photophysical, and electrochemical properties can be easily controlled.

Brunner first reported a functional dendrimer with a pyridine-containing Schiff-base as a Cu(I)-binding core [71]. The cyclopropanation of styrene with ethyl diazoacetate was investigated for which almost no asymmetric induction takes place. Many other dendrimers with a catalytic group at the core have also been synthesized and studied [72]. For example, Oosterom and coworkers [72b] synthesized a series of diphosphine ligands having phosphorus donor atoms in the core of a carbosilane dendrimer (Figure 1.10) and studied their use in a palladium-catalyzed allylic alkylation.

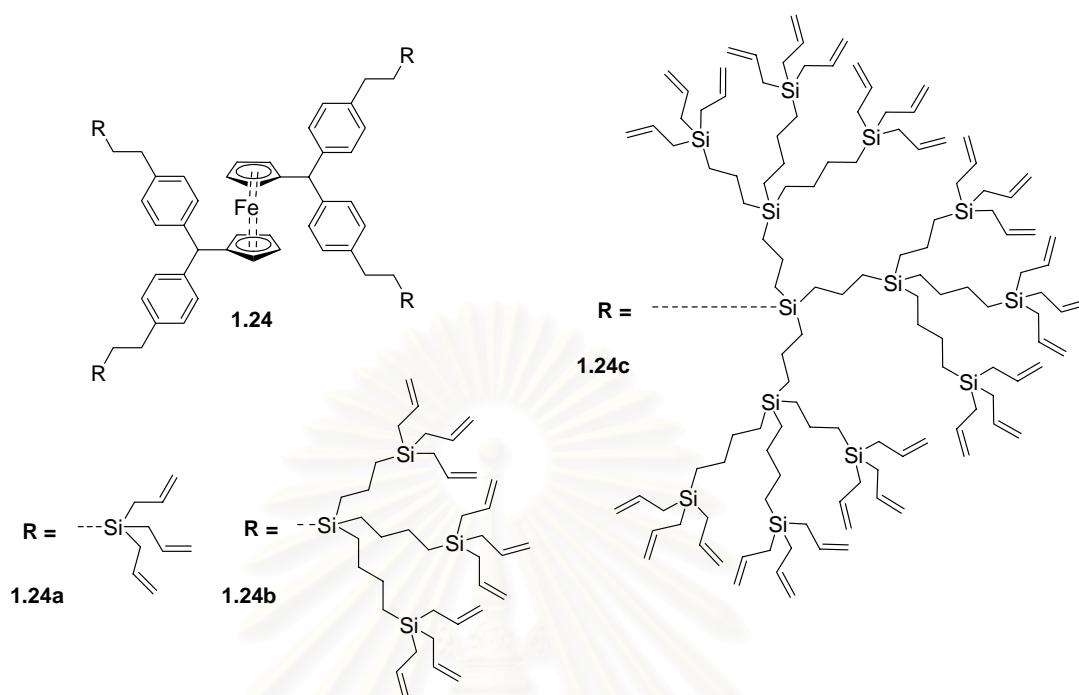


Figure 1.10 Carbosilane dendrimers synthesized by Oosterom and coworkers [72b].

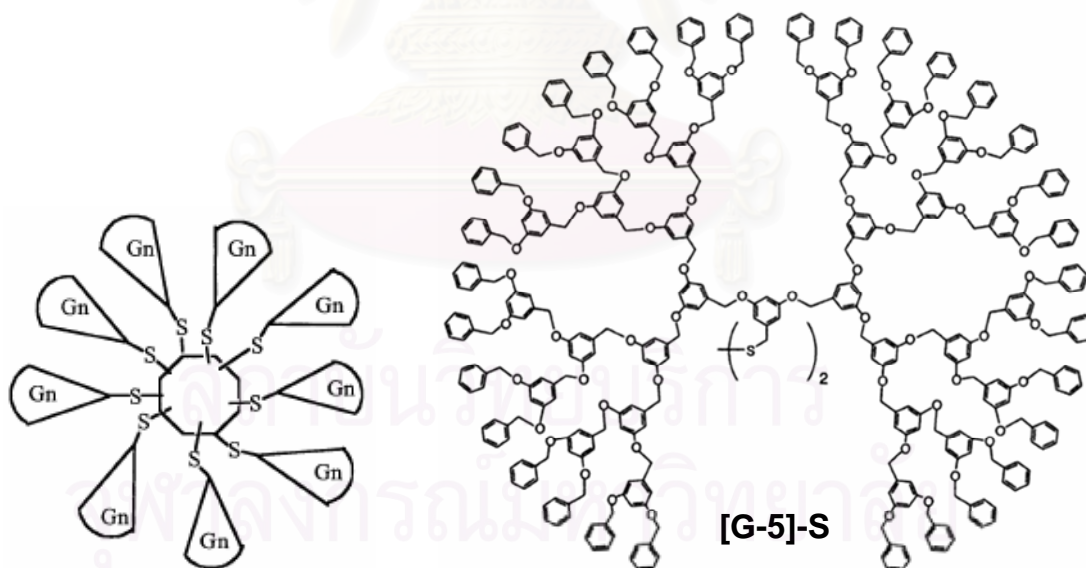


Figure 1.11 Nanoparticle-core dendrimers (NCDs) synthesized by Fox and coworkers.

Gold is popular for being chemically inert and appeared for long time an essentially useless material for catalysis. Ironically, the extremely facile Au^0 -catalyzed oxidation of CO to CO_2 is the most striking result in Au^0 -catalytic chemistry [73], but only when Au^0 exists as metal nanoparticles supported on suitable metal oxides. This potential catalytic application of gold nanoparticles inspired Fox and coworkers [74] to synthesize a series of nanoparticle-core dendrimers (NCDs, Figure 1.11). However, the catalytic activities of these NCDs have not been reported yet.

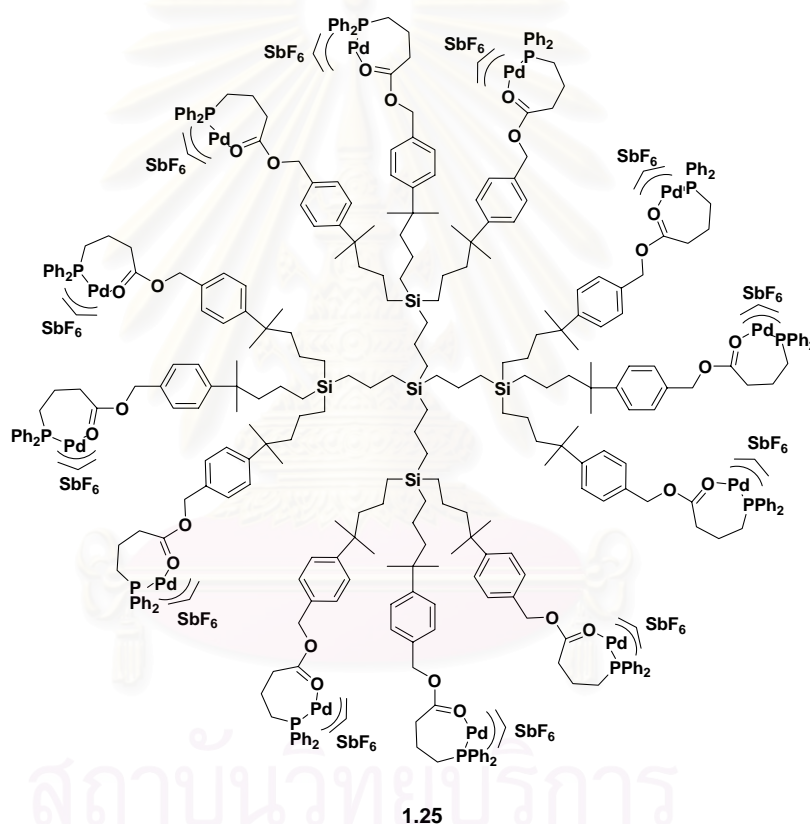


Figure 1.12 The carbosilane dendrimers **1.25** synthesized by Van Koten and coworkers.

b) Functional dendrimers with peripheral catalytic Sites

The periphery of dendrimers can be used to attach many catalytic sites on one molecule, possibly resulting in anomalous and favorable catalytic behavior. Ford and coworkers [75] reported the first dendrimer with 36 peripheral quaternary ammonium ions. This dendrimer accelerates both the decarboxylation of 6-nitrobenzoxazole-3-carboxylate and the hydrolysis of *p*-nitrophenyl diphenyl phosphate in water. Later on, more dendrimers with peripheral catalytic sites were synthesized and their catalytic activities were studied [76]. For example, Van Koten and Vogt and coworkers [77a] synthesized carbosilane dendrimers **1.25** (Figure 1.12). The palladium complexes of this system can efficiently catalyze hydrovinylation of styrene, an important reaction since it provides easy access to chiral building blocks for the synthesis of fine chemicals.

c) Transition metal nanocomposites in the dendrimer interior

Recently, a new concept of making catalytic metal nanoparticles was reported independently by the groups of Crooks [77] and Tomalia [78]. Hydroxyl-terminated poly(amido amine) dendrimers (PAMAM) are excellent templates for the preparation of precise metal nanoclusters within the dendrimer interiors. Precise construction of metal nanoparticles in the cavities of dendrimers leads to both metal cluster stability and full control over size and size distributions. The dendrimer branches can be used as selective gates to control access of substrates to the catalytically active encapsulated nanoparticles. In addition, the peripheral groups can be tailored to control solubility of the nanocomposite and used as linkage attaching to surfaces and other polymers.

Cu^{2+} ions have been extracted into the interior of PAMAM dendrimers with terminal hydroxyl groups and bound to the outermost tertiary amine groups. Chemical reduction leads to stable, soluble Cu^0 nanoclusters (Figure 1.13). Pd^0 and Pt^0 nanoparticles were synthesized similarly. Dendrimer-encapsulated Au, Ag, Pd and Pt nanoclusters were prepared by metal-displacement reactions with Cu. Such intradendrimer exchange reactions are fast and quantitative. Moreover, the resulting nanoparticles are stable and relatively monodispersed. The water-soluble nanocomposite

G4-OH(Pd₄₀) has a high catalytic activity for the hydrogenation of alkenes in water. Turnover frequencies are higher than that of water-soluble polymer-bound Rh^I catalysts and comparable to PVP-stabilized Pd dispersion in water (PVP: poly(vinyl pyrrolidone)). These dendrimer-encapsulated catalysts are sufficiently stable for recycling and reuse.

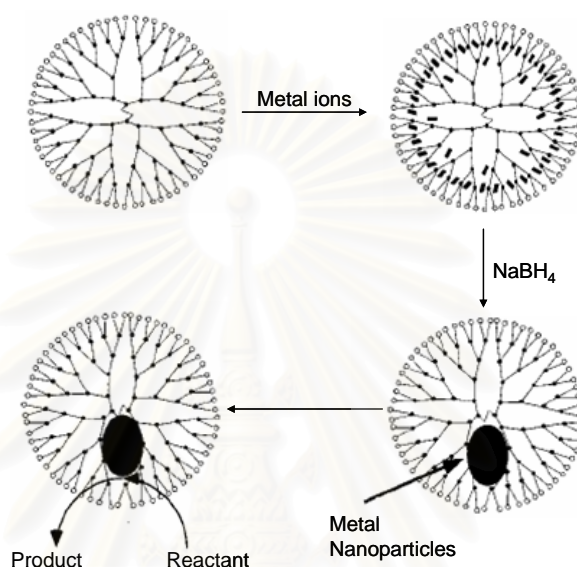


Figure 1.13 Synthesis of dendrimer-encapsulated metal nanoparticles and their application in catalysis.

1.2.8.2 Functional dendrimers for light-harvesting applications

Besides dendrimers with efficient energy-transfer properties, there has also been considerable effort to design dendrimers with favorable electron-transfer properties [79]. However, efforts to combine these two steps, energy transfer and charge transfer, to mimic both preliminary events of the photosynthesis, have been more limited [80]. Figure 1.14 shows the sequence of events [81].

A donor molecule first transfers its energy to the core acceptor, which then is able to oxidize the donor and form a charge separated state. In such a system, the donor plays two roles: energy harvester and electron donor. Dendrimers are also interesting scaffolds for photoinduced charge transfer from the core to the periphery. As one moves from the

core to the periphery of the dendrimers, the number of units at least doubles with each layer. Therefore, dendrimers could provide an entropic driving force for charge separation from the core to the periphery. Guldi and coworkers [82] reported conjugated phenylene vinylene-based dendrimers, in which an energy level dependent energy transfer and/or electron transfer was achieved. In conjugated dendrimers, the backbone serves as a vehicle for the through-bond communication both for electron and energy transfer.

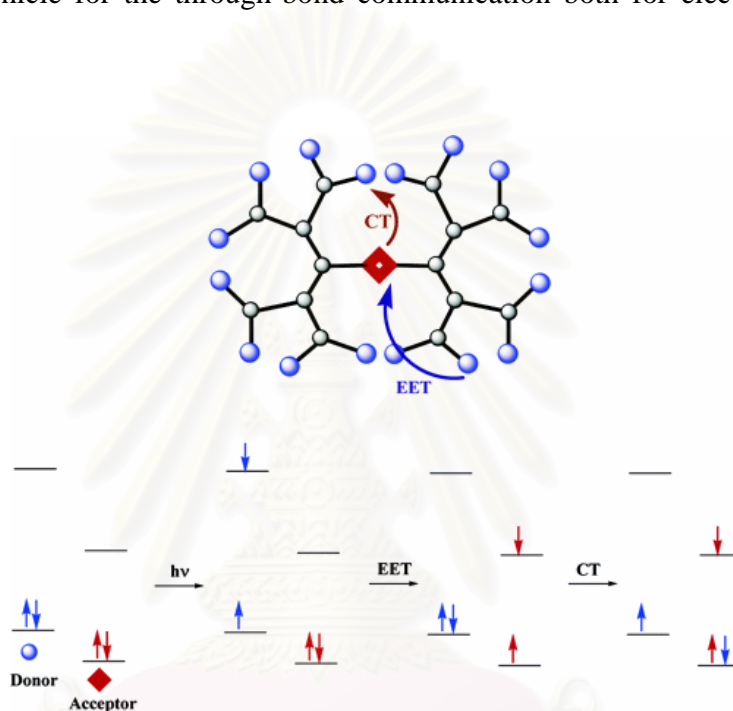


Figure 1.14 Cartoon of dendrimers for light harvesting.

1.2.8.3 Functional dendrimers in supramolecular chemistry

Due to their unique structural features, dendrimers offer new possibilities for molecular recognition and self-assembly, which are two important areas in supramolecular chemistry. Molecular recognition and self-assembly are based on supramolecular interactions such as hydrogen bonding, hydrophobic effect, metal-ligand coordination, π - π stacking, etc. For example, Percec and coworkers [83] reported the self-assembly of gallic acid dendrons. The driving force of self-assembly is the hydrophobic and fluorophobic effect. Depending on the form of the dendrons (wedge-

shape or cone-shape), cylindrical or spherical aggregates were formed. These supramolecular aggregates come together to form even larger structures. While the cylindrical supramolecular structures form hexagonal columnar phases, the spherical aggregates arrange to cubic superstructures (Figure 1.15).

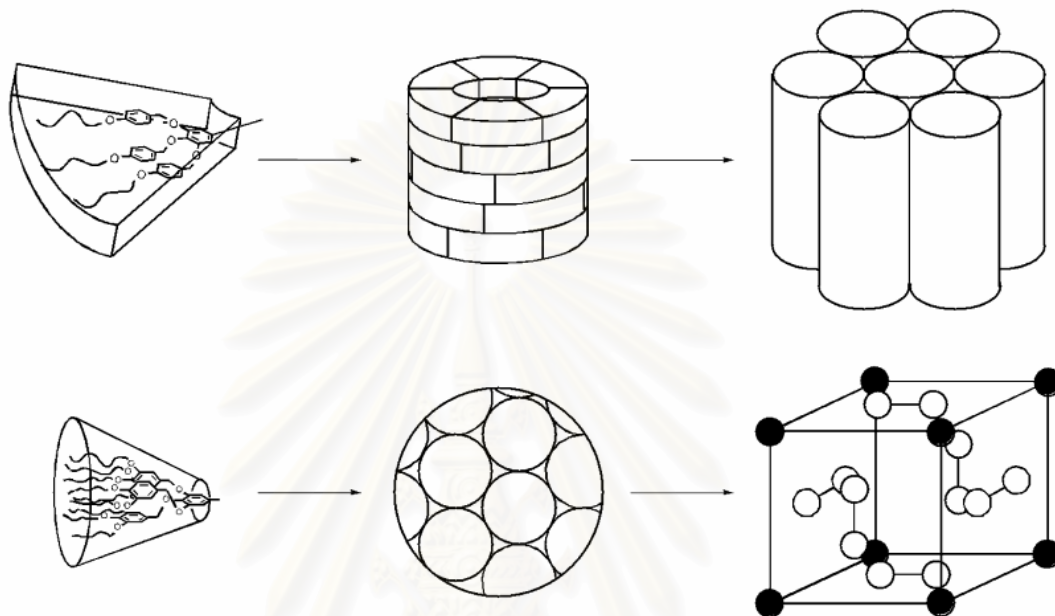


Figure 1.15 Gallic acid dendrons self-assembling to supramolecular dendrimers, which again organize themselves in thermotropic, liquid-crystalline phases.

1.3 Objectives and outline of this dissertation

The objectives of this dissertation are as follows:

- (1) To design ditopic sensor in the present of azacalix[3]arene component;
- (2) To explore the applications of azacalix[3]arene which connected to conjugated polymer networks (CPNs) to be a sensor for real system;
- (3) To expand thiophene and carbazole dendrimers chemistry by introducing functional groups on the periphery;
- (4) To study supramolecular assembly and their electropolymerization properties of carbazole dendrons with dendrimers.

The rest of this dissertation is organized into three chapters. Chapter 2 exposes the secret properties of azacalix[3]arene based on understanding their plate form (**L1**) and

chemistry of azacalix[3]arene after modification included cone (**L2**) and partial-cone (**L3**) conformations as well as their binding properties. To implement its application, the preparation and the metal ion sensing of polycarbazole-ultrathin film incorporating the hexahomotriazacalix[3]arene moiety as a neutral cation-binding receptor will be describe.

Chapter 3 composes of two parts. The first one demonstrates supramolecular complexes of PAMAM and electropolymerizable surfmer dendrons which were prepared resulting in nano-ring structures electrodeposited on conducting substrates. The second part describes the functionalization of poly(amidoamine) dendrimers with thiophene and carbazole dendrons, the preparation of dendrimer-encapsulated metal nanoparticles, and absorption behavior of the resulting nanocomposites.

Finally, Chapter 4 provides a general summary of all the different projects and the impact they will have on future studies.



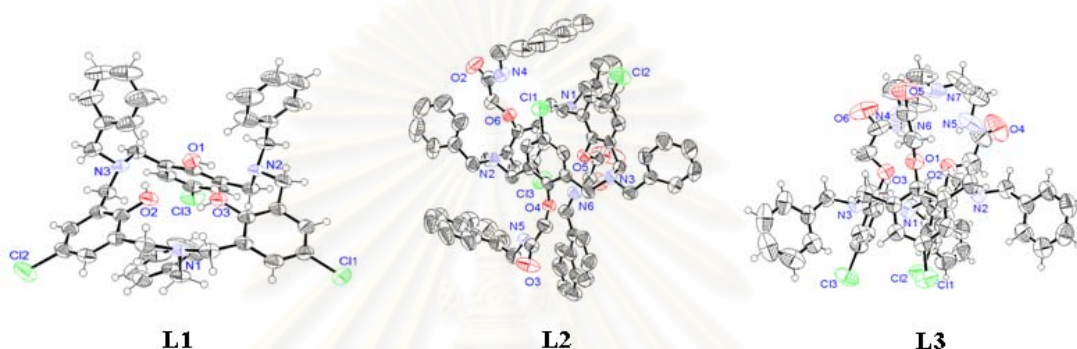
สถาบันวิทยบริการ
จุฬาลงกรณ์มหาวิทยาลัย

CHAPTER II

SYNTHESIS AND BINDING PROPERTIES OF DITOPIC RECEPTORS BASED ON HEXAHOMOTRIAZACALIX[3]ARENE

2.1 Ditopic receptors based on hexahomotriazacalix[3]arene

2.1.1 Introduction



Based on the concepts provided by host-guest chemistry, cations and anions sensing have recently risen to a dominant position in research devoted to the detection of designated species [84]. This rapid growth is derived from the realization of the diverse roles played by cations and anions in biological and chemical systems [85]. Current effort is paid for developing supramolecular systems that simultaneously bind both of a cation and an anion. Two strategies have been presented in literature: 1) the so-called ‘dual receptor strategy’ involving a binary mixture of a cation-receptor and an anion-receptor [86] and 2) the so-called ‘ditopic receptor strategy’ consisting of a single ditopic receptor with defined cation and anion binding sites [87]. Calixarenes and related macrocycles have received a lot of attention due to their molecular recognition properties [6,21]. The advantages of azacalix[3]arene compared to calixarene are more coordinating sites in which 3-D cavity is suitable for binding cations [16]. Moreover, the presence of soft nitrogen atoms in azacalixarenes is envisioned to bind soft cations such as transition metals according to the hard soft acid and base principle (HSAB) as well as other specific features such as building sophisticated receptors, metal ligand systems, etc. [15,16]. However, they have received relatively little attention, mainly because they can be synthesized only in rather low overall yields. There is no specific functionalization condition to obtain a

specific conformation. Moreover, there have only been limited studies of the solution conformations, solid-state structures, and complexation properties of this molecule.

2.1.2 Objectives of this research

According to the previous reports, the profound understanding on properties of azacalix[3]arene is insufficient, despite its wide application. Therefore, this receptor is ready for our lab to explore. Several research groups have focused on studying only the cation binding site of azacalix[3]arenes, especially in transition metal ions. The selectivity depends on their cavity sizes and hard-soft acid and base between cations and nitrogen donor atoms of these compounds. Normally, when azacalix[3]arene combined with cations the hydroxyl protons are not located on the oxygen atoms but are transferred to nitrogen atoms and form intramolecular zwitter-ionic structures [16]. On the other hand, they can bind with anions through hydrogen bond at the phenol groups. This is an interesting character of this molecular platform. With this in mind, we decide to study the complexation of **L1** with anions in order to expose other properties of azacalix[3]arene template and get an excellent anion receptor.

Previously, Hampton and coworkers [89] showed that the conformations of azacalix[3]arenes are cone and partial cone based on NMR and X-ray single crystal studies. Previous reports have focused on the functionalization and complexation of the cone conformation. On the other hand, partial cone conformation has rarely been studied which was changed both of selectivity and geometry in this template. To further understand the properties of azacalix[3]arene in partial cone conformation, we report a conformational selective synthesis, the X-ray crystal structures, and the binding properties of *N*-benzylhexahomotriaza-*p*-chlorocalix[3]-trinaphthylamide (**L2**) towards cations and anions. This is the first time to expose complexation ability of partial cone azacalix[3]arene.

The azacalix[3]arene is chosen to elaborate a novel anion receptor due to the fact that not only their chemistry has a high potential to be developed for anion receptors but their structural C_{3v} symmetry accompanied by a hydrophobic cavity wider than that of calix[4]arene is also able to accept large substrates. In addition, we report the synthesis, the conformational analysis, the X-ray crystal structure and binding properties of cone conformation (C_{3v} -symmetrical N_7 -hexahomotriazacalix[3]-cryptand or N_7 -azacalix[3]-cryptand (**L3**)) which combines

C_{3v} symmetrical '*N*-benzylhexahomotriaza-*p*-chlorocalix[3]arene' element and a 3-fold symmetric 'tren' residue [8]. This integration results in a system that can bind anions through a hydrogen bonding with amide groups. The inner rim of azacalix[3]arene was also used to complex with cation in order to tune the anion binding property of N_7 -azacalix[3]-cryptand (**L3**).

2.1.3 Experimental section

2.1.3.1 Synthesis of heteroditopic receptors based on azacalix[3]arene

a) General procedure

a1) Materials

Unless otherwise specified, the solvent and all materials were reagent grades purchased from Fluka, BHD, Aldrich, Carlo Erba, Merck or J.T. Baker and were used without further purification. Commercial grade solvents such as acetone, dichloromethane, hexane, methanol and ethylacetate were purified by distillation before used. Acetonitrile and dichloromethane for set up the reaction were dried over calcium hydride and freshly distilled under nitrogen atmosphere prior to use. Tetrahydrofuran was dried and distilled under nitrogen from sodium benzophenone ketyl immediately before use.

Column chromatography was carried out on silica gel (Kieselgel 60, 0.063-0.200 nm, Merck). Thin layer chromatography (TLC) was performed on silica gel plates (Kieselgel 60, F₂₅₄, 1 mm, Merck) and used to detect the compounds by the UV-light. All manipulations were carried out under nitrogen atmosphere. For titration experiments, dimethyl sulfoxide (DMSO) used as solvent was spectroscan grade (LAB-SCAN). Tetrabutylammonium hexafluorophosphate (TBAPF₆, purum, Fluka) was used as supporting electrolyte. Metal salts, used without further purification, were as following: LiClO₄, NaClO₄ and KClO₄, CoCl₂ (GR ACS grade, Merck), NiCl₂, and CuCl₂ (RPE grade, Carlo Erba), ZnCl₂ (purum, Fluka), CdCl₂, and HgCl₂ (GR ACS grade, Merck), PbCl₂ (purum, Riedel-de-Haën[®]) and Pb(NO₃)₂ (puriss, Riedel-de-Haën[®]). In quantitative determination of metal using the EDTA (ethylenediaminetetraacetic acid) titration, reagents were used as following: EDTA standard solution (Idranal[®] III 0.10 M, for metal titration, Riedel-de-Haën[®]), hexamethylenetetramine (Hexamine, analytical reagent grade, Riedel-de-Haën[®]), Murexide (for complexometry, Riedel-de-Haën[®]), and Xylenol orange (for metal

titration, Riedel-de-Haën®). Anion salts, used without further purification, were as following: TBAF, TBACl (GR ACS grade, Merck), TBABr, TBAI, TBANO₃, TBAHSO₄, TBAClO₄, TBACH₃COOH and TBAPhCOOH (purum, Fluka).

a2) Instrumentations

Nuclear magnetic resonance (NMR) spectra were recorded on a Varian 400 MHz spectrometer in deuterated solvents. Chemical shifts (δ) are reported in parts per million and the residual solvent peaks are used as internal standards.

Absorption spectra were measured by a Varian Cary 50 UV-vis spectrometer. UV-vis titration spectra were measured by a Perkin Elmer Lambda 25 spectrophotometer at 25 °C.

Fluorescence spectra were recorded by Perkin Elmer SL50B fluorescence spectrophotometer.

FT-IR spectra were obtained using a Nicolet Impact 410. KBr pellets were prepared by first mixing the sample solutions with KBr, removing solvents under vacuum and then pressing the KBr using a 10-ton hydraulic press.

MALDI-TOF mass spectra were recorded on a Biflex Bruker Mass spectrometer with 2-cyano-4-hydroxycinnamic acid (CCA) or 2,5-dihydroxy-benzoic acid (DHB) as matrix.

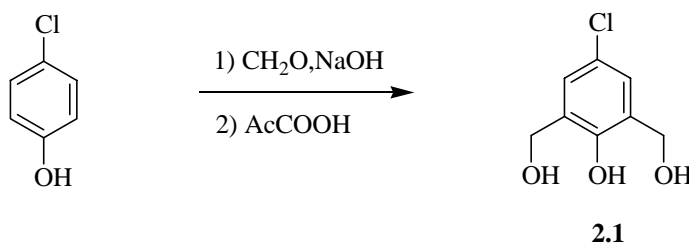
Elemental analysis was carried out on CHNS/O analyzer by Perkin Elmer PE2400 series II.

b) Synthesis

b1) Synthesis of *N*-chlorobenzylhexahomotriazacalix[3]-arene

(L1)

Synthesis of 4-chloro-2,6-bis(hydroxymethyl)phenol (2.1)



2.1 was synthesized according to the general procedure reported by Robinson and Hakimelahi [90].

Into a solution of *p*-chlorophenol (55.50 g), formaldehyde (95.40 mL) and sodium hydroxide (21.68 g) were added. The reaction mixture was stirred for 7 – 10 days at room temperature under nitrogen atmosphere. The sodium salts of **2.1** were isolated by removal of the solvent under reduced pressure. Acidification of the sodium salts with acetic acid in acetone, removal of sodium acetate by filtration and recrystallization from ethyl acetate resulted 4-chloro-2,6-bis(hydroxymethyl)phenol (**2.1**) with 72% yield.

Characterization data for 2.1

IR (neat)/cm⁻¹: 3412, 3300, 2967, 2914, 2888, 1478, 1456, 1211, 1068, 1010

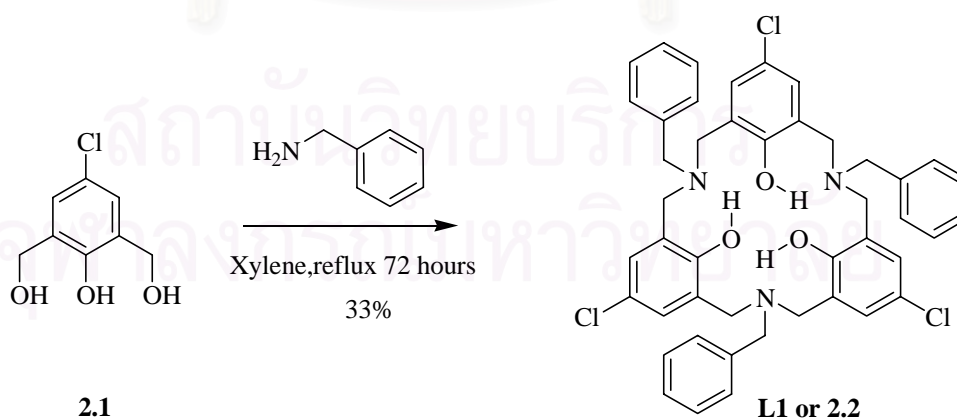
¹H-NMR (400 MHz, CD₃OD): δ (ppm) 7.14 (s, 2H, ArH), 4.72 (s, 4H, HOCH₂Ar)

MALDI-TOF : m/z Calcd for [C₈H₉ClO₃]⁺: m/z 188.02

Found: [C₈H₉ClO₃ + H]⁺: m/z 189.00

All spectroscopic data are consistent with those reported in the literatures [90].

p-chloro-N-benzylhexahomotriazacalix[3]arene (**2.2**)



This procedure was modified from the procedure reported by Thuéry and co-workers [23].

Into a solution of **2.1** (6.00 g, 32.52 mmol) in 100 mL of xylene, benzylamine (3.39 g, 31.67 mmol) dissolved in 50 mL of xylene was added dropwise. The reaction mixture was refluxed for 72 hours and the water generated was removed during the course of the reaction with a Dean-Stark condenser. The mixture was evaporated to dryness affording deep yellow oil. The residue was dissolved in dichloromethane (100 mL) and washed with saturated NaHCO₃ (2 × 50 mL). The organic layer was dried over anhydrous sodium sulfate and purified by column chromatography (hexane : EtOAc = 9 : 1, v/v) providing **2.2** as a white solid (2.73 g, 3.50 mmol) in 33 % yields.

Characterization data for L2 or 2.2

IR (neat)/cm⁻¹: 3412, 3300, 2967, 2914, 2888, 1478, 1456, 1211, 1068, 1010

¹H-NMR (400 MHz, CDCl₃): δ (ppm) 11.2 (br s, 3H, ArOH), δ 7.29 (br s, 15H, ArH), 7.01 (s, 6H, ArH) 3.69 (s, 6H, NCH₂Ar), 3.64 (s, 12H, NCH₂Ar)

¹³C-NMR (100 MHz, CDCl₃): δ (ppm) 155.5, 136.4, 129.6, 129.4, 128.1, 127.3, 125.0, 122.7, 58.0, 56.7

MALDI-TOF: m/z Calcd for [C₄₅H₄₂Cl₃N₃O₃]⁺: m/z 777.23

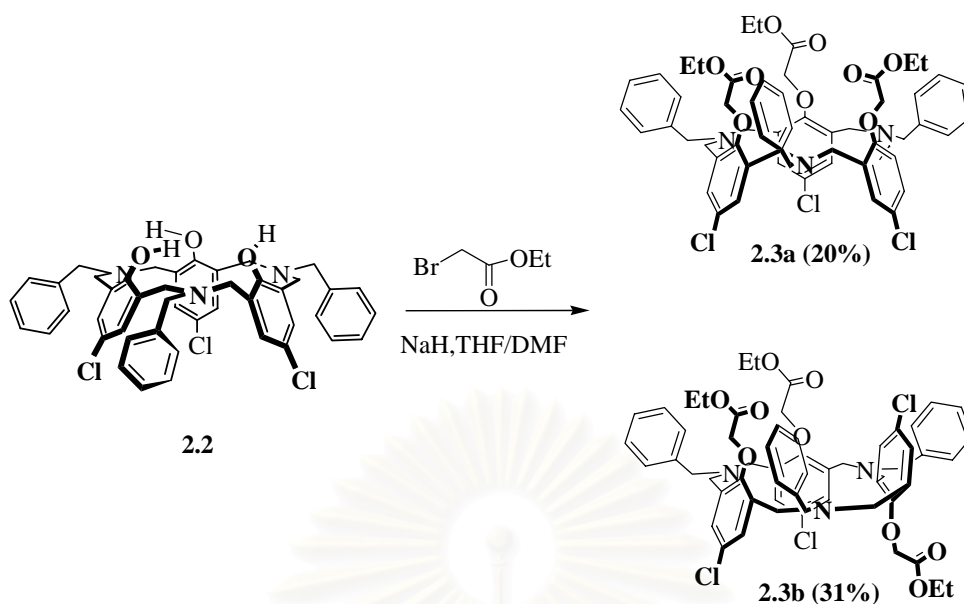
Found: [C₄₅H₄₂Cl₃N₃O₃ + H]⁺: m/z 778.69

Elemental analysis: Anal Calcd. for C₄₅H₄₂Cl₃N₃O₃: C, 69.36; H, 5.43; N, 5.39

Found. C, 69.44; H, 5.49; N, 5.28

b2) Synthesis of N-benzylhexahomotriaza-p-chlorocalix-[3]-trinaphthylamide (L2)

N-benzylhexahomotriaza-p-chlorocalix[3]-tri(ethylacetate (2.3)



Into a solution of *N*-benzylhexahomotriaza-*p*-chlorocalix[3]arene **2.2** (0.67 g, 0.85 mmol) and NaH (0.14 g, 2.99 mmol) in THF (30 mL) and DMF (10 mL) was added with a solution of ethylbromoacetate (0.499 g, 2.99 mmol) in THF (10 mL). After stirring for 2 days at 80 °C, the reaction mixture was evaporated, extracted with CH₂Cl₂ (2 × 30 mL), and washed with NaHCO₃ (2 × 30 mL). The organic layer was dried over anhydrous Na₂SO₄, filtered, and evaporated to dryness by a rotary evaporator. Column chromatography on silica gel (hexane/EtOAc = 9:1, v/v) afforded **2.3a** (0.135 g, 0.130 mmol) in 21 % yield as a deep yellow oil and **2.3b** in 31 % yield as pale yellow solid.

Characterization data for **2.3a**

IR (neat)/cm⁻¹: 3063, 3028, 2981, 2929, 2803, 1757, 1448, 1372, 1292, 1188, 1118, 1065, 1030, 879, 743, 701

¹H-NMR (400 MHz, CDCl₃): δ (ppm) 7.34-7.26 (m, 12H, ArH), 7.18 (t, 3H, *J*_{H-H}=7.2 Hz, ArH), 6.90 (s, 6H, ArH), 4.28 (s, 6H, OCH₂CO), 4.22 (q, 6H, *J*_{H-H}=7.6 Hz, OCH₂CH₃), 3.61 (s, 6H, NCH₂Ar), 3.44 (dd, 12H, *J*_{H-H}=14.4, 7.6 Hz, NCH₂Ar), 1.28 (t, 9H, *J*_{H-H}=7.2 Hz, OCH₂CH₃)

¹³C-NMR (100 MHz, CDCl₃): δ (ppm) 169.1, 152.3, 139.2, 133.9, 130.1, 129.0, 128.9, 128.9, 128.6, 127.3, 71.0, 62.4, 52.5, 52.1, 14.4

MALDI-TOF: m/z Calcd for [C₅₇H₆₀Cl₃N₃O₉]⁺: m/z 1035.34

Found: [C₅₇H₆₀Cl₃N₃O₉ + H]⁺: m/z 1036.92

Elemental analysis: *Anal Calcd.* for $C_{57}H_{60}Cl_3N_3O_9$: C, 65.99; H, 5.83; N, 4.05

Found. C, 65.95; H, 5.71; N, 4.00

Characterization data for 2.3b

IR (neat)/ cm^{-1} : ν 3063, 3028, 2981, 2922, 2852, 2804, 1756, 1446, 1376, 1291, 1187, 1121, 1063, 1030, 891, 743, 700

1H -NMR (400 MHz, $CDCl_3$): δ (ppm) 7.57 (d, $J = 7.6$ Hz, 2H, ArH), 7.31 (t, $J = 7.6$ Hz, 3H, ArH), 7.38-7.30 (m, 10H, ArH), 7.02 (s, 4H, ArH), 6.98 (s, 2H, ArH), 4.31 (br d, 2H, OCH_2CO), 4.15 (s, 4H, OCH_2CH_3), 4.13 (s, 2H, OCH_2CH_3), 4.11 (br d, 2H, OCH_2CO), 3.79-3.22 (m, 20H, OCH_2CO and NCH_2Ar), 1.24 (m, 9H, OCH_2CH_3)

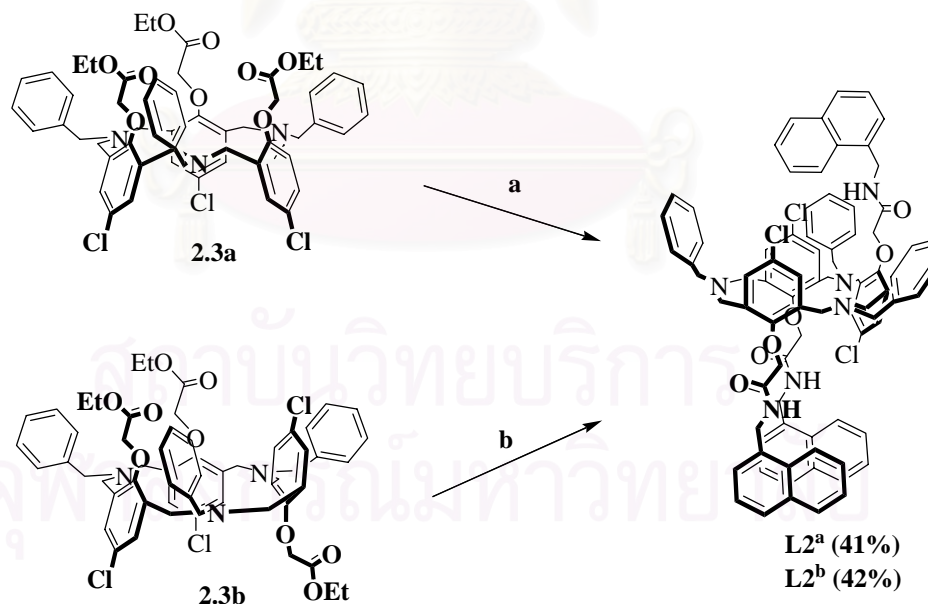
MALDI-TOF: m/z Calcd for $[C_{57}H_{60}Cl_3N_3O_9]^+$: m/z 1035.34

Found: $[C_{57}H_{60}Cl_3N_3O_9 + H]^+$: m/z 1036.92

Elemental analysis: *Anal Calcd.* for $C_{57}H_{60}Cl_3N_3O_9$: C, 65.99; H, 5.83; N, 4.05

Found. C, 65.82; H, 5.92; N, 3.93

N-benzylhexahomotriaza-p-chlorocalix[3]-trinaphthylamide (L2)



Condition a: into a solution of **2.3a** (0.14 g, 0.13 mmol) was charged with a solution of 1-naphthylmethanamine (0.07 g, 0.46 mmol) in 1:1 methanol : toluene mixture (10 mL). The solution was reflux for 3 days. After removing the solvents, the crude mixture was purified with column chromatography of the precipitate on silica

gel (hexane/EtOAc = 3:2, v/v) gave **L2^a** (0.07 g, 0.05 mmol, 41 % yield) as a white solid.

Condition b: into a solution of **2.3b** (0.21 g, 0.20 mmol) was charged with a solution of 1-naphthylmethylamine (0.21 g, 0.70 mmol) in 1:1 methanol : toluene mixture (10 mL). The solution was reflux for 7 days. After removing the solvents, the crude mixture was purified with column chromatography of the precipitate on silica gel (hexane/EtOAc = 3:2, v/v) gave **L2^b** (0.11 g, 0.09 mmol, 42 % yield) as a white solid.

Characterization data for L2

IR (neat)/cm⁻¹: ν 3419, 3059, 2921, 2837, 2810, 1679, 1594, 1524, 1436, 1364, 1251, 1193, 1124, 1041, 884, 797, 789, 745, 701

¹H-NMR (400 MHz, CDCl₃): δ (ppm) 8.10-8.08 (m, 3H, ArH_{nap}), 8.01-7.97 (m, 4H, ArH_{nap}), 7.91 (d, J_{H-H} = 7.2 Hz, 2H, ArH_{nap}), 7.64-7.57 (m, 8H, ArH_{nap}), 7.64-7.57 (m, 4H, ArH_{nap}), 7.32-7.21 (m, 9H, ArH_{calix}), 7.14 (d, J_{H-H} = 6.8 Hz, 2H, ArH_{calix}), 7.09 (d, J_{H-H} = 7.6 Hz, 4H, ArH_{calix}), 7.02 (s, 1H, CH₂NHCO), 6.86 (s, 2H, CH₂NHCO), 6.51 (s, 2H, ArH_{calix}), 6.44 (s, 2H, ArH_{calix}), 6.36 (s, 2H, ArH_{calix}), 5.11 (d, J_{H-H} = 4.8 Hz, 2H, ArCH₂NH), 5.04 (d, J_{H-H} = 5.6 Hz, 1H, ArCH₂NH), 5.00 (d, J_{H-H} = 4.8 Hz, 1H, ArCH₂NH), 4.93 (d, J_{H-H} = 4.8 Hz, 1H, ArCH₂NH), 4.89 (d, J_{H-H} = 5.2 Hz, 1H, ArCH₂NH), 3.91 (d, J_{H-H} = 15.2 Hz, 2H, ArCH₂N), 3.80 (s, 2H, OCH₂CO), 3.58 (d, J_{H-H} = 14.8 Hz, 2H, ArCH₂N), 3.09 (s, 2H, OCH₂CO), 2.99-2.71 (m, 12H, ArCH₂N and OCH₂CO), 2.57 (d, J_{H-H} = 12.8 Hz, 2H, ArCH₂N), 2.28 (d, J_{H-H} = 14.0 Hz, 2H, ArCH₂N)

MALDI-TOF: m/z Calcd for [C₈₄H₇₅Cl₃N₆O₆]⁺: m/z 1368.48

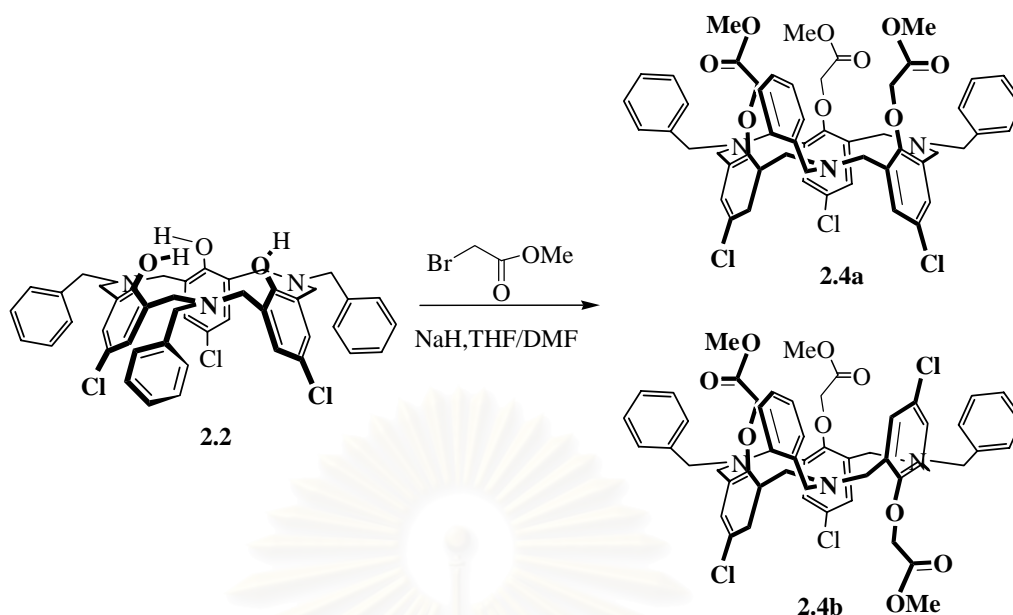
Found: [C₈₄H₇₅Cl₃N₆O₆ + H]⁺: m/z 1369.67

Elemental analysis: *Anal Calcd.* for C₈₄H₇₅Cl₃N₆O₆: C, 73.59; H, 5.51; N, 6.31

Found. C, 73.56; H, 5.53; N, 6.14

b3) Synthesis of *N*₇-hexahomotriaza-*p*-chlorocalix-[3]cryptand (L3**)**

N-benzylhexahomotriaza-*p*-chloro-calix[3]-tri(methyl acetate) (**2.4**)



Into a solution of *N*-benzylhexahomotriaza-*p*-chlorocalix[3]arene **2.2** (1.17 g, 1.50 mmol) and NaH (0.25 g, 10.50 mmol) in THF (40 mL) and DMF (30 mL) was added with a solution of methyl bromoacetate (0.90 g, 5.85 mmol) in THF (10 mL). After stirring for 2 days at 80 °C, the reaction mixture was evaporated, extracted with CH₂Cl₂ (2 × 30 mL), and washed with saturated NaHCO₃ (2 × 30 mL). The organic layer was dried over anhydrous Na₂SO₄, filtered, and evaporated to dryness under vacuum. Column chromatography on silica gel (hexane/EtOAc = 3:2, v/v) afforded **2.4a** (0.24 g, 0.24 mmol) in 16 % yield as a deep yellow oil and **2.4b** (pale yellow solid, 33 % yield).

Characterization data for **2.4a**

IR (neat)/cm⁻¹: 3427, 2949, 2918, 2844, 2357, 1762, 1435, 1365, 1182, 1123, 1057, 878, 750, 691

¹H-NMR (400 MHz, CDCl₃): δ (ppm) 7.46-7.38 (m, 9H, ArH), 7.32-7.29 (m, 6H, ArH), 7.01 (s, 6H, ArH), 4.42 (s, 6H, OCH₂CO), 3.90 (s, 9H, OCH₃), 3.72 (s, 6H, NCH₂Ar), 3.54 (br s, 12H, NCH₂Ar)

¹³C-NMR (100 MHz, CDCl₃): δ (ppm) 169.1, 152.3, 139.2, 133.9, 130.1, 129.0, 128.9, 128.9, 128.6, 127.3, 71.0, 62.4, 52.5, 52.1

MALDI-TOF: m/z Calcd. for [C₅₄H₅₄Cl₃N₃O₉]⁺: m/z 993.29

Found: [C₅₄H₅₄Cl₃N₃O₉ + H]⁺: m/z 994.69

Elemental analysis: *Anal Calcd.* for $C_{54}H_{54}Cl_3N_3O_9$: C, 65.61; H, 5.47; N, 4.22

Found. C, 65.12; H, 6.17; N, 4.08

Characterization data for 2.4b

IR (neat)/ cm^{-1} : 3427, 2949, 2918, 2844, 2357, 1762, 1435, 1365, 1182, 1123, 1057, 878, 750, 691

1H -NMR (400 MHz, $CDCl_3$): δ (ppm) 7.55 (d, $J = 7.6$ Hz, 2H, ArH), 7.45 (t, $J = 7.6$ Hz, 2H, ArH), 7.38-7.30 (m, 11H, ArH), 7.16 (s, 2H, ArH), 7.14 (s, 2H, ArH), 7.09 (s, 2H, ArH), 4.32 (s, 4H, OCH_2CO), 3.93-3.68 (m, 19H, OCH_2CO , NCH_2Ar and OCH_3), 3.72 (s, 6H, NCH_2Ar), 3.59 (s, 2H, NCH_2Ar), 3.56 (s, 2H, NCH_2Ar), 3.46-3.35 (m, 6H, NCH_2Ar)

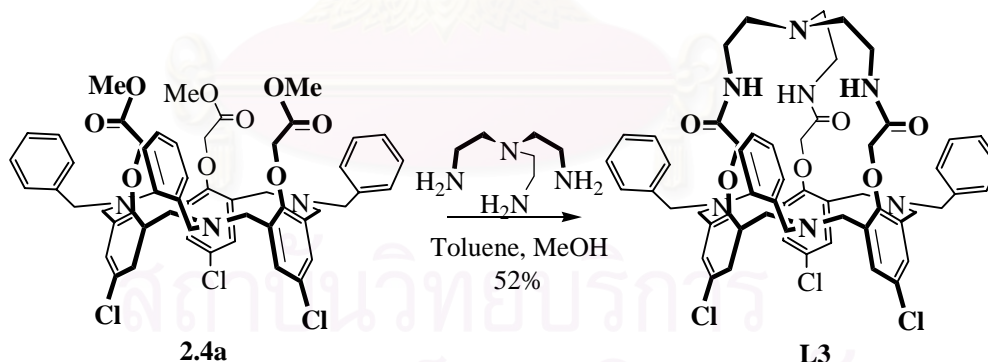
MALDI-TOF: m/z Calcd for $[C_{54}H_{54}Cl_3N_3O_9]^+$: m/z 993.29

Found: $[C_{54}H_{54}Cl_3N_3O_9 + H]^+$: m/z 994.69

Elemental analysis: *Anal Calcd.* for $C_{54}H_{54}Cl_3N_3O_9$: C, 65.61; H, 5.47; N, 4.22

Found. C, 65.12; H, 6.17; N, 4.08

N_7 -hexahomotriaza-*p*-chlorocalix[3]-cryptand (L3)



Into a solution of **2.4a** (0.49 g, 0.47 mmol) was mixed with a solution of tris(2-aminoethyl)amine (0.07 g, 0.47 mmol) in 1:1 methanol : toluene mixture (10 mL). The solution was reflux for 38 hours and, then, a second crop of tris(2-aminoethyl)amine (0.03 g, 0.24 mmol) was added. The mixture was refluxed for additional 72 hours. After removing off the solvents, the crude product was

precipitated with methanol. Column chromatography of the precipitate on silica gel (acetone/CH₂Cl₂ = 3 : 7, v/v) gave **L3** (0.26 g, 0.24 mmol, 52 % yield) as a white solid.

Characterization data for L3

IR (neat)/cm⁻¹: 3443, 3388, 2925, 2844, 2361, 1668, 1513, 1439, 1353, 1182, 1120, 1038, 849, 867, 746, 695

¹H-NMR (400 MHz, CDCl₃): δ (ppm) 7.33-7.30 (m, 9H, ArH), 7.27-7.20 (m, 6H, ArH), 6.94 (s, 6H, ArH), 4.01 (s, 6H, OCH₂CO), 3.54 (s, 6H, ArCH₂N), 3.38 (br s, 6H, NCH₂CH₂NH), 3.30 (s, 12H, NCH₂Ar), 2.70 (br s, 6H, NCH₂CH₂NH)

¹³C-NMR (100 MHz, CDCl₃): δ (ppm) 167.8, 151.2, 138.2, 133.3, 131.2, 129.4, 129.0, 128.7, 127.7, 73.0, 62.0, 56.0, 52.1, 38.0

MALDI-TOF: m/z Calcd for [C₅₇H₆₀Cl₃N₇O₆]⁺: m/z 1043.37

Found: [C₅₇H₆₀Cl₃N₇O₆ + H]⁺: m/z 1044.11

Elemental analysis: *Anal Calcd.* for C₅₇H₆₀Cl₃N₇O₆: C, 65.48; H, 5.78; N, 9.38

Found. C, 65.13; H, 5.91; N, 9.36

2.1.3.2 Complexation studies

a) Complexation studies of ligand L1, L2 and L3 by using the ¹H-NMR spectroscopy

Typically, an excess (10 equivalents and 4 equivalents) of tetrabutylammonium salts were added into NMR tubes. A solution of 10 mM of **L1**, **L2** and **L3** (0.055 mmol) in CDCl₃ 5 mL was prepared and 0.5 mL of this solution was added in each NMR tube. The ¹H-NMR spectra were recorded after addition of anions and checked every 24 hours until the complexation reached to the equilibrium.

b) Complexation studies by using the UV-vis spectroscopy

b1) Complexation studies of L2 and L3 with metal ions by using the UV-vis titration

Stock solutions of ligand kept concentration approximately 1 mM have been prepared by measuring amounts of each ligand on the Mettler Toledo model AT 201 balances and dissolving in DMSO with ionic strength kept constant at 10 mM using TBAPF₆. The stock solutions were diluted with the same solvent system until

obtained concentration was approximately 0.1 mM, named ligand solutions. In the case of stock solutions of metal, actually concentration of metal stock solutions could be determined by the EDTA titration [91] before these solutions would be diluted with DMSO/TBAPF₆ system in which metal solutions were controlled concentration by an optimal condition of each complexation studied.

2 mL of ligand solution was placed in spectrophotometric cell of 1-cm path length and its absorbance was recorded extending from 200 to 400 nm. A metal solution had been then added directly and successively into the cell by a microburette and was stirred for 40 seconds after each addition of metal solutions. Spectral variations were recorded after each addition. The stability constants were refined from spectrometric data using the program Sirko [92].

b2) Complexation studies of L1, L2 and L3 with anions by using the UV-vis titration

Stock solutions with 10 mM constant ionic strength using TBAPF₆ were prepared as described for metal ion complexation study. The UV-vis titrations were carried out in the same manner as mentioned in titration with metal ions. The stability constants were also refined from spectrometric data using the program Sirko.

c) Complexation studies by using the fluorescent spectroscopy

c1) Complexation studies between L2 with cations by using the fluorescent spectroscopy

Typically, a solution of 0.001 mM of a ligand **L2** in a 0.01 M TBAPF₆ in dried DMSO were prepared by adding 0.01 mL of a stock solution of ligand **L2** (0.1 mM) in a 10 mL volumetric flask. Stock solutions of 30 mM of cations in dried DMSO were prepared in a 10 mL volumetric flasks.

Fluorescent spectra of **L2** and cation complexes were recorded from 290-600 nm at ambient temperature. The solutions of excess (300 equivalents) cations were added directly to 2.00 mL of 0.001 mM ligand **L2** in a 1-cm quartz cuvette, stirred and recorded after addition and every 24 hours until the complexation reached the equilibrium.

c2) Complexation studies between L1 and L2 with anions by using the fluorescent spectroscopy

Table 2.1 Concentration of anions ($X^- = F^-$, $H_2PO_4^-$, CH_3COO^- and $PhCOO^-$) used in anion complexation studies with ligand **L1** and the final ratios of guest : host.

Point	X ⁻ /L1	[L1], μM	[X ⁻], μM	V of X ⁻ (mL)	V total (mL)
1	0	0.100	0.000	0.00	2.00
2	0.2	0.099	0.020	0.02	2.02
3	0.4	0.098	0.039	0.04	2.04
4	0.6	0.097	0.058	0.06	2.06
5	0.8	0.097	0.077	0.08	2.08
6	1.0	0.096	0.096	0.10	2.10
7	1.4	0.094	0.131	0.14	2.14
8	1.8	0.092	0.166	0.18	2.18
9	2.2	0.090	0.199	0.22	2.22
10	2.6	0.089	0.231	0.26	2.26
11	3.0	0.087	0.262	0.30	2.30
12	3.8	0.084	0.320	0.38	2.38
13	4.6	0.082	0.375	0.46	2.46
14	5.4	0.079	0.427	0.54	2.54
15	6.2	0.077	0.475	0.62	2.62
16	7.0	0.074	0.520	0.70	2.70
17	8.0	0.072	0.573	0.80	2.80
18	9.0	0.069	0.623	0.90	2.90
19	10.0	0.067	0.669	1.00	3.00
20	11.0	0.065	0.712	1.10	3.10
21	12.0	0.063	0.753	1.20	3.20
22	13.0	0.061	0.791	1.30	3.30
23	14.0	0.059	0.826	1.40	3.40
24	15.0	0.057	0.860	1.50	3.50

Typically, a solution of 0.001 mM of a **L2** in a 10 mM TBAPF₆ in dried DMSO were prepared by adding 0.01 mL of a stock solution of them (0.1 mM) in a 10 mL volumetric flask and a solution of **L1** (0.1 mM) in 10 mM TBAPF₆ in dried DMSO 50 mL. A stock solution of 30 mM of anions in dried DMSO was prepared in a 10 mL volumetric flask.

Fluorescent spectra of **L1**, **L2** and their anion complexes were recorded at ambient temperature from 400-700 and 290-600 nm, respectively. The solution of an excess (300 equivalents) anions were added directly to 2.00 mL of 0.001 mM ligand **L2** and 2.00 mL of 0.05 mM ligand **L1** in a 1-cm quartz cuvette, stirred and recorded after addition and every 24 hours until the complexation reached to the equilibrium. For the fluorescent titrations of **L1**, the solution of anions were added to 2.00 mL of 0.05 mM ligand **L1** in a 1-cm quartz cuvette by microburette and stirred for 40 seconds. Fluorescent spectra were measured after each addition. Table 2.1 shows the concentration of anion which used in anions complexation and ratio of anions : host.

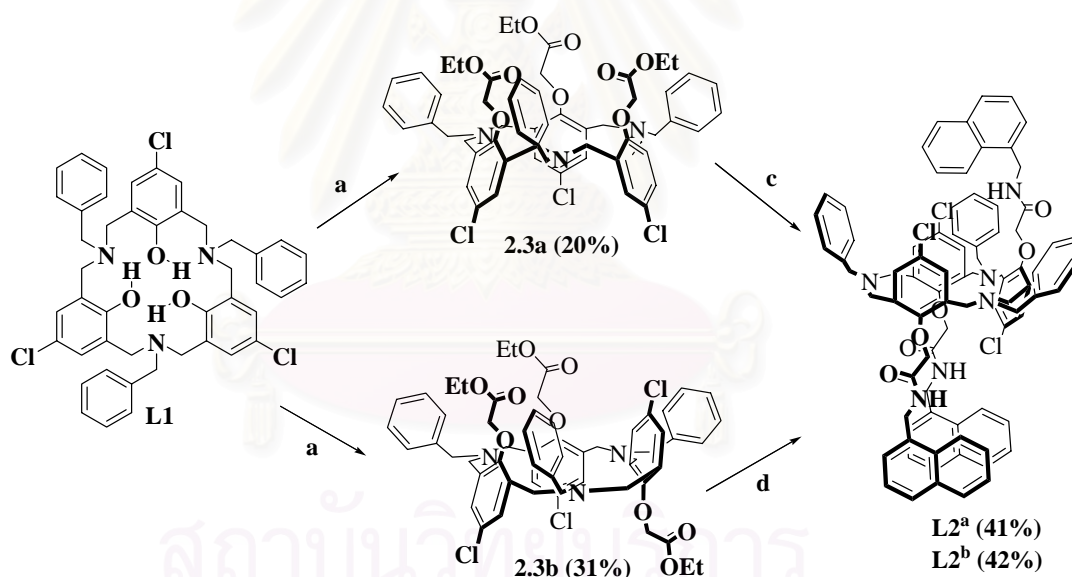
2.1.4 Results and discussion

2.1.4.1 Synthesis and characterization of sensor **L1**, **L2** and **L3**

The synthesis of desired compound **L2** was carried out as shown in Scheme 2.1. Alkylation of *N*-benzylhexahomotriaza-*p*-chlorocalix[3]arene with ethylbromoacetate in the presence of NaH in THF/DMF to produce compounds **2.3a** (*cone conformation*) in 20% yield, in which its structure was confirmed by X-ray single crystal spectroscopy as shown in Figure 2.1a, and **2.3b** (*partial cone conformation*) in 20% yield. The reactions between **2.3a** and **2.3b** with 1-aminomethylnaphthalene afforded only the partial cone conformer of the *N*-benzylhexahomotriaza-*p*-chlorocalix[3]-trinaphylamide (**L2**) in 41% and 42% yields started of **2.3a** or **2.3b**, respectively.

The partial cone conformation of **L2** was confirmed by ¹H, ¹³C, 2D-NMR and X-ray single crystal spectroscopies [94]. In the ¹H-NMR spectrum of **L2**, the methylene protons of the Ar_{calix}CH₂N bridges present as two AB doublets at δ 3.91 (*J*_{H-H} = 15.2 Hz), 3.58 (*J*_{H-H} = 14.8 Hz), 2.57 (*J*_{H-H} = 12.8 Hz), 2.28 (*J*_{H-H} = 14.0 Hz) and a signal in a multiplet at 2.99-2.71 ppm. The other doublets for the methylene protons of Ar_{nap}CH₂NH appear at 5.11, 5.04, 5.00, 4.93 and 4.89 ppm with coupling

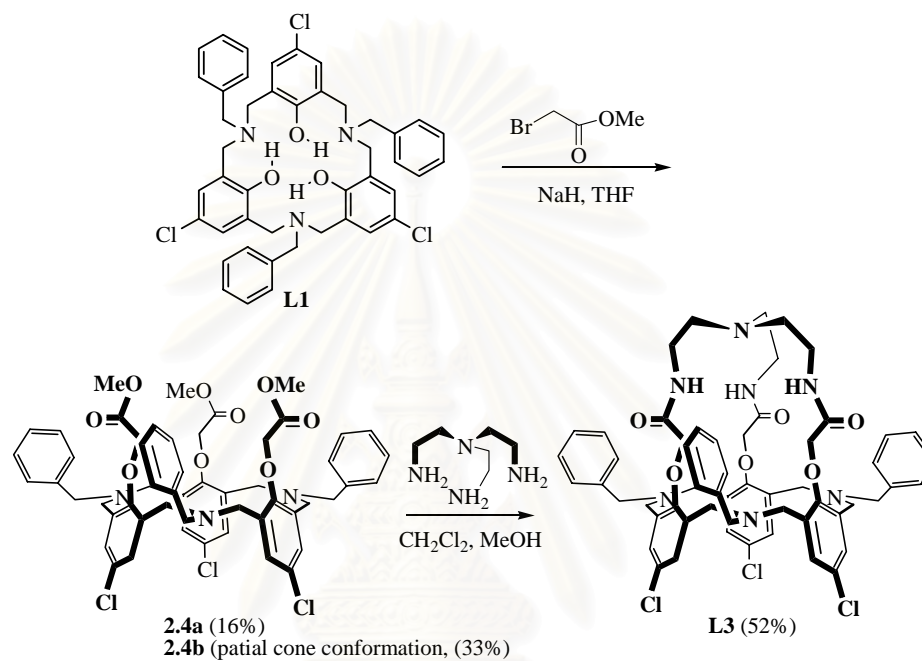
constants of 4.8, 5.6, 4.8, 4.8 and 5.2 Hz, respectively. In the parent hexahomotriazacalix[3]arene [95], which adopts a regular C_{3v} cone conformation, the signal of 6 protons of $Ar_{calix}H$ exists as a singlet at δ 7.01 ppm. However, in **L2**, the three singlets of $Ar_{calix}H$ were observed at 6.51, 6.43 and 6.36 ppm. The ^{13}C -NMR spectrum also confirms the partial cone conformation of azacalix[3]arene macroring of **L2**. $Ar_{nap}CH_2NH$ appeared as two peaks at 41.6, 41.2 ppm and the carbons of methylene bridges ($Ar_{calix}CH_2N$) splitted to four peaks at 72.8, 52.7, 52.5 and 52.0 ppm. The aromatic carbons of Ar_{calix} which connected with hydrogen also gave three signals at 130.2, 130.1 and 129.5 ppm. Therefore, **L2** exists in a stable partial cone conformation. The X-ray single crystal structure of **L2** was also a solid proof for the partial cone conformation as shown in Figure 2.1b. The cavity for cation ($7.92 \times 4.92 \text{ \AA}^2$) and free N-H for anion binding sites were observed. More interestingly, during the preparation of **L2** by starting with **2.3a**, the conformation changed from cone to partial cone conformations, which is more stable as a result of steric effect.



Scheme 2.1 Synthesis pathway of **L2** (a) ethylbromoacetate, NaH, THF, DMF, reflux, 72 hours; (b) 1-aminomethylnaphthalene, toluene:MeOH(1:1), RT, 3 days, **L2a** (41%); and (c) 1-aminomethyl-naphthalene, toluene:MeOH(1:1), RT, 7 days, **L2b** (42%).

The synthesis of **L3** (Scheme 2.2) began by the reaction of *N*-benzylhexahomotriaza-*p*-chlorocalix[3]arene (**L1**) with 3 equivalents of $BrCH_2CO_2Me$ and 7 equivalents of NaH as base in THF for 2 days to provide two *N*-

benzylhexahomotriaza-*p*-chlorocalix[3]tris(methyl acetate) isomers: **2.4a** (deep yellow oil, 16%) and **2.4b** (pale yellow solid, 33%). Based on ¹H-NMR, IR, and MS spectroscopies, **2.4a** was shown to be in a *cone conformation* while the *partial-cone conformation* was found for **2.4b**. Compound **2.2a** was refluxed with 3 equivalents of N(CH₂CH₂NH₂)₃ or tren in a 1:1 mixture of methanol/toluene for 5 days to afford *N*₇-azacalix[3]cryptand (**L3**) in 52% yield.



Scheme 2.2 Synthesis pathway of *N*₇-Azacalix[3]cryptand (**L3**).

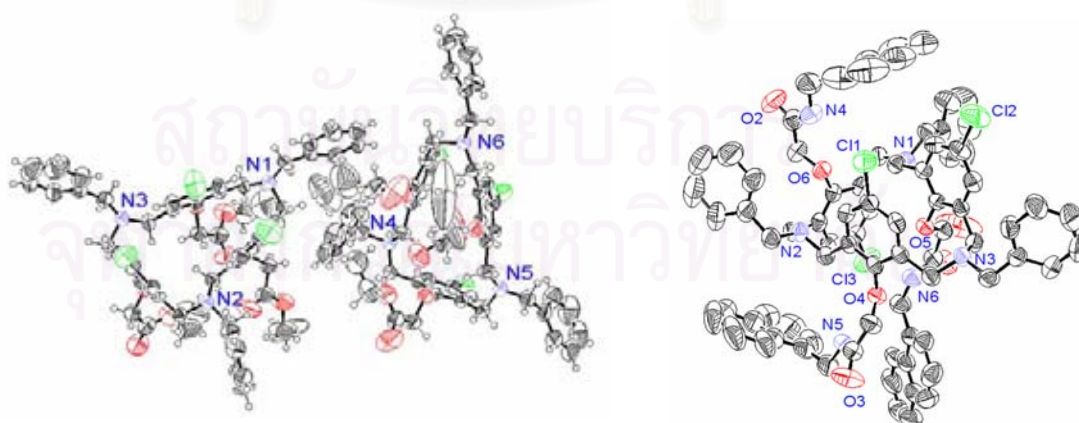


Figure 2.1 ORTEP drawing of *N*-benzylhexahomotriaza-*p*-chlorocalix[3]-tri(ethyl acetate) (**2.3a**) (a) and *N*-benzylhexahomotriaza-*p*-chlorocalix[3]-trinaphthylamide (**L2**) (b). The displacement ellipsoids are drawn at the 50% probability level.

L3 exists in a cone conformation due to the presence of only one singlet at 3.63 ppm for the ArCH₂N protons in ¹H-NMR spectrum showing that the azacalix[3]arene macrocoring retains a C_{3v} symmetry. The X-ray crystallographic analysis [93] clearly confirms that **L3** was in a cone conformation (see Figure 2.3). They mutually interact outside the cavity to furnish a unique crystal structure stabilized by intermolecular CH/Cl interactions (see Figure 2.2).

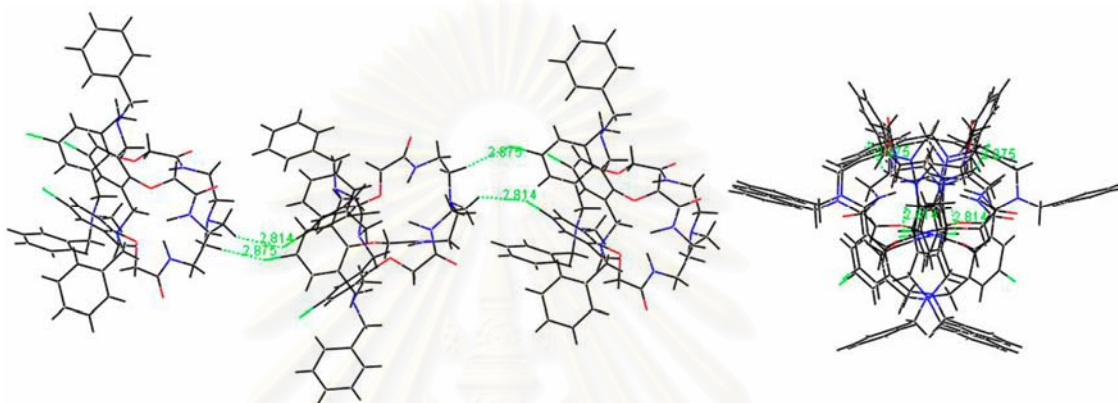


Figure 2.2 Formation of solid structure **L3** stabilized by intermolecular CH/Cl hydrogen bond interactions.

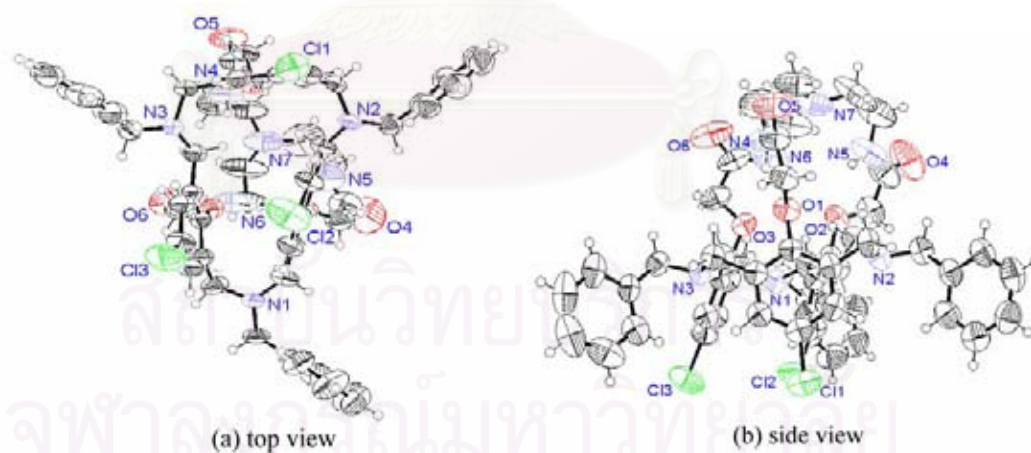


Figure 2.3 ORTEP drawing of *N*₇-azacalix[3]cryptand (**L3**). The displacement ellipsoids are drawn at the 50% probability level.

2.1.4.2 Investigation of binding ability

Cations and anions binding studies of all compounds were carried out by ¹H-NMR spectroscopy, UV-vis and fluorescence titrations. Compound **L1** contains

phenolic hydroxyl groups serving as anion binding sites. Compounds **L2** and **L3** can bind with transition metals through cation-dipole interaction with nitrogen atoms of the azacalix[3]arene macroring and anions through hydrogen bonding with primary acetamide groups.

a) Complexation studies of ligand L1 with various anions by using $^1\text{H-NMR}$, UV-vis and fluorescent spectroscopies

In our preliminary experiments, we found that all ligands were able to dissolve in $\text{DMSO-}d_6$. For $^1\text{H-NMR}$ spectroscopy, this technique allows access to the detail of the interaction between a host and a guest molecule and has been widely employed to investigate receptor-substrate interactions.

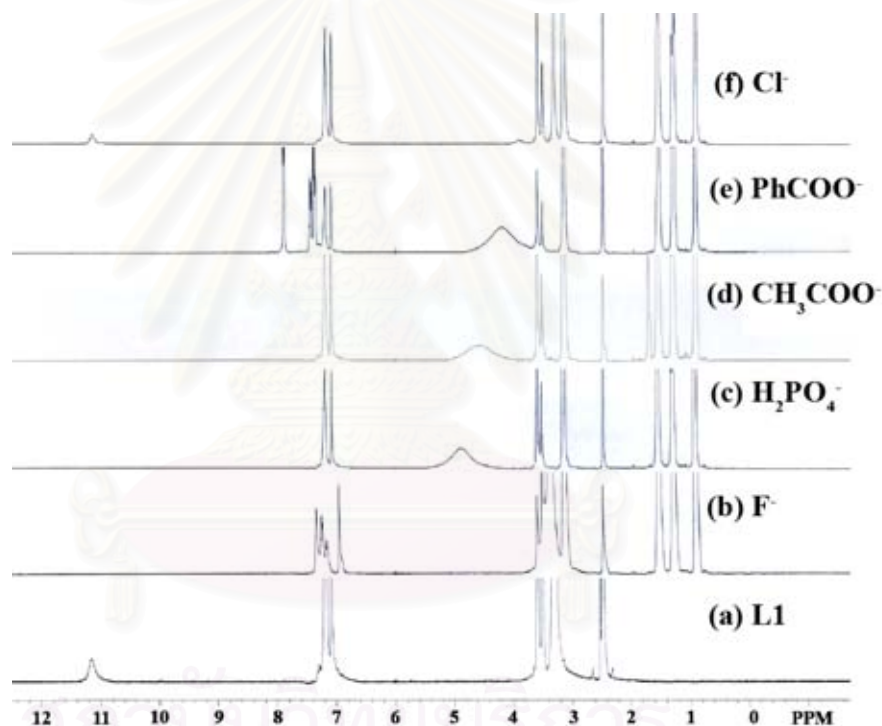


Figure 2.4 $^1\text{H-NMR}$ spectra (400 MHz, $\text{DMSO-}d_6$) (a) azacalix[3]arene (**L1**), (b) **L1** $\supset\text{F}^-$, (c) **L1** $\supset\text{H}_2\text{PO}_4^-$, (d) **L1** $\supset\text{CH}_3\text{COO}^-$, (e) **L1** $\supset\text{PhCOO}^-$, and (f) **L1** $\supset\text{Cl}^-$ complexes obtained upon addition of a CDCl_3 solution of **L1** into NBu_4^+X^- salts (10 equivalents).

The inclusion of an anion by the ligand can be monitored by observing the singlet peak of phenolic OH protons at 11.15 ppm. In case of H_2PO_4^- , the signal of phenol protons at 11.15 ppm in $^1\text{H-NMR}$ spectra (Figure 2.4) disappeared after addition of 4 equivalents of anions. The similar behaviors were observed in the case

of F^- , CH_3COO^- and $PhCOO^-$. After addition F^- , the signal of aromatic protons of phenolic groups shows a small upfield shift from 7.1 to 6.9 ppm which may be caused by the deprotonation of phenolic OH groups by F^- ion. Besides, the signals of aromatic protons of benzyl moieties also shifted to downfield and splitted into multiplets. However, when the solution of **L1** was added to the excess (4 equivalents) of Br^- , I^- , NO_3^- , PF_6^- and ClO_4^- salts, no displacement of signals in the 1H -NMR spectra was observed which implies that they could not form complex with **L1**.

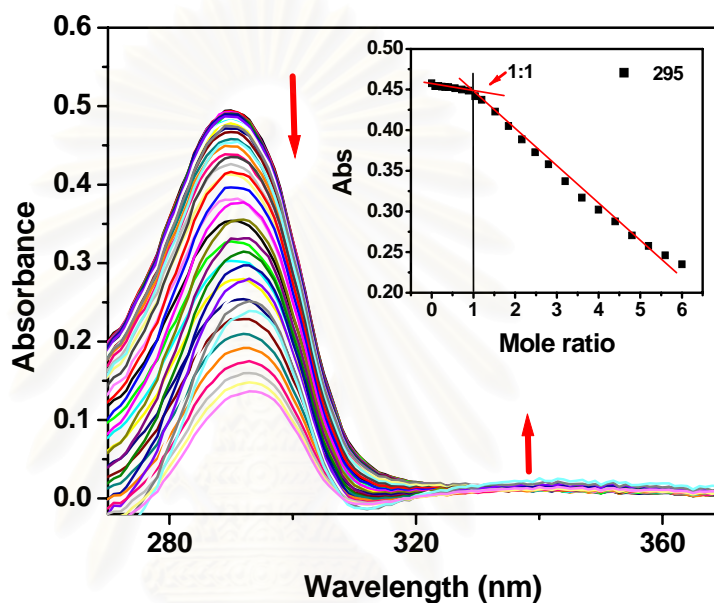


Figure 2.5 Spectral change in the UV absorption of **L1** ($C_L = 5 \times 10^{-5}$ M) upon addition of $NBu_4^+F^-$ ($C_A = 0.04$ M) in DMSO ($0 \leq C_A/C_L \leq 6$).

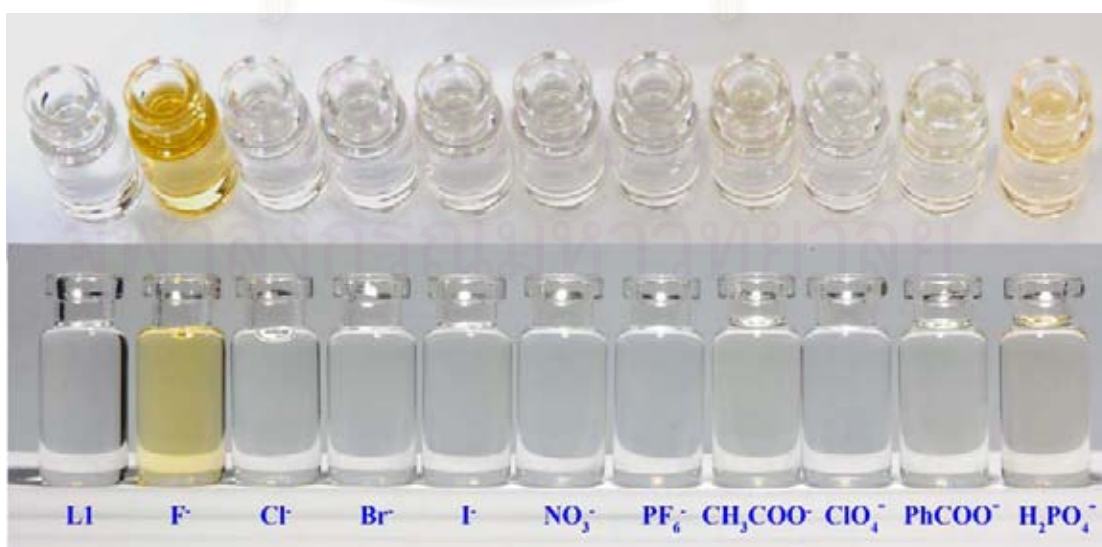


Figure 2.6 Color changes of **L1** in DMSO after addition of 30 equivalents of anions.

In complexation studies between metal ions and ligands using UV-vis spectrophotometric titration, spectral changes are usually employed for monitoring the complex formation. Most of all absorption spectra of complexes studied in this research exhibited hypochromic shifts upon addition of NBu_4^+X^- into solutions of **L1** (Figure 2.5). Free compound **L1** displayed a strong absorption band at 295 nm. The inserted curve in Figure 2.5 shows the mole ratio plot which confirms the 1:1 stoichiometry.

Interestingly, after addition of 30 equivalents of anions, the color of the solution changed from colorless to orange and light orange in the case of F^- (see Figure 2.6) by which UV-vis spectra are positively proved by observation of new peaks at 350 nm (F^-) and 325 nm (H_2PO_4^-) as shown in Figure 2.7. This may come from the deprotonation process [96] at the phenolic protons to provide phenoxide ion. However, in the case of Cl^- , Br^- , I^- , NO_3^- , PF_6^- and ClO_4^- ions, no detectable color change was observed. This sensor, thus, allows the selective colorimetric detection of F^- . The excited state would be more stabilized by anion binding, resulting in a bathochromic shift in the absorption maxima as well as colors change.

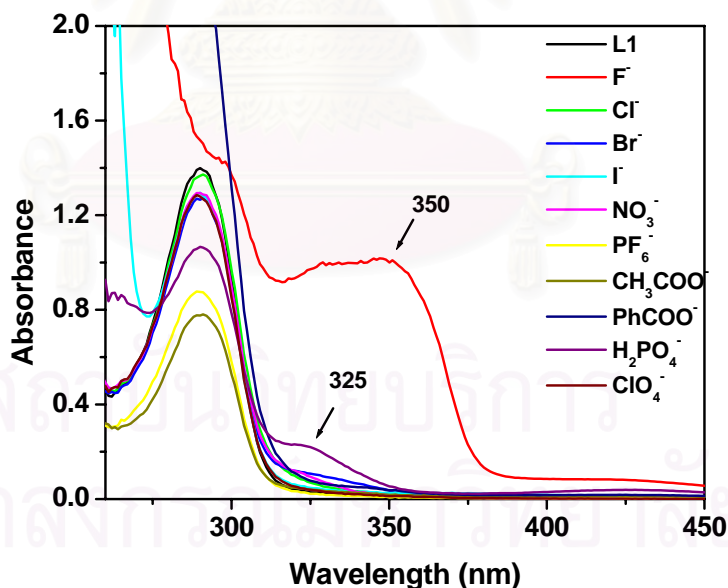


Figure 2.7 Absorption spectra of ligand **L1** ($[\text{L}] = 1 \times 10^{-4} \text{ M}$) upon addition excess of anions (30 equivalents).

The emission spectra ($\lambda_{\text{ex}} = 270 \text{ nm}$) of **L1** ($1 \times 10^{-4} \text{ M}$) in the presence of 30 equivalents of anions are shown in Figure 2.8. It can be seen that the fluorescence intensity ($\lambda_{\text{em}} = 470 \text{ nm}$) of **L1** significantly increases and shifts to 508 nm upon addition of F^- and H_2PO_4^- . The enhancement of fluorescence with a change of maximum wavelength in both anions is due to charge transfer (CT) mechanism (amine donor to chlorophenol acceptor) which is in good agreement with the deprotonation process.

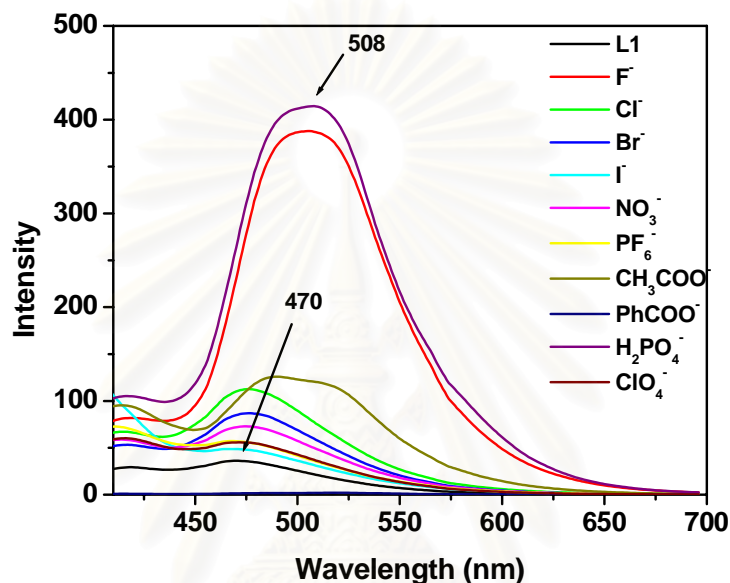


Figure 2.8 Emission spectra of ligand **L1** ($[\text{L}] = 1 \times 10^{-4} \text{ M}$) upon addition excess of anions (30 equivalents).

Moreover, the anion complexation abilities of ligand **L1** with various sizes, geometries, and basicity of anions such as chloride, nitrate, benzoate, dihydrogen phosphate, etc. were investigated by using the UV-vis titrations in DMSO.

The stoichiometries and binding constants of complexes could be determined from changes in photophysical properties of host **L1** induced by a guest bound. The changes in absorbance of the DMSO solution between 200-400 nm were used for evaluating of complex formation constants and stoichiometries by using the SIRKO program [52] which are reported in Table 2.2.

It can be concluded that the order of the formation constants of **L1** with anions were $\text{PhCOO}^- \sim \text{CH}_3\text{COO}^- > \text{H}_2\text{PO}_4^- > \text{F}^-$ for 1:1 complexes and $\text{H}_2\text{PO}_4^- \sim \text{CH}_3\text{COO}^- > \text{F}^-$ for 1:2 complexes. This suggests that the anion binding ability of **L1** depends on basicity of anions as well as their geometries [96].

Table 2.2 Stability constants ($\log \beta$)^a of hexahomotriazacalix[3]arene (**L1**) complexes with anion in DMSO by UV-vis titration method ($T = 25\text{ }^{\circ}\text{C}$, $I = 0.01\text{ M Bu}_4\text{NPF}_6$).

anions	$\log \beta\ (\text{M}^{-1})$
F^-	3.47 (0.08) ^b , 7.69 (0.01) ^c
Cl^-	< 1.50
Br^-	1.99 (0.01) ^b
I^-	3.31 (0.01) ^b
NO_3^-	1.51 (0.01) ^b
PF_6^-	< 1.50
CH_3COO^-	5.40 (0.07) ^b , 10.29(0.09) ^c
PhCOO^-	5.53 (0.01) ^b , 8.62 (0.01) ^d
H_2PO_4^-	4.07 (0.01) ^b , 11.26 (0.02) ^c
ClO_4^-	1.50 (0.01) ^b

^aMean values of $n \geq 3$ independent determinations, with standard deviation σ_{n-1} on the mean in parentheses. ^b1:1 complex (AL). ^c2:1 complex (A_2L). ^d1:2 complex (AL_2).

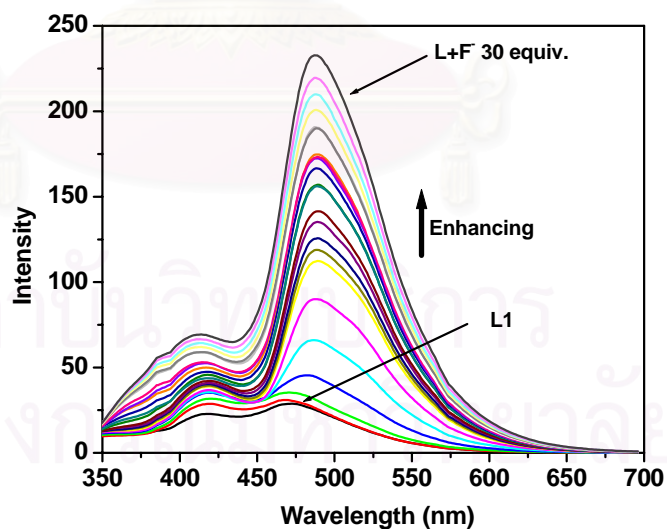


Figure 2.9 Intensity of emission spectra of **L1** ($1 \times 10^{-5}\text{ M}$) enhanced by addition of F^- ($\lambda_{\text{ex}} = 295\text{ nm}$) in DMSO.

Compound **L1** contains the chlorophenol groups as fluorophore which bind anions by hydrogen bonding. This interaction can also be easily monitored by which

anion complexation induced a change in enhanced fluorescent intensity with attribute to formation of chorophenoxide anions during addition of anions. For example, Figure 2.8 presents changes in absorption spectra of ligand **L1** upon addition of F⁻. From the fluorimetric titration, binding constant can be determined by plotting of $I_F^0/(I_F - I_F^0)$ against the reciprocal of the anions concentration $[M]^{-1}$ as shown in the equation below where a and b is a constant. The stability constant (β) is obtained from the ratio of intercept/slope [97].

$$\frac{I_F^0}{I_F - I_F^0} = \left(\frac{a}{b - a} \right) \left(\frac{1}{K[M]} + 1 \right) \quad (2.1)$$

Based on this equation, β for 1:1 stoichiometry of F⁻ = 10721, CH₃COO⁻ = 11990, H₂PO₄⁻ = 7607 and PhCOO⁻ = 4427 dm³mol⁻¹ were obtained. With all of the results it has been noted that **L1** can be used to be a colorimetric sensor for F⁻.

b) Fluorogenic properties of ligand **L2**

It is well-known that hexahomotriazacalix[3]arene which is a stronger metal ion complexing agent [16,95] than the parent calixarenes and amide derivatives can complex with anions [95]. Generally, a naphthalene-based fluorophore can form a monomer and excimer [98] and can be detected in fluorescent spectrum of **L2** at wavelengths of 336 and 423 nm, respectively. However, the excimer formation of fluorophore containing more than one fluorogenic unit can be inter- or intramolecular manners which the former one depends on concentration and solvent polarity. The ratio of excimer to monomer can be observed by using the ratio of intensities of excimers to monomers ($I_{\text{excimer}}/I_{\text{monomer}}$ or I_e/I_m). From fluorescent spectrum, we also discovered that free **L2** exhibits a strong monomer emission at 336 nm and an excimer emission at 423 nm suggesting that the two naphthalene units are in the face-to-face π -stack so as to form a dynamic excimer [98]. The ratio of I_e/I_m increased when the concentration of fluorophore **L2** decreased (Figure 2.10). Because of at the low concentration which was no intermolecular interaction, the two naphthyl groups are on the same side of azacalix[3]arene platform formed an intramolecular excimer and gave an excimer emission at 423 nm.

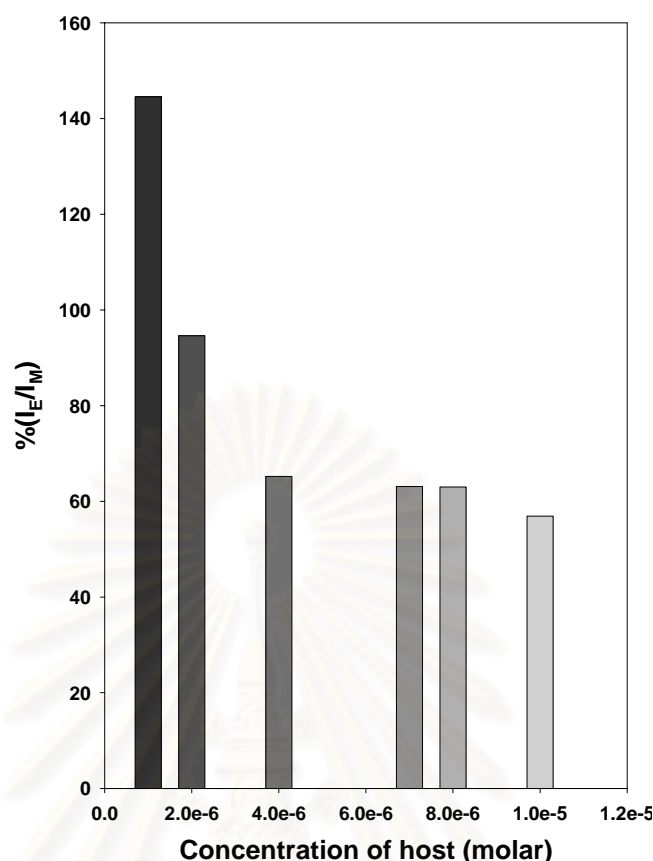


Figure 2.10 Plot of the ratio of excimer to monomer emission versus concentration of ligand **L2**.

While, the other naphthyl moiety which is on the opposite side remain a monomer but its fluorescent emission at 336 nm was quenched for the reason that it was included by the azacalix[3]arene framework as found in the fluorescent quenching of red dye by calix[6]arene [99]. On the other hand, at higher concentrations, the intermolecular interaction increased leading to a decrease of intramolecular inclusion of naphthyl fluorophore. However, the hydrogen bond between the amide groups prevented the face-to-face stacking of naphthyl moieties leading to more monomer emission.

c) Complexation studies of ligand **L2** with various anions by using $^1\text{H-NMR}$, UV-vis and fluorescent spectroscopies

We investigated fluorescent intensity changes of **L2** to determine the cation and anion binding abilities. In the case of cations, we found that **L2** exhibits Pb^{2+} , Hg^{2+} and Co^{2+} (quenching) and Cd^{2+} (enhancing) selectivity over other metal cations studied as shown in Figure 2.11. The quenching phenomena are ascribed to the PET

(photo-induced electron transfer) mechanism and metal ion effects [100]. The electron transfer from lone pair of amido-nitrogen to naphthalene group occurs when the carbonyl moiety of amide group binds with metal such as Pb^{2+} [101].

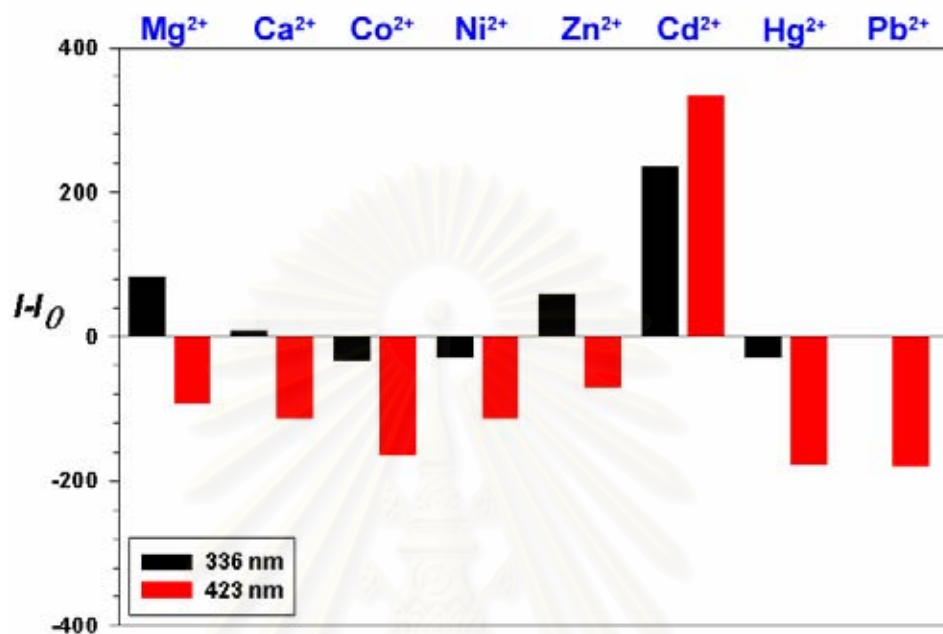


Figure 2.11 Fluorescence changes ($I - I_0$) of **L2** upon addition of various metal ions. Condition: **L2** ($1 \mu\text{M}$) in DMSO, excitation at 285 nm, metal nitrate and chloride (300 equivalents) in DMSO. I : fluorescence emission intensity of complexes **L2**. I_0 : fluorescence emission intensity of free **L2**.

On the other hand, in the case of Cd^{2+} , both monomer and excimer emissions increased which strongly suggests that the Cd^{2+} ion prefers to bind to nitrogen of azacalix[3]arene macrocyclic rather than to the amide groups indicating that the photoinduced electron transfer (PET) and heavy metal ion effects are excluded. Moreover, the azacalix[3]arene has a similar structure to azacrown ether and exhibits an excellent binding with Cd^{2+} which shows, for the first time, the advantage of azacalixarene framework over the parent calixarenes [102]. UV-vis spectroscopy was employed to determine the stoichiometries and stability constants of complexes by using SIRKO program. According to the extent of the absorption spectra changes, we could obtain the association constants of **L2** as shown in Table 2.3. This indicates that the ligand **L2** binds strongly with Pb^{2+} ($\log \beta = 4.68 \text{ M}^{-1}$) and Cd^{2+} ($\log \beta = 4.53 \text{ M}^{-1}$).

The titration profiles of absorption changes of **L2** with Cd^{2+} and Pb^{2+} are shown in Figures 2.12 and 2.13.

Table 2.3 Stability constants ($\log \beta$)^a of 1:1 complexes of **L2** with cations in DMSO by UV-vis titration method ($T = 25\text{ }^\circ\text{C}$, $I = 0.01\text{ M Bu}_4\text{NPF}_6$).

Cations	Size(Å)	$\log \beta$ (M^{-1})
Mg^{2+}	1.60	2.13 (0.01)
Ca^{2+}	1.97	2.01 (0.04)
Co^{2+}	0.75	4.08 (0.09)
Ni^{2+}	0.69	1.83 (0.04)
Cu^{2+}	0.69	2.06 (0.08)
Zn^{2+}	0.74	3.23 (0.09)
Cd^{2+}	0.95	4.53 (0.04)
Hg^{2+}	1.02	2.12 (0.01)
Pb^{2+}	1.19	4.68 (0.04)

^aMean values of $n \geq 3$ independent determinations, with standard deviation σ_{n-1} on the mean in parentheses.

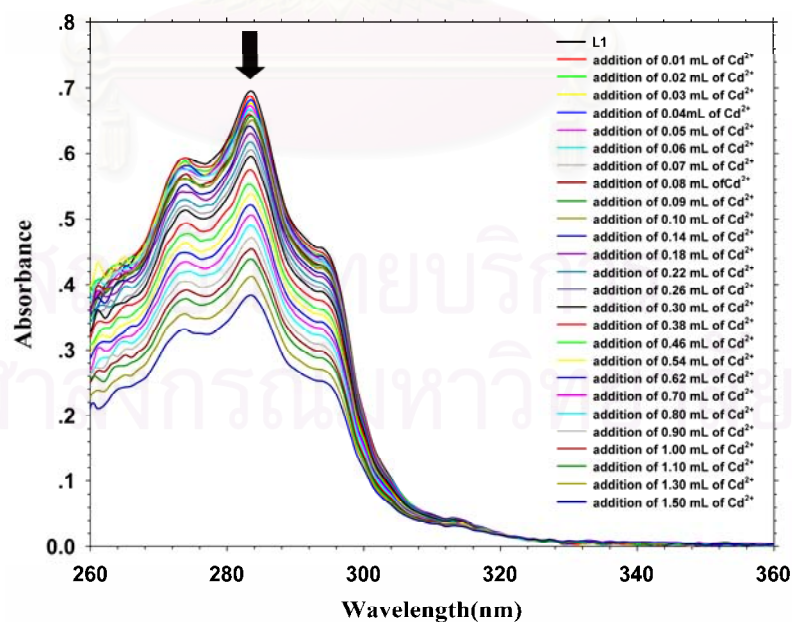


Figure 2.12 Spectral change in the UV-vis absorption of **L2** ($C_L = 3 \times 10^{-5}\text{ M}$) upon addition of Cd^{2+} ($C_C = 1.2 \times 10^{-3}\text{ M}$) in DMSO ($0 \leq C_A/C_L \leq 30$).

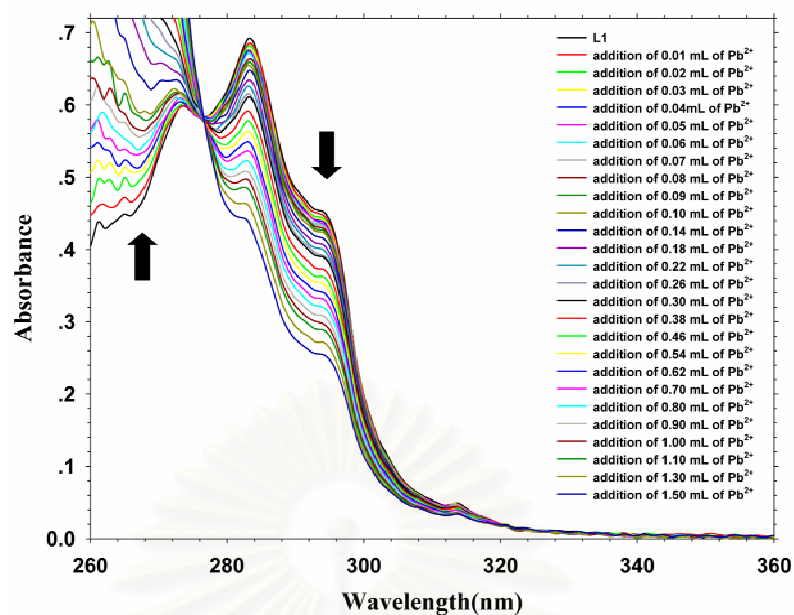


Figure 2.13 Spectral change in the UV-vis absorption of **L2** ($C_L = 3 \times 10^{-5}$ M) upon addition of Pb^{2+} ($C_C = 1.2 \times 10^{-3}$ M) in DMSO ($0 \leq C_A/C_L \leq 30$).

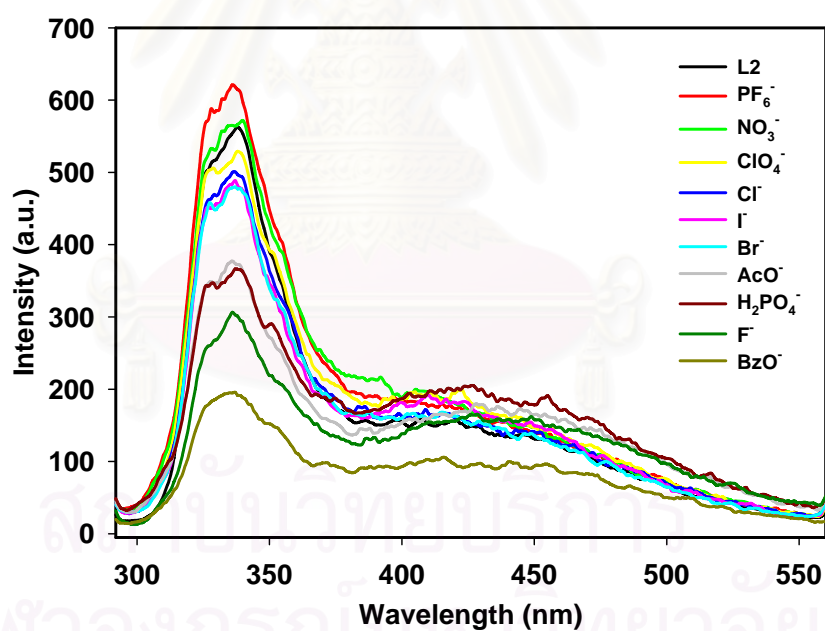


Figure 2.14 Fluorescence changes of **L2** upon addition of various anions. Condition: **L3** (0.1 μ M) in DMSO, excitation at 285 nm, TBAX (300 equivalents) in DMSO.

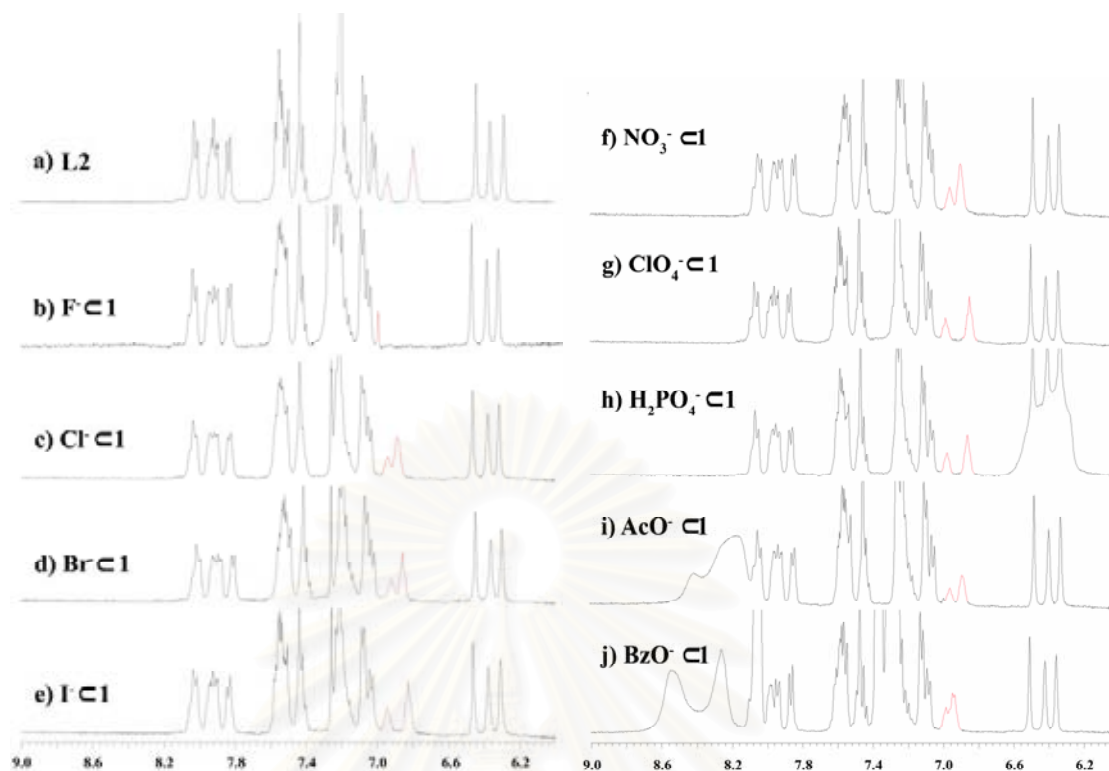


Figure 2.15 ^1H -NMR spectra of **L2** with 10 equivalents of TBAX in CDCl_3 .

Table 2.4 Variation in absorbance of compound **L2** in the absence or presence of various anions^a ($\lambda=293$ nm).

Entry	Solution of ligand L2 with	A/A_0^b
1	free ligand L2	1.00
2	TBA^+F^-	0.71
3	TBA^+Cl^-	1.03
4	TBA^+Br^-	0.84
5	TBA^+I^-	0.86
6	$\text{TBA}^+\text{NO}_3^-$	1.03
7	$\text{TBA}^+\text{ClO}_4^-$	1.01
8	$\text{TBA}^+\text{H}_2\text{PO}_4^-$	0.86
9	$\text{TBA}^+\text{CH}_3\text{COO}^-$	0.72
10	$\text{TBA}^+\text{PhCOO}^-$	0.44

^aIn DMSO, at 25 °C, concentration of host = 0.03 mM and concentration of guests = 1.2 mM, added as their tetrabutylammonium salts. ^b A_0 and A are the absorbances of the host solution in the absence or presence of guests, respectively.

For anion sensor study, the fluorescence excess spectra (Figure 2.14) of the **L2** \supset anions still have quenching effect from PET mechanism on monomer peak. The excimer peaks were still intact indicating that allosteric effect-induced conformation change does not favor the binding of anions. The $^1\text{H-NMR}$ spectra of $1\supset$ anions is also a positive proof because only the signal of amide protons shifted (Figure 2.15) which implies that anion was bound amide groups through hydrogen bond.

Table 2.5 Stability constants ($\log \beta$)^a of complexes of **L2** with anions in DMSO by UV-vis titration method ($T = 25\text{ }^\circ\text{C}$, $I = 0.01\text{ M Bu}_4\text{NPF}_6$).

Anion	$\log \beta\ (\text{M}^{-1})$
F^-	4.21(0.09) ^b , 9.71(0.01) ^c
Cl^-	2.37(0.05) ^b
Br^-	< 1.50
I^-	< 1.50
NO_3^-	2.03(0.01) ^b
ClO_4^-	2.20(0.01) ^b
H_2PO_4^-	< 1.50
CH_3COO^-	2.43(0.02) ^b , 9.29(0.03) ^c
PhCOO^-	2.83(0.01) ^b , 9.43(0.03) ^c

^a Mean values of $n \geq 2$ independent determinations, with standard deviation σ_{n-1} on the mean in parentheses. ^b 1:1 complex (AL). ^c 2:1 complex (A_2L).

To get insight into its selectivity of anion binding, UV-vis spectroscopy was employed to study the interaction of compounds **L2** with anionic guests. The complexation abilities of ligand **L2** with anions were investigated by using spectrophotometric titration in DMSO at $25\text{ }^\circ\text{C}$. The spectrum was recorded from 260-360 nm. Upon the addition of anions, there was change in the absorption spectra of **L2** (Table 2.4). The stability constants (Table 2.5) were calculated from spectrometric data using program SIRKO which can be concluded that **L2** prefers to complex F^- over other anions tested by forming a 1:1 complex.

d) Complexation studies of ligand L3 with various anions by using ¹H-NMR and UV-vis spectroscopies

The ability of **L3** to coordinate anions was investigated by ¹H-NMR spectroscopy. The solutions of **L3** in CDCl₃ were reacted with 10 equivalents of tetrabutylammonium halides (NBu₄⁺X⁻). All of the resulting ¹H-NMR spectra (see Figure 2.16 and Table 2.6) displayed peaks shifts of OCH₂CO, NCH₂Ar, and NCH₂CH₂ toward downfield. This implies the formation of *endo* complexes while keeping the C_{3v} symmetry of the free ligand. Moreover, the signals of aromatic protons of benzyl moieties are also displaced in the same manner, which may be due to a conformational reorganization.

The complexation abilities of ligand **L3** with zinc and anions of various sizes, geometries, and basicity such as chloride, nitrate, benzoate, dihydrogen phosphate, etc. were investigated by using UV-vis spectrophotometric titration in DMSO at 25°C (see Figure 2.17). When necessary, Bu₄NPF₆ was employed to keep the ionic strength at 0.01 M.

Table 2.6 Relative affinities of the halide salts toward host **L3** and ¹H-NMR chemical Induced downfield shifts (CIS) observed through their *endo*-complexation in CDCl₃.

Entry	tetrabutylammonium halide	CIS (ppm) ⁱ			
		a	e	c	b
1	TBA+F ⁻	-0.066	-0.066	-0.066	-0.063
2	TBA+Cl ⁻	-0.025	-0.036	-0.036	-0.030
3	TBA+Br ⁻	-0.060	-0.058	-0.056	-0.053
4	TBA+I ⁻	-0.069	-0.066	-0.064	-0.063

ⁱCIS defined as $\Delta\delta = \delta(\text{complexed halide}) - \delta(\text{free host})$. a, e, c, b refer to the relative position of the protons to charge when host encapsulation halide anion.

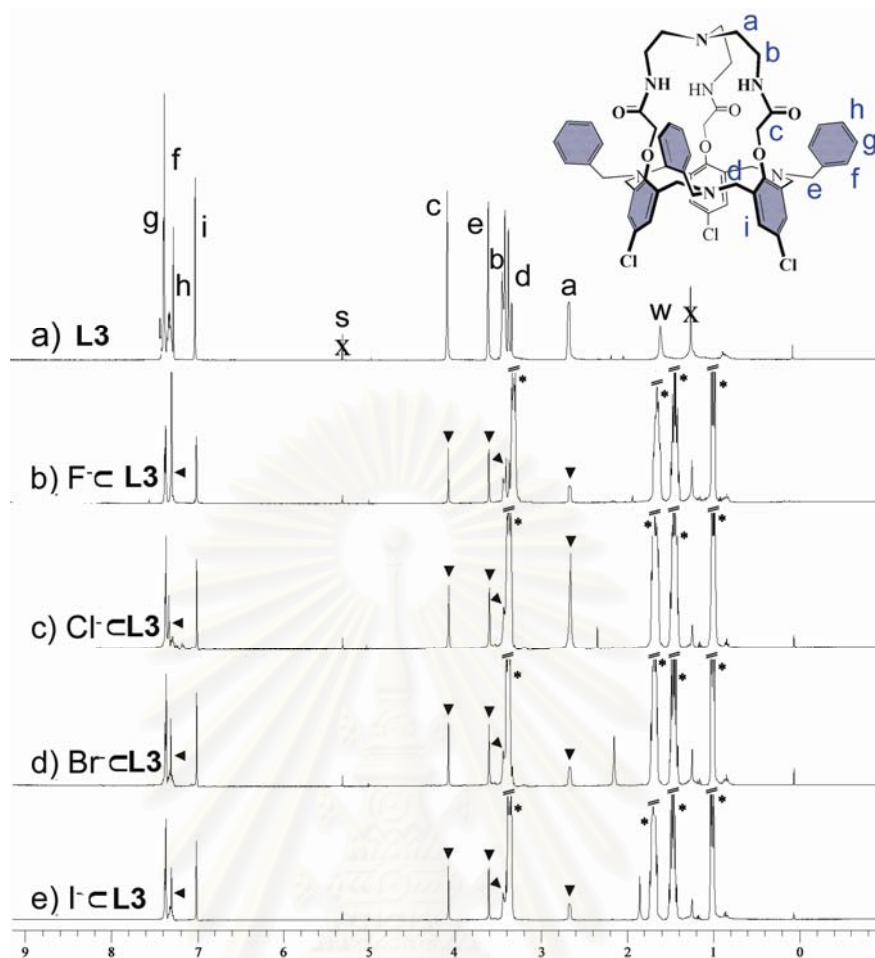


Figure 2.16 ^1H -NMR spectra (400 MHz, CDCl_3) (a) N_7 -azacalix[3]-cryptand (**L3**), (b) $\text{L3} \cdot \text{F}^-$, (c) $\text{L3} \cdot \text{Cl}^-$, (d) $\text{L3} \cdot \text{Br}^-$, and (e) $\text{L3} \cdot \text{I}^-$ complexes obtained upon addition of NBu_4^+X^- (10 equivalents) into a CDCl_3 solution of **L3**. ▼: signals of $\text{L3} \cdot \text{X}^-$; *: signals of NBu_4^+ . Residual solvents and partially protonated water are labeled as “S” and “W” respectively.

Typically, the solution of ion of interest was added directly and successively into the cuvette containing ligand **L3** and the spectral variation was recorded after each addition. The final guest-to-host ratios were varied case by case to obtain the optimal condition for complexation. In all cases, hypochromic shifts were observed upon addition of NBu_4^+X^- into solutions of **L3**. The stoichiometries and stability constants of the complexes were refined by the SIRKO program and are summarized in Table 2.7.

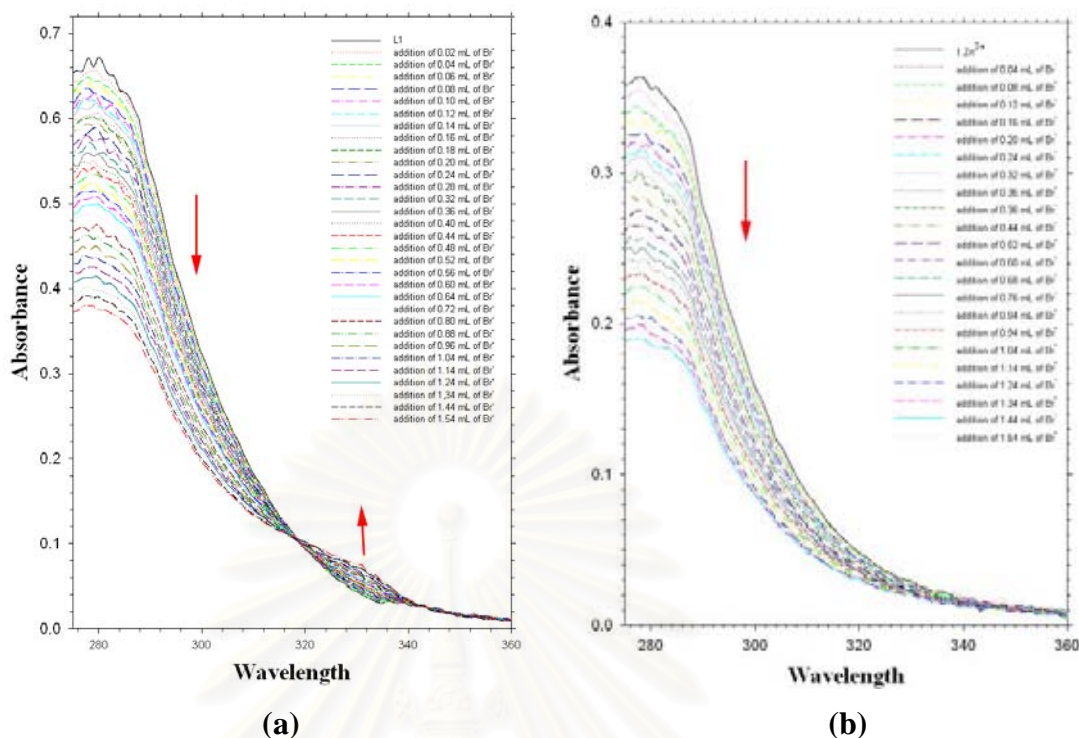


Figure 2.17 Spectral changes in the UV absorption of (a) **L3** ($C_L = 6 \times 10^{-5}$ M) upon addition of $\text{NBu}_4^+\text{Br}^-$ ($C_A = 8 \times 10^{-4}$ M) in DMSO ($0 \leq C_A/C_L \leq 10.3$), and (b) **L3.Zn**²⁺ ($C_L = 3.429 \times 10^{-5}$ M) upon addition of $\text{NBu}_4^+\text{Br}^-$ ($C_A = 8 \times 10^{-4}$ M) in DMSO ($0 \leq C_A/C_L \leq 18$).

It can be seen that **L3** prefers to complex with halide anions over CH_3COO^- , PhCOO^- , NO_3^- , PF_6^- , and ClO_4^- by forming 1:1 complexes. Anion selectivity of **L3** was obtained (as percentage of various free halide anion (% FA)) (see Table 2.7 and Figure 2.18) by calculations using the Hltafall program [9]. For the halide ions, it may be concluded that **L3** prefers to bind $\text{Cl}^- > \text{Br}^- > \text{I}^- > \text{F}^-$. This trend implies that the cavity size of receptor **L3** is suitable for complexation with Cl^- . Though the NO_3^- ion (1.79 Å) has a similar size compared with the Cl^- ion (1.81 Å), the stability constant of the NO_3^- complex is inferior to that of Cl^- . This can be explained by the ease of orientation of the anion inside the rigid cavity of receptor **L3** to form hydrogen bonds with amide groups.

Table 2.7 Stability constants ($\log \beta$)^a of *N*₇-azacalix[3]-cryptand (**L3**) complexes with anion in DMSO by UV-vis titration method ($T = 25\text{ }^{\circ}\text{C}$, $I = 0.01\text{ M Bu}_4\text{NPF}_6$).

anions	$\log \beta\text{ (M}^{-1}\text{)}$	% FA ^b
F ⁻	2.78 (0.01) ^c	40.80
Cl ⁻	4.55 (0.03) ^c	1.38
Br ⁻	3.97 (0.01) ^c	4.97
I ⁻	2.72 (0.01) ^c	43.87
NO ₃ ⁻	1.77 (0.01) ^c	89.87
ClO ₄ ⁻	< 1.50	-
CH ₃ COO ⁻	2.92 (0.01) ^c , 6.06(0.01) ^d	0.03
PhCOO ⁻	2.36 (0.06) ^c , 6.26(0.01) ^d	0.04

^aMean values of $n \geq 3$ independent determinations, with standard deviation σ_{n-1} on the mean in parentheses. ^bPercentage of various free halide anion at $C_L, C_A = 10^{-3}\text{ M}$. ^c1:1 complex (AL). ^d2:1 complex (A₂L).

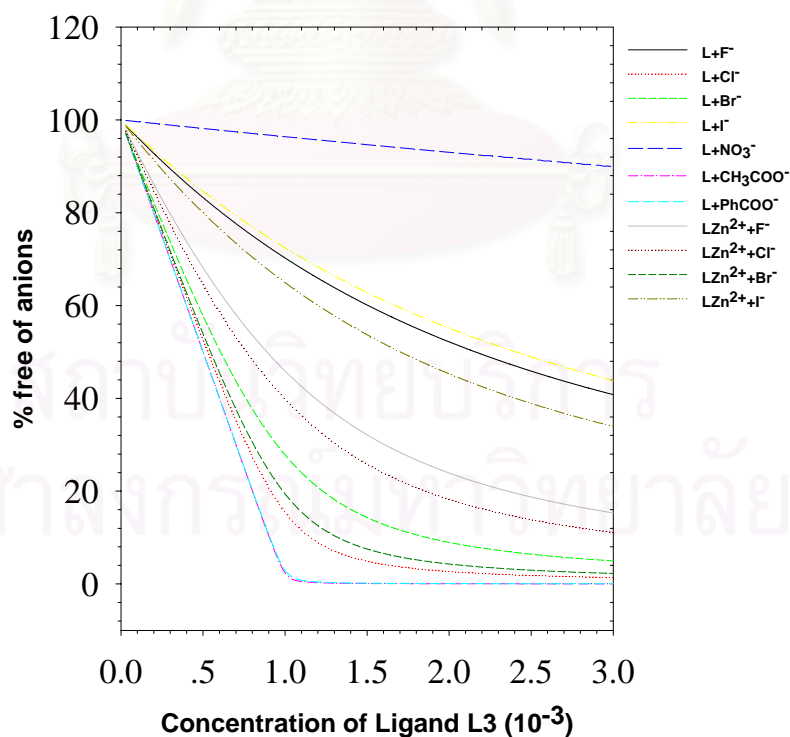


Figure 2.18 Percentage of free anions by each ligand studied as a function of ligand **L3** concentration ($C_L = 1 \times 10^{-3}\text{ M}$).

For CH_3COO^- and PhCOO^- anions, two species of complexes (1:1 and 2:1 (anion:ligand)) were obtained leading to the lower percentages of free halide anion (% FA). This implies that the complexation may occur in an exo fashion. As it was reported that the azacalix[3]arene can bind soft cations such as transition metals [15,16] which can enhance anion binding by electrostatic force, we decided to study the effects of Zn^{2+} on anion complexation of **L3**. In the presence of Zn^{2+} , hypochromic shifts increased in cases of F^- , Br^- , and I^- complexes while they decreased in the case of Cl^- , leading to incremental stability constants of halide complexation except for Cl^- (Table 2.8). This can be rationalized in the following manner: upon addition of Zn^{2+} , one can assume that the Zn^{2+} binds to the azacalix[3]arene part of **L3** to give rise to a $\text{L3}\cdot\text{Zn}^{2+}$ complex which is positively charged and thus increases the stability constants of $\text{L3}\cdot\text{Zn}^{2+}/\text{X}^-$ by electrostatic interactions [87]. In the case of Cl^- , the electronic interaction between Zn^{2+} and Cl^- may reduce the hydrogen bond interaction between **L3** and Cl^- , which leads to a decrease of the stability constant.

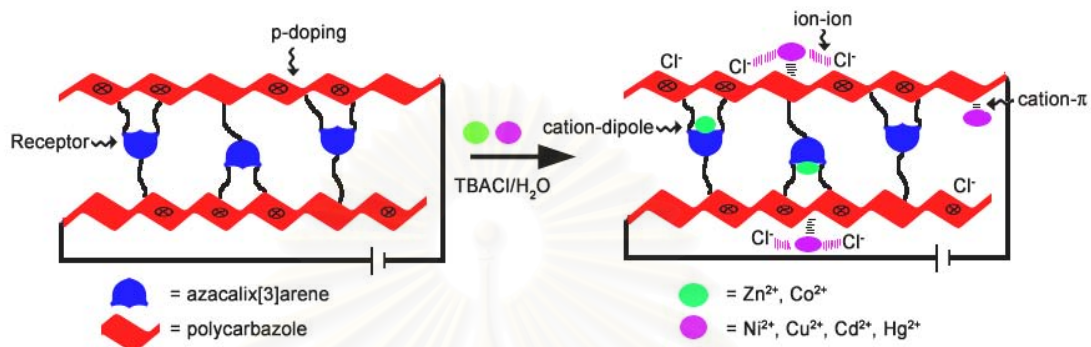
Table 2.8 Stability constants ($\log \beta'$)^a of $\text{L3}\cdot\text{Zn}^{2+}$ complexes with anion in DMSO by UV-vis titration method ($T = 25\text{ }^\circ\text{C}$, $I = 0.01\text{ M Bu}_4\text{NPF}_6$).

anions	$\log \beta'$ (M^{-1})	% FA ^b
F	3.41 (0.08) ^c	15.31
Cl-	3.58 (0.07) ^c	11.09
Br-	4.33 (0.03) ^c	2.26
I	2.92 (0.05) ^c	33.94

^aMean values of $n \geq 3$ independent determinations, with standard deviation σ_{n-1} on the mean in parentheses. ^bPercentage of various free halide anion at $C_L, C_A = 10^{-3}\text{ M}$. ^c1:1 complex or AL.

2.2 Ultrathin films of azacalixarene-carbazole conjugated polymer networks (CPN) for specific cation sensing

2.2.1 Introduction



The basic recognition element of a chemical sensor is essentially a molecular or macromolecular structure designed to recognize a specific analyte. The binding or complexation constant, K_{asso} , of the analyte is dependent on the strength of non-covalent interaction and accessibility to this structure. A high surface area is also a factor as it affects the diffusion kinetics of the analyte to the binding site. In the presence of a conducting (π -conjugated) polymer, a polymeric chemosensor system can be made electrochemically active, electrically conducting, and fluorescent, depending on the structure of the polymer, mode of electric field application, and wavelength excitation. The presence of a conducting polymer can make a polymeric chemosensor be able to conduct the electricity and show fluorescence spectrum as well as be active electrochemically. Thus, it is unnecessary for the receptor-analyte unit of the polymeric chemosensor to have an inherently high K_{asso} . Only partial occupancy of the recognition sites may be required for signal transduction since the conjugated polymer also contributes to signal amplification and improved sensitivity [103].

A number of well-investigated π -conjugated polymers such as polythiophenes, polypyrroles, polyanilines, etc. have been used successfully for sensor and device applications [104]. As a class of semi-conducting polymers, polycarbazole possesses

good electroactivity and useful thermal, electrical, and photophysical properties which have led to its use in redox catalysis, electrochromic displays, electroluminescent devices, and sensors [105]. For example, polycarbazole has been used to develop copper(II) ion selective microelectrochemical transistors [106a] and L-dopa selective sensors [106b] due to its negligible sensor response hysteresis and greater chemical and thermal stability compared to other conducting polymers [106].

2.2.2 Objectives of this research

To prepare a new class of chemical recognition elements for sensors, we have synthesized hexahomotriazacalix[3]arene-carbazole as a precursor for the formation of conjugated polymer networks (CPNs) as shown in Figure 2.19. To the best of our knowledge, there has been no report on the use of azacalix[3]arene in partial-cone conformation combined with polycarbazoles in a chemical sensor material system. Using electropolymerization, these precursors can be deposited as ultrathin films on Au and indium tin oxide (ITO) electrode substrates. This electrochemical process results in the formation of a conjugated polymer network (CPN) due to the inherent inter-molecular and intra-molecular reactivity of pendant carbazole units [107]. The films were characterized by UV-vis spectroscopy, fluorescence spectroscopy, and atomic force microscopy (AFM). The electrochemical and sensing properties were investigated in conjunction with various electrochemically hyphenated optical and acoustic techniques, e.g., electrochemical quartz crystal microbalance (EC-QCM), electrochemical surface plasmon spectroscopy (EC-SPR) and open-circuit potentiometry. It is expected that the partial-cone conformation of azacalix[3]arene allows a gain in the kinetic binding property, with its selectivity remaining intact with electropolymerization, leading to a high specificity for cations.

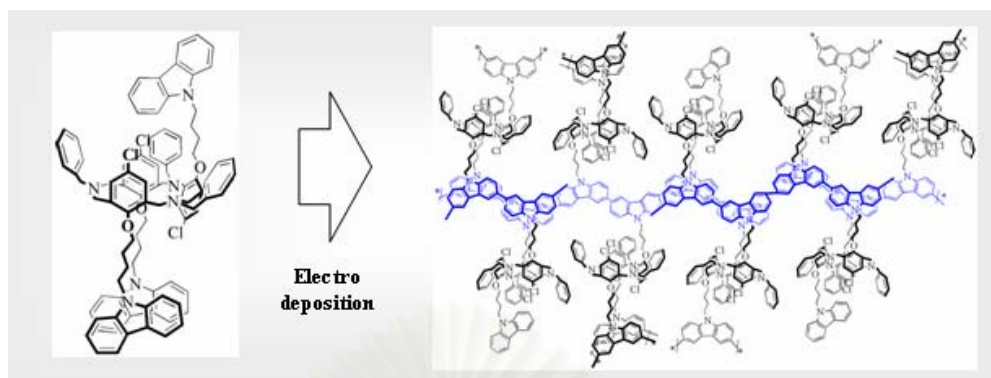


Figure 2.19 Electrochemical polymerization (cross-linking) of *p*-chloro-*N*-benzylhexahomotriazaacalix[3]-tri(buthyl carbazole) or monomer **L4**.

2.2.3 Experimental section

2.2.3.1 Synthesis of sensor based on azacalix[3]arene

a) General procedure

a1) Materials

Unless otherwise specified, the solvent and all materials were reagent grades purchased from Fluka, BHD, Aldrich, Carlo Erba, Merck or J.T. Baker and were used without further purification. Commercial grade solvents such as acetone, dichloromethane, hexane, methanol and ethylacetate were purified by distillation before use. Acetonitrile and dichloromethane for set up the reaction were dried over calcium hydride and freshly distilled under nitrogen atmosphere prior to use. Tetrahydrofuran was dried and distilled under nitrogen from sodium benzophenone ketyl immediately before use.

Column chromatographies were carried out on silica gel (Kieselgel 60, 0.063-0.200 nm, Merck). Thin layer chromatography (TLC) was performed on silica gel plates (Kieselgel 60, F₂₅₄, 1mm, Merck). Compound on TLC plates were detected by the UV-

light. All manipulations were carried out under nitrogen atmosphere. Tetrabutylammonium chloride (TBACl, purum, Fluka) used as supporting electrolyte. Metal salts, used without further purification, were as following: LiClO₄, NaClO₄ and KClO₄, CoCl₂ (GR ACS grade, Merck), NiCl₂, and CuCl₂ (RPE grade, Carlo Erba), ZnCl₂ (purum, Fluka), CdCl₂, and HgCl₂ (GR ACS grade, Merck).

a2) Instrumentations

Nuclear magnetic resonance (NMR) spectra were recorded on a Varian 400 MHz spectrometer and a General Electric QE-300 spectrometer at 300 MHz in deuterated solvent. Chemical shifts (δ) are reported in parts per million and the residual solvent peak was used as an internal standard.

Absorption spectra were measured by a Varian Cary 50 and HP-8453 UV-vis spectrometer. UV-vis titration spectra were measured by a Perkin Elmer Lambda 25 spectrophotometer at 25 °C.

Fluorescence spectra were recorded by Perkin Elmer SL50B fluorescence and a PerkinElmer LS 45 spectrophotometer.

FT-IR spectra were obtained using a FTS 7000 Spectrometer (Digilab now Varian Inc.) equipped with a liquid N₂-cooled MCT detector and a Nicolet Impact 410. KBr pellets were prepared by first mixing the sample solutions with KBr, removing solvents under vacuum and then pressing the KBr using a 10-ton hydraulic press.

MALDI-TOF mass spectra were recorded on a Biflex Bruker Mass spectrometer with 2-Cyano-4-hydroxycinnamic acid (CCA) or 2,5-Dihydroxy-benzoic acid (DHB) as matrix.

Elemental analysis was carried out on CHNS/O analyzer (Perkin Elmer PE2400 series II).

The cyclic voltammetry (CV) experiments were carried out on a Princeton Applied Research Parstat 2263 with a modified ITO substrate as the working electrode coupled with a Pt plate counter and Ag/AgCl reference electrode. Cyclic voltammetry was utilized to prepare the cross-linked films from a 0.1 wt % of the precursor polymer solution of 0.1 M TBAPF₆/CH₂Cl₂.

The QCM apparatus, probe, and crystals are available from Maxtek Inc. The data acquisition was done using a RQCM (Research Quartz Crystal Microbalance, Maxtek, Inc.) system equipped with a built-in phase lock oscillator and the RQCM Data-Log Software. This was coupled with the Amel potentiostat to generate EC-QCM results. A 5 MHz AT-cut CBzC11SH (2.8) modified on Au-coated quartz crystal with an effective area of 1.327 cm² was used as a working electrode. Platinum as a counter electrode and Ag/AgCl as a reference were used to measure *in situ* polymerization during cyclic voltammetry. To initiate the experiment, an inert probe was firstly immersed in methylene chloride until a stable frequency was obtained.

Surface plasmon resonance spectroscopy (SPR) on Au-coated glass (~45 nm) was performed using a commercially available instrument (Multiskop) with a Kretschmann configuration and attenuated total reflection (ATR) conditions. The reflectance was monitored with a *p*-polarized He-Ne laser (632.8 nm) as a function of angle of incidence.

Electrochemical surface plasmon resonance spectroscopy (EC-SPR) measurements were performed using a SPR setup combined with a three-electrode electrochemical cell in a Kretschmann configuration for the excitation of surface plasmons. The details of this setup are described in the sensing part. Surface plasmons were excited by reflecting *p*-polarized laser light off the Au-coated base of the prism. The excitation source employed was a He-Ne laser: $\lambda = 632.8$ nm. Kinetic measurements were performed to monitor the formation of the film. Reflectivity-angular measurements were also performed by scanning an incident angle range before and after *in situ*

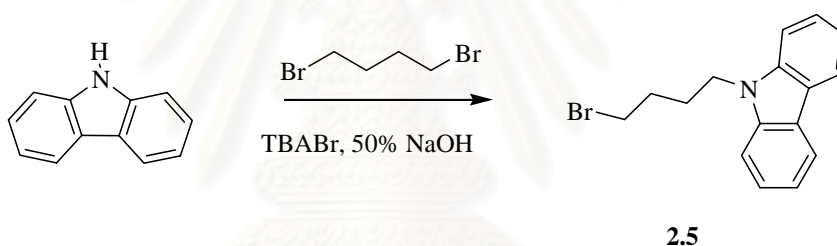
polymerization. For these experiments, the gold film thickness (~45 nm) was chosen for optimum excitation of the surface plasmons. The electrode surface area was 0.785 cm².

Atomic force microscopy (AFM) imaging was examined in ambient conditions with a PicoSPM II (PicoPlus System, Molecular Imaging [now Agilent Technologies Tempe, AZ.] in the Tapping mode (AAC mode)).

b) Synthesis

b1) Synthesis of *p*-Chloro-*N*-benzylhexahomotri-azacalix[3]-tri(buthyl carbazole) (L4)

9-(4-bromobutyl)-9*H*-carbazole (2.5)



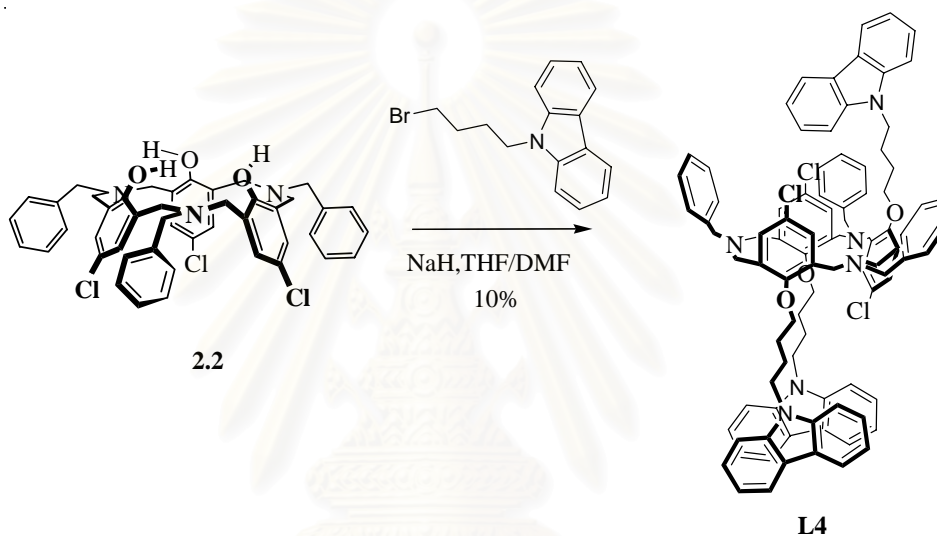
To a solution of 59.10 g (237.70 mmol) of 1,4-dibromobutane, 1.00 g of tetrabutylammonium bromide, 5.16 g (30.86 mmol) of carbazole, 50 mL of aqueous 50% sodium hydroxide, and 50 mL benzene was added and stirred at 40 °C for 6 hours. The organic layer was separated, and the aqueous layer was extracted three times with chloroform (3 × 30 mL). The combined organic layer was washed three times with water (3 × 40 mL) and dried over anhydrous Na₂SO₄. The organic solvent was distilled over a water bath, the unreacted 1,4-dibromobutane was removed by vacuum distillation, and the residue was recrystallized from ethanol to give a white needle-like solid. Yield: 5.80 g (62%).

Characterization data for 2.5

IR (neat)/cm⁻¹: ν 3045, 2939, 2925, 2855, 1620, 1593

¹H-NMR (300 MHz, CDCl₃): δ (ppm) 8.06 (d, 2H, ArH), 7.11–7.47 (m, 6H, ArH), 4.29 (t, 2H, NCH₂), 3.32 (t, 2H, CH₂CH₂Br), 1.98 (m, 4H, ArCH₂CH₂)

p-Chloro-N-benzylhexahomotriazacalix[3]-tri(buthyl carbazole) (L4)



To a solution of **2.2** (0.50 g, 0.64 mmol), NaH (0.11 g, 4.42 mmol) in THF (20 mL) and DMF (5 mL) was added a solution of 9-(4-bromobutyl)-9H-carbazole (0.68 g, 2.25 mmol) in THF (10 mL). After stirring for 2 days at 80 °C, the reaction mixture was evaporated, extracted with CH₂Cl₂, and washed with saturated NaHCO₃. The organic layer was dried over anhydrous Na₂SO₄, filtered, and evaporated. Column chromatography on silica gel (hexane/EtOAc = 9:1, v/v) afford **L4** (0.09 g, 0.06 mmol) in 10 % yields as deep white oil.

Characterization data for L4

IR (neat)/cm⁻¹: 2977, 2937, 2880, 1470, 1386, 1320, 1243, 1168, 1107, 1059, 1035, 929, 879, 817, 738

¹H-NMR (300 MHz, CDCl₃): δ (ppm) 8.12 (br m, 6H, ArH), 7.52 (br m, 12H, ArH), 7.31 (m, 15H, ArH), 7.04 (s, 4H, ArH), 7.01 (s, 2H, ArH), 4.13 (t, *J* = 7.2 Hz, 2H, OCH₂CH₂), 3.74 (t, *J* = 7.2 Hz, 4H, OCH₂CH₂), 3.78-3.00 (br m, 24H, NCH₂Ar and CH₂CH₂N), 1.76-1.18 (br m, 12H, , CH₂CH₂CH₂)

¹³C-NMR (75 MHz, CDCl₃): δ (ppm) 157.5, 155.5, 141.0, 140.9, 139.6, 139.7, 135.0, 134.0, 133.6, 131.4, 129.9, 129.5, 129.4, 129.1, 128.9, 127.9, 127.7, 126.2, 123.4, 121.0, 120.94, 119.5, 119.4, 119.3, 109.3, 109.2, 75.0, 74.7, 63.4, 62.8, 60.4, 53.2, 52.2, 51.4, 43.5, 43.3, 30.3, 28.2, 28.2, 26.4, 26.2

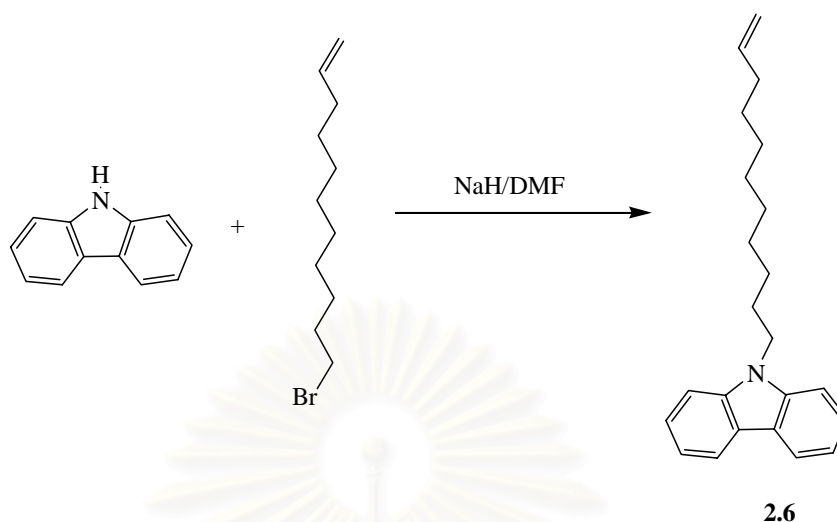
MALDI-TOF: m/z Calcd for [C₉₃H₈₇Cl₃N₆O₃]⁺: m/z 1443.08

Found: [C₉₃H₈₇Cl₃N₆O₃+ H]⁺: m/z 1443.08

b2) Synthesis of 11-(9H-carbazol-9-yl)-undecane-1-thiol (2.8)

9-(Undec-10-enyl)-9H-carbazole (2.6)

สถาบันวิทยบริการ
จุฬาลงกรณ์มหาวิทยาลัย



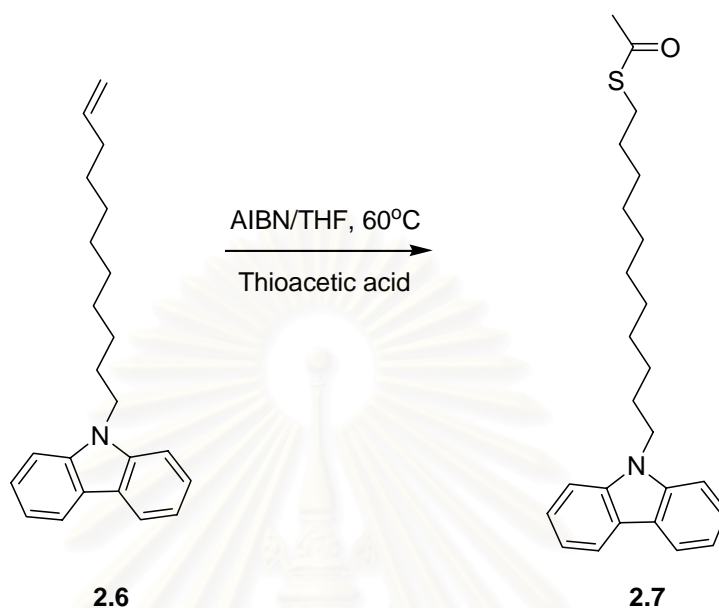
To a stirred solution of 6.00 g (36.00 mmol) of carbazole in 15 mL dimethylformamide (DMF), NaH 1.83 g (39.60 mmol) was added in portions and after complete addition the mixture was heated to 60 °C for 2 hours. After the mixture was cooled, a solution of 11-bromoundec-1-ene 9.40 g (40.00 mmol) in 5 mL DMF was added dropwise to the reaction mixture and was allowed to stir for 48 hours at room temperature. The reaction mixture was then poured in water and was extracted using methylene chloride and dried over anhydrous Na₂SO₄. After evaporating the solvent, the crude product was purified by column chromatography using hexane as an eluent giving **2.6**, 9.5 g in 83% yields.

Characterization data for 2.6

¹H-NMR (300 MHz, CDCl₃): δ (ppm) 8.14 (d, 2H, ArH), 7.53–7.42 (m, 4H, ArH), 7.27(t, 2H, ArH), 5.80 (m, 1H, CH₂CH=CH₂), 4.95 (m, 2H, CH₂CH=CH₂), 4.29 (t, 2H, NCH₂CH₂), 2.02 (p, 2H, CH₂CH₂CH), 1.86 (p, 2H, CH₂CH₂CH₂), 1.35–1.22 (m, 12H, CH₂CH₂CH₂)

¹³C-NMR (75 MHz, CDCl₃): δ (ppm) 140.6, 139.3, 125.7, 123.1, 120.3, 118.9, 114.3, 109.9, 43.4, 34.2, 29.8, 29.7, 29.4, 29.3, 29.2, 27.7

11-(9H-Carbazol-9-yl)undecyl Ethanethioate (2.7)



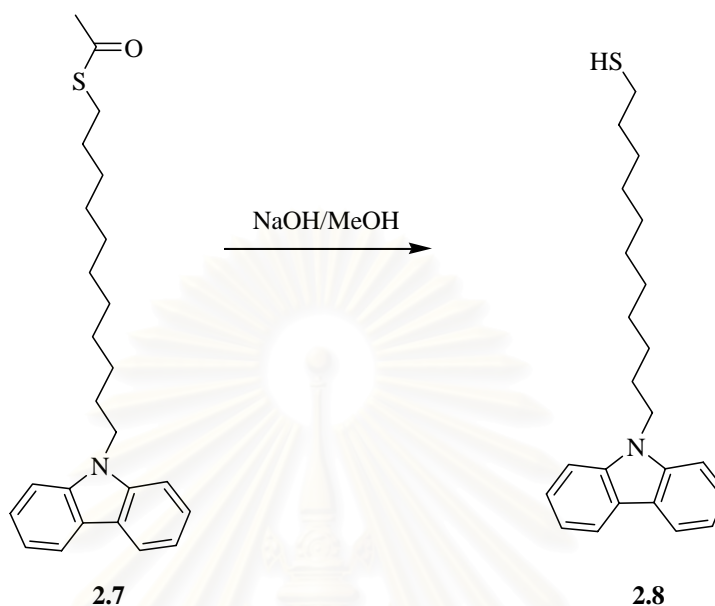
To a solution of **2.6**, 1.91 g (6.00 mmol) in dry tetrahydrofuran (THF; 20 mL) containing thioacetic acid 0.63 g (8.32 mmol) and 2,2'-azobis(2-methylpropanionitrile) (AIBN) 56.00 mg (0.17 mmol) was refluxed at 60 °C for 12 hours under nitrogen. After cooling the reaction flask, 20.00 mg of AIBN and 0.30 g thioacetic acid was added and refluxed for another 4 hours. Concentration of the reaction mixture followed by flash column chromatography (4:1 hexane/CH₂Cl₂) gave **2.7**, 2.10 g in 87% yields.

Characterization data for 2.7

¹H-NMR (300 MHz, CDCl₃): δ (ppm) 8.14 (d, 2H, ArH), 7.53–7.42 (m, 4H, ArH), 7.27(t, 2H, ArH), 4.29(t, 2H, NCH₂CH₂), 2.70(t, 2H, CH₂CH₂CO), 2.35 (s, 3H, COCH₃), 1.92–1.88 (m, 2H, CH₂CH₂CH₂), 1.74–1.69 (m, 2H, CH₂CH₂CH₂), 1.38–1.26 (m, 14H, CH₂CH₂CH₂)

¹³C-NMR (75 MHz, CDCl₃): δ (ppm) 196, 140.6, 125.7, 123.1, 120.3118.6, 108.9, 43.0, 39.1, 35.1, 32.1, 30.5, 29.4, 29.3, 29.1, 28.9, 27.3

11-(9*H*-carbazol-9-yl)-undecane-1-thiol (2.8)



To a solution **2.7**, 1.00 g (2.52 mmol) was dissolved in 10 mL methanol, and CH_2Cl_2 was added dropwise to make the suspension clear. To this solution 1 mL of 50 wt% NaOH was added under nitrogen and was further allowed to stir overnight. The reaction mixture was neutralized by adding acetic acid. The neutralized solution was then poured into 25 mL water and the organic phase was extracted using methylene chloride. The organic phase was then washed with brine and dried over anhydrous Na_2SO_4 . After filtering and concentrating under vacuum, the crude product was further washed with hexane to give the pure product as 0.78 g (88%) of slightly yellowish oil.

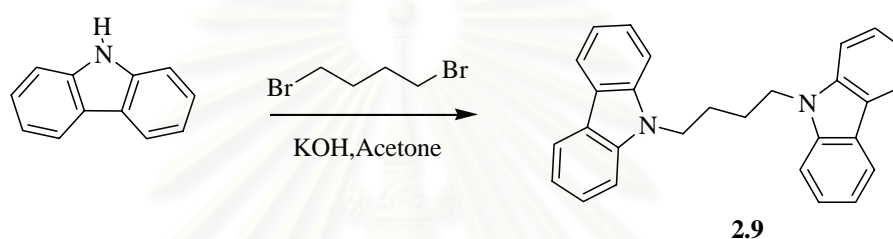
Characterization data for 2.8

$^1\text{H-NMR}$ (300 MHz, CDCl_3): δ (ppm) 8.14 (d, 2H, ArH), 7.53–7.42 (m, 4H, ArH), 7.27 (t, 2H, ArH), 4.29 (t, 2H, NCH_2CH_2), 2.68 (t, 2H, $\text{CH}_2\text{CH}_2\text{SH}$), 1.92–1.88 (m, 2H, $\text{CH}_2\text{CH}_2\text{CH}_2$), 1.74–1.69 (m, 2H, $\text{CH}_2\text{CH}_2\text{CH}_2$), 1.38–1.26 (m, 15H, $\text{CH}_2\text{CH}_2\text{CH}_2$ and SH)

$^{13}\text{C-NMR}$ (75 MHz, CDCl_3): δ (ppm) 140.6, 125.7, 123.1, 120.3118.6, 108.9, 43.0, 39.1, 35.1, 32.1, 29.3, 29.1, 29.0, 28.9, 28.4, 27.3

b3) Synthesis of 9-(4-(9H-carbazol-9-yl)butyl)-9H-carbazole (2.9)

9-(4-(9H-carbazol-9-yl)butyl)-9H-carbazole (2.9)



To a solution of carbazole (5.00 g, 30.00 mmol), KOH (1.68 g, 30.00 mmol) in acetone (20 mL) was added dropwise into a solution of dibromobutane (2.60 g, 12.00 mmol) in acetone (5 mL). After stir for 24 hours at room temperature, the reaction mixture was evaporated and then extracted with CH_2Cl_2 , and finally washed with EtOH and THF. The filter was dried in vacuum to afford **9** (3.26 g, 8.39 mmol) in 70 % yields as a white solid.

Characterization data for 2.9

$^1\text{H-NMR}$ (300 MHz, CDCl_3): δ (ppm) 8.10 (d, 4H, ArH), 7.44 (br m, 8H, ArH), 7.23 (m, 4H, ArH), 4.24 (t, $J = 7.2$, 4H, NCH_2CH_2), 1.98 (p, 4H, $\text{CH}_2\text{CH}_2\text{CH}_2$)

2.2.3.2 Electrochemical synthesis of cross-linked polymers (P-L4)

The precursor polymers were synthesized using the cyclic voltammetry (CV) technique. In a three-electrode cell, 0.10 M tetra-butylammonium hexafluorophosphate (TBAPF₆) was used as a supporting electrolyte along with 0.10 wt % polymer dissolved in anhydrous methylene chloride in separate cells. The electropolymerization of each precursor polymer was performed by sweeping the voltage at a scan rate of 50 mV/s from 0 to 1.0, 1.3, 1.5 V against Ag/AgCl as a reference electrode and platinum as a counter electrode. The ITO, gold-coated slides and CBzC11SH coated gold substrates were used both as a working electrode and as a substrate.

2.2.3.3 Sensitivity and selectivity studies of P-L4 by using potentiometry

Polymerized on ITO substrates by sweeping the voltage at scan rate 50 mV/s from 0-1.3 V, hexahomotriazacalix[3]arene-carbazole was studied as a sensor using 0.01 M TBACl as electrolyte. Using Teflon cell, TBACl of 0.01 M was injected, until potential signal was kept constant. To study sensitivity and selectivity of the polymer, different concentrations of cations was held constant for 1000 sec.

The change in potential (ΔE), [ΔE] = Observed potential (E_0) – Initial potential (E_i)] was recorded simultaneously as a function of time.

2.2.3.4 Sensitivity and selectivity studies of P-L4 by using EC-QCM and QCM

EC-QCM was used to polymerize L4 on 2.8 coated gold substrates. The electropolymerization was performed by sweeping the voltage at the scan rate of 50 mV/s from 0 to 1.0 V. The sensitivity and selectivity were monitored in aqueous solution. From Figure 2.20, we injected water into the sample cell and kept this cell constant at room temperature for 1000 sec. After that, such cell was dried in vacuum oven for 10 mins, and

each delta frequency shown in Figure 2.20 was measured in air by QCM each time for 20 mins as the function of cations' concentration being as follows 10^{-6} , 10^{-5} , 10^{-4} and 10^{-3} M.

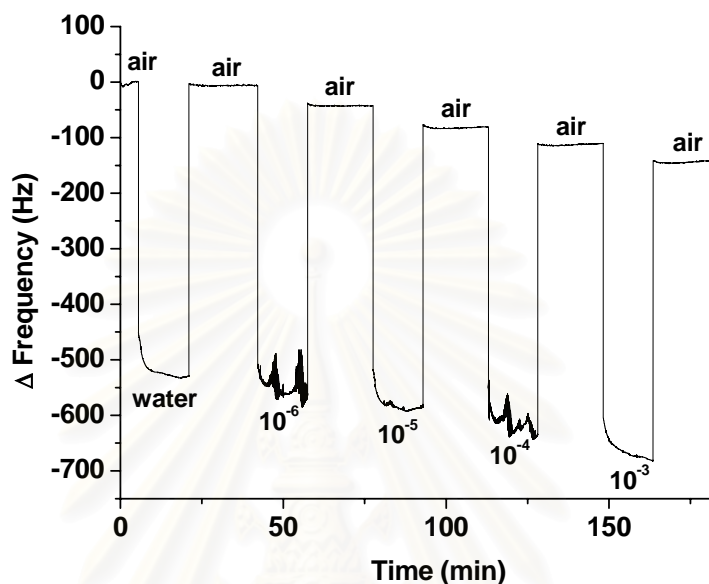


Figure 2.20 Sensor diagram studied by using QCM.

2.2.3.5 Sensitivity and selectivity studies of P-L4 by using EC-SPR and SPR

EC-SPR was used to polymerize **L4** on **2.8** coated gold substrates. The electropolymerization was performed by sweeping the voltage at the scan rate of 50 mV/s from 0 to 1.0 V. The sensitivity and selectivity were monitored in aqueous solution. Figure 2.21 shows the sensor set up by SPR and EC-SPR. We injected water into the sample cell and kept this cell constant at room temperature for 1000 sec. After that, the sensing experiment was performed by injecting different concentrations of cations (10^{-6} , 10^{-5} , 10^{-4} and 10^{-3} M) at regular intervals by starting at the lowest concentration.

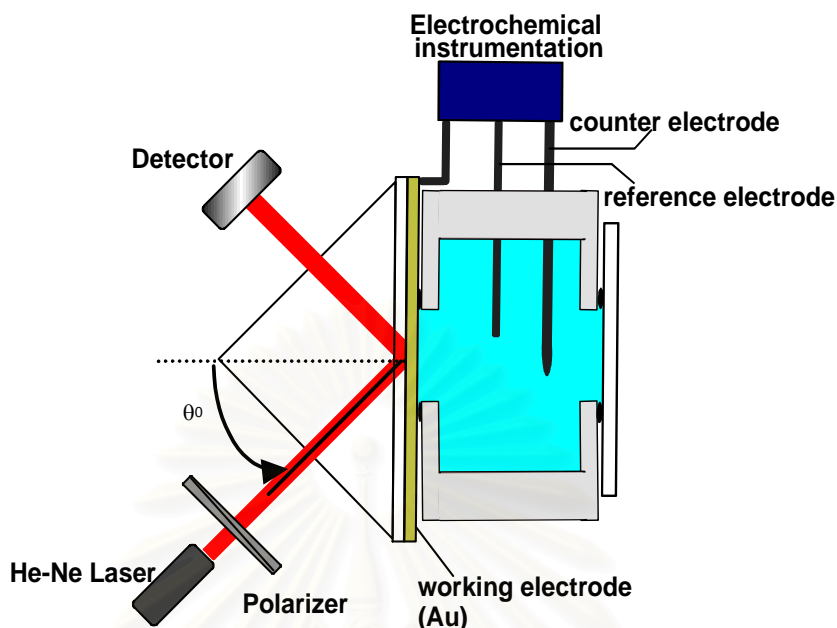


Figure 2.21 Sensor setup for *in situ* EC-SPR/SPR measurement.

2.2.4 Results and discussion

2.2.4.1 Synthesis of macrocyclic receptor monomer (L4)

The synthesis of monomer **L4** was completed by reacting *N*-benzylhexahomotriaza-*p*-chlorocalix[3]arene with 3.5 equivalents of 9-(4-bromobutyl)-9H-carbazole and 3.5 equivalents of NaH as base in THF/DMF solution for 2 days. Column chromatography (silica gel, 90/10 hexane/ethyl acetate) was used to afford monomer **L4** in 10% yields. The carbazole functionalized hexahomotriazacalix[3]arene monomer was then characterized by FT-IR, ¹H-NMR, ¹³C-NMR and MALDI-TOF MS as summarized in the experimental section.

It was found that hexahomotriazacalix[3]-tricarbazole (**L4**) was fixed as a partial cone conformation as evidenced by the presence of 2 triplet $-CH_{-azacalix}$ aromatic at 7.04 ppm ($J=7.2$ Hz) and 7.01 ppm ($J=7.2$ Hz) and multiplet peaks of $-NCH_2Ar-$ at 3.78-3.00

ppm in the $^1\text{H-NMR}$ spectrum. The $^{13}\text{C-NMR}$ spectrum also gave evidence of the changes, consistent with the previous study from a cone conformation spectrum [95], i.e. $-\text{OCH}_2\text{CH}_2-$ showed two peaks (75.0, 74.7 ppm) and the $-\text{C}-$ of the aromatic azacalix split into three peaks (135.0, 134.0 and 133.5 ppm).

2.2.4.2 Electropolymerization of L4

Electropolymerization by cyclic voltammetry (CV) is a widely used method for preparing polycarbazole (PCBz) films [108,109]. To test the ability to form network ultra-thin films, monomer **L4** was electropolymerized and deposited on three working electrodes: plain gold-coated glass substrate, CBzC11SH (thiol-undec-9*H*-carbazole, **2.8**) self-assembled monolayer (SAM) coated gold substrate, and ITO substrate. All the CV trace diagrams of monomer **L4** deposited onto the different substrates are also shown in Figure 2.22. Deposition on bare gold-coated slide was first attempted. The current increase was low and the CV was not well-behaved. When the **2.8** SAMs coated gold substrate was used (Figure 2.22a), the monomer was shown to be electropolymerized anodically at 1.0 V.

After several cycles, the oxidation and reduction peaks are observed at 0.85 V and 0.77 V, respectively. The current was low on the first cycle but increased in the second and slightly changed with further cycles. Thus, compared to the bare-Au electrode, more material was deposited on this **2.8** coated gold substrate based on a higher current increase at 0.85 V. On the other hand, the best films were obtained when ITO was used as the electrode-substrate with applied potential window from 0 to 1300 mV (electropolymerization was initially attempted with applied potential up to 1500 mV, Figure 2.22d). The linear increase in the oxidation current and high cyclic reversibility is indicative of a uniform film growth. The anodic current trace splits into two peaks with further cycles. At the first cycle, the broad anodic peak is centered at 0.90 V and the reduction peak is at 0.75 V. When the eighth cycle was reached, two consecutive anodic peaks centered at 0.85 V and 0.96 V became more pronounced. The two anodic current

peaks can be assigned to the doping of anions into the polymerized carbazole from the electrolyte solution and oxidation of carbazole, leading to a radical cation species [107]. This is reasonable because only one reduction peak is observed, which decreases from 0.75 V to 0.71 V. Thus, the reduction from the previously oxidized but uncrosslinked species may be the source of this peak. Dedoping may also be involved in this reduction process but is not favored considering polycarbazole is a *p*-type semiconductor polymer.

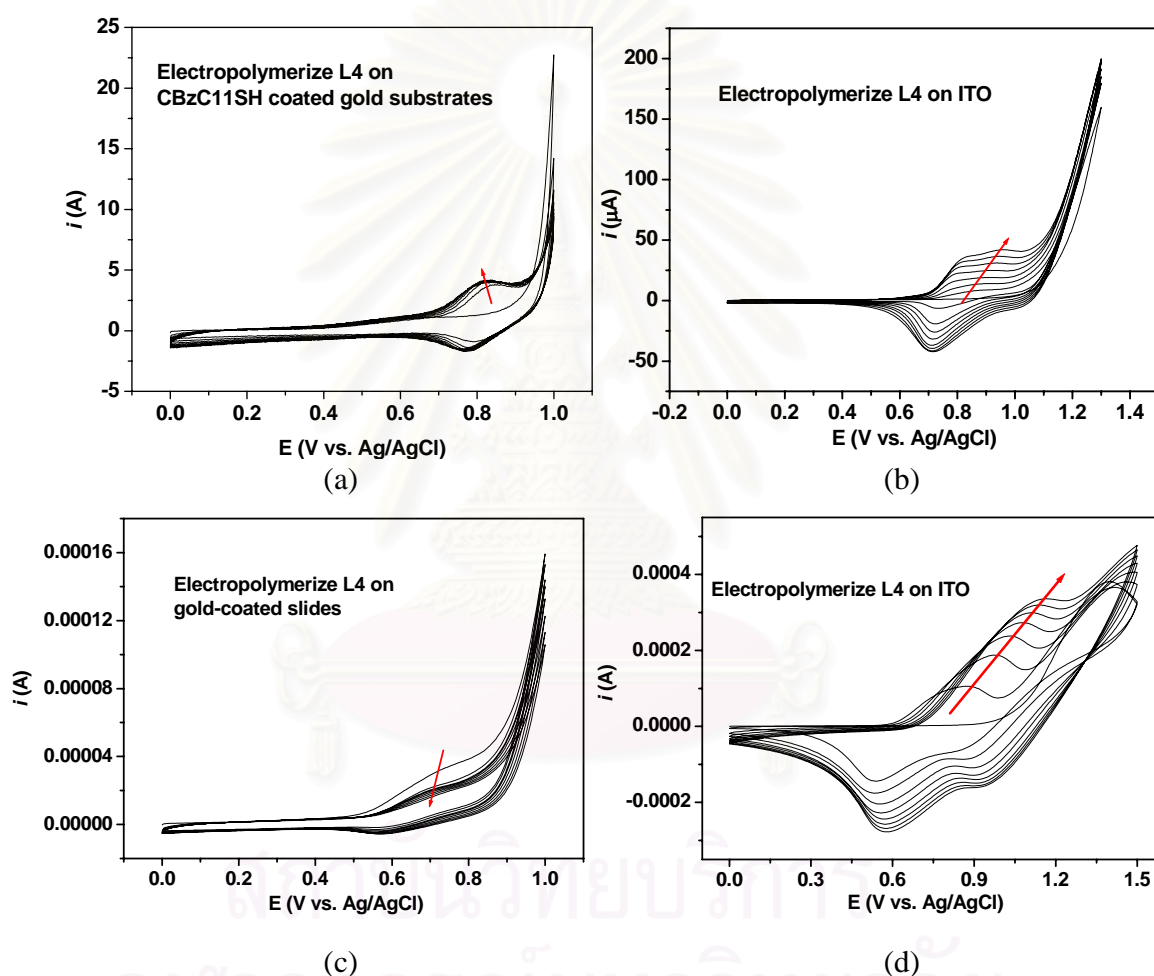


Figure 2.22 Cyclic voltammograms of the electrochemical cross-linking/deposition of **L4** at a scan rate of 50 mV/s, 8 cycles: (a) deposited material on **2.8** coated gold substrates (0-1.0 V), (b) on ITO substrates (0-1.3 V), (c) on gold-coated slides (0-1.0 V), and (d) on ITO substrates (0-1.5 V).

2.2.4.3 Morphological studies

The morphology before and after electropolymerization on the ITO, gold-coated slides, and **2.8** SAM coated gold substrates were characterized by AFM (Figure 2.23, Figure 2.24). **L4** was electropolymerized for 8 cycles at a range of 0 to 1000 mV at a scan rate 50 mV/s in 0.1 M TBAPF₆/anhydrous CH₂Cl₂ as electrolyte (WE, gold-coated slide; CE, Pt wire; RE, Ag/AgCl wire). In the case of direct deposition on unfunctionalized gold substrate, the morphology appeared to be more similar to bare gold, indicating very small quantity was deposited. When **2.8** SAM coated gold was used, the morphologies are relatively rough (Figure 2.23c). It implied that the deposition of the precursor material was achieved better on **2.8** coated gold substrates but were not as uniform as expected. The nucleation of **2.8** SAM may play a very important role during the polymerization, according to a previous report on polythiophene electrodeposition [110]. For the ITO substrates, a highly uniform morphology was observed with applied potentials from 0 to 1.3 V (Figure 2.24b). However in the case of higher applied potential (up to 1.5 V), the polymer films tended to give a rougher and patchy film (but complete coverage) as shown in Figure 2.24c.

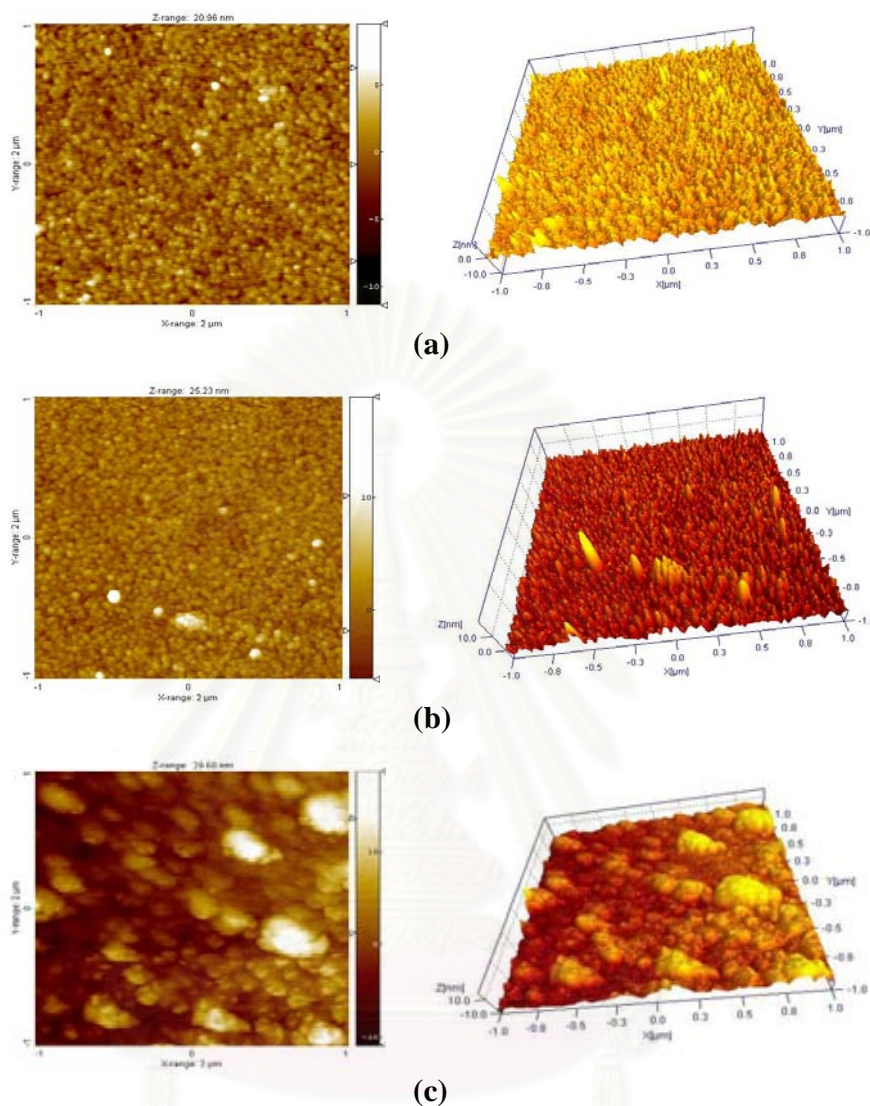


Figure 2.23 AFM images, the topological or height images (left) and three-dimensional topographic images (right): (a) bare gold, (b) poly hexahomotriazacalix[3]arene-carbazole (**PL4**) electropolymerized at 50 mV/s (0 to 1.0), 8 cycles in TBAPF₆/CH₂Cl₂ electrolyte (WE, gold-coated slides; CE, Pt wire; RE, Ag/AgCl wire), and (c) after electropolymerization of **PL4** at 50 mV/s (0 to 1.0), 8 cycles in TBAPF₆/CH₂Cl₂ electrolyte (WE, **2.8** coated gold substrates; CE, Pt wire; RE, Ag/AgCl wire).

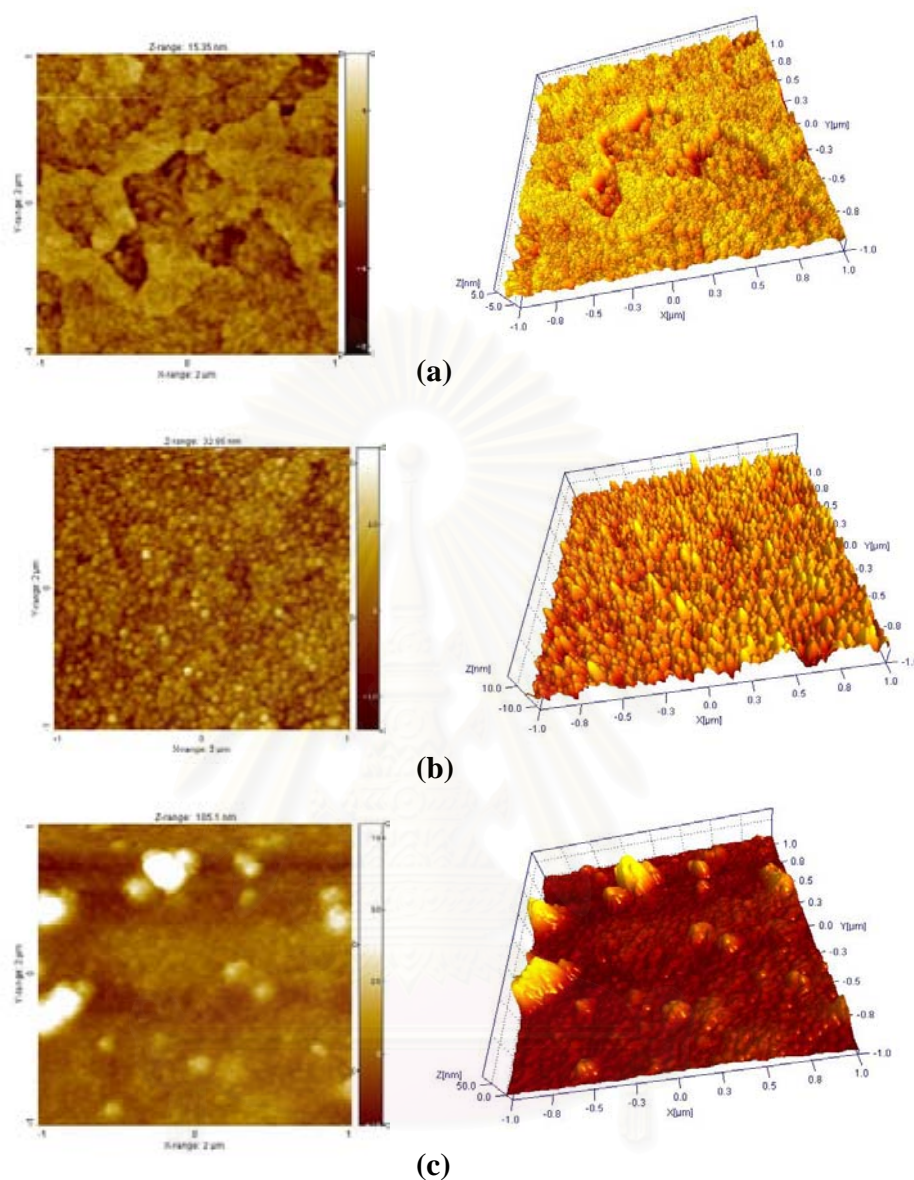


Figure 2.24 AFM images, the topological or height images (left) and three-dimensional topographic image (right): (a) bare ITO, (b) after electropolymerization of **L4** at 50 mV/s (0 to 1.3), 8 cycles in TBAPF₆/CH₂Cl₂ electrolyte (WE, ITO; CE, Pt wire; RE, Ag/AgCl wire), and (c) after electropolymerization of **L4** at 50 mV/s (0 to 1.5), 8 cycles in TBAPF₆/CH₂Cl₂ electrolyte (WE, ITO; CE, Pt wire; RE, Ag/AgCl wire).

2.2.4.4 Spectroelectrochemical studies

Spectroelectrochemical measurements were performed using a previously described set-up [111]. The spectroelectrochemical measurement of **PL4** was performed to investigate the cross-linking polymerization process *in-situ* and the presence of polaronic states associated with the formation of a more conjugated polymer.

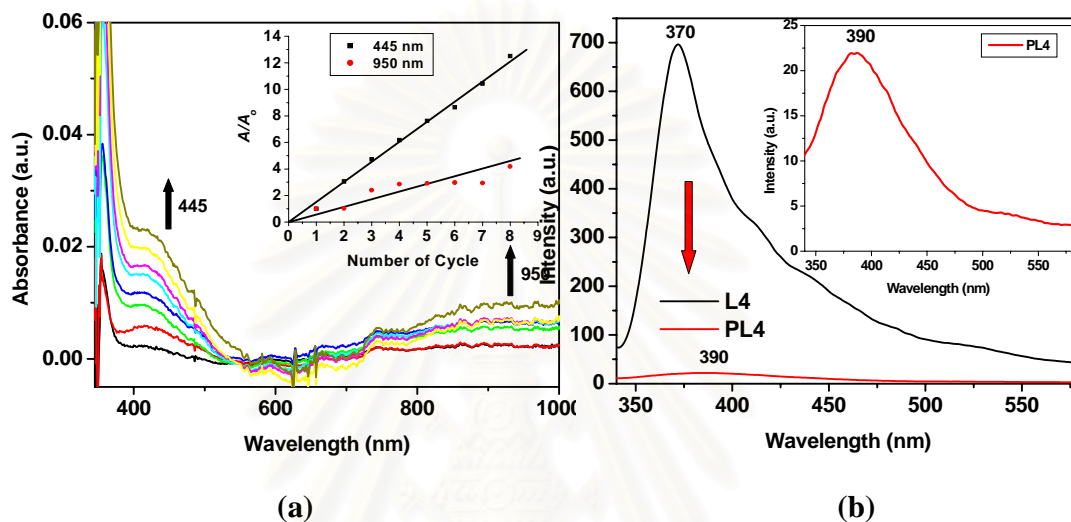


Figure 2.25 (a) Spectroelectrochemical analysis performed in 0.1 M TBAPF₆/CH₂Cl₂ of **L4**, growth of the 445 and 950 nm peaks during electrodeposition of **PL4**, spectra taken in situ at 0 V during each CV cycle, and (b) Fluorescence spectra before and after electropolymerization of **L4** which are taken at the excitation wavelength $\lambda = 320$ nm.

The *in-situ* UV-vis absorption spectra of **L4** were measured simultaneously with electropolymerization in a 0.10 M TBAPF₆/CH₂Cl₂ solution as electrolyte (WE, ITO; CE, Pt wire; RE, Ag/AgCl) at a scan rate of 50 mV/s. Figure 2.25a shows the extended appearance of the π - π^* transition at 307 nm and a shoulder at 445 nm, which are attributed to polycarbazole [112]. The broad peak centered at 950 nm can be assigned to the polaronic and bipolaronic bands originating from the formation of the conjugated polycarbazole species and their complexed ion redox couple with hexafluorophosphate ions. From the spectra, the peaks at 445 and 950 nm were tracked and showed a linear increase with increasing CV cycles indicating an even deposition of the polymer. In

addition to the electronic absorption properties, the fluorescence emission properties of polycarbazole further confirmed the crosslinking reaction [112]. It was found that the azacalix[3]arene-carbazole precursor shows a different fluorescence spectra before and after crosslinking. The fluorescence peak of the carbazole units present on **L4** was observed at 370 nm (Figure 2.25b) (film). After electropolymerization, this peak is quenched in the case of the solid state PPC-CBz film, where a new peak arises at 390 nm attributed to the formation of polycarbazole. This was also observed previously as in the case of CBz functionalized polybenzyl ether dendrimers in solution and solid-state carbazole containing polystyrenic CPN films [112].

2.2.4.5 Selectivity and sensitivity studies by using potentiometric measurements

The selectivity and sensitivity studies were first investigated by open-circuit potentiometry (an electrochemical cell potential set at zero current). The changes in potential (ΔE) were recorded simultaneously as a function of time at constant zero-current voltage. The experiment also tracks the redox state of the polymer since it can be influenced by either introducing an electric charge or adding a reagent (analyte) which interferes with the redox equilibrium. An increase in negative value of ΔE from the zero potential indicates an increase in conductivity. The selectivity studies by potentiometry were first performed using the electrochemically cross-linked **PL4** film on ITO against 100 mM of the various cations (TBACl 10 mM is present as supporting electrolyte). As shown in Figure 2.26a, the highest selectivity (biggest change in ΔE) was observed from Zn^{2+} compared with other cations. A priori, this situation may be due to the exact size and fit of the Zn^{2+} cation on the azacalix[3]arene, steric effect from the polymerback bone and hard soft acid and base principle (HSAB) [15,16]. The presence of the nitrogen atoms considered as a soft atom in azacalix[3]arenes allows them to bind soft cations (such as transition metals) [23,95]. Moreover, our previous work [95] have been shown that the azacalix[3]arene template can be specified sensor for Zn^{2+} in organic solution.

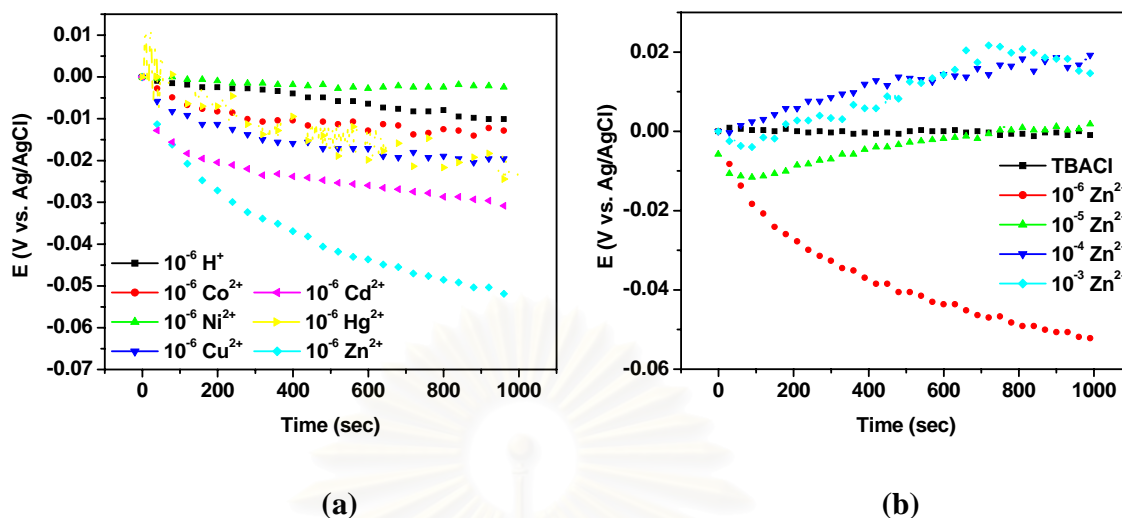


Figure 2.26 Potentiometric profiles of **PL4** on ITO in 10 mM TBACl aqueous solution: (a) various cation analytes, and (b) various concentrations of Zn^{2+} . Plotted data are within 5% deviation from several measurements.

However, by design, the hexahomotriazacalix[3]-tri(buthylcarbazole) was made to be specific for the Zn^{2+} cations compared to the other transition metals. In this case, the conductivity of the cross-linked polymer may increase with binding of the Zn^{2+} cations to the azacalix[3]arene pocket. This seemed to be readily achieved at 10^{-6} M where the other cations have little effect on the potential change since they did not have an exact fit on the azacalix[3]arene and thus showed little deviation from the zero point potential.

In general for the Zn^{2+} cations, after the lowest concentration (10^{-6} M), the ΔE did not decrease much over time (Figure 2.26b). For the other concentrations, the potential decreases in the first 100 seconds, followed by a gradual increase until it reaches a steady state. This is generally observed for all the other cations at higher concentrations (10^{-5} – 10^{-3} M). (see Figure 2.27). This indicates that the decrease of potential at 10^{-6} M of the cations over time is primarily due to the first cations being encapsulated in the cavity of azacalix[3]arene through cation-dipole interaction [95]. With increasing concentrations, the limited amount of the cavities does not allow further encapsulation and therefore

cations are free to complex with other species in the polymer backbone, i.e. driven by the interaction between the cations with doped anions (Cl^- and PF_6^-) and with extended π -conjugated polymer on the backbone. Thus, the potentiometric changes can be attributed from the increasing interference of the Zn^{2+} on charged species in the polymer such as polarons and bipolarons along with their neutralizing counterions which are independent species.

Clearly, on the basis of the potentiometric measurements in the presence of 10^{-6} M cations, the Zn^{2+} showed the best performance in terms of selectivity and sensitivity compared to the other cations. However, there is a need to further explain this phenomenon of the ΔE change beyond the HSAB principle and the presence of other independent ionic species in the polymer. The basic premise is that the other ions when not bound to the azacalix[3]arene cavity via a cation-dipole interaction are primarily involved with ion-pairing on the doped conjugated polymer and cation- π interaction between cations and π -extended conjugated polymer.

To begin with, the observed behavior can be correlated with the effect of charge-carrier properties on a conjugated polymer, i.e., hole transport and electron transfer properties of the polycarbazole to the cations. There are two explanations for the potential changes after the addition of different cations along with different concentrations: 1) one can first consider the contribution of electron transfer from the lone pair of nitrogen on the azacalix[3]arene moiety to the conjugated polymer backbone. This was confirmed by studying the complexation of protons with the azacalix[3]arene (see Figure 2.27a). As shown in Scheme 2.3a, protonation of nitrogen (ammonium formation) gives less efficiency for electron transfer to the polycarbazole. As a consequence, fewer holes can be generated and thus less conductivity enhancement or a smaller potential decrease would be expected, which is indeed the case; 2) the other consideration is based on the hole-transport throughout the whole polymer network in a three dimensional manner. Since the Zn^{2+} are complexed in the azacalix[3]arene cavities by ion-dipole interaction,

the holes not only move along the polymer backbones but also hop through the cations to improve the hole transport pathways in-between chains [114a].

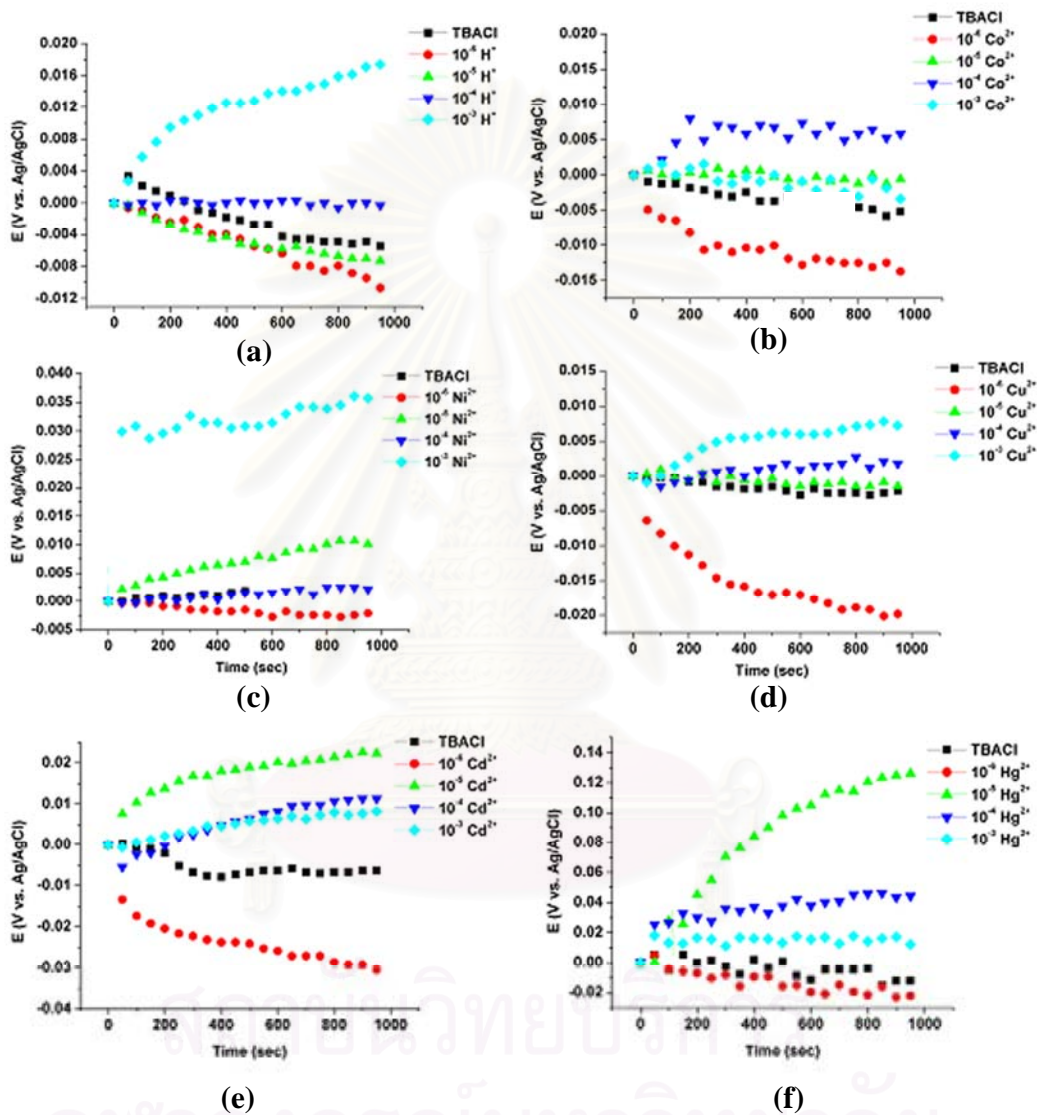
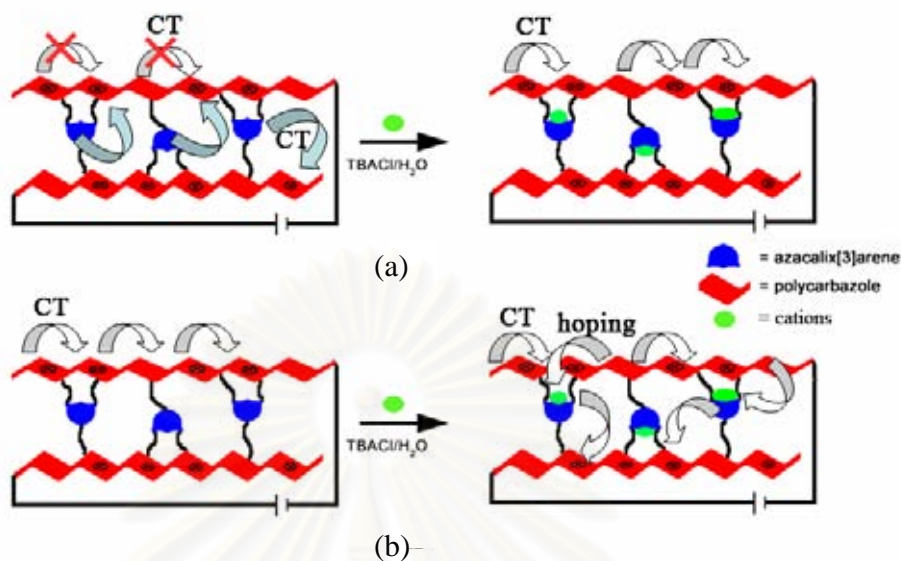


Figure 2.27 Potentiometric profiles of PL4 on ITO in aqueous solution in different concentration of cations at 0 V: (a) H^+ , (b) Co^{2+} , (c) Ni^{2+} , (d) Cu^{2+} , (e) Cd^{2+} , and (f) Hg^{2+} .



Scheme 2.3 The two explanations for the potential changes after the addition of cations (a) cations can be protected electron transfer to the conjugated polymer backbone, and (b) cations complexation can be a hole to improve the hole transport pathways in-between chains.

The other effect to consider is the competition with the free ions (overall ionic strength) and the ions bound on the doped polymer. With increasing concentration of the cations, the ion-ion and cations- π interactions increase and begin to reside proximal to the polymer backbones, pairing with the anions (Cl^- and PF_6^-) on the doped sequences of the polymer. Thus they tend to decrease the doping level of the polymer films by removing the anions paired to the polymer backbone and the stabilization of π -extended conjugated polymer by reducing electron cloud on the polymer backbone. Consequently, the net potential shift is attributed from the competition of these two effects. The flux of the cations into the polymer films may proceed in two steps: at first they diffuse into the polymer and selectively bind with the azacalix[3]arene cavities, which enhances the conductivity. If all the cavities have been filled up, the cations would slowly disperse to

the sequences occupied by the dopants, which interrupts the polymeric conjugation and decreases the hole mobility.

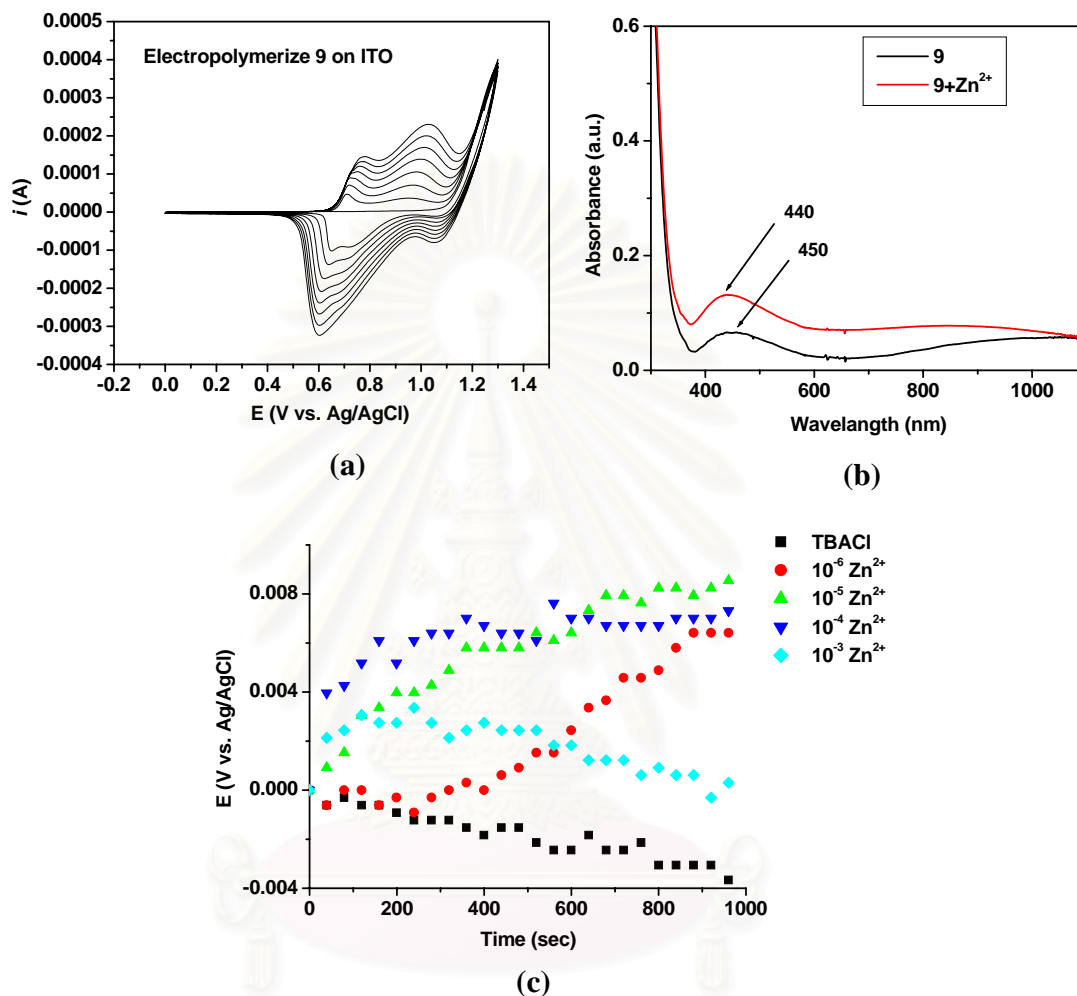


Figure 2.28 (a) Cyclic voltammograms electrochemical cross-linking/deposition of **2.9** polymerization at a scan rate of 50 mV/s, 8 cycle deposited material on ITO substrates., (b) The UV-Vis absorption spectrum of **2.9** films before and after addition of Zn^{2+} cations $10^{-3} M$ on ITO substrates, and (c) Potentiometric profiles of **2.9** on ITO in aqueous solution in different concentration of Zn^{2+} at 0 V.

In principle the conductivity of conjugated polymers can be fine tuned by changing charge transport pathways. Previous studies [114] correlated that the three-dimensional connectivity for bipolaron migration was caused by the close contacts between planar π -extended polymers which efficiently promote an interstrand charge hopping and consequently facilitates charge delocalization. On the other hand, the minimization of cross-communication of the conjugated polymer backbones can remarkably change the conductivity profile by reducing the dimensionality of charge transporting pathways [115]. As a control experiment, 9-(4-(9H-carbazol)-9H-carbazole (**2.9**) was used. The data showed only a little increase of ΔE in the Figure 2.28.

2.2.4.6 Selectivity and sensitivity studies by using spectroelectrochemical measurements

Spectroelectrochemical studies were also performed to support the order of cation sensitivity and selectivity. As expected, the addition of 10^{-3} M cations into the cell containing the films resulted in different changes in the absorption spectra. The blue shift (≈ 45 nm) from 455 nm to 405 nm and 950 nm to 910 nm upon the addition of Ni^{2+} , Cu^{2+} , Cd^{2+} and Hg^{2+} suggests that conjugation of the polycarbazole is indeed decreased, consistent with the above discussion in the potentiometric measurements. However, little change in the absorption spectra of **PL4** was observed upon the addition of Zn^{2+} and Co^{2+} and can be attributed primarily to an allosteric effect. This suggests that the Zn^{2+} and Co^{2+} ions are primarily bound in the cavity of azacalix[3]arene by cation-dipole interaction. This was also confirmed by the addition of protons. As can be seen from Figure 2.29, there is a slight blue shift with protons primarily bound on the nitrogen of azacalix[3]arene, but the interference is much weaker than the metal ions, maintaining the polymeric conjugation to a large extent. From the Co^{2+} spectrum, this may imply that Co^{2+} ion may compete with Zn^{2+} for the azacalix[3]arene specificity. However, the blue shift (~ 10 nm) from 450 to 440 nm occurred upon the addition of Zn^{2+} in the control

experiment (Figure 2.28b). From this data, the blue shift can be explained by cation- π interactions between the cations and the conjugated polymers.

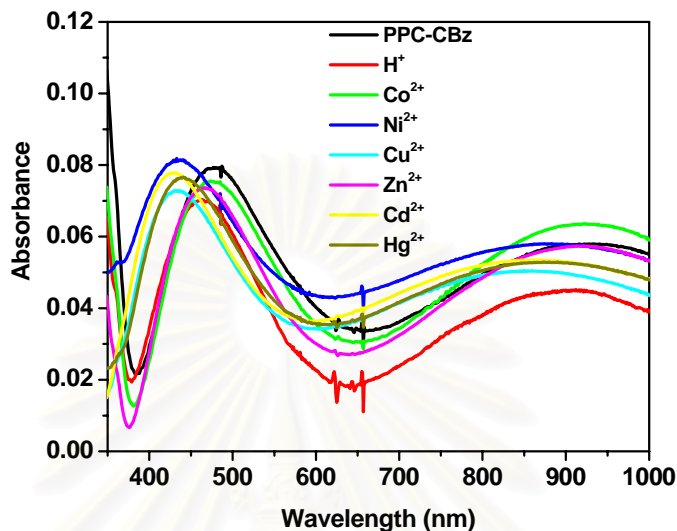


Figure 2.29 The UV-vis absorption spectrum of **PL4** films upon the addition of different cations with the concentration 10^{-3} M on ITO substrates.

2.2.4.7 Selectivity and sensitivity studies by using electrochemistry and quartz crystal microbalance method (EC-QCM)

Additionally, we combined electrochemistry and quartz crystal microbalance method (EC-QCM) to confirm the sensitivity and selectivity of **PL4**. This method is very informative for probing mass-transport processes into thin films [111]. The mass deposition per cycle was measured during electropolymerization and showed a general decrease in frequency with each cycle over time, indicating a continuous deposition on the substrate (Figure 2.30a). After the deposition of **PL4** on the EQCM probe, aqueous solutions of the cations were added. In general, the Butterworth-van Dyke (BD) equation provides a method for relating the electrical properties of the quartz resonator to the mechanical properties of the deposited film [116]. The relationship between ΔR and Δf under liquid loading was derived from BD equation [117]. The increase in ΔR is

correlated with an increase in the viscoelasticity of the layer adjacent to the crystal surface while a small change in ΔR is indicative of a more rigid adsorbed layer.

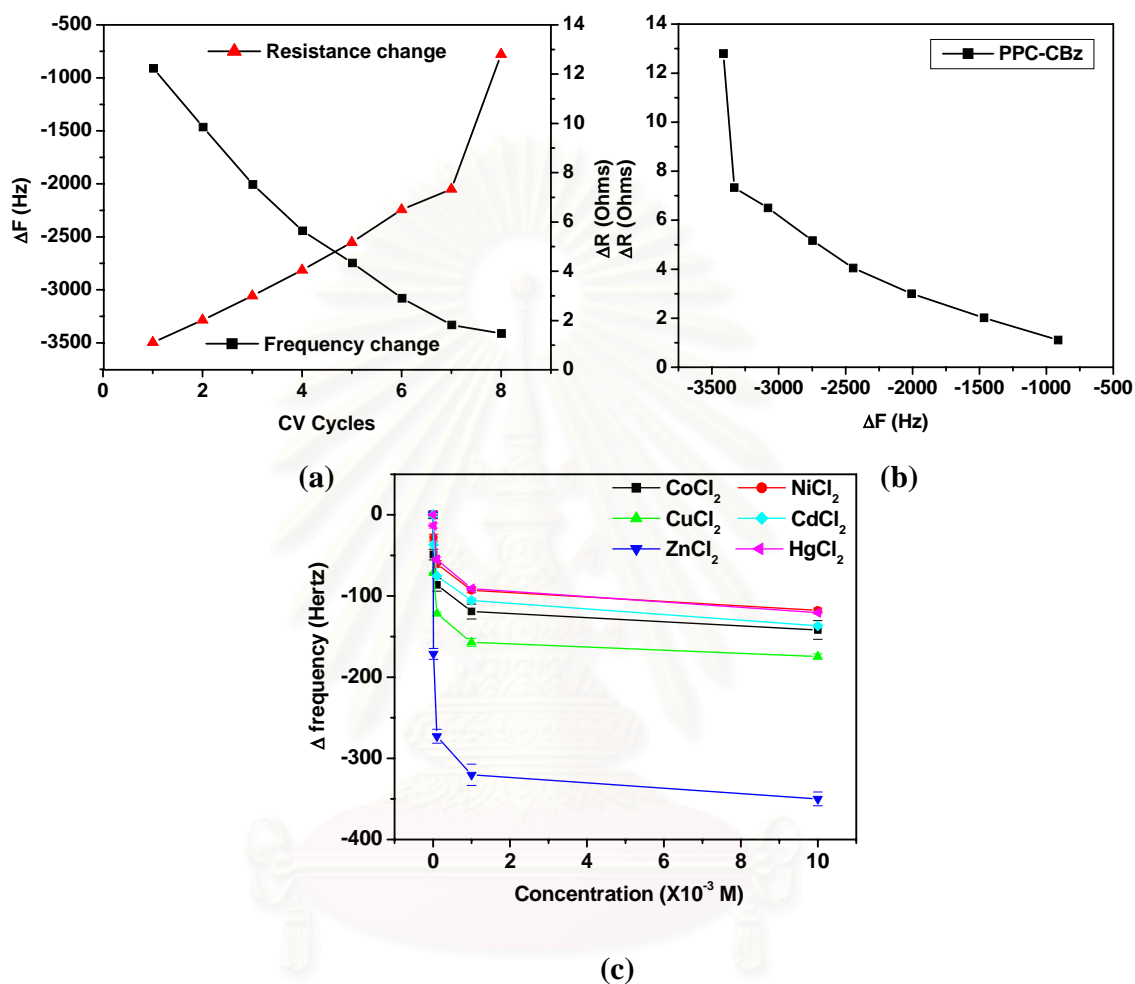


Figure 2.30 Electrochemical quartz crystal microbalance studies: (a) ΔF , frequency change and ΔR , resistance change during the CV cycling., (b) Changes in the viscoelastic behavior in the polymers., and (c) ΔF , frequency change as a function of different cations concentration.

From Figures 2.30a and 2.30b, the resistance increased with each cycle indicating increasing rigidity (viscoelastic behavior) of the films with more layers deposited. In

general, with oxidation and reduction, the change in resistance indicates the transport of the ions in and out of the cross-linked film. After cross-linking, the addition of Zn^{2+} caused a rapid increase of the mass of the deposited polymer (Figure 2.30c). This was the highest for the Zn^{2+} as compared to the other ions. Analysis of the mass-concentration relationship, according to the Langmuir equation ($1/\Gamma = 1 + 1/KC_M$, where $\Gamma = \Delta m/\Delta m_{\max}$, C_M is the metal ion concentration and K the complexation constant) was made [118]. The binding ability of **PL4** towards cations thus varies as follows: Zn^{2+} ($K = 1.1 \times 10^6 \text{ M}^{-1}$) > $\text{Cu}^{2+} \approx \text{Co}^{2+}$ ($K = 9.0 \times 10^5 \text{ M}^{-1}$) > $\text{Ni}^{2+} \approx \text{Hg}^{2+}$ ($K = 3.3 \times 10^5 \text{ M}^{-1}$) > Cd^{2+} ($K = 2.5 \times 10^5 \text{ M}^{-1}$).

2.2.4.8 Selectivity and sensitivity studies by using electrochemistry and surface plasmon spectroscopy method (EC-SPR)

SPR spectroscopy was combined with an electrochemistry setup to study the efficiency of transport and sensitivity of Zn^{2+} ions with **PL4** films. As shown in the EC-SPR measurements (Figure 2.31), the reflectivity increases with increasing CV cycles, indicating the continuous deposition of the film onto the **2.8** SAM coated gold substrates. The subsequent doping and dedoping of the films with oxidation and reduction cycles are shown in the reversible reflectivity change which consists of either a change in dielectric constant or thickness [119]. The sensing experiment was conducted by injecting different concentrations of Zn^{2+} into SPR cell embedded with the as-deposited polymer film on Au working electrode. From the SPR sensorogram (Figure 2.31b), a sudden change was observed on the reflectivity upon injecting 10^{-6} and $10^{-5} \text{ M Zn}^{2+}$ and a peak saturation was observed upon injection of 10^{-4} M and higher concentrations. The concentrations at this level are not expected to give a measurable change in reflectivity [120]. This indicated that the association of Zn^{2+} with the film primarily induced the dielectric constant change assuming the thickness was constant. It is also interesting to note that the highest change was observed with 10^{-6} and $10^{-5} \text{ M Zn}^{2+}$ concentrations, indicating that at these concentrations, the azacalix[3]arene units are fully bounded and that excess ions do

not participate in a significant dielectric constant change to the film, similar to the results with open-circuit potentiometry. This confirms that the allosteric effect is mostly observed only at lower concentrations of the Zn^{2+} cation and that at higher concentrations, the excess ion does not participate in binding to the azacalix[3]arenes.

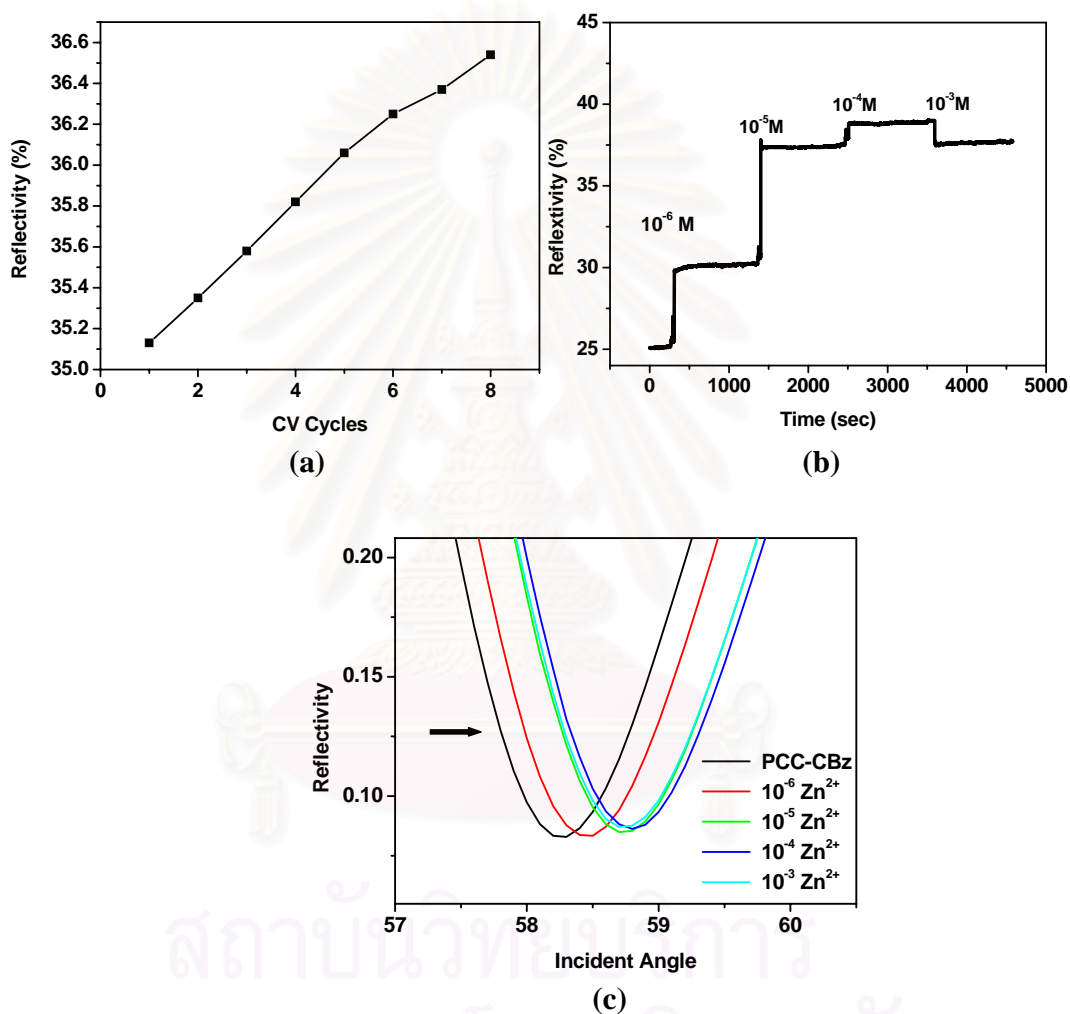


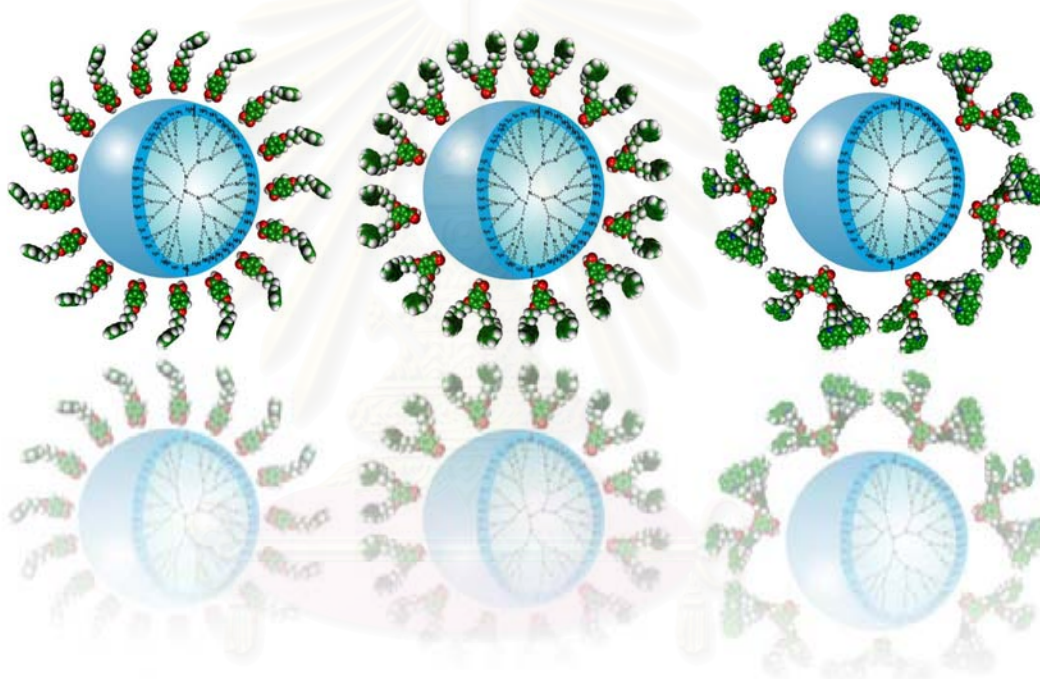
Figure 2.31 EC-SPR and SPR studies of **PL4** on **2.8** coated gold substrates: (a) kinetic measurement during deposited film, (b) kinetic sensorogram at different concentrations of Zn^{2+} , and (c) angular sensorogram at different concentrations of Zn^{2+} .

CHAPTER III

ELECTROCHEMICALLY REACTIVE DENDRIMERS

3.1 Lord of the nano-rings: self-assembly and electropolymerization of PAMAM-carbazole dendron surfmer complexes

3.1.1 Introduction



Supramolecular nanostructures derived from self-organizing molecules and macromolecules are of high interest for achieving new functions and properties in the fields of material science and chemical biology [121]. Dendrimeric self-assembly [67,122] especially in the case of polyamidoamine (PAMAM) dendrimers, have attracted increasing attention in recent years because of their unique structure, interesting properties, and ready availability. Their potential applications in medicine, catalysis, gene therapy, and nanoreactor systems have been explored in the last decade or so [123]. These dendrimers are composed of a central core (ethylenediamine core, in this study)

with amidoamine branching units that extend outward in a symmetric fashion and consist of n generations (layers). It is a monodispersed, highly branched macromolecule with primary amine functional groups on the surface and amido units at the branch points in the interior. Recently, a number of studies have focused on the interaction and aggregation behavior between PAMAM dendrimers and surfactants in aqueous solution such as SDS [124], poly(ethylene glycol) [125], and dodecanoic acid [126]. However, up to now, there has been no attempt to use PAMAM-surfactant complexes as templates for direct polymerization.

Template polymerization is a useful method to obtain multicomponent materials [127]. A polymer can be used as a template to associate monomers by non-covalent interactions such as hydrogen bonding, electrostatic forces, dipole forces, and other interactions, followed by polymerization of the monomers on the contours of the template [128]. Thus a template acts as a structure-directing agent guiding the topology of the polymerization process. In direct templating, a change of dimensions or phase transitions occurs, and the templated material becomes a 1:1 copy of a template. Template polymerization of polyelectrolyte-surfactant monomer (surfmmer) complexes is a primary example and has been previously reviewed [129,130,131]. They were successfully demonstrated in the polymerization of a variety of lipid assemblies with preservation of the mesostructures. However, γ -irradiation have been shown to degrade the monomer in the initiation step of a polymerization reaction within smectic liquid-crystalline layers [132]. Recently, Faul et al. [129] have been able to preserve the lamellar phase structure of polyelectrolyte-surfmmer surfactant (di(undecenyl)phosphate and α - ω -diene) complexes through a dithiol polyaddition strategy.

Electroactive groups such as pyrrole [133a,133b] and thiophene [133c,133d] containing surfactants has the potential for producing new hybrid and electro-optical materials. Because of the electroactive moieties, they are not only polymerizable but also potentially electrically conductive when polymerized. Nanowire structures of pyrrole and thiophene have been realized which could serve as new conducting fibers. On the other

hand, carbazole polymers have been of recent interest due to their interesting electrochemical homopolymerization and copolymerization behavior [112]. They exhibit interesting electrochromic properties as well [134]. The ability of polycarbazole to form two distinct oxidation states further leads to multichromic effects [107]. Furthermore, polycarbazole is well-known as a hole transport material [135].

3.1.2 Objectives of this research

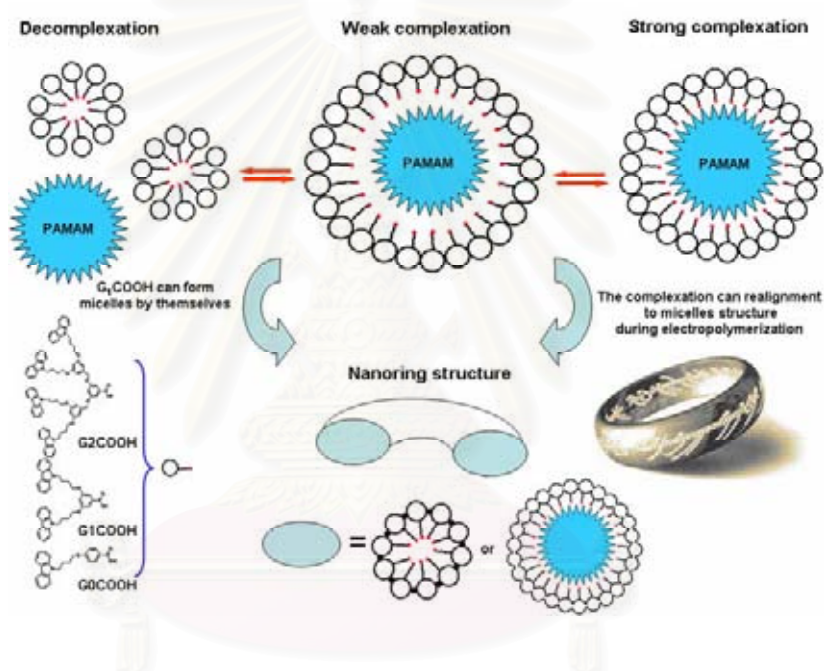


Figure 3.1 PAMAM dendrimer generation 4 with carboxylic acid terminal dendrons containing peripheral electroactive carbazole groups of different generations (G₀COOH, G₁COOH and G₂COOH) and possibility to form nano-ring structures.

In this part, we report a detailed and quantitative study on the supramolecular complexation of amine functionalized PAMAM dendrimer generation 4 with carboxylic acid terminal dendrons containing peripheral electroactive carbazole groups of different

generations ($G_0\text{COOH}$, $G_1\text{COOH}$ and $G_2\text{COOH}$) (Figure 3.1). The focus is on a detailed understanding and mechanism of complex formation and subsequent electropolymerization properties with the different generation of the dendron surfmers. In the process, we observed the formation of interesting nano-ring structures that preceded the electropolymerization process. The rest of the work involved understanding the nature of this nanostructure formation. We believe that this is only one of a few rare reports in which template polymerization was applied with a dendrimer-surfmer complex via electropolymerization.

3.1.3 Experimental section

3.1.3.1 Synthesis of carbazole dendrons to complex with dendrimer

a) General procedure

a1) Materials

Unless otherwise specified, the solvents and all materials were reagent grades purchased from Fluka, BHD, Aldrich, Carlo Erba, Merck or J.T. Baker and were used without further purification. Commercial grade solvents such as acetone, dichloromethane, hexane, methanol and ethylacetate were purified by distillation before used. Acetonitrile and dichloromethane for set up the reaction were dried over calcium hydride and freshly distilled under nitrogen atmosphere prior to use. Tetrahydrofuran was dried and distilled under nitrogen from sodium benzophenone ketyl immediately before use. Column chromatographies were carried out on silica gel (Kieselgel 60, 0.063-0.200 nm, Merck). Thin layer chromatography (TLC) were performed on silica gel plates (Kieselgel 60, F₂₅₄, 1mm, Merck). Compound on TLC plates were detected by the UV-light. All manipulations were carried out under nitrogen atmosphere.

a2) Instrumentations

Nuclear magnetic resonance (NMR) spectra were recorded on a Varian 400 MHz spectrometer and a General Electric QE-300 spectrometer at 300 MHz in deuterated solvent. Chemical shifts (δ) are reported in parts per million and the residual solvent peak was used as an internal standard.

Absorption spectra were measured by a Varian Cary 50 and HP-8453 UV-vis spectrometer. UV-vis titration spectra were measured by a Perkin Elmer Lambda 25 spectrophotometer at 25 °C.

Fluorescence spectra were recorded by Perkin Elmer SL50B fluorescence and a PerkinElmer LS 45 spectrophotometer.

FT-IR spectra were obtained using a FTS 7000 Spectrometer (Digilab now Varian Inc.) equipped with a liquid N₂-cooled MCT detector and a Nicolet Impact 410. KBr pellets were prepared by first mixing the sample solutions with KBr, removing solvents under vacuum and then pressing the KBr using a 10-ton hydraulic press.

MALDI-TOF mass spectra were recorded on a Biflex Bruker Mass spectrometer with 2-Cyano-4-hydroxycinnamic acid (CCA) or 2,5-Dihydroxy-benzoic acid (DHB) as matrix.

Water contact angle measurements (Model CAM-Micro, Tantec Inc.) were taken before and after complexation to ensure modification on PAMAM by monitoring the change in hydrophilicity of the surface for the glass substrates.

Elemental analysis was carried out on CHNS/O analyzer (Perkin Elmer PE2400 series II).

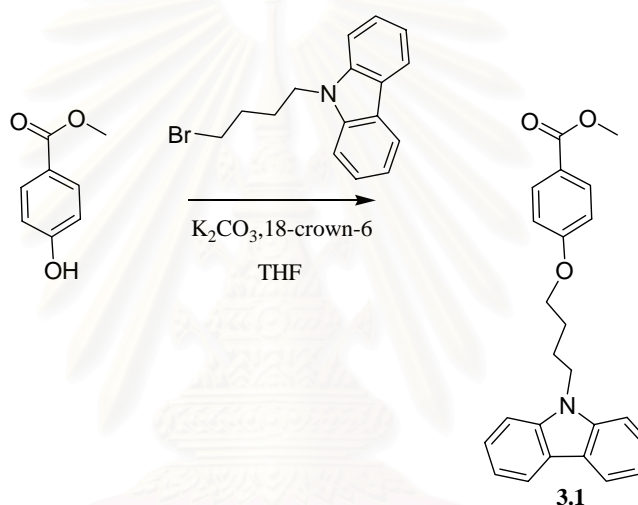
The cyclic voltammetry (CV) experiments were carried out on a Princeton Applied Research Parstat 2263 with a modified ITO substrate as the working electrode coupled with a Pt plate counter and Ag/AgCl reference electrode. Cyclic voltammetry was utilized to prepare the cross-linked films from very concentration of the precursor polymer solution of 0.1 M TBAPF₆/CH₂Cl₂.

Atomic force microscopy (AFM) imaging was examined in ambient conditions with a PicoSPM II (PicoPlus System, Molecular Imaging [now Agilent Technologies Tempe, AZ.] in the Tapping mode (AAC mode)).

b) Synthesis

b1) Synthesis of carbazole dendrons ($G_0\text{COOH}$, **3.2**)

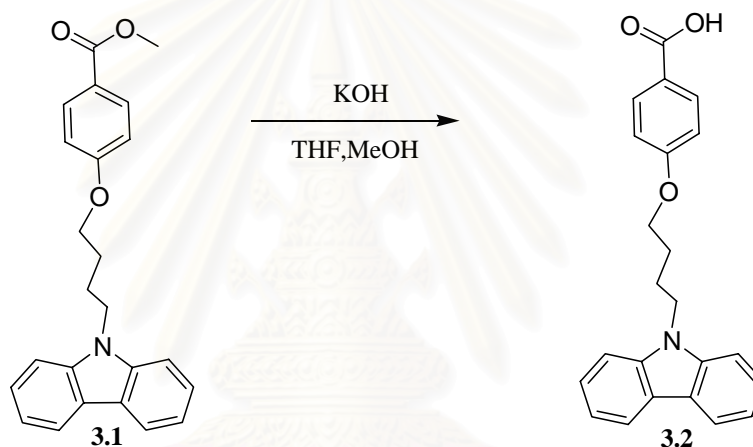
Methyl 4-[4-(9H-Carbazol-9-yl)butoxy]benzoate ($G_0\text{COOC}_2\text{H}_5$, **3.1**)



A mixture of 9-(4-bromobutyl)-9H-carbazole (9.03 g, 29.87 mmol), methyl 4-hydroxybenzoate (5.00 g, 32.86 mmol), anhydrous potassium carbonate (12.39 g, 89.63 mmol), and 18-crown-6 (3.95 g, 14.94 mmol) in anhydrous THF (150 mL) was refluxed with vigorous stirring under nitrogen for 72 hours. After cooling to room temperature, the mixture was concentrated to dryness under reduced pressure. The residue was partitioned between CH₂Cl₂ and H₂O and the aqueous layer was extracted with CH₂Cl₂ (3×50 mL). The combined organic layers were dried with anhydrous Na₂SO₄ and the solvents evaporated. The product was purified by column chromatography on silica gel eluting with CH₂Cl₂/hexane (3:7) to give **3.1** as a white solid (8.60 g, 70 % yield).

Characterization data for 3.1

¹H-NMR (300 MHz, CDCl₃): δ (ppm) 8.23 (d, *J* = 7.8 Hz, 2H, Ar*H*), 8.08 (d, *J* = 8.7 Hz, 2H, Ar*H*), 7.50-7.58 (m, 4H, Ar*H*), 7.38 (t, *J* = 1.2 Hz, 2H, Ar*H*), 6.94 (d, *J* = 6.6 Hz, 2H, Ar*H*), 4.47 (t, *J* = 6.6 Hz, 2H, NCH₂CH₂), 4.02 (t, *J* = 6.6 Hz, 2H, OCH₂CH₂), 4.00 (s, 3H, OCH₃), 2.12 (m, 2H, NCH₂CH₂CH₂), 1.93 (m, 2H, OCH₂CH₂CH₂)

4-[4-(9H-Carbazol-9-yl)butoxy]benzoic Acid (G₀COOH, 3.2)

A mixture of compound **3.1** (3.73 g, 10.00 mmol) and KOH (5.61 g, 100.00 mmol) in tetrahydrofuran/methanol (55 mL/110 mL) was refluxed with vigorous stirring for overnight. After cooling to room temperature, the mixture was concentrated to dryness under reduced pressure. The residue was acidified to pH 2-3 with HCl, then the precipitate was filtered and washed with ether to give **3.2** as a white solid (3.32 g, 92 % yield).

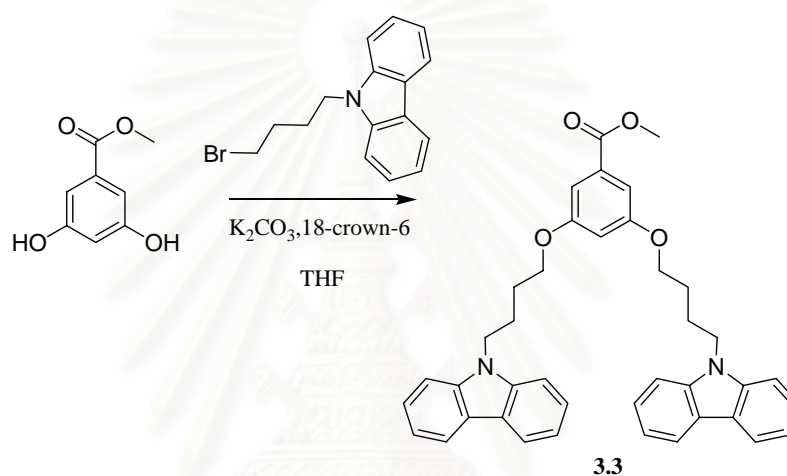
Characterization data for 3.2

¹H-NMR (300 MHz, CDCl₃): δ (ppm) 8.20 (d, *J* = 7.5 Hz, 2H, Ar*H*), 8.12 (d, *J* = 8.4 Hz, 2H, Ar*H*), 7.59-7.49 (m, 4H, Ar*H*), 7.33 (t, *J* = 7.8 Hz, 2H, Ar*H*), 6.96 (d, *J* = 8.7 Hz,

2H, ArH), 4.51 (t, $J = 6.6$ Hz, 2H, NCH₂CH₂), 4.08 (t, $J = 5.4$ Hz, 2H, OCH₂CH₂),), 2.20 (m, 2H, NCH₂CH₂CH₂), 1.96 (m, 2H, OCH₂CH₂CH₂)

b2) Synthesis of carbazole dendrons (G₁COOH, 3.4)

Methyl 3,5-Bis[4-(9H-carbazol-9-yl)butoxy]benzoate (G₁COOCH₃, 3.3)

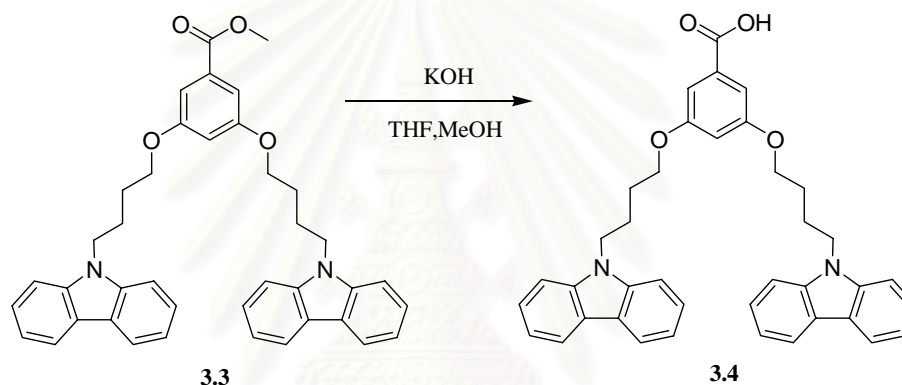


A mixture of *N*-(4-bromobutyl)-9*H*-carbazole (15.22 g, 50.37 mmol), methyl 3,5-dihydroxybenzoate (3.94 g, 23.40 mmol), anhydrous potassium carbonate (21.00 g, 159.94 mmol), and 18-crown-6 (0.45 g, 2.8 mmol) in anhydrous acetone (500 mL) was refluxed with vigorous stirring under nitrogen for 72 hours. After cooling to room temperature, the mixture was concentrated to dryness under reduced pressure. The residue was then partitioned between CH₂Cl₂ (500 mL) and H₂O (400 mL). The combined organic layers were dried with anhydrous Na₂SO₄. After removal the solvent, the residue was recrystallized from ethyl acetate to give **3.3** as a white solid in 70 % yield.

Characterization data for 3.3

$^1\text{H-NMR}$ (300 MHz, CDCl_3): δ (ppm) 8.19 (d, $J = 7.8$ Hz, 4H, ArH_{CBz}), 7.57-7.49 (m, 8H, ArH_{CBz}), 7.35-7.29 (m, 4H, ArH_{CBz}), 6.71 (s, 2H, ArH), 4.49 (t, $J = 7.2$ Hz, 4H, NCH_2CH_2), 4.04 (t, $J = 5.4$ Hz, 4H, OCH_2CH_2), 2.27 (s, 3H, OCH_3), 2.21 (m, 4H, $\text{NCH}_2\text{CH}_2\text{CH}_2$), 1.95 (m, 4H, $\text{OCH}_2\text{CH}_2\text{CH}_2$)

3,5-Bis[4-(9H-carbazol-9-yl)butoxy]benzoic Acid, G_1COOH , 3.4



A mixture of compound **3.3** (3.00 g, 4.91 mmol) and KOH (2.76 g, 49.12 mmol) in tetrahydrofuran/methanol (30 mL/60 mL) was refluxed with vigorous stirring for overnight. After cooling to room temperature, the mixture was concentrated to dryness under reduced pressure. The residue was acidified to pH 2-3 with HCl, and then the precipitate was filtered and washed with ether to afford **3.4** as a white solid (2.76 g, 94 % yield).

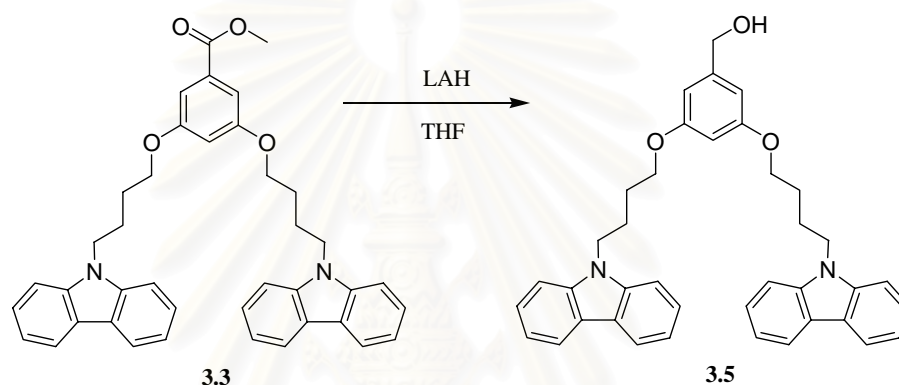
Characterization data for 3.4

$^1\text{H-NMR}$ (300 MHz, CDCl_3): δ (ppm) 8.09 (d, $J = 7.8$ Hz, 4H, ArH), 7.84-7.39 (m, 8H, ArH), 7.24-7.17 (m, 4H, ArH), 7.16 (s, 2H, ArH), 6.57 (s, 1H, ArH), 4.40 (t, $J = 6.3$ Hz,

4H, NCH₂CH₂), 3.94 (t, *J* = 6.0 Hz, 4H, OCH₂CH₂), 2.08 (m, 4H, NCH₂CH₂CH₂), 1.84 (m, 4H, OCH₂CH₂CH₂)

b3) Synthesis of carbazole dendrons (G₂COOH, 3.7)

3,5-bis(4-(9H-carbazol-9-yl)butoxy)phenyl)methanol (G₁COH, 3.5)

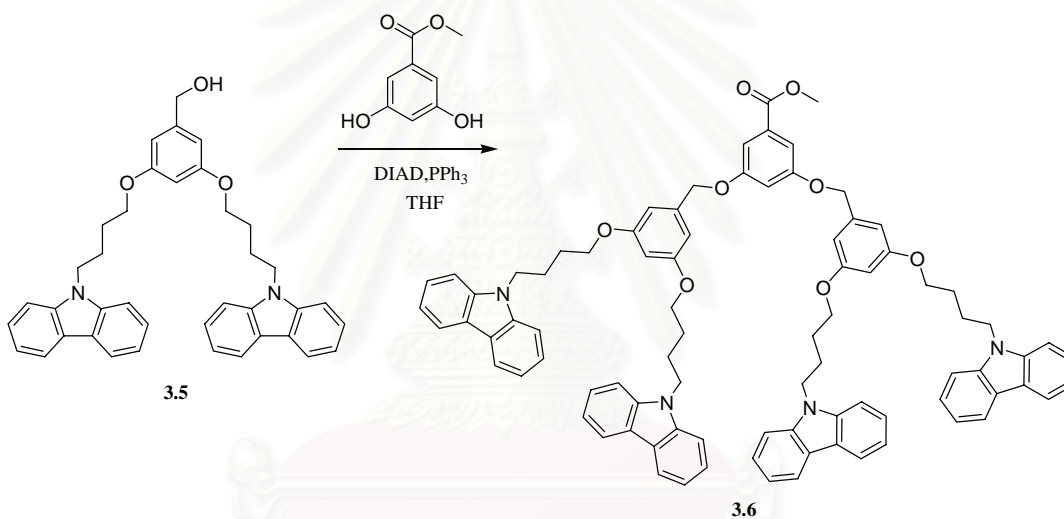


A solution of compound **3.3** (9.50 g, 15.50 mmol) in 400 ml of THF was slowly added dropwise into a suspension of LAH 1.0 g (23.30 mmol) in 300 ml of THF cooled to 0 °C with an ice bath. The suspension was stirred at room temperature for 4 hours. The reaction was quenched by addition of water, and THF was removed under reduced pressure. The crude residue was neutralized by HCl and extracted with CH₂Cl₂. The combined organic layers were dried with anhydrous Na₂SO₄ and solvents were evaporated off. The product was purified by column chromatography on silica gel eluting with CH₂Cl₂/hexane/ethyl acetate: 20/4/1 to give **3.5** as a white solid (8.13 g, 90 % yield).

Characterization data for 3.5

¹H-NMR (300 MHz, CDCl₃): δ (ppm) 8.10 (d, *J* = 7.5 Hz, 4H, Ar*H*), 7.53-7.42 (m, 8H, Ar*H*), 7.25-7.22 (m, 4H, Ar*H*), 6.45 (d, 2H, *J* = 2.1 Hz, Ar*H*), 6.28 (t, 1H, *J* = 2.1 Hz, Ar*H*), 4.59 (s, 2H, ArCH₂OH), 4.39 (t, *J* = 6.9 Hz, 4H, NCH₂CH₂), 3.91 (t, *J* = 6.2 Hz, 4H, OCH₂CH₂), 2.12-2.02 (m, 4H, NCH₂CH₂CH₂), 1.87-1.78 (m, 4H, OCH₂CH₂CH₂)

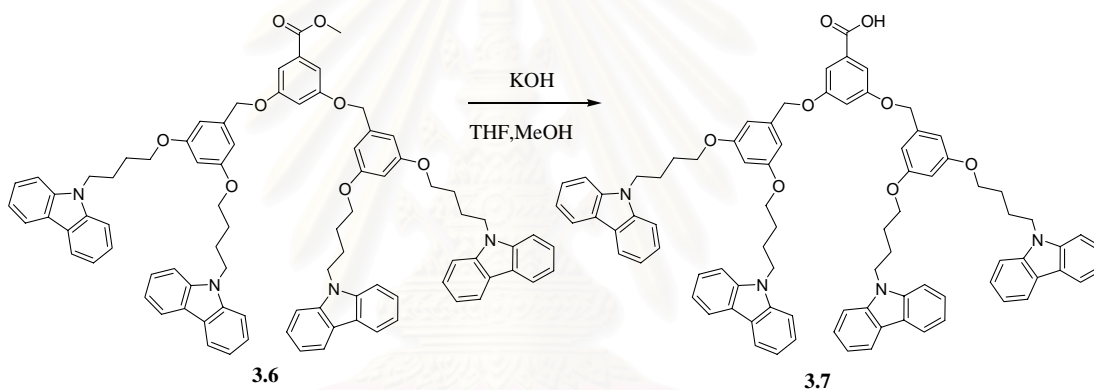
Methyl-3,5-bis(3',5'-bis(4-(9H-carbazol-9-yl)butoxy)benzyloxy)benzoate (G₂COOCH₃, 3.6)



A mixture of methyl 3,5-dihydroxybenzoate (0.86 g, 5.15 mmol), compound **3.5** (6.00 g, 10.30 mmol) and PPh₃ (2.70 g, 10.30 mmol) in 50 mL THF was cooled to 5 °C with an ice bath. A solution of DIAD (2.08 g, 10.30 mmol) in 3 mL THF was added dropwise under nitrogen. The solution was stirred for 1.5 hours. The product was purified on silica gel by using 4:1 CH₂Cl₂: hexane as eluent to afford **3.6** as a white solid in 84 % yield.

Characterization data for 3.6

¹H-NMR (300 MHz, CDCl₃): δ (ppm) 8.09 (d, *J* = 7.5 Hz, 8H, Ar*H*), 7.48-7.39 (m, 16H, Ar*H*), 7.27-7.21 (m, 8H, Ar*H*), 7.19 (d, 2H, *J* = 2.1 Hz, Ar*H*), 6.76 (t, 1H, *J* = 2.1 Hz, Ar*H*), 6.50 (d, 4H, *J* = 2.1 Hz, Ar*H*), 6.31 (t, 2H, *J* = 2.1 Hz, Ar*H*), 4.94 (s, 4H, ArCH₂OAr), 4.37 (t, *J* = 7.5 Hz, 8H, NCH₂CH₂), 3.91-3.87 (m, 11H, OCH₂CH₂ and COOCH₃), 2.08-2.03 (m, 8H, NCH₂CH₂CH₂), 1.85-1.78 (m, 8H, OCH₂CH₂CH₂)

3,5-bis(3',5'-bis(4-(9H-carbazol-9-yl)butoxy)benzyloxy)benzoic acid (G₂COOH, 3.7)

A mixture of compound **3.6** (2.00 g, 1.56 mmol) and KOH (0.87 g, 15.41 mmol) in tetrahydrofuran/methanol (30 mL/60 mL) was refluxed with vigorous stirring for overnight. After cooling to room temperature, the mixture was concentrated to dryness under reduced pressure. The residue was acidified to pH 2-3 with HCl, and then the precipitate was filtered and washed with ether to give **3.7** as a white solid (1.51 g, 75 % yield).

Characterization data for 3.7

¹H-NMR (300 MHz, CDCl₃): δ (ppm) 8.07 (d, $J = 7.8$ Hz, 8H, ArH), 7.45-7.37 (m, 16H, ArH), 7.30-7.17 (m, 10H, ArH and ArH), 6.79 (s, 1H, ArH), 6.48 (s, 4H, ArH), 6.30 (s, 2H, ArH), 4.93 (s, 4H, ArCH₂OAr), 4.35 (t, $J = 7.2$ Hz, 8H, NCH₂CH₂), 3.87 (t, $J = 6.0$ Hz, 8H, OCH₂CH₂), 2.04 (m, 8H, NCH₂CH₂CH₂), 1.80 (m, 8H, OCH₂CH₂CH₂)

3.1.3.2 Electrochemical synthesis of cross-linked dendron complexations

The precursor dendron complexes were electropolymerized using the cyclic voltammetry (CV) technique. In a three-electrode cell, 0.10 M tetra-butylammonium hexafluorophosphate (TBAPF₆), using a supporting electrolyte, and 10⁻⁵, 10⁻⁶ M of PAMAM-G₀COOH and PAMAM-G₁COOH were dissolved in 2 mL of chloroform. The electropolymerization of the spherical supramolecular assembled complexes were performed by sweeping the voltage at a scan rate of 50 mV/s from 0 to 1.0, 1.3, 1.5 V against Ag/AgCl as a reference electrode and platinum as a counter electrode. The ITO slides were used as a working electrode and also as a substrate.

3.1.3.3 Complex preparation

The amine-terminated, ethylene diamine core, generation 4 poly(amidoamine) dendrimer (G₄[EDA] PAMAM-NH₂, >99% purity) was purchased from Sigma-Aldrich and used without further purification. It has 64 primary amines on the surface and 180 tertiary amines at branch points within the core. The anionic carabzole (CBz) dendrons (G₀COOH, G₁COOH and G₂COOH) were prepared according to the modified procedure that has been recently reported by our group [136].

Complex preparation: Zero-, first- and second-generation anionic dendronized polymers were selected to form ionic supramolecular complexes as illustrated in Scheme 1. The entire set of complexations between dendron surfactants and PAMAM was carried out at stoichiometric ratio of carboxylic on dendrons and primary amine on the surface. A

suspension of CBz dendrons (6.4 μmol) was prepared in MeOH (0.82 mL). It was then stirred at 25 °C, after which PAMAM G₄ solution (0.1 μmol in 0.18 mL of MeOH) was added dropwise. After 24 hours, a clear solution was obtained. ¹H-NMR spectroscopy was then used to monitor the complexation behavior of the CBz dendron and PAMAM for every 2 hours, until complexation was complete. All samples were kept under nitrogen so as to avoid any contamination by atmospheric carbon dioxide.

3.1.4 Results and discussion

3.1.4.1 Formation of the spherical assemblies of the G₀COOH, G₁COOH and G₂COOH with G₄-PAMAM

The formation of the spherical assemblies of the G₀COOH and G₁COOH with G₄-PAMAM was then monitored by ¹H-NMR spectroscopy in CDCl₃. In the absence of PAMAM, the ¹H-NMR spectra chemical shifts of G₁COOH were very clear, sharp, and assignable as shown in Figure 3.2 and G₀COOH in Figure 3.3. When PAMAM was titrated into the G₀COOH and G₁COOH solutions, all signals shifted upfield and the resonance for the spectrum broadened after stirring for 24 hours, representing the translational movement and compact aggregation of the dendrons to the PAMAM surface [137].

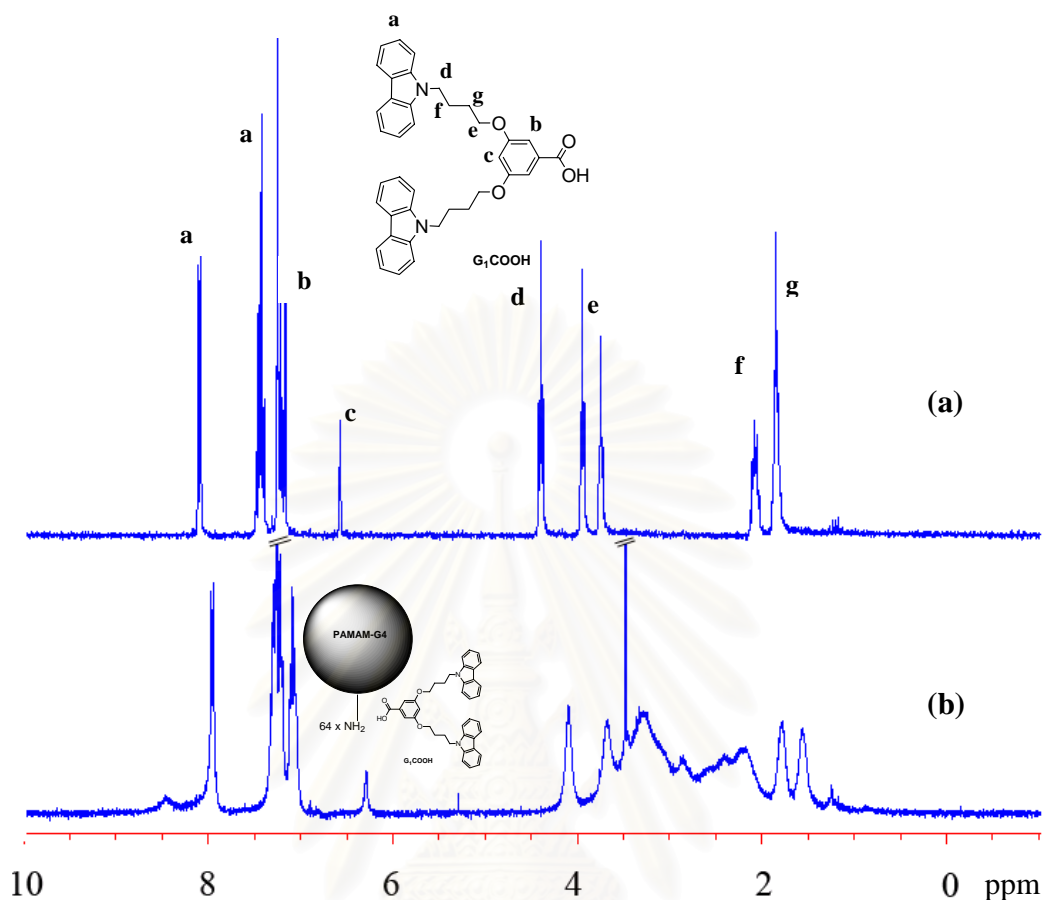


Figure 3.2 $^1\text{H-NMR}$ spectra (300 MHz, 298 K) in CDCl_3 of 2 mM solutions (based on the concentration of PAMAM): (a) G_1COOH , and (b) complex of PAMAM- G_1COOH .

The chemical shift of the PAMAM dendrimer was also detected at $\delta = 2.0\text{-}3.5$ ppm. However, despite several attempts, complexation of G_2COOH with PAMAM was not observed, which may be the result of steric effects (Figure 3.4) and lack of solubility in the G_2COOH . The UV-vis spectra before and after complexation of G_0COOH and G_1COOH with PAMAM in CHCl_3 are shown in Figures 3.5a and 3.6a. Absorption peaks are observed at 265, 295, 330 and 345 nm, which are typically assigned to the $\pi\text{-}\pi^*$ and $n\text{-}\pi^*$ transitions of carbazole [107,138]. In the case of the PAMAM+ G_1COOH , it can be

dissolved in polar (MeOH) and non-polar (CHCl_3) solvents. In MeOH, the peaks are ~ 5 nm blue-shifted when compared with those of CHCl_3 solution. On the other hand, G_0 could solubilize very well in CHCl_3 but was insoluble in MeOH. This eventually influenced the G_0 -PAMAM to have stronger aggregation characteristics compared to the G_1 -PAMAM in MeOH.

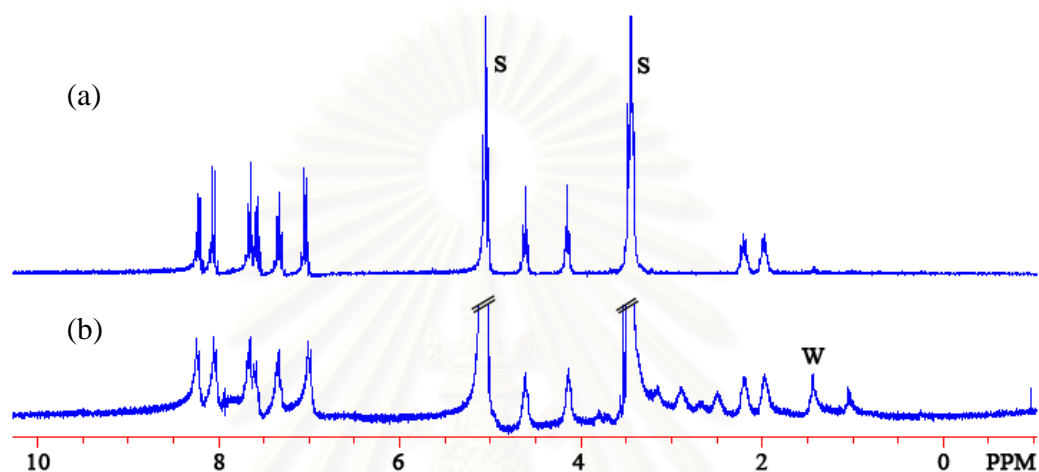


Figure 3.3 ^1H -NMR spectra (300 MHz, 298 K, DMSO) of a 2 mM solution (based on the concentration of PAMAM) of (a) $G_0\text{COOH}$, and (b) complex of PAMAM+ $G_0\text{COOH}$.

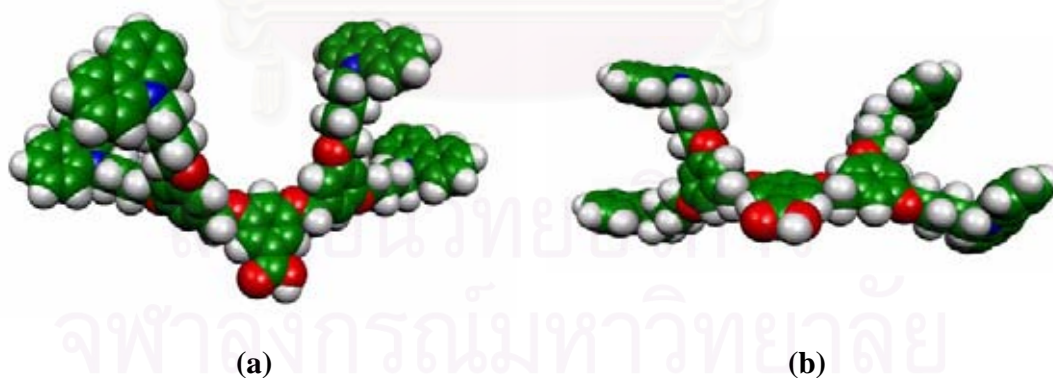


Figure 3.4 Optimized structures of $G_2\text{COOH}$ built from the Gaussian 98 B3LYP/STO-3G output using the “Molekel” software (a) side view, and (b) top view.

In all cases, hypsochromic shifts were observed upon addition of PAMAM into solutions of G₁COOH. As shown in Figure 3.5b and Figure 3.6b, fluorescence studies revealed a decrease in fluorescence emission of up to 70% upon addition of PAMAM. The quenching phenomena is attributed to a photo-induced electron transfer (PET) mechanism, that is, electron transfer from the lone pair of nitrogen of the amino group to the carbazole group and self-quenching due to aggregation of the carbazole groups.

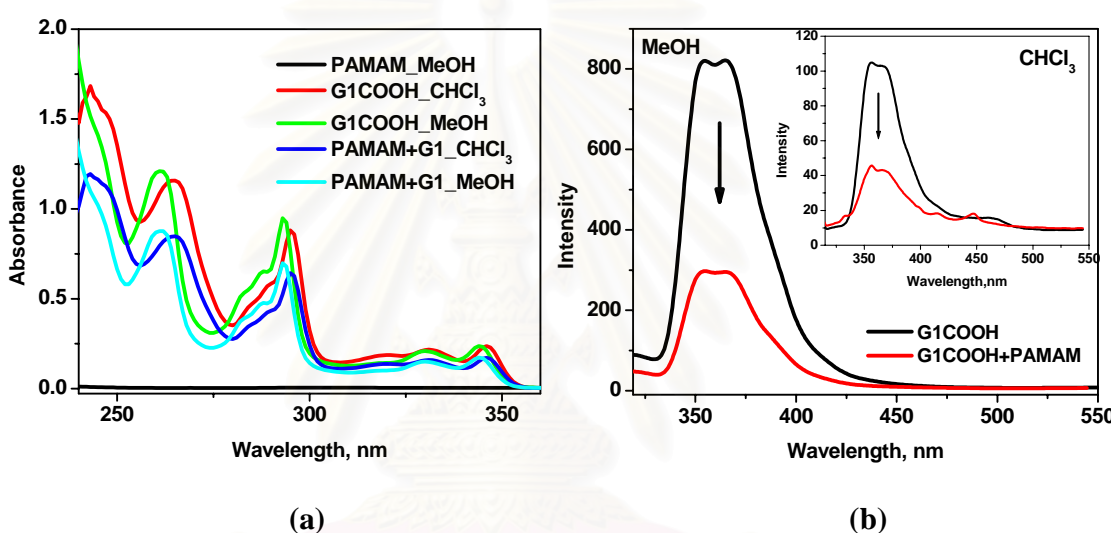


Figure 3.5 (a) UV-vis absorption spectra of G₁COOH solutions in MeOH and CHCl₃ before and after complexation with PAMAM, and (b) fluorescence emission spectra of G₁COOH before and after complexation with PAMAM, $\lambda_{\text{ex}} = 293 \text{ nm}$, $\lambda_{\text{em}} = 360 \text{ nm}$.

It should be noted that the equilibrium between complexation and decomplexation has an influence on the percentage of quenching. Accordingly, up to 30 % of the quenching with G₀- PAMAM is attributed to the formation of complex species, consistent with their aggregation properties.

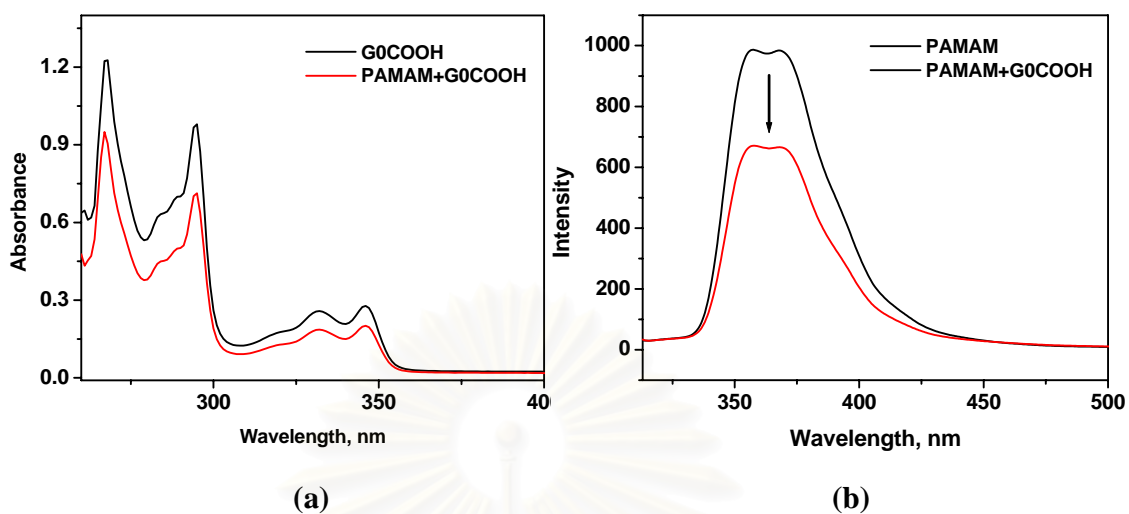


Figure 3.6 (a) UV-vis absorption spectra of G_0COOH before and after complexation with PAMAM, and (b) fluorescence emission spectra of G_0COOH before and after complexation with PAMAM, $\lambda_{ex} = 293$ nm, $\lambda_{em} = 360$ nm.

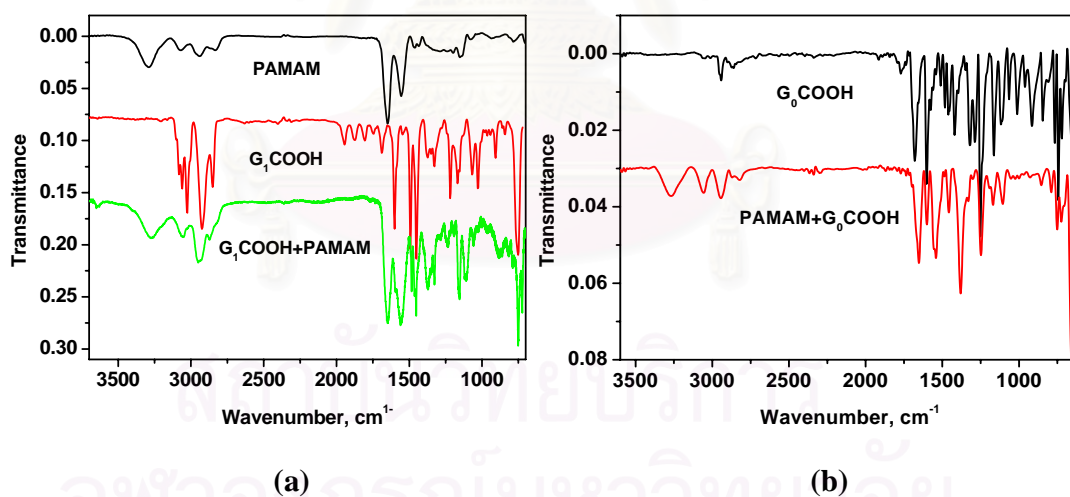


Figure 3.7 FT-IR spectra of (a) PAMAM, G_1COOH and G_1COOH -PAMAM complex., and (b) G_0COOH and G_0COOH -PAMAM complex. Resolution is at 4 cm^{-1} for each spectrum.

To further confirm that the PAMAM actually formed complexes with G₀COOH and G₁COOH, FT-IR spectra have been recorded after the 24 hours addition of PAMAM solution to G₀COOH and G₁COOH (at 25 °C, clear solutions were obtained). IR spectra of PAMAM, G₁COOH, and the G₁COOH-PAMAM complex are shown in Figure 3.7. The carboxylic acid vibrations for G₁COOH were found to be at 1690 cm⁻¹ (C=O stretch, dimer) and at 1373 cm⁻¹ (C-O stretch, dimer) and changed to a broad diffuse band between 1500 and 1760 cm⁻¹ in the spectrum of G₁COOH-PAMAM complex resulting from the ionic ammonium carboxylate structures. The same results were observed on the studies of PAMAM-G₀COOH, where the carboxylic dimer peaks at 1758 and 1303 cm⁻¹ changed to broad diffuse bands of ionic carboxylate structures between 1500 and 1600 cm⁻¹. According to these results, it can be concluded that 1:1 stoichiometric complexes were formed similar to previously reported fluorinated [139a] and nonfluorinated [139b] polyethyleneimine complexes.

Contact angle measurements were also carried out to investigate the complexation. In this case, the complexation should reduce the hydrophilicity of the PAMAM and the dendrons (Figure 3.8). The dilute solutions of the PAMAM and the complexes were spin-coated on a pre-cleaned and plasma treated Si-wafer flat substrate. The films prepared from the complexes of G₀COOH and G₁COOH and the PAMAM solutions, resulted in a change of the static water contact angle (WCA) (0° to 55.7°, G₁, and 0° to 80.3°, G₀). This confirmed the complexation of PAMAM with dendrons based on a change in the hydrophilic-lipophilic balance (HLB) compared to the completely wetted PAMAM-Si-wafer substrate, with a WCA of 0°. The large increase in WCA is due to the hydrophobicity of the carbazole groups forming the outer shell of the dendrimers. From these results, it can also be inferred that the G₀COOH is strongly aggregated on the peripheral of dendrimer and is fully-complexed compared to G₁COOH, as confirmed by the larger WCA increase on the former.

The formation of the individual PAMAM-G₁COOH dendrimer-surfmer complexes was directly observed by atomic force microscopy (AFM) as shown in Figure

3.9. Very dilute solutions of $1\mu\text{M}$ of the PAMAM- G_1COOH complexes in MeOH and CHCl_3 were spin-casted onto a mica substrate. Isolated nanoparticle dendrimer complexes were observed at concentration 10^{-6} M on the surface.

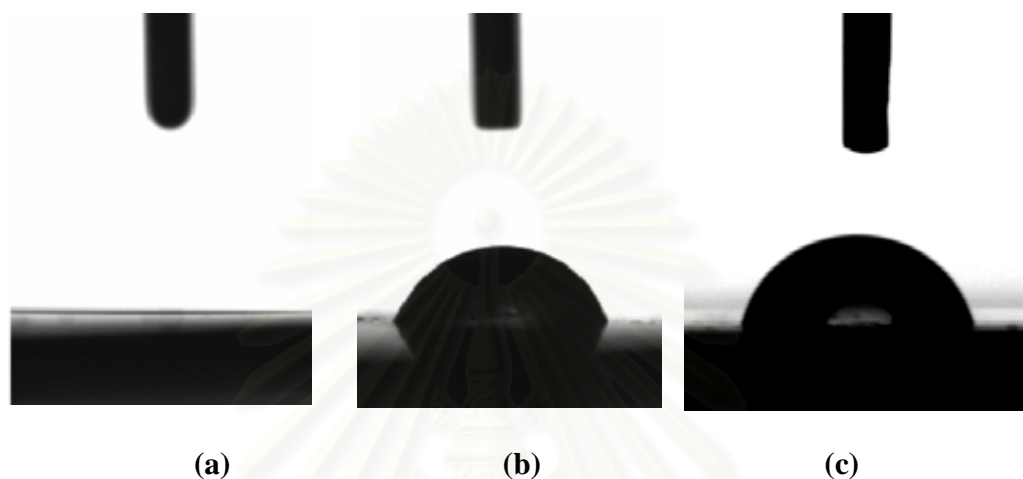


Figure 3.8 WCA measurement for: (a) PAMAM (0°), (b) complex PAMAM- G_1COOH (55.7°), and (c) complex PAMAM- G_0COOH (80.3°).

The particle diameter of PAMAM is $\sim 4.0\pm 0.5$ nm, and PAMAM- G_1COOH complexes in MeOH and CHCl_3 are $\sim 7.0\pm 0.5$ and 16.5 ± 1.0 nm, respectively. The difference in sizes of the complexes was verified by molecular modeling (Gaussian 98 with B3LYP/STO-3G basic set) [140], Figure 3.10. From optimization of the structures, two different conformers were found to have the same minimum energy. The sizeable increase with complexation is dependent on the polarity of solvent. It can be noted that conformer **a** will be present in MeOH to avoid the polar solvent and conformer **b** will be present in CHCl_3 , a more nonpolar solvent. Moreover, by decreasing the generation of dendron to G_0COOH , a smaller increase of the diameter was found (diameter $\sim 4.3\pm 0.5$ nm), as demonstrated in Figure 3.11. It is clear that G_0COOH has a stronger aggregation after complexation.

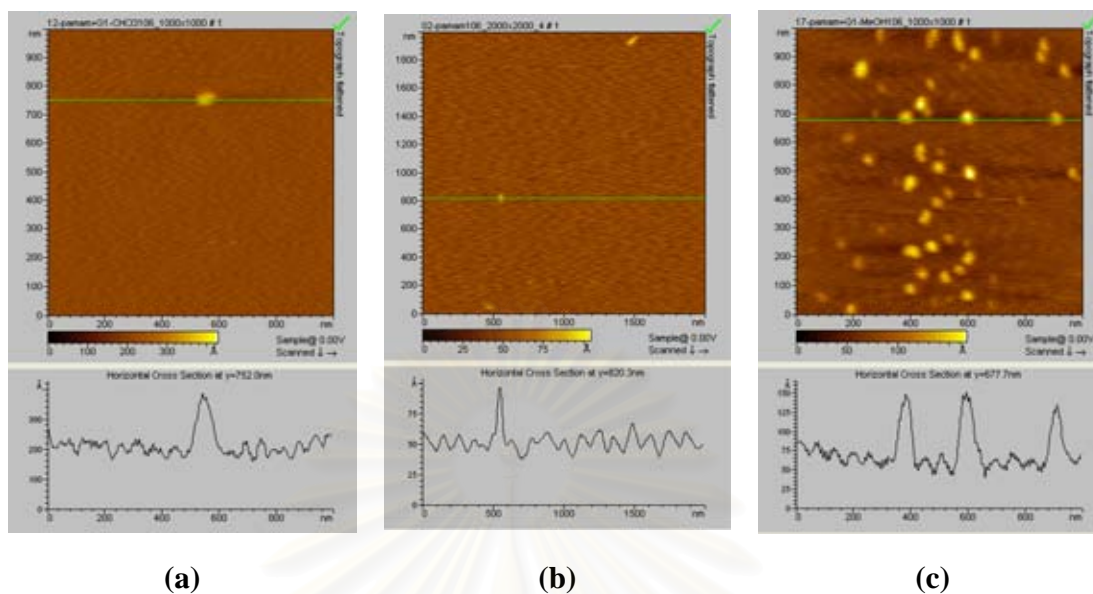


Figure 3.9 AFM images complex on a mica substrate of (a) PAMAM G_4 (b) PAMAM- G_1 COOH complex in CHCl_3 , and (c) PAMAM- G_1 COOH complex in MeOH.

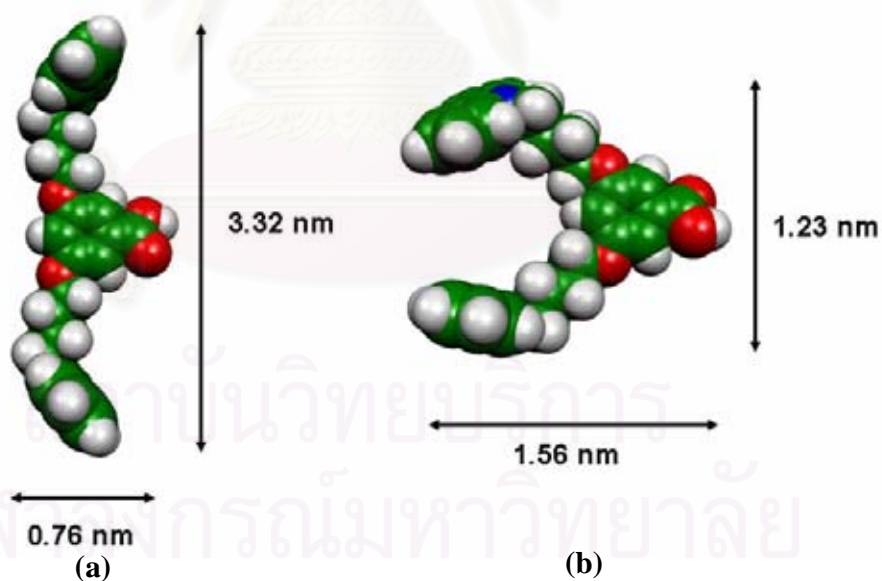


Figure 3.10 Optimized structures built from the Gaussian 98 B3LYP/STO-3G output file using the “Molekel” software [140].

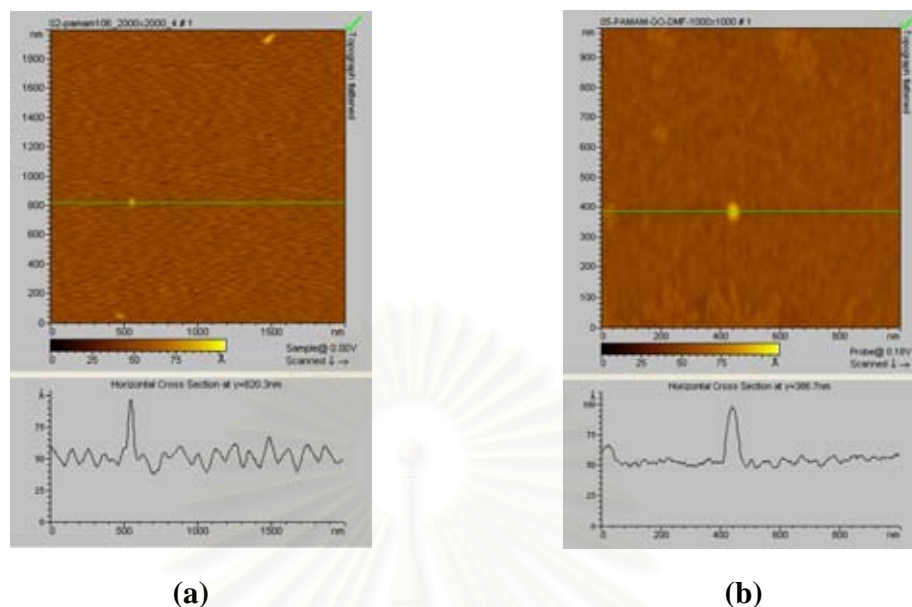


Figure 3.11 AFM images on a mica substrate of (a) PAMAM G_4 , and (b) PAMAM+ G_0 COOH complex in MeOH.

3.1.4.3 Electrochemical studies of dendron surfmer complexes

The precursor complexes (PAMAM- G_0 COOH and PAMAM- G_1 COOH) were electropolymerized and deposited on ITO substrates. The cyclic voltammetry (CV) curves are shown in Figures 3.12, and 3.13. The potentials were cycled from 0 to 1.0, 1.3, 1.5 V at a scan rate of 50 mV/s against Ag/AgCl reference electrode and platinum counter electrode. The cyclic voltammograms of the dendron complexes shows unusually sharper reversible redox peaks compared to those of the conventional voltammograms of polycarbazole [141]. This obviously suggests that there is an optimal conformational freedom required to allow extended conjugation during cross-linking for these dendrimers. This could also possibly lead to both 3,6 and 2,7 type cross-linkings in the dendrimers. The presence of a small reduction peak between 0.9 and 1.1 V is indication of some 2,7 cross-linking [142a], but the majority of cross-linking still occurs via the 3,6-position [142b] as indicated by strong reduction peaks observed between 0.5 and 0.7 V. At a concentration of 10^{-6} M PAMAM- G_1 COOH, no redox peaks were observed on the

anodic scan up to a potential of 1.1 V. (Figure 3.14). Nevertheless, we have recently investigated the linear increase in oxidation onset potentials in each cycle in applied potential windows of up to 1.3 and 1.5 V (as shown in Figure 3.12). This means that the formation of a conjugated polymer was observed at a higher potential but it decomposed when the potential went over to 1.5 V limit. Both 10^{-6} and 10^{-5} M of PAMAM- G_1 COOH showed characteristic peaks for the formation of polycarbazole units. A small difference of the oxidation onsets was recorded in there anodic scans as shown in Figure 3.12 and as summarized Table 3.1.

However, shape and peak positions are obviously unique for different concentrations and potential windows of the dendron complexes. At higher concentration (10^{-5} M), the oxidation process observed in the first cycle ($E_{pa} \approx 0.87$ V) was attributed to dimerization of carbazole, and then shifted toward higher potentials in subsequent scans ($E_{pa} \approx 1.15$ V) due to a higher oxidation potential of the dimer.

We believe that the aggregation and globular formation during complexation affects the availability of the electroactive groups. Different CV features were also demonstrated with PAMAM- G_0 COOH (Figure 3.13). For all cases, the oxidation peaks were higher in intensity in the first cycle, which indicates that almost all of the materials were deposited initially on the ITO substrate. In the second cycle, a sudden decrease of oxidation peak intensities was observed which indicate a weaker complexation between PAMAM and G_0 COOH and a more polymerized G_0 COOH that could lead to film degradation.

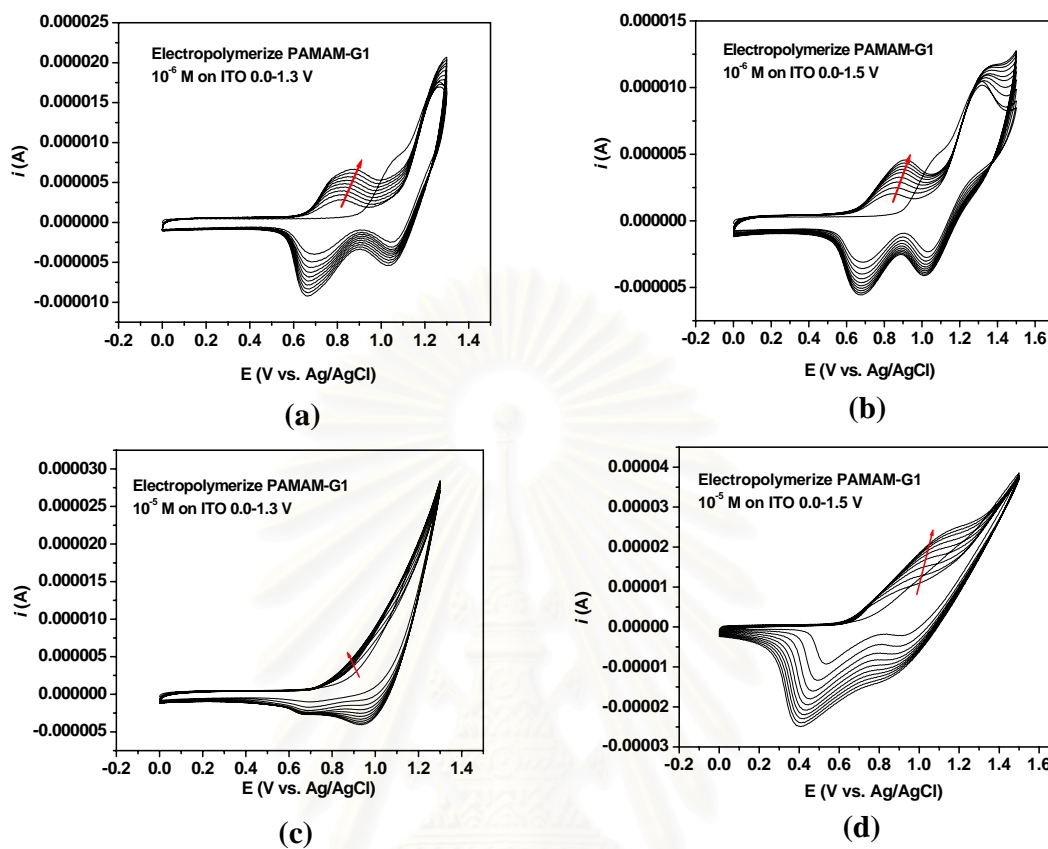


Figure 3.12 Cyclic voltammograms of the electrochemical cross-linking/deposition of PAMAM-G₁COOH complex at a scan rate of 50 mV/s, 10 cycles: (a) concentration of 10^{-6} M, potential window from 0-1.3 V, (b) concentration of 10^{-6} M, potential window from 0-1.5 V, (c) concentration of 10^{-5} M, potential window from 0-1.3 V, and (d) concentration of 10^{-5} M, potential window from 0-1.5 V.

สถาบันวิทยบริการ
จุฬาลงกรณ์มหาวิทยาลัย

Table 3.1 Anodic and cathodic currents/potentials of precursor polymers and their corresponding onsets of oxidation potential.

PAMAM-D _n	Conditions	Onsets	E_{pa} (V)	I_{pa} (μ A)	E_{pc} (V)	I_{pc} (μ A)
G ₀ COOH	10 ⁻⁵ , 1300 mV	0.63	0.87	6.63	0.66	9.20
	10 ⁻⁵ , 1500 mV	0.61	0.91	4.53	0.67	5.55
	10 ⁻⁶ , 1300 mV	0.73	0.93	6.18	0.65	2.61
	10 ⁻⁶ , 1500 mV	0.66	1.13	23.8	0.41	24.9
G ₁ COOH	10 ⁻⁵ , 1300 mV	0.56	0.97	8.89	0.84	3.12
	10 ⁻⁵ , 1500 mV	0.56	0.99	9.20	0.85	3.88
	10 ⁻⁶ , 1300 mV	0.67	1.02	21.8	0.84	11.0
	10 ⁻⁶ , 1500 mV	0.62	0.89	11.2	0.85	7.05

However, there was a peak shift toward higher oxidation potential after three cycles that can be attributed to aggregation. The CV results also suggest that raising the generation of the dendron surfmer increases the amount of longer conjugated segments formed along the cross-linked species. From Table 3.1, it is obvious that PAMAM-G₁COOH shows a higher ΔE ($E_{pa} - E_{pc}$) value than that of PAMAM-G₀COOH which indicates a more heterogeneous and slow electron-transfer rate for these complexes [138]. This heterogeneous electron transfer is also likely a consequence of a thicker film deposited during each CV cycle and is also an indication of a higher degree of cross-linking.

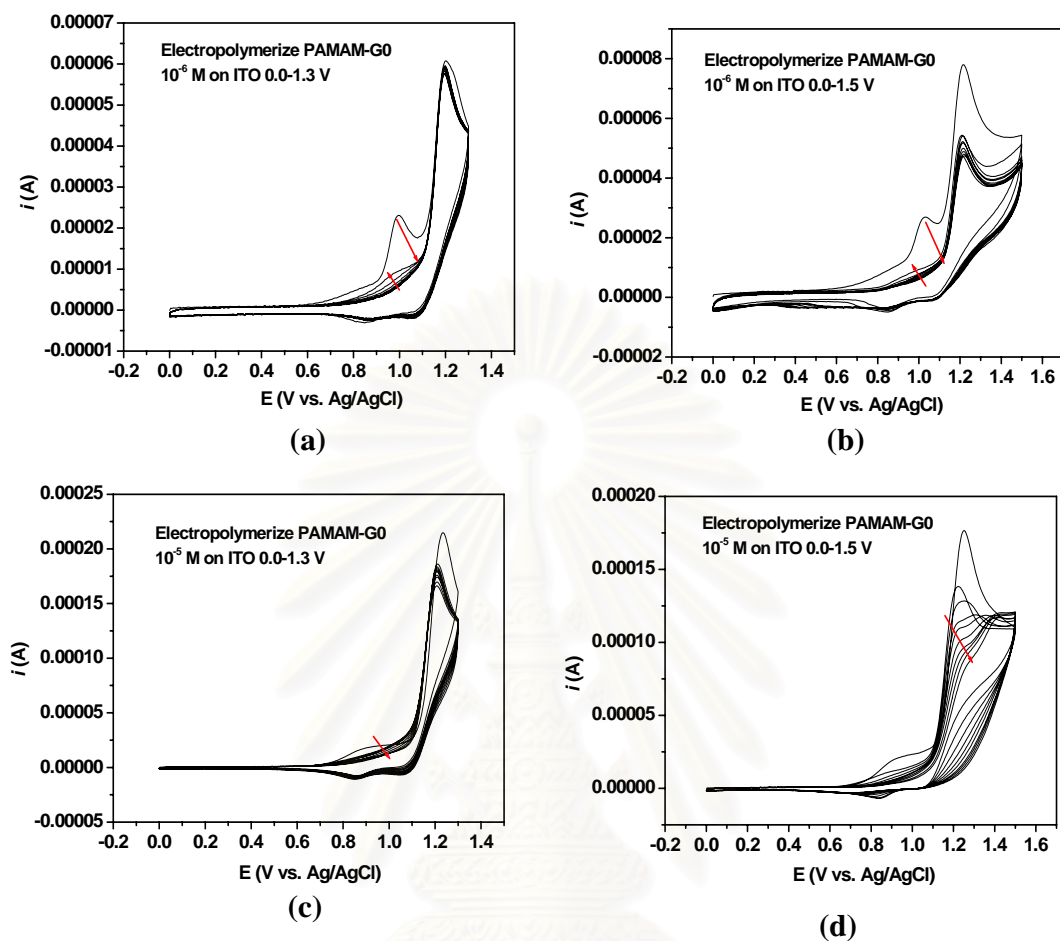


Figure 3.13 Cyclic voltammograms of the electrochemical cross-linking/deposition of PAMAM-G₀COOH complexes at a scan rate of 50 mV/s, 10 cycles: (a) concentration of 10^{-6} M, potential window from 0-1.3 V, (b) concentration of 10^{-6} M, potential window from 0-1.5 V, (c) concentration of 10^{-5} M, potential window from 0-1.3 V, and (d) concentration of 10^{-5} M, potential window from 0-1.5 V.

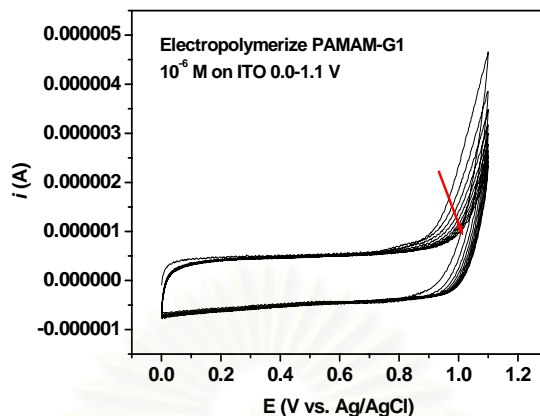


Figure 3.14 Cyclic voltammograms of the electrochemical cross-linking/deposition of PAMAM-G₁COOH complexes at a scan rate of 50 mV/s, 10 cycles: concentration 10^{-6} M, potential window from 0-1.1 V.

3.1.4.4 Spectro-electrochemical studies of dendron surfmer complexes

The cross-linked films were further characterized by electrochemical UV-vis spectroscopy. The extent of increasing π orbital overlap between neighboring repeating units on conjugated polymers can directly affect the observed energy of the π - π^* transition which appears as the absorption maxima in the electronic spectra. This could be due to the possibility of either inter/intramolecular cross-linking dominating the π - π^* transition.

The values of the absorption maxima for the different generations are closely linked to their degree of polymerization. The extended appearance of the π - π^* transition at 380-403 nm, which is attributed to polycarbazole is shown in Figure 3.15 [138,139]. The peak between 700-1000 nm can be assigned to the polaronic band originated from the formation of conjugated polycarbazole species and their complex ion redox couple with hexafluorophosphate ions. From the spectrum, the peaks at high concentration and high applied potential shows extraordinary increases of the peak intensity at 380-403 nm

(polycarbazole) and appearance of the peak at the 600-900 nm (bipolaron formation) region confirms the highly crosslinked and conjugated nature of the materials deposited on the ITO substrate.

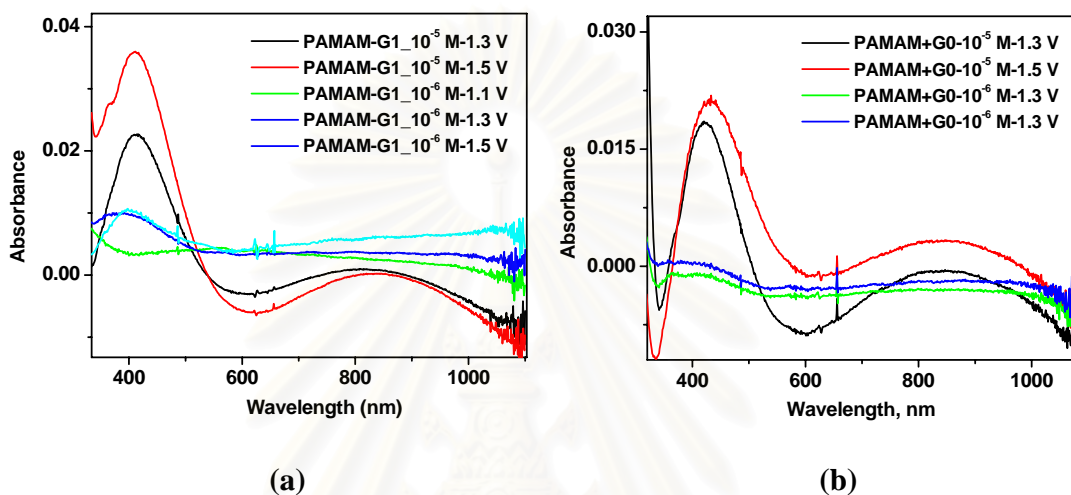


Figure 3.15 Absorption spectra analysis performed in 0.1 M TBAPF₆/CHCl₃ on ITO substrate in the present of different concentrations and potential windows. (a) PAMAM-G₁COOH, and (b) PAMAM-G₀COOH.

3.1.4.5 Morphological studies

The morphology and molecular orientation of the dendron complexes after electropolymerization on ITO substrates have been studied using AFM measurements. In the case of PAMAM-G₁COOH at low concentration (10^{-6} M) and applied potential of 0-1.3 V, the AFM image (Figure 3.16b), a unique nanostructure was observed. A ring-like structure with diameters in the range of 100-150 nm and a height and width of ~15 nm was detected. Interestingly, the height is equivalent to the full diameter of a PAMAM-G₁COOH nanoparticle diameter.

The nano-ring diameter could also closely resemble a donut shape particle that may likely contain a PAMAM-core with the G₁COOH shell (Figure 3.1). This kind of feature was found repeatedly with solute evaporation [143] and is presumably related to the overall hydrophobic-hydrophilic balance property [144]. To investigate the mechanisms that drives the morphological change from nanospheres (before electropolymerization) to ring-like (donut) nanostructures, two experiments were performed to determine when the nano ring structures are formed as illustrated in Scheme 3.1.

The micellization phenomenon of G₁COOH was first investigated. If the critical micelle concentration (CMC) is equal to and/or less than the concentration of G₁COOH that was used to make PAMAM-G₁COOH complexes, the nano-ring can be generated between the equilibrium of the G-COOH micellization and the weak-complexation equilibrium with the PAMAM. However, if the CMC is lower than the concentration of G₁COOH used, thus the equilibrium between decomplexation and weak-complexation with PAMAM is preferred. We have studied the solubilization of the dye Nile Red as a function of the concentration of G₁COOH in order to determine the CMC [145]. Shown in Figure 3.17a is the UV-vis spectra before and after micelle formation while Figure 3.17b represented the fluorescence spectra at $\lambda_{ex}=570$ and $\lambda_{ex}=655$ nm of different solutions of G₁COOH. The dendron solution was stirred for 2 hours in the presence of Nile red and then filtered to remove unsolubilized dye. The CMC of this system was found to be 70.0 μ M. From the experiment, a 6.4 mM concentration of G₁COOH was used for dendron complexation, and a concentration of 6.4×10^{-5} M was used for the CV. This means that the nanoring structures could have only formed at the equilibrium between the decomplexation and weak-complexation stage as presented in Figure 3.1 since there is not enough unimers to form free G₁COOH micelles based on these concentrations.

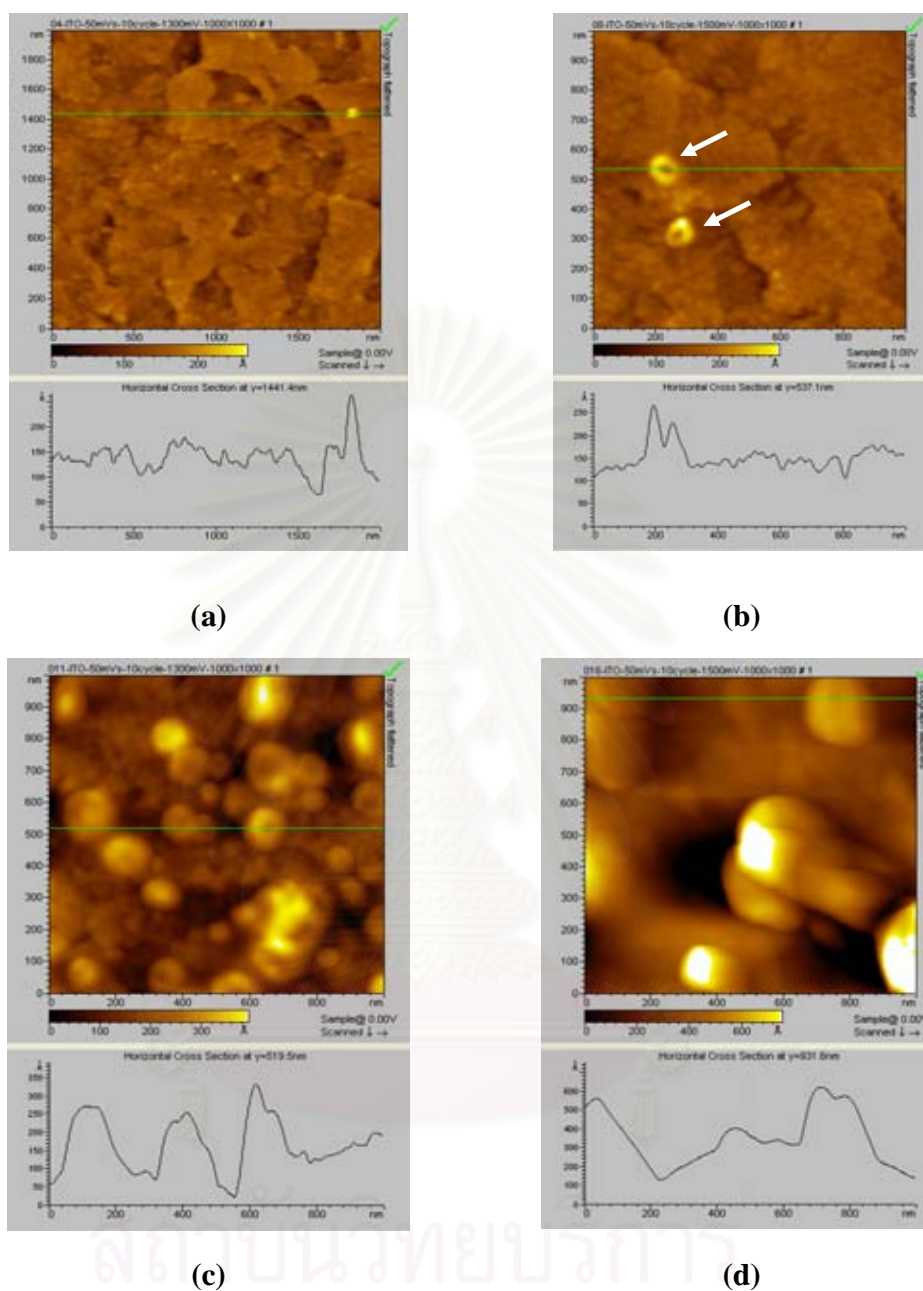


Figure 3.16 AFM images of PAMAM-G₁COOH complex after electropolymerization on ITO at a scan rate of 50 mV/s, 10 cycles: (a) concentration of 10^{-6} M, potential window from 0-1.3 V, (b) concentration of 10^{-6} M, potential window from 0-1.5 V, (c) concentration of 10^{-5} M, potential window from 0-1.3 V, and (d) concentration of 10^{-5} M, potential window from 0-1.5 V.

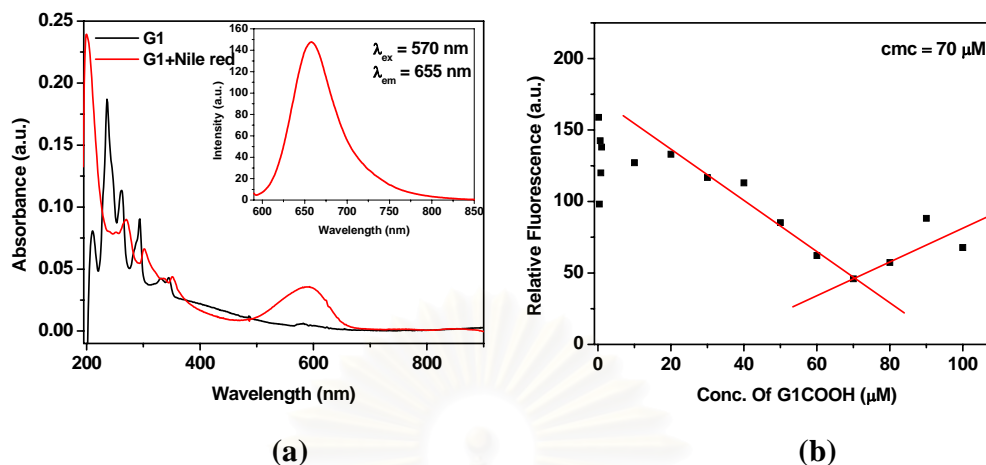


Figure 3.17 (a) Absorption spectra of Nile red in a solution of 70 μM G_1COOH , and (b) Emission intensity of different saturated solutions of Nile red at 640 nm ($\lambda_{\text{ex}}=570$ nm) versus concentration of G_1COOH in 0.1 M TBAPF_6 .

To confirm that nano-ring structures could not have developed in the absence of PAMAM, we also studied the electropolymerization of G_1COOH alone. The CV curves in Figure 3.18 exhibited the oxidation and reduction peaks of cross-linked polycarbazole. The linear current increase and ΔE change indicated that G_1COOH can also be effectively deposited on ITO with even greater efficiency than the PAMAM- G_1COOH . The in-situ spectroelectrochemical studies also showed the typical π - π^* and polaronic bands of polycarbazole [18,20]. However, no ring-like nanostructures were observed on the morphology from the AFM images (Figure 3.19).

To further understand the components of the deposited film on the ITO, XPS spectroscopy was used to determine the composition of the deposited film based on C/N ratio. Shown in Figure 3.20 is the high-resolution XPS spectrum of PAMAM- G_1COOH cross-linked polymer on ITO for C and N atoms. In all quantitative analyses, the theoretical value is assumed on the basis of 100% electrografting.

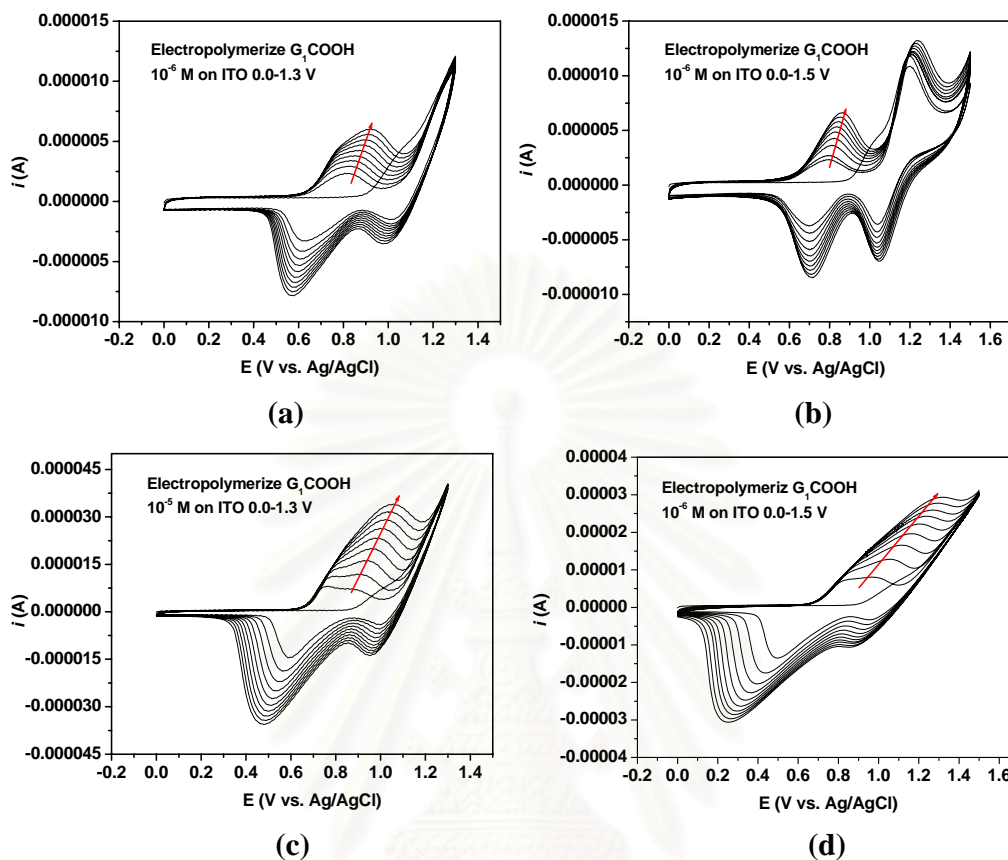


Figure 3.18 Cyclic voltammograms of the electrochemical cross-linking/deposition of G₁COOH at a scan rate of 50 mV/s, 10 cycles: (a) concentration of 10⁻⁶ M, potential window from 0-1.3 V, (b) concentration of 10⁻⁶ M, potential window from 0-1.5 V, (c) concentration of 10⁻⁵ M, potential window from 0-1.3 V, and (d) concentration of 10⁻⁵ M, potential window from 0-1.5 V.

For the 10⁻⁶ M of PAMAM-G₁COOH electrodeposited with a reductive potential of up to 1.5 V, an experimental value of $C/N = 7.95$ was obtained which is higher than the theoretical value of PAMAM-G₁COOH at $C/N = 7.07$. This higher value indicates the incorporation of a slightly larger amount of the surfmer compared to the PAMAM. Thus during the electrodeposition of the dendrimer-complex, it is possible that the PAMAM

was decomplexed into the solution subphase during the nano-ring formation near the weak-complexation equilibrium. Furthermore, since the surfmers are not likely to form micelles at the 10^{-6} M concentration used, the ring formation resulted in expulsion of the PAMAM and at the same time the electropolymerization of the dendron surfmer units. This explains the higher experimental C/N ratio observed from XPS and is supported by AFM, CMC, and even fluorescence data (carbazole aggregation). The rings then are formed largely due to the formation of a higher ordered core-shell ring (donut) composed of a higher content $G_1\text{COOH}$ shell with the PAMAM remaining as an interior template-support during the electrochemical CV procedure.

To confirm the uniqueness of the dendron complexation phenomenon, we covalently bonded the $G_1\text{COOH}$ to PAMAM to form a carbazole amide functionalized dendrimer (PC) (synthesis procedure as shown in part 3.2). The synthesis, purification and characterization of this derivative are reported in the supporting information. The electropolymerization was done with the same parameters as with the PAMAM- $G_1\text{COOH}$ complexes.

At the low potential application (1.3 V), a good trend of increasing oxidation potential onset was observed with increasing of cycles but the CV curves shifted to higher anodic potential (E_{pa}) and the reduction peaks shifted to lower cathodic potential (E_{pc}) compared to the non-covalent PAMAM-dendron complexes as shown in Figure 3.22. Degradation was observed after applying a higher potential (1.5 V) which may come from the lack of availability of more mobile electroactive monomers. Moreover, the UV-vis spectra revealed the formation of less conjugated polycarbazole species (predominantly dimerization) as shown in Figure 3.21 in which the $\pi-\pi^*$ transition at 380-403 nm is weaker. From the morphology (Figure 3.23) as imaged by AFM, the cross-linked PC film did not show nano ring formation at all but a rough and patchy film that was macroscopically more non-uniform.

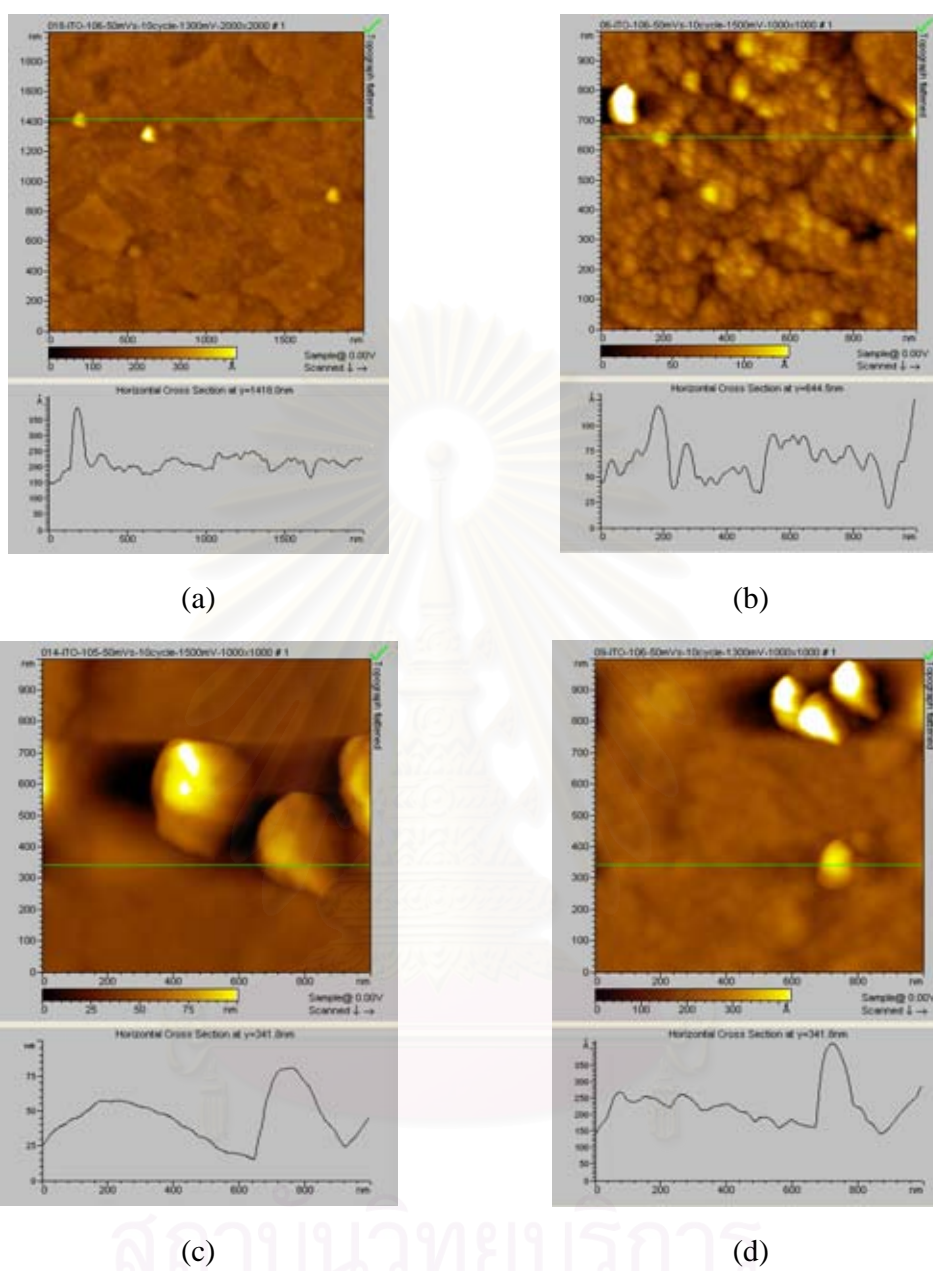


Figure 3.19 AFM images of G₁COOH after electropolymerization on ITO at a scan rate of 50 mV/s, 10 cycles: (a) concentration of 10^{-6} M, potential window from 0-1.3 V, (b) concentration of 10^{-6} M, potential window from 0-1.5 V. (c) concentration of 10^{-5} M, potential window from 0-1.3 V, and (d) concentration of 10^{-5} M, potential window from 0-1.5 V.

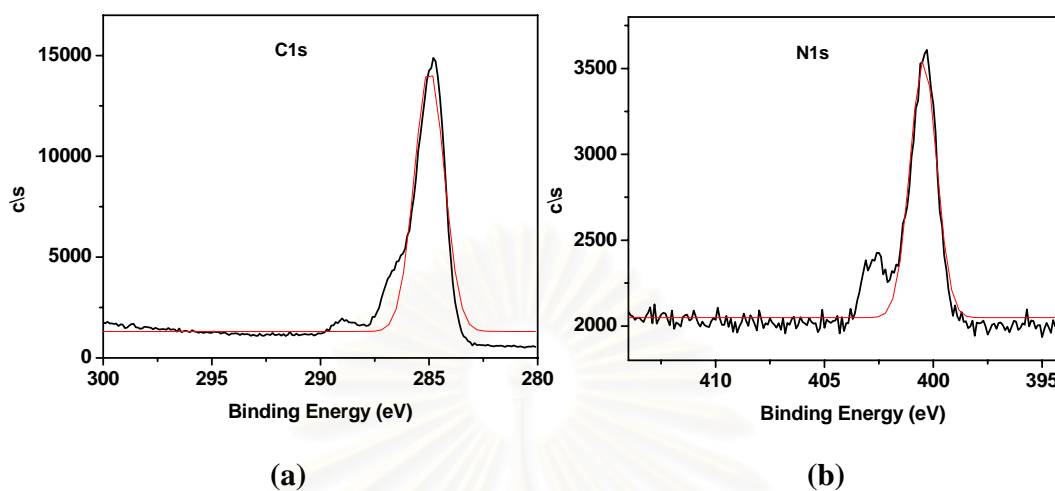


Figure 3.20 High-resolution XPS spectra of the cross-linked polymer: (a) C 1s, and (b) N 1s.

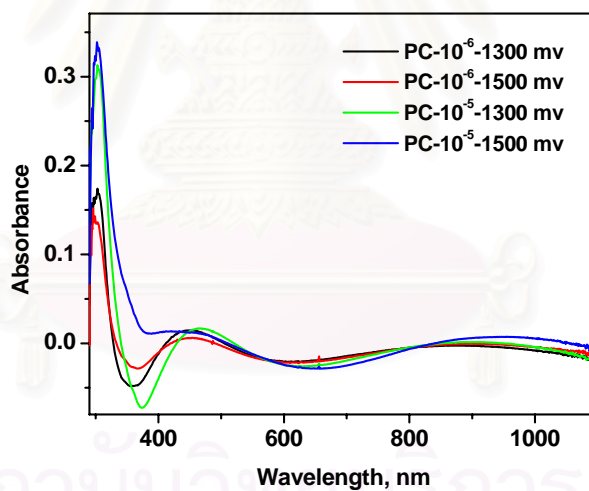


Figure 3.21 Spectroelectrochemical analysis performed in 0.1 M TBAPF₆/CHCl₃ on ITO substrate in the present of different concentrations and potential windows of PC.

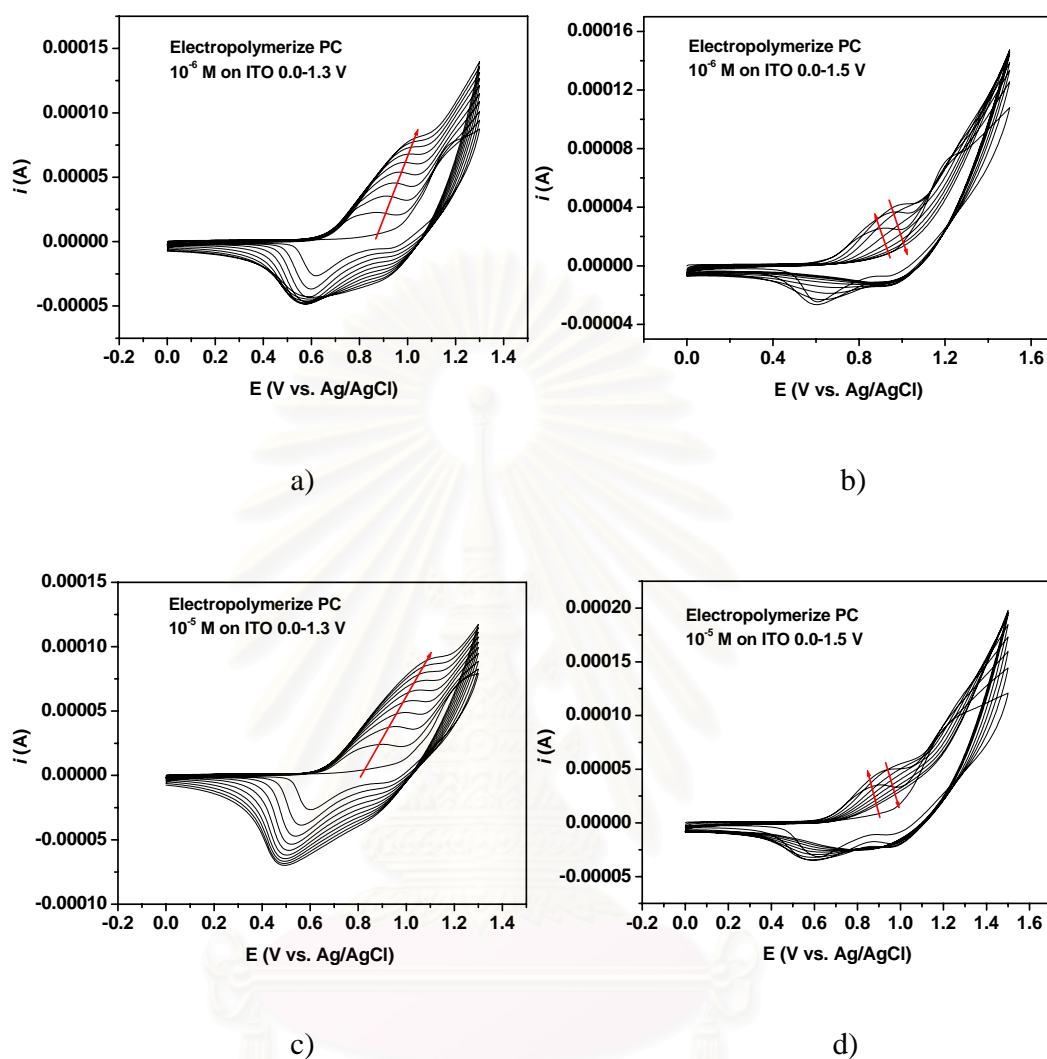


Figure 3.22 Cyclic voltammograms of the electrochemical cross-linking/deposition of (3,5-Bis(4-(9H-carbazol-9-yl)butoxy)-benzoyl-Functionalized Dendrimer PAMAM (PC) at a scan rate of 50 mV/s, 10 cycles: (a) concentration of 10^{-6} M, potential window from 0-1.3 V, (b) concentration of 10^{-6} M, potential window from 0-1.5 V, (c) concentration of 10^{-5} M, potential window from 0-1.3 V, and (d) concentration of 10^{-5} M, potential window from 0-1.5 V.

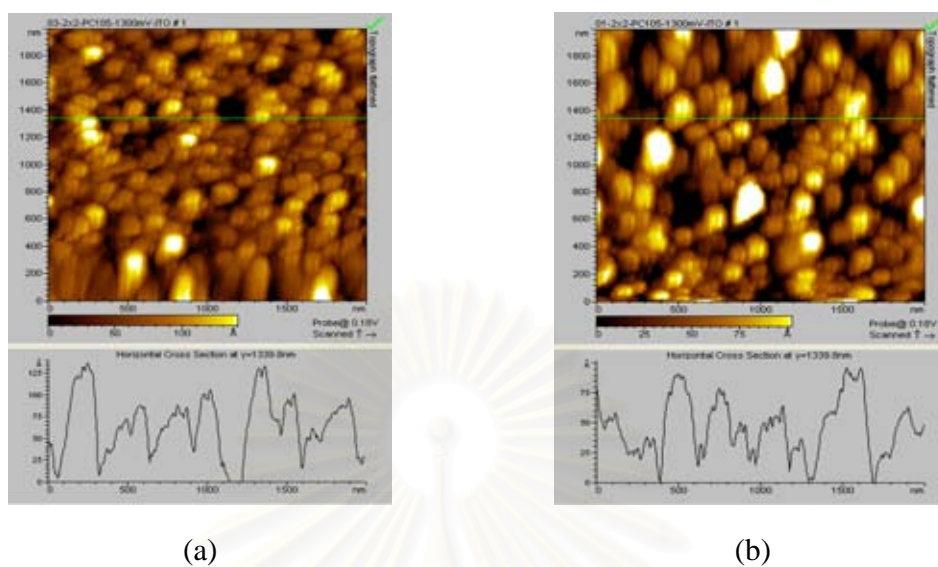
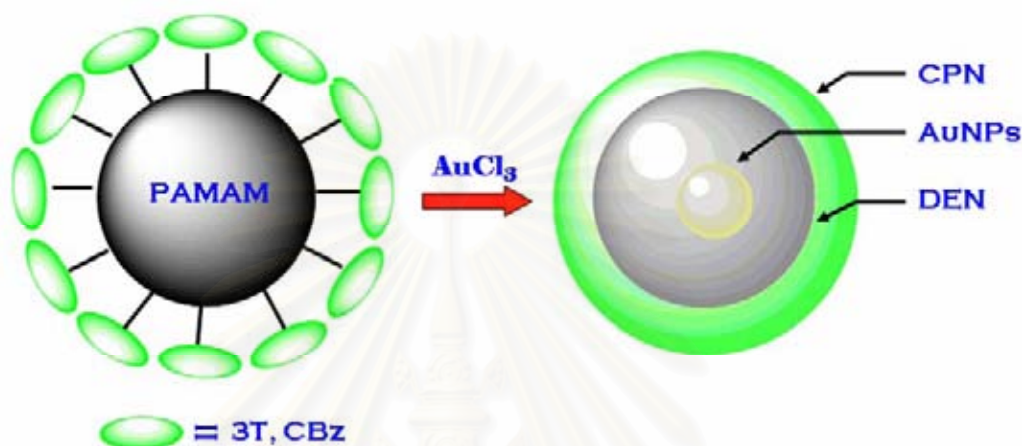


Figure 3.23 AFM topography images of **PC** after electropolymerization on ITO at a scan rate of 50 mV/s, 10 cycles: (a) concentration of 10^{-6} M, potential window from 0-1.3 V, and (b) concentration of 10^{-5} M, potential window from 0-1.3 V.

3.2 Redox nanoreactor dendrimer boxes: *in-situ* hybrid gold nanoparticles via terthiophene and carbazole-PAMAM dendrimer oxidation

3.2.1 Introduction



Dendrimer-encapsulated nanoparticles (DENs), the nanocomposite materials are synthesized by complexing metal ions within dendrimers and then reducing the composites to yield zerovalent DENs. DENs are of great interest because they combine the desirable physical and chemical properties of the encapsulated nanoparticles with the tunable solubility and surface reactivity of the dendrimer template. Dendrimers are particularly well-suited for hosting metal nanoparticles for the following reasons [146]: 1) the dendrimer templates themselves are of fairly uniform composition and structure, and therefore they yield well-defined nanoparticle replicas; 2) the nanoparticles are stabilized by encapsulation within the dendrimer, and therefore they do not agglomerate; 3) the encapsulated nanoparticles are confined primarily by steric effects, and therefore a substantial fraction of their surface is unpassivated and available to participate in catalytic reactions; 4) the dendrimer branches can be used as selective gates to control access of small molecules (substrates) to the encapsulated (catalytic) nanoparticles; 5) the terminal

groups on the dendrimer periphery can be tailored to control solubility of the hybrid nanocomposite and used as handles for facilitating linking to surfaces and other polymers.

Especially, PAMAM dendrimers can bind a defined number of transition metal cations, create an ideal environment for trapping guest species [146,148], which can be a template and stabilize metal oxide or metal nanoparticles [149]. Furthermore, the nanoparticle size, composition, and structure can be controlled by taking advantage of the dendrimer structure and the means by which the metal ions are introduced into the dendrimer. In a part few decades, several methods for making gold nanoparticles by using chemical reduction of hydrogen tetrachloroaurate (III) and gold (III) chloride have been developed. The most popular one used for a long time was the citrate reduction of HAuCl_4 in water, which was introduced by Turkevitch in 1951 [150]. Biphasic synthesis were performed to produce organic soluble gold colloids (<5 nm). Recently, the electroactive groups such as pyrrole [151], aniline [152], thiophene [153], EDOT [156], or others which can be oxidized to prepare gold nanoparticles and at the same time they can be polymerized to conducting polymers are currently investigated.

In particular, thiophene and carbazole copolymers have been of recent interest due to their interesting electrochemical copolymerization behavior [112] and electrochromic properties [134]. It has been shown that electropolymerization of terthiophene leads to the formation of highly electrochromic and conducting polythiophenes [154]. On the other hand, polycarbazole is well-known as a hole transport material [107]. Furthermore, electrochemically polymerized carbazoles show interesting chromic properties because of the conjugation breaks that are present due to the inclusion of a 3,6-linkage. These broken conjugation lengths generate radical cations, which are separated from one another and do not combine. Therefore, the ability of polycarbazole to form two distinct oxidation states further leads to multichromic effects [134].

3.2.2 Objectives of this research

In this work, we report the synthesis of PAMAM dendrimers functionalized with terthiophene (PT) and carbazole (PC) dendrons on their periphery. The formation of DENs consisting of gold nanoparticles protected with PAMAM (inner shelf) and π -conjugated polymer (outer shelf) will be described. UV-vis spectroscopy was used to monitor the formation of these hybrid nanoparticles. FT-IR was used to study the stabilization effect of gold nanoparticles with functionalized PAMAM dendrimer PC and PT. Finally, we have investigated the energy transfer between the nanoparticles and thiophene, carbazole-dendron on the periphery.

3.2.3 Experimental section

3.2.3.1 Synthesis of carbazole and terthiophene dendrons to modify dendrimer

a) General procedure

a1) Materials

Unless otherwise specified, the solvents and all materials were reagent grades purchased from Fluka, BHD, Aldrich, Carlo Erba, Merck or J.T. Baker and were used without further purification. Commercial grade solvents such as acetone, dichloromethane, hexane, methanol and ethylacetate were purified by distillation before use. Acetonitrile and dichloromethane for set up the reaction were dried over calcium hydride and freshly distilled under nitrogen atmosphere prior to use. Tetrahydrofuran was dried and distilled under nitrogen from sodium benzophenone ketyl immediately before use.

Column chromatographies were carried out on silica gel (Kieselgel 60, 0.063-0.200 nm, Merck). Thin layer chromatography (TLC) was performed on silica gel plates

(Kieselgel 60, F₂₅₄, 1mm, Merck). Compound on TLC plates were detected by the UV-light. All manipulations were carried out under nitrogen atmosphere.

a2) Instrumentations

Nuclear magnetic resonance (NMR) spectra were recorded on a General Electric QE-300 spectrometer at 300 MHz in deuterated solvent. Chemical shifts (δ) are reported in parts per million and the residual solvent peak was used as an internal standard.

Absorption spectra were measured by a HP-8453 UV-vis spectrometer. Fluorescence spectra were recorded by a PerkinElmer LS 45 spectrophotometer.

FT-IR spectra were obtained using a FTS 7000 Spectrometer (Digilab now Varian Inc.) equipped with a liquid N₂-cooled MCT detector. KBr pellets were prepared by first mixing the sample solutions with KBr, removing solvents under vacuum and then pressing the KBr using a 10-ton hydraulic press.

MALDI-TOF mass spectra were recorded on a Biflex Bruker Mass spectrometer with 2-Cyano-4-hydroxycinnamic acid (CCA) or 2,5-Dihydroxy-benzoic acid (DHB) as matrix.

Elemental analysis was carried out on CHNS/O analyzer (Perkin Elmer PE2400 series II).

Atomic force microscopy (AFM) imaging was examined in ambient conditions with a PicoSPM II (PicoPlus System, Molecular Imaging [now Agilent Technologies] Tempe, AZ.) in the Tapping mode (AAC mode).

Morphology studied by SEM was performed using a JSM 6330F (JEOL) instrument operating at 15 kV.

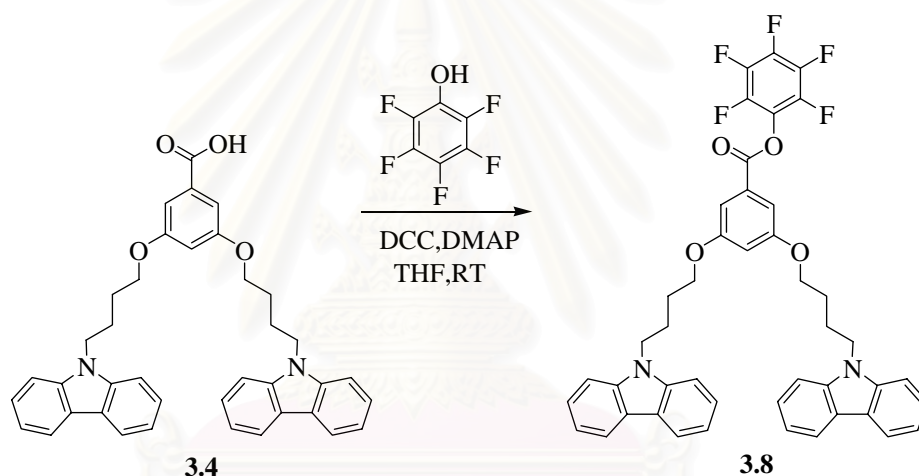
X-ray photoelectron spectroscopy (XPS) was carried out on a Physical Electronics 5700 instrument with photoelectrons generated by the non-monochromatic Al K α irradiation (1486.6 eV). Photoelectrons were collected at a takeoff angle of 45° using a hemispherical analyzer operated in the fixed retard ratio mode with an energy resolution

setting of 11.75 eV. The binding energy scale was calibrated prior to analysis using the Cu 2p_{3/2} and Ag 3d_{5/2} lines. Charge neutralization was ensured through cobombardment of the irradiated area with an electron beam and the use of the nonmonochromated Al K α source.

b) Synthesis

b1) Synthesis of (3,5-bis(4-(9H-carbazol-9-yl)butoxy)-benzoyl)-functionalized dendrimer (PC, 3.13)

Perfluorophenyl-3,5-bis(4-(9H-carbazol-9-yl)butoxy)benzoate (G₁COOPP, 3.8)

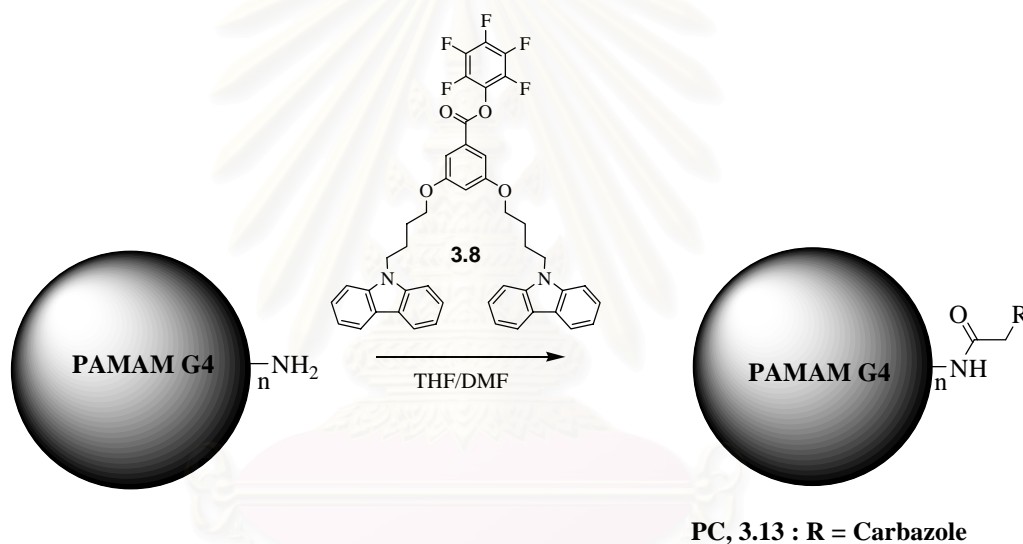


A mixture of compound **3.4** (0.20 g, 0.34 mmol) and pentafluorophenol (0.08 g, 0.42 mmol) were allowed to react in 20 mL of dry THF in the presence of dicyclohexylcarbodiimide (DCC) (0.10 g, 0.50 mmol) and *p*-(dimethylamino)pyridine (DMAP) (0.06 g, 0.49 mmol) for 2 days. After separation of dicyclohexylurea by filtration, the solvent was removed by rotary evaporation. The resulting residue was purified by column chromatography on silica gel (CH₂Cl₂/*n*-hexane (1:1)). The compound **3.8** was obtained as an orange crystal (0.15 g, 68% yield).

Characterization data for 3.8

¹H-NMR (300 MHz, CDCl₃): δ (ppm) 8.10 (d, $J = 7.5$ Hz, 4H, ArH_{CBz}), 7.50-7.40 (m, 8H, ArH_{CBz}), 7.24-7.20 (m, 4H, ArH_{CBz}), 6.63 (s, 1H, ArH), 6.62 (s, 1H, ArH), 6.61 (s, 1H, ArH), 4.38 (t, $J = 6.6$ Hz, 4H, NCH₂CH₂), 3.94 (t, $J = 6.0$ Hz, 4H, OCH₂CH₂), 2.08 (m, 4H, NCH₂CH₂CH₂), 1.85 (m, 4H, OCH₂CH₂CH₂)

(3,5-Bis(4-(9H-carbazol-9-yl)butoxy)-benzoyl-Functionalized Dendrimer (PC, 3.13)



PAMAM-(NH₂)₆₄ (18.40 mg, 1.30 μ mol) with 64 primary amine groups was dissolved in a mixture of 10 mL of dried THF and 10 mL of dried DMF. To this solution was slowly added with a solution of **3.8** (74.00 mg, 97.5 μ mol) in a dropwise fashion. After the addition was completed, the reaction mixture was refluxed for 2 days, yielding an orange solution. The solvent was removed by rotary evaporation. The obtained crude product was washed with diethyl ether twice and recrystallized from CH₂Cl₂/MeOH to afford pure **3.13** as a yellow solid (42.00 mg, 85% yield).

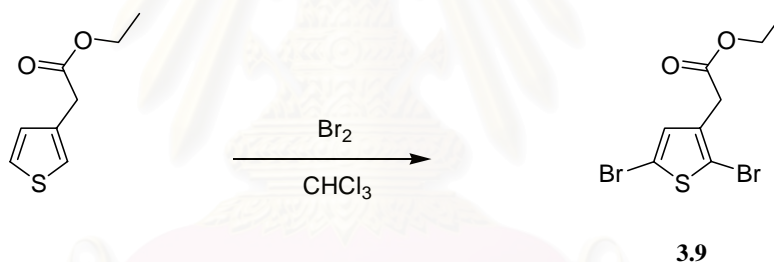
Characterization data for 3.13

¹H-NMR (300 MHz, CDCl₃): δ (ppm) 8.10 (br s, 184H, ArH), 7.34-7.15 (m, 552H, ArH), 6.75 (br s, 138H, ArH), 6.30 (br s, 46H, ArCONHCH₂), 4.10 (br s, 184H, NCH₂CH₂), 3.57 (br s, 184H, OCH₂CH₂), 3.49-2.11 (m, 1138H, CH₂CH₂NHCO, NCH₂CH₂N and CH₂NH₂), 1.78 (br s, 184H, NCH₂CH₂CH₂), 1.55 (br s, 184H, OCH₂CH₂CH₂)

UV-vis (Toluene): λ_{max} = 332 and 345 nm

b2) Synthesis of 2-(2,5-di(thiophen-2-yl)thiophen-3-yl) acetoxy-functionalized dendrimer (PC, 3.14)

Ethyl-2,5-Dibromothiophene-3-acetate (3TOET, 3.9)

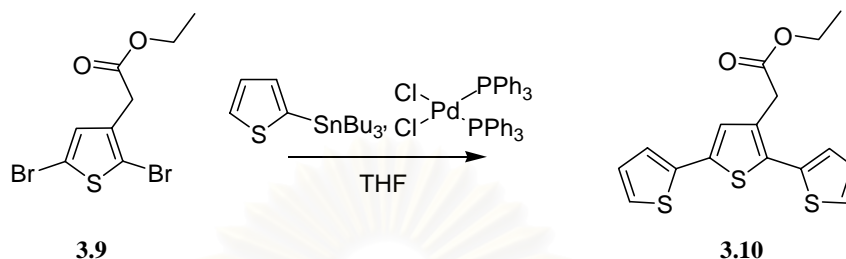


A solution of 3.94 mL (77.00 mmol) of bromine was added to a solution of 5.94 g of ethyl thiophene-3-acetate in 100 mL of chloroform. The solution was stirred for 4 hours, then quenched with a 10% aqueous sodium hydroxide solution and washed with distilled water, dried with MgSO₄, and evaporated. The resulting residue was distilled, 200 °C under reduced pressures, yielding of **3.9**, (10.90 g, 95% yield).

Characterization data for 3.9

¹H-NMR (300 MHz, CDCl₃): δ (ppm) 6.8 (s, 1H, ArH), 4.06 (q, *J* = 7.15 Hz, 2H, OCH₂CH₃), 3.46 (s, 2H, ArCH₂CO), 1.18 (t, *J* = 7.14 Hz, 4H, OCH₂CH₃)

Ethyl-2-(2,5-di(thiophen-2-yl)thiophen-3-yl)acetate (3TOET, 3.10)



A solution of **3.9** (3.20 g, 10.00 mmol) and 2-(tributylstannyl) thiophene (7.45 g, 20.00 mmol) were added to a THF solution of dichlorobis-(triphenylphosphine)palladium (0.46 g, 0.4 mmol). The mixture was heated at 80 °C for 24 hours. The solvent was removed under vacuum, and the residue was dissolved in CH_2Cl_2 , washed with water, and dried with MgSO_4 . The crude product was purified by chromatography on silica gel with toluene as eluent. A total of **3.10**, 1.68 g of ethyl 2-(2,5-di(thiophen-2-yl)thiophen-3-yl)acetate was obtained (50%).

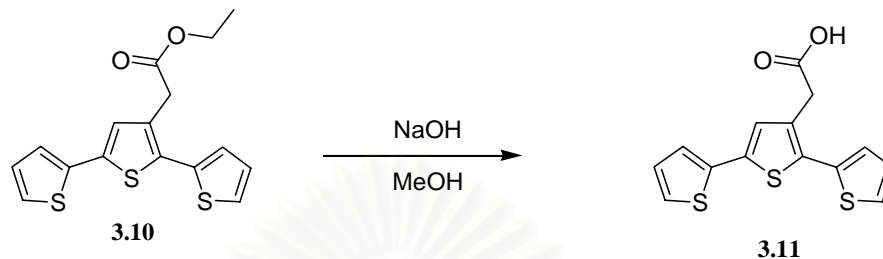
Characterization data for 3.10

$^1\text{H-NMR}$ (300 MHz, CDCl_3): δ (ppm) 6.8-7.2 (m, 7H, ArH), 4.06 (q, $J = 7.15$ Hz, 2H, OCH_2CH_3), 3.46 (s, 2H, ArCH_2CO), 1.18 (t, $J = 7.14$ Hz, 3H, OCH_2CH_3)

MALDI-TOF: m/z Calcd for $[\text{C}_{16}\text{H}_{14}\text{O}_2\text{S}_3]^+$: m/z 334.02

Found: $[\text{C}_{16}\text{H}_{14}\text{O}_2\text{S}_3 + \text{H}]^+$: m/z 335.21

2-(2,5-di(thiophen-2-yl)thiophen-3-yl)acetic acid (3TOH, 3.10)



A solution of **3.10** (3.40 g, 10.00 mmol) was dissolved in methanol and added to a 20% aqueous sodium hydroxide solution (300 mL). The mixture was refluxed for 4 hours. After concentration the aqueous solution was washed with ether, acidified with concentrated HCl to pH 1 and extracted by ether. The ether solution was washed up to pH 7, evaporation of ether yielded **3.11**, 2.80 g (90%) of 2-(2,5-di(thiophen-2-yl)thiophen-3-yl)acetic acid.

Characterization data for 3.11

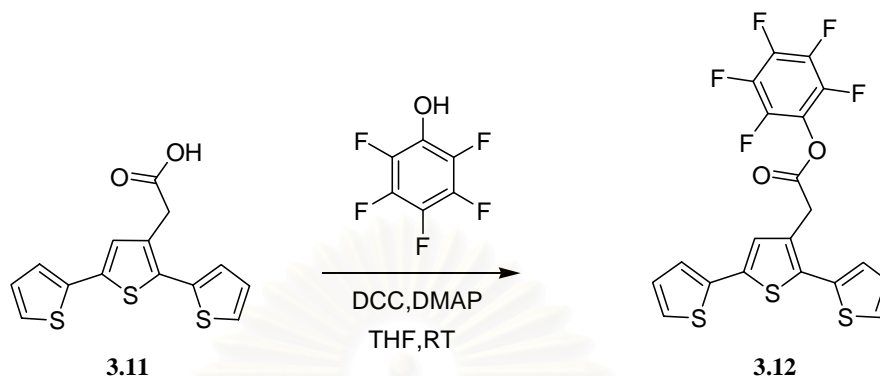
¹H-NMR (300 MHz, CDCl₃): δ (ppm) 6.8-7.2 (m, 7H, ArH), 3.46 (s, 2H, ArCH₂CO

MALDI-TOF: m/z Calcd for [C₁₄H₁₀O₂S₃]⁺: m/z 305.98

Found: [C₁₄H₁₀O₂S₃ + H]⁺: m/z 306.71.

สถาบันวิทยบริการ
จุฬาลงกรณ์มหาวิทยาลัย

Perfluorophenyl-2-(2,5-di(thiophen-2-yl)thiophen-3-yl)acetate (3TCOOPP, 3.12)



Compound **3.12** was prepared by the same procedure of **3.8** by using compound **3.11** (0.20 g, 0.65 mmol), pentafluorophenol (0.15 g, 0.82 mmol), dicyclohexylcarbodiimide (DCC) (0.20 g, 0.98 mmol) and *p*-(dimethylamino)pyridine (DMAP) (0.12 g, 0.98 mmol) in 20 mL of anhydrous THF. After purification by column chromatography on silica gel ($\text{CH}_2\text{Cl}_2/n$ -hexane (1:1)), compound **3.12** was obtained as an orange crystal (0.03 g, 10% yield).

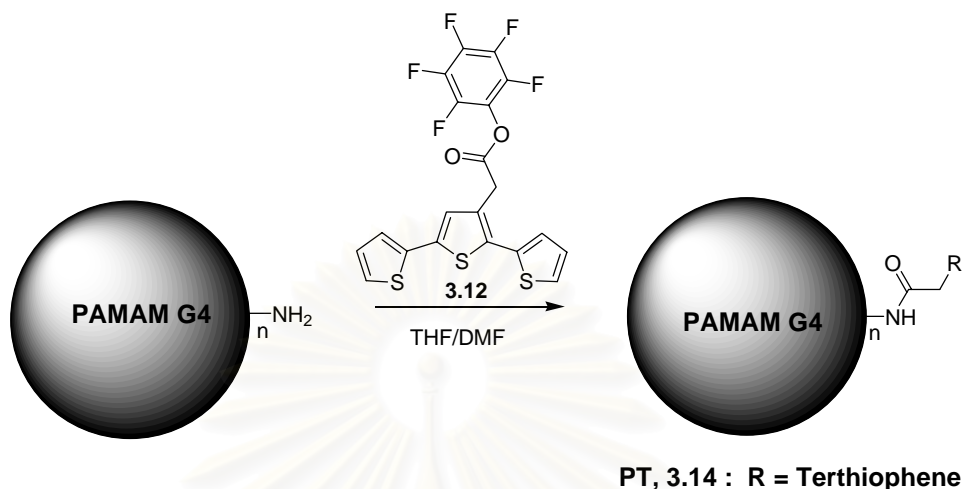
Characterization data for 3.12

$^1\text{H-NMR}$ (300 MHz, CDCl_3): δ (ppm) 7.49-7.10 (m, 7H, ArH), 4.17 (s, 2H, ArCH₂COOAr)

MALDI-TOF: m/z Calcd for $[\text{C}_{20}\text{H}_9\text{F}_5\text{O}_2\text{S}_3]^+$: m/z 471.97

Found: $[\text{C}_{20}\text{H}_9\text{F}_5\text{O}_2\text{S}_3 + \text{H}]^+$: m/z 473.02

2-(2,5-di(thiophen-2-yl)thiophen-3-yl) acetyl-Functionalized Dendrimer (PC, 3.14)



Dendrimer **14** was synthesized by using the same methodology as dendrimers **3.13** with PAMAM-(NH₂)₆₄ (12.20 mg, 0.0009 mmol) with 64 primary amine groups and perfluorophenyl-2-(2,5-di(thiophen-2-yl)thiophen-3-yl)acetate (**3.4**) (30.00 mg, 0.0635 mmol) in a mixture of 10 mL of dried THF and 10 mL of dried DMF. Dendrimer **3.14** was obtained as a yellow solid (21.00 mg, 83% yield).

Characterization data for 3.14

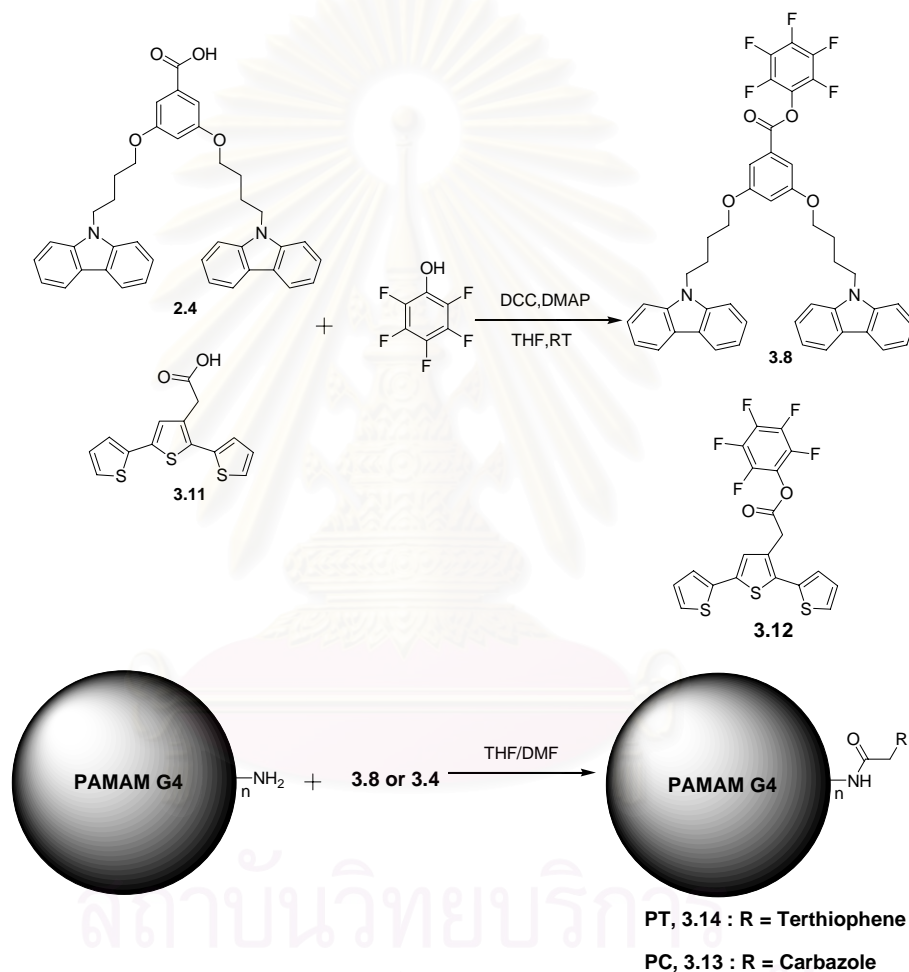
¹H-NMR (300 MHz, CDCl₃): δ (ppm) 8.23 (br s, 44H, CH₂CONHCH₂), 7.54-7.15 (m, 308H, ArH_{3t}), 3.75 (br s, 88H, ArCH₂CONH), 3.43-2.39 (m, 1160H, CH₂CH₂NHCO, NCH₂CH₂N and CH₂NH₂)

UV-vis (Toluene): λ_{max} = 344 nm

3.2.4 Results and discussion

3.2.4.1 Synthesis of derivative of PAMAM dendrimers

The starting materials, ethyl 2-(2,5-di(thiophen-2-yl)thiophen-3-yl)acetate and methyl-3,5-bis[4-(9*H*-carbazol-9-yl)butoxy]benzoate, were prepared according to the procedures reported in literature [165,166].



Scheme 3.1 Electroactive groups (terthiophene, T and carbazole, C) of modified PAMAM dendrimer were used in this study.

Hydrolyzation of both compounds was performed by using KOH in THF/MeOH, followed by reaction with an excess of pentafluorophenol in the presence of DCC/DMAP in THF. The active ester perfluorophenyl-3,5-bis(4-(9H-carbazol-9-yl)butoxy)benzoate (**3.3**) and perfluorophenyl-2-(2,5-di(thiophen-2-yl)thiophen-3-yl)acetate (**3.4**) were obtained in 68% and 10%, respectively. Amidation reactions of **3.3** and **3.4** with PAMAM were accomplished in THF/DMF to obtain PC (85%) and PT (83%) (as shown in Scheme 3.1).

3.2.4.2 Preparation of Au DENs

The attempt to prepare Au-NPs encapsulated in PT and PC dendrimers were initiated by adding an aliquot of 55 μL and 110 μL of AuCl_3 (1×10^{-3} M) in MeOH into a solution containing PT and PC (1×10^{-6} M) in toluene, respectively. These pale yellow solutions were vigorously stirred for 30 mins to incorporate AuCl_3 into the dendrimer templates. The reduction to zero valent Au-NPs simultaneous with the oxidative chemical polymerization of carbazole or terthiophene in the periphery of the dendrimers is expected, i.e., $\text{PT} \rightarrow \text{PPT}$ and $\text{PC} \rightarrow \text{PPC}$.

In a typical procedure, PT was reacted with 55 equivalents of the gold precursor. Upon adding the AuCl_3 solution into the PT solution, the color of the solution changed immediately from pale yellow to blue. After 30 mins, a dark blue solution was observed. The blue color is probably due to electron transfer from the terthiophene to Au^{3+} (metal to ligand charge transfer or MLCT). It has been reported that polyelectrolyte complex (PEC) with water-soluble terthiophene derivative also changed in color successively after addition of Au^{3+} [155]. A similar procedure was also employed for the PC. From the initial experiment, using 55 equivalents of gold, no color change can be observed. Therefore, a larger ratio of AuCl_3 to PC was employed. When 110 equivalents of gold precursor was used, the color change from pale yellow to deep yellow and the color was found to be stable in the media even after several weeks. The fact that a higher ratio of

AuCl_3 to PC was needed may be due to the higher oxidation onset potential (monomer) (0.8-1.0 mV) for the carbazole compared to terthiophene at about 0.22 V [107,113].

3.2.4.3 Formation of DENs by UV-vis, FT-IR and fluorescent spectrometry

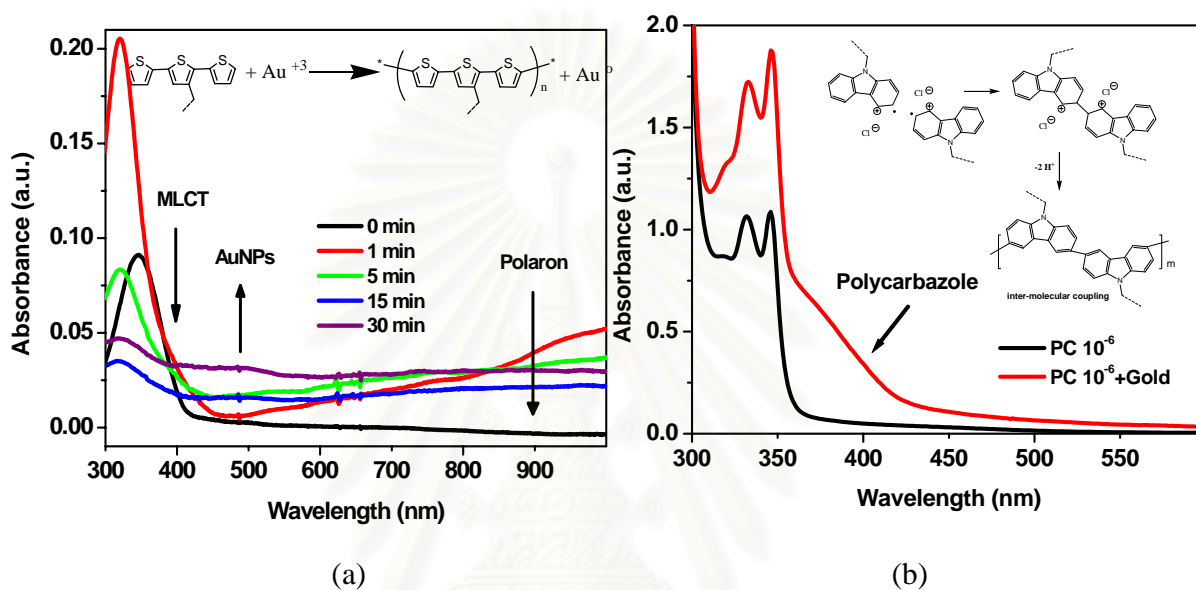


Figure 3.24 UV-vis absorption spectra of PAMAM dendrimers functionalized with terthiophene (PT) and carbazole (PC) dendrons 10^{-6} M before and after adding with AuCl_3 in toluene. (a) PT at different time (0-30 mins), and (b) PC after adding AuCl_3 30 mins. Dendrimer PT and PC show their characteristic absorption bands at 345, 333 and 346 nm, respectively.

The formation of DENs can be tracked by monitoring the change in UV-vis absorbance at various time intervals. The main absorption band observed at 320 nm is attributed to the terthiophene unit. The UV-vis optical spectra of 1×10^{-6} M of PT in toluene after addition of 55 μL of AuCl_3 at 0, 1, 5, 15 and 30 mins is shown in Figure 3.24a. The observed peaks at 320 nm and at 850 to 1000 nm corresponds to the π - π^* and polaron- π , π - π , and polaron- π^* transitions, respectively. The peak shift from 345 nm to

320 nm is due to the presence of MLCT transitions. This peak gradually decreases with time. After vigorous stirring for 30 mins, the absorption band of polythiophene and the surface plasmons of Au nanoparticles appeared at 410-550 nm.

However, it may be difficult to totally distinguish the Au-NP surface plasmon band by this technique due to the overlap between the Au-NP and polythiophene peaks [156]. Nevertheless, one interesting evidence is the coincident decrease of the MLCT region at 345 nm for Au⁺³ to thiophene, increase at the 500 nm for Au-NP, and decrease in polaron band with time (Figure 3.24a). The latter indicates convincing evidence of Au⁰ formation since the electron charge (polaron, radical cation) will tend to reside on the Au⁰ surface rather than on the conjugated polythiophene species when present. The UV-vis spectrum for PC (1×10^{-6} M) to PPC conversion is shown in Figure 3.24b. The absorbances at 333 and 346 nm which are characteristic of the carbazole group were observed [107,113]. After mixing the PC solution with 110 equivalents of AuCl₃ for 30 mins, a peak at 315 nm increased and a slight hypsochromic shift is observed [157]. On the other hand, the π - π^* transition of carbazole was red shifted and an absorption tail extending into the visible range centered at 385 nm on the PPC is observed. This indicated the formation of higher π -conjugated species. However, this spectrum seemingly lacked the characteristic plasmon band at the 500 nm region. In general, the simultaneous oxidative polymerization of PT and PC and AuNPs formation were performed until no further change was observed.

The steady state fluorescence emission spectra of solutions of PT, PPT-AuNPs, PC and PPC-AuNPs are shown in Figure 3.25. Without AuNPs, the terthiophene modified PAMAM dendrimer, PT, exhibited a strong characteristic emission of terthiophene with the emission maximum at 433 nm and one shoulder around 415 nm upon excitation at 345 nm (in Figure 3.25a) while the carbazole modified PAMAM dendrimer, PC, showed a characteristic emission at 356 and 365 nm upon excitation at 333 nm (in Figure 3.25b) [107]. The emission of PT was quenched dramatically in the PPT-AuNPs hybrid and also slightly shifted when the PC was used as a substrate due to a

highly efficient energy transfer between PPT, PPC to AuNPs [158] and self-quenching with formation of conjugated polymer species [113]. These were confirmed by the observation of a new peak at 545, 510 nm in PT and PC, respectively. This is due to the AuNPs quenching for the PT but most likely represents a Au^{+3} - MLCT quenching effect for the PC dendrimer because of the absence of the plasmon band from the UV-vis absorption spectrum.

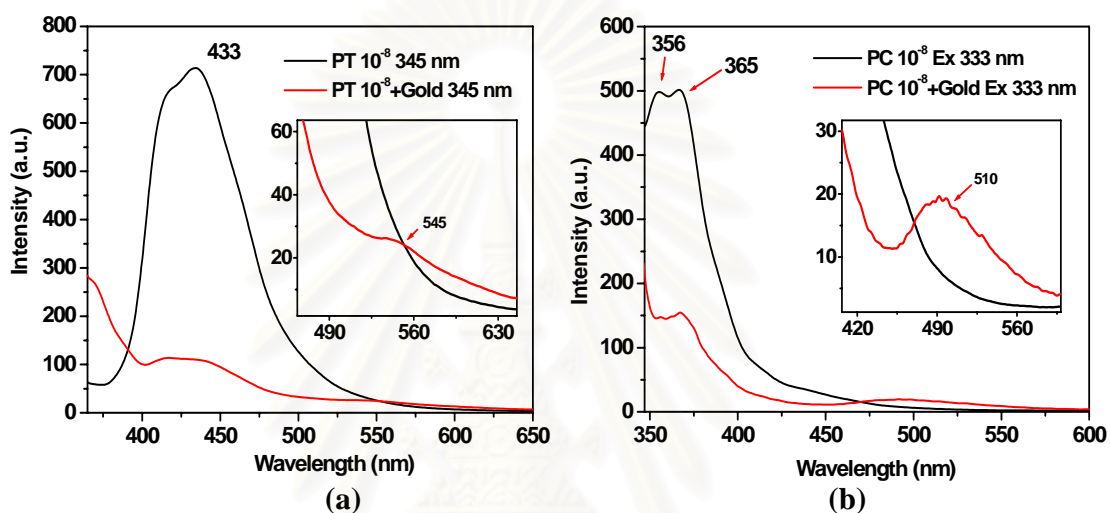


Figure 3.25 Steady-state fluorescent spectra of PAMAM dendrimers functionalized with terthiophene (PT) and carbazole (PC) dendrons 10^{-6} M before and after treated with $AuCl_3$ in toluene by using excitation wavelengths at 345 and 333 nm, respectively. ET mechanism was proved by quenching phenomena and new peaks of AuNPs.

The preparation of the hybrid nanoparticles was also monitored by FT-IR spectra (Figure 3.26). The characteristic peaks were observed at 1636 and 1690 cm^{-1} corresponding to the two amide bands of PAMAM. The $=C-H$ in-plane and out-of-plane vibrations of the substituted terthiophene ring is assigned to $1,240$ and 825 cm^{-1} , respectively. These two bands disappeared for the DEMNs which formed upon the oxidation of terthiophene by $\alpha-\alpha'$ coupling to form polythiophene with Au^{3+} to Au^0

conversion. The PAMAM characteristic peaks were also observed for the PC and in addition, 1230, 1325, 1450, and 1533 cm^{-1} peaks representing the carbazole aromatic (C-H), (C-N)_{ring} and carbazole (C=C)_{ring} vibrations [107b]. We also observed the disappearance of the =C-H in-plane and out-of-plane vibrations of PC at 1325 and 847 cm^{-1} , respectively with complexation. In general, both the loading of metal ions and the presence of nanoparticles shifted the amide vibration to longer cm^{-1} .

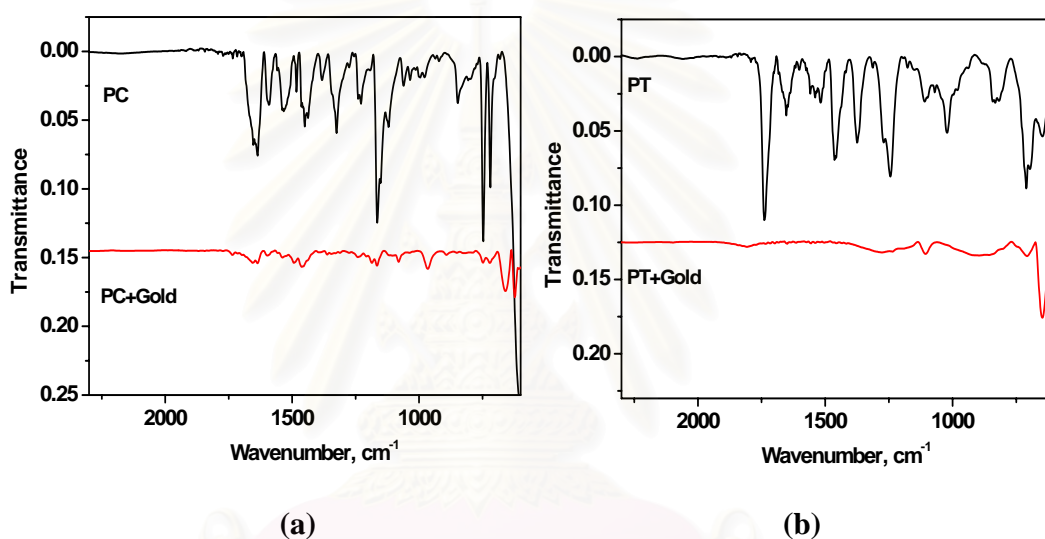


Figure 3.26 FT-IR spectra of films (drop-cast on ITO substrate, from top to bottom) of PAMAM dendrimers functionalized with 10^{-6} M of PC (a) and PT (b) dendrons before and after treated with AuCl_3 in toluene.

3.2.4.4 Characterization of DENs by XPS, and AFM

The formation of the hybrid materials was also examined by XPS. A solution of the Au-NP-PT dendrimer complex was solution cast on planar Si wafer. The Au^0 spectra based on Au 4f $_{7/2}$ and Au 4f $_{5/2}$ doublet appeared at 84.4 and 88.1 eV, respectively (Figure 3.27a). These features were in agreement with results reported for self-assembled

alkanedithiol [159], alkanethiols on AuNPs and/or bulk gold substrates [160] as well as for bulk gold [161]. However, it was hard to detect Au NPs from the AuCl₃ and PC procedure in toluene. This can imply that the conjugated polycarbazole modified dendrimer was not able to fully convert a majority of the Au⁺³ precursor to Au-NPs. The redox coupling was observed only with carbazole species and the MLCT was primarily with Au⁺³ species. No distinct plasmon band was observed with the UV-vis spectra supports this fact. Thus compared to the PC, the PT was a more effective oxidant to form Au-NPs DEMNs in the inner shelf and simultaneously forming the conjugated polythiophene PPT in the outer shelf [162].

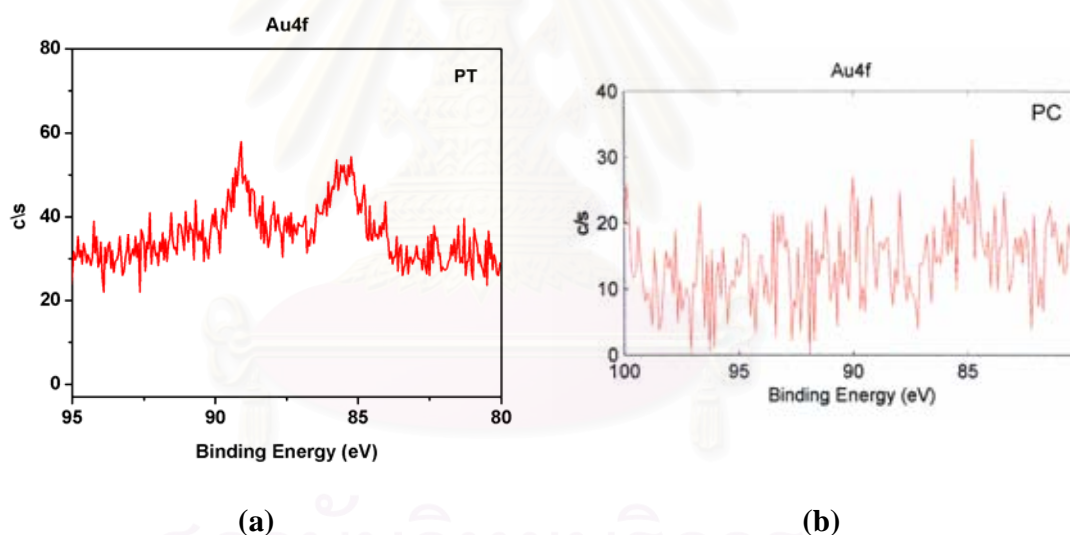


Figure 3.27 High-resolution XPS of the informative elements for the structure determination of (a) PPT-AuNPs and (b) PPC-AuNPs.

The particle morphology and distribution of the dendrimers before and after treatment with AuCl₃ have also been studied using AFM measurements (Figures 3.28 and 3.29). A droplet of a 1×10^{-6} M of toluene solution was placed on mica and the solution

was allowed to evaporate in spin-coating technique. Shown in Figure 3.28b is the AFM image of a large ordered two-dimensional array of PPT-Au NPs on a mica substrate. The image demonstrates the near homogenous distribution of the particles which tends to form very large aggregates at higher concentrations and on hydrophobic substrates.

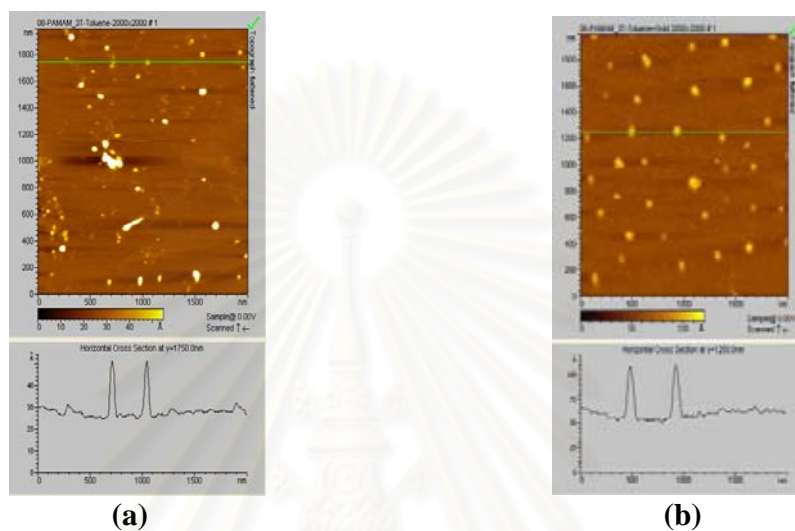


Figure 3.28 AFM image ($2 \times 2 \mu\text{M}$) of PT (a) and PPT-AuNPs (b) on mica substrate.

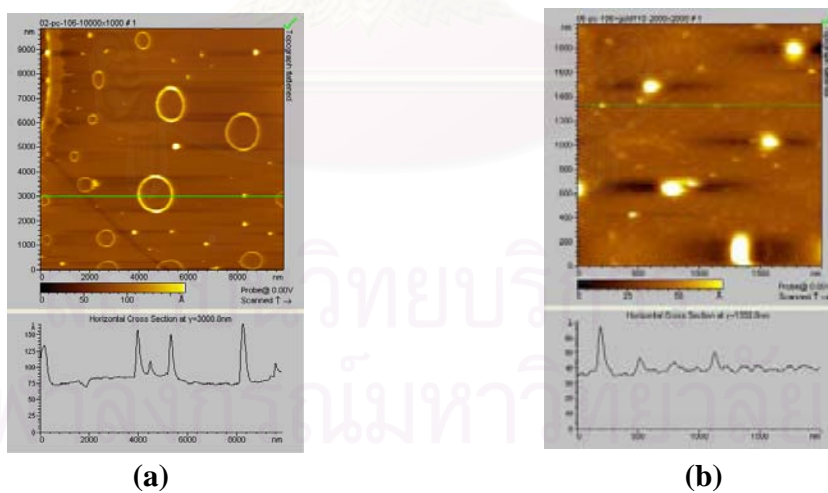


Figure 3.29 AFM image ($2 \times 2 \mu\text{M}$) of PC (a) and PPC-AuNPs (b) on mica substrate.

Detailed cross-sectional measurements performed on a large number of isolated features revealed an average height of 2.4 ± 1.0 nm for the PT alone and after the formation of the hybrid Au-NP within the PT, a more uniform and twice higher average height (height of $\sim 5.2 \pm 0.2$ nm) of particles were observed (Figure 3.28b).

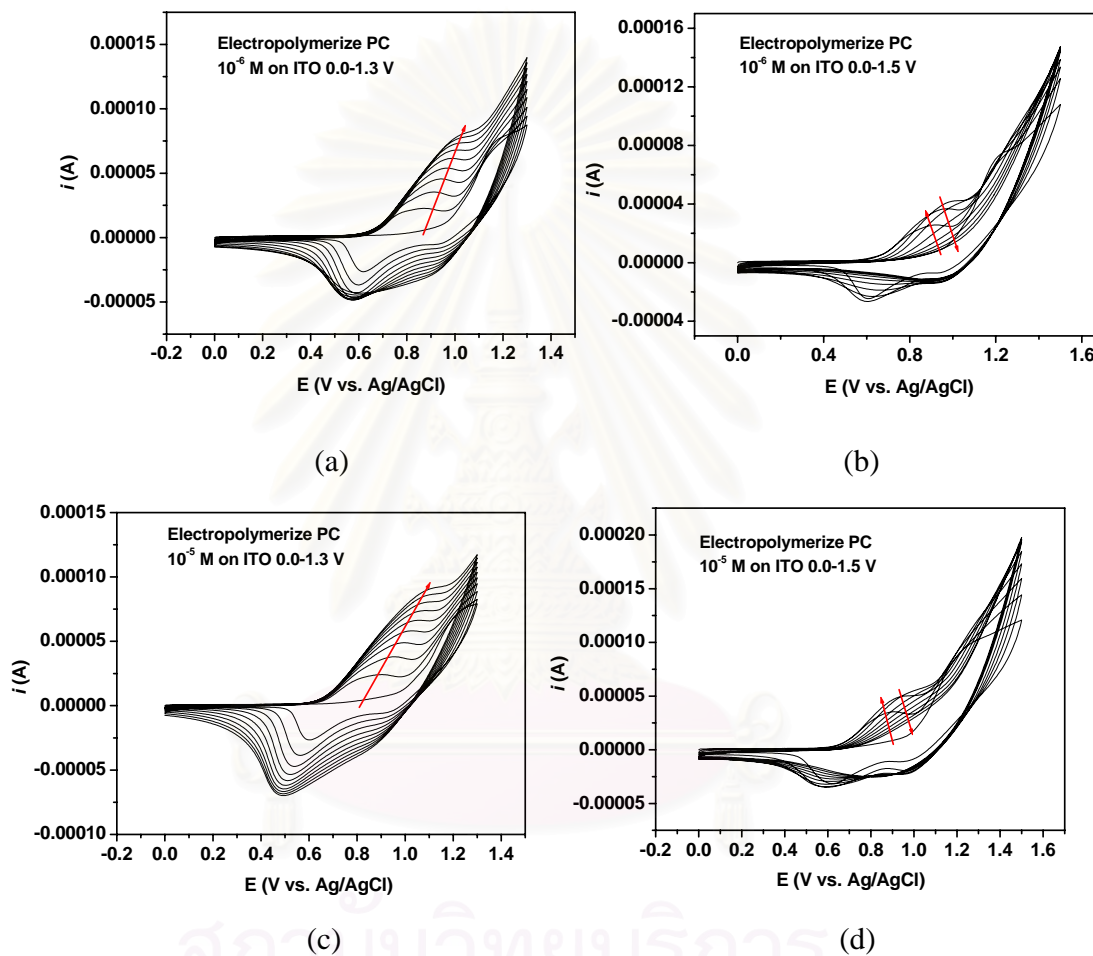


Figure 3.30 Cyclic voltammograms of the electrochemical cross-linking/deposition of PC at a scan rate of 50 mV/s, 10 cycles: (a) concentration of 10^{-6} M, potential window from 0-1.3 V, (b) concentration of 10^{-6} M, potential window from 0-1.5 V, (c) concentration of 10^{-5} M, potential window from 0-1.3 V, and (d) concentration of 10^{-5} M, potential window from 0-1.5 V.

For the PC, the entire substrate surface (of the large and small nanoparticles) was roughly covered with the dendrimer molecules. It is believed that the use of toluene as a solvent is the reason for aggregation between the dendrimer molecules on the hydrophilic substrate to form larger aggregates [163]. However, no individual DENs were observed as demonstrated in Figure 3.29. Thus, these results reveal evidence on the mechanism for a favorable in-situ formation of Au-NPs within PT. At first, metal ions were complexed with terthiophene by ion-dipole interaction and, then, oxidative polymerization of terthiophene occurred concurrent with Au-NPs formation. Surprisingly, when we investigated the PC dendrimers alone, we observed nano ring structures with different sizes on mica substrate (Figure 3.29a). These structures are comparable to the results obtained by Nolte and co-workers [164] on the formation of ring like structures of porphyrin molecules when solutions of porphyrins were allowed to evaporate fast. However, our results indicate a poor ability to mediate Au-NP reduction, although the PC to PPC oxidation (formation of more conjugated species) was observed electrochemically by cyclic voltammetry experiments (Figure 3.30). In the future, it should be possible to test this concept with different PAMAM generations.

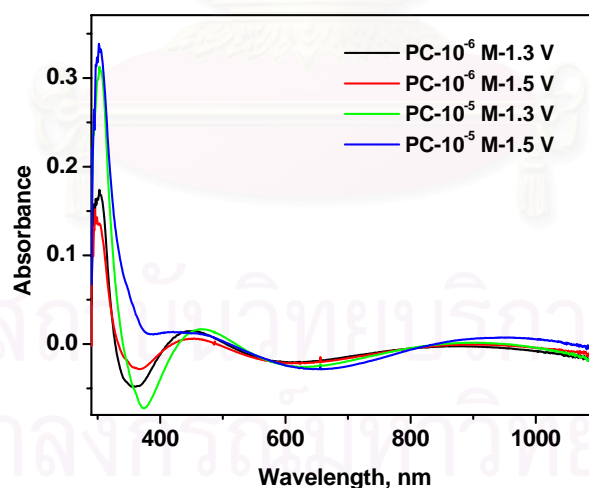


Figure 3.31 Spectroelectrochemical analysis performed in 0.1 M TBAPF₆/CHCl₃ on ITO substrate in the presence of different concentrations and potential windows of PC.

CHAPTER IV

CONCLUSIONS

4.1 Synthesis and binding properties of ditopic receptors based on hexahomotriazacalix[3]arene

4.1.1 Ditopic receptors based on hexahomotriazacalix[3]arene

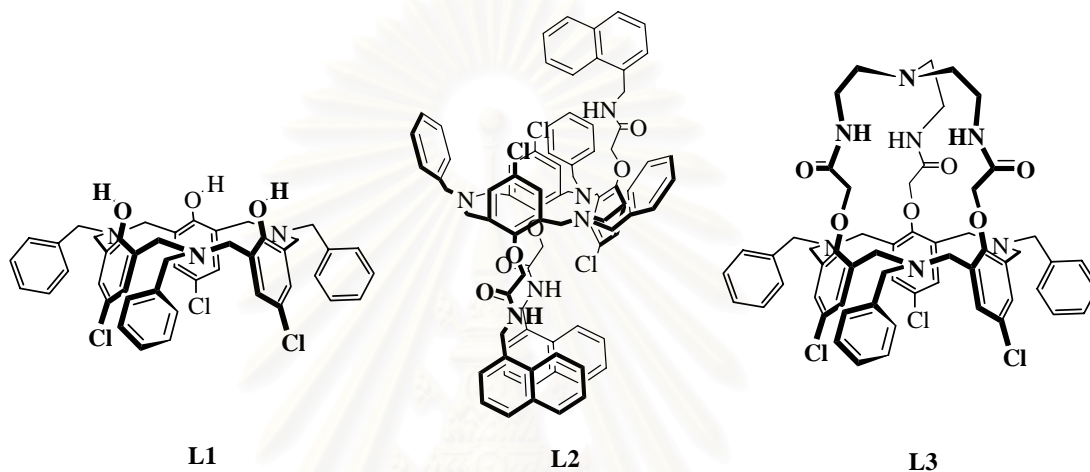


Figure 4.1 The derivative receptors based on hexahomotriazacalix[3]arene.

We have been successful to synthesize a novel C_{3v} -symmetrical N_7 -hexahomotriazacalix[3]cryptand (**L2**), N -benzylhexahomotriaza- p -chlorocalix[3]-trinaphthylamide (**L3**) and a new function of azacalix[3]arene template [**L1**] have been discovered as well. The reason why these three azacalix[3]arenes have drawn our attention was that they reflected all abilities of azacalix[3]arenes. First, **L1** showed ability to bind anions through hydrogen bonds which were dependent on the basicity of anions. As the color change from colorless to deep yellow after traced with fluoride, we can use this one to be a colorimetric sensor. The change of color has been derived from the deprotonate mechanism which confirmed by ^1H NMR, UV-vis and fluorescent spectroscopy. Second, **L2** and **L3** have first shown their potentials. Their conformations were proved by ^1H NMR spectroscopy and X-ray single-crystal structure determination. Complexation studies showed that **L2** was a selective receptor for Cl^- ion. **L2** turned out to bind Br^- in the presence of Zn^{2+} , which was called the allosteric effect. Monitored by fluorescence, UV-vis and ^1H -NMR spectrometric titration, partial-cone ligand **L3** binds strongly Cd^{2+} , Pb^{2+} and F^- using

nitrogens of azacalix[3]arene framework, amide groups and hydrogen bonds, respectively.

4.1.2 Ultrathin films of azacalixarene-carbazole conjugated polymer networks (CPN) for specific cation sensing

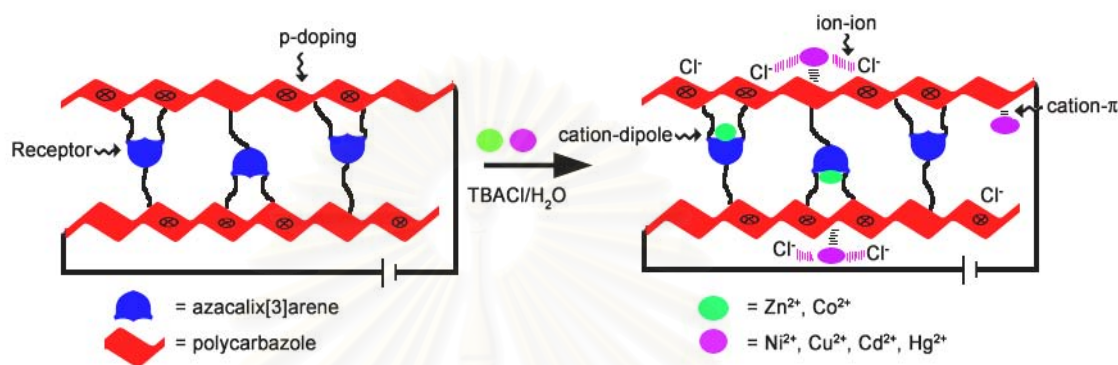


Figure 4.2 Molecular device based on hexahomotriazacalix[3]arene.

We have successfully developed a new class of chemosensor recognition elements based on *conjugated polymer network ultra-thin films* from electrochemical crosslinking of hexahomotriazacalix[3]arene-carbazole. We also demonstrated its selectivity and sensitivity towards Zn^{2+} by using potentiometry, QCM and SPR combined with electrochemistry. The results showed that *cation interaction to the film* might increase charge carrier transport properties on a *conjugated polymer* through azacalix[3]arene bound cations. It also reduces the doping states by interfering ions through ion-ion interaction and disturbs electron cloud on the π -extended conjugated polymer through cation- π interaction. Specifically, these observed changes in the electrical and spectroelectrochemical properties of the films are related to the cation-dipole interaction between Zn^{2+} and azacalix[3]arene resulting in a higher binding constant and its subsequent specificity for chemical sensing.

4.2 Electrochemically active dendrimers

4.2.1 Lord of the nano-rings: self-assembly and electropolymerization of PAMAM-carbazole dendron surfmer complexes

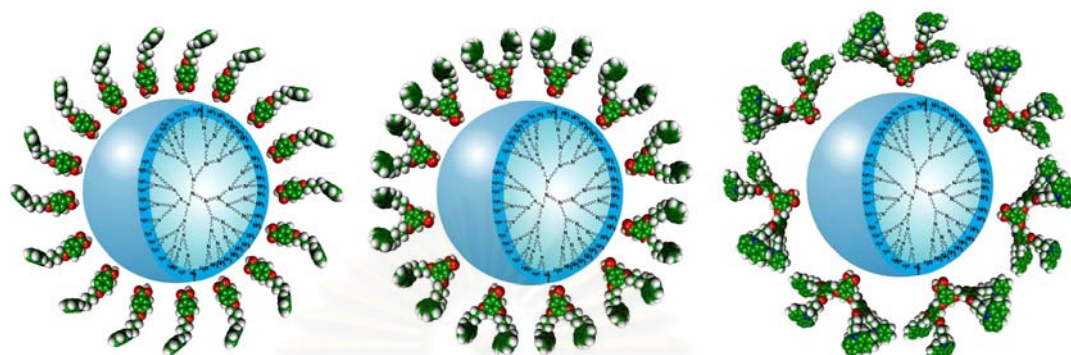


Figure 4.3 Self-assembly of PAMAM-carbazole dendron surfmer complexes.

We have demonstrated the successful self-assembly and complexation between dendrimer template (PAMAM G4) and dendron surfmers ($G_0\text{COOH}$, $G_1\text{COOH}$). An increasing steric hindrance of a dendron was a problem in complexation as demonstrated in the case of $G_2\text{COOH}$. Hypochromic shifts in the UV-vis spectra and quenching of fluorescence indicated that $G_1\text{COOH}$ was trapped around the dendrimer. Ammonium and carboxylate species were investigated by FTIR. The isolated sphere size was observed on the mica substrates. The stronger complexation was found in PAMAM- $G_1\text{COOH}$. The electrochemical cross-linking of dendrimer complexes as thin films revealed unusual CV behavior depending upon the generation. PAMAM- $G_1\text{COOH}$ showed a higher extent of inter- and intramolecular cross-linking while PAMAM- $G_0\text{COOH}$ showed a higher degree of aggregation. More interestingly nanoring structures were observed as the complex was deposited on ITO indicating a type of supramolecularly-based template electropolymerization of a dendrimer-surfmer complex. The CMC, AFM and XPS revealed a ring-like or donut structure most likely composed of the PAMAM-core and dendron-carbazole shell. This was formed at the equilibrium of decomplexation and weak complexation. In principle, different generation of dendrons, different dendrimer topologies, and other electroactive surfmer moieties can result in a wider applicability of this method, for electro-optical applications, drug delivery, sensing, and other nanoscience and materials directions.

4.2.2 Redox nanoreactor dendrimer boxes: *in-situ* hybrid gold nanoparticles via terthiophene and carbazole-PAMAM dendrimer oxidation

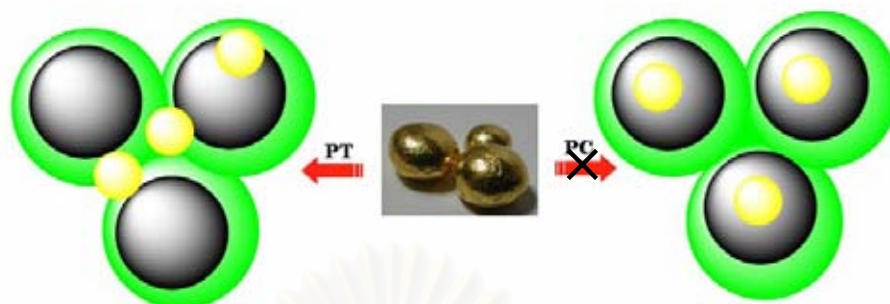


Figure 4.4 The possibility to form hybrid gold nanoparticles via terthiophene and carbazole-PAMAM dendrimer oxidation.

π -conjugated dendrimer-protected gold nanoparticles in stable colloidal form have been successfully prepared via simultaneous reduction of AuCl_3 with oxidation of terthiophene (PT) and carbazole (PC) peripheral functionalized PAMAM dendrimers. The hybrid dendrimer-metal materials were characterized using UV-vis, fluorescence, and FT-IR spectroscopy. XPS and AFM analysis were also employed. The differences in gold nanoparticle (AuNP) formation between the two PAMAM derivatives were discussed. In case of PT dendrimer, AuNPs can be stabilized by thiophene to construct PAMAM-AuNPs hybrid materials. For the PC dendrimer, the redox reaction afforded PPC formation without necessarily forming AuNPs as demonstrated in Figure 4.4.

4.3 Suggestion for future works

From all obtained results and discussion, future works should be focused on;

- 4.3.1 X-ray crystal structures of compound and their complexes with various anionic guests should be obtained in order to understand the structure of the synthetic receptors and their coordination chemistry.
- 4.3.2 Computational optimization of compound and their complexes with various anionic and cationic guests should be investigated to obtain complexation energies and physical properties upon complexation.
- 4.3.3 The possibility of using compound as a molecular device should be explored using many techniques such as membrane electrodes.

REFERENCES

- [1] Vicens, J.; Bohmer, V. *Calixarenes: A Versatile class of compounds*. Eds., Dordrecht: Kluwer Academic Publishers; **1991**.
- [2] Asfari, Z.; Böhmer, V.; Harrowfield, J.; Vicens, J. *Calixarenes 2001*, Eds., Dordrecht: Kluwer Academic Publishers; **2001**.
- [3] Gutsche, C.D.; Stoddart, J.F.; Calixarenes, Monographs in *Supramolecular chemistry Vol. 1*, Eds., Cambridge: The Royal Society of Chemistry; **1989**.
- [4] Gutsche, C. D.; Dhawan, B.; No, K. H.; Muthukrishnan, R. "The synthesis, characterization, and properties of the calixarenes from *p*-tert-butylphenol" *J. Am. Chem. Soc.* **1981**, *103*, 3782-3792.
- [5] Zinke, A.; Ziegler, E. "Zur Kenntnis des Härtingsprozesses von Phenol-Formaldehyd-Harzen, X. Mitteilung" *Chem. Ber.* **1944**, *77*, 264-272.
- [6] Gutsche, C. D.; Muthukrishnan, R. "Calixarenes. 1. Analysis of the product mixtures produced by the base-catalyzed condensation of formaldehyde with para-substituted phenols" *J. Org. Chem.* **1978**, *43*, 4905-4906.
- [7] Gutsche, C. D.; Dhawan, B.; Levine, J. A.; No, K. H.; Bauer, L. J. "Calixarenes 9: Conformational isomers of the ethers and esters of calix[4]arenes" *Tetrahedron.* **1983**, *39*, 409-426.
- [8] (a) Iwamoto, K.; Araki, K.; Shinkai, S. "Conformations and structures of tetra-O-alkyl-*p*-tert-butylcalix[4]arenes. How is the conformation of calix[4]arenes immobilized?" *J. Org. Chem.* **1991**, *56*, 4955-4962; (b) Araki, K.; Iwamoto, K.; Shinkai, S.; Matsuda, T. *Chem. Lett.* **1989**, 1747-1750.
- [9] Guelzim, A.; Khrifi, S.; Baert, F.; Loeber, C.; Asfari, Z.; Matt, D.; Vicens, J. *Acta Crystallogr.* **1993**, *C49*, 72-74.
- [10] Izatt, R. M.; Lamb, J. D.; Hawkins, R. T.; Brown, P. R.; Izatt, S. R.; Christensen, J. J. "Selective M^+H^+ coupled transport of cations through a liquid membrane by macrocyclic calixarene ligands" *J. Am. Chem. Soc.* **1983**, *105*, 1782-1785.
- [11] (a) Delaigue, X.; Hosseini, M. W. "Multicavitands II: Synthesis of a non centrosymmetric hollow molecular unit (koiland) based on fusion of two *p*-tert-butylcalix[4]arenes by both silicon and titanium atoms" *Tetrahedron Lett.* **1993**, *47*, 7561-7564. (b) Delaigue, X.; Hosseini, M. W. "Multicavitands III: Synthesis and NMR studies of a tri-directional koiland composed of three *p*-tert-butylcalix[4]arene units fused by two silicon atoms" *Tetrahedron Lett.*

- 1994**, 35, 1711-1714. (c) Martz, J.; Graf, E.; Hosseini, M. W.; Cian, A. De.; Fisher, J. "Molecular tectonics: design, synthesis and structural analysis of a molecular network based on inclusion processes using a doubly fused *p*-isopropylcalix[4]arene" *J. Mater. Chem.* **1998**, 8(11), 2331-2333.
- [12] Olmstead, M. M.; Sigel, G.; Hope, H.; Xu, X.; Power, P. P. "Metallocalixarenes: syntheses and x-ray crystal structures of titanium(IV), iron(III), and cobalt(II) complexes of *p*-tert-butylcalix[4]arene" *J. Am. Chem. Soc.* **1985**, 107, 8087-8091.
- [13] (a) Dhawan, B.; Gutsche, C.D. "Calixarenes. 10. Oxacalixarenes" *J. Org. Chem.* **1983**, 48, 1536-1539. (b) Hampton, P.D.; Bencze, Z.; Tong, W.; Daitch, C.E. "A New Synthesis of Oxacalix[3]arene Macrocycles and Alkali-Metal-Binding Studies" *J. Org. Chem.* **1994**, 59, 4838-4843. (c) Ashram, M.; Mizyed, S.; Georghiou, P.E. "Synthesis of Hexahomotrioxacalix[3]naphthalenes and a Study of Their Alkali-Metal Cation Binding Properties" *J. Org. Chem.* **2001**, 66, 1473-1479. (d) Tsubaki, K.; Morimoto, T.; Otsubo, T.; Kinoshita, T.; Fuji, K. "Synthesis, Structure, and Ion-Binding Properties of New Tetraoxacalix[3]arenes" *J. Org. Chem.* **2001**, 66, 4083-4986.
- [14] Masci, B.; Nierlich, M.; Thuéry, P. "Supramolecular assemblies from uranyl ion complexes of hexahomotrioxacalix[3]arenes and protonated [2.2.2]cryptand" *New J. Chem.* **2002**, 26, 766-774.
- [15] Takemura, H.; Shinmyozu, T.; Miyura, H. "Synthesis and properties of N-substituted azacalix[3]arene" *J. Incl. Phenom. Macro.* **1994**, 19, 193-206.
- [16] (a) Khan, I. U.; Takemura, H.; Suenaga, M.; Shinmyozu, T.; Inazu, T. "Azacalixarene-new macrocycles with dimethyleneaza-bridged calix[4]arene system" *J. Org. Chem.* **1993**, 58, 3158-3161. (b) Takemura, H.; Shinmyozu, T.; Inazu, T. "Nitrogen-bridged macrocycles: Synthesis, structures and inclusion phenomena" *Coord. Chem. Rev.* **1996**, 156, 183-200.
- [17] Ebata, T.; Watanabe, T.; Mikami, N. "Evidence for the Cyclic Form of Phenol Trimer: Vibrational Spectroscopy of the OH Stretching Vibrations of Jet-Cooled Phenol Dimer and Trimer" *J. Phys. Chem.* **1995**, 99, 5761-5764 and references therein.
- [18] (a) Murahashi, S.; Kondo, K.; Hakata, T. *Tetrahedron Lett.* **1982**, 23, 229-232. (b) Bernotas, R.C.; Cube, R. V. *Tetrahedron Lett.* **1991**, 32, 161-164.

- (c) Watanabe, Y.; Tsuji, Y.; Ohsugi, Y. *Tetrahedron Lett.* **1981**, 22, 2667-2670.
- [19] (a) Takemura, H.; Yoshimura, K.; Khan, I. U.; Shinmyozu, T.; Inazu, T. "The first synthesis and properties of hexahomotriazacalix[3]arene" *Tetrahedron Lett.* **1992**, 33, 5775-5778.
- [20] Hampton, P. D.; Tong, W. D.; Wu, S. and Duesler, E. N. "Synthesis, X-ray structure and alkali-metal binding properties of a new hexahomotriazacalix[3]arene" *J. Chem. Soc., Perkin Trans. 2.* **1996**, 1127-1130.
- [21] Lumetta, G. J.; Rogers, R. D.; Gopalan, A. S. *Calixarenes for separations*. Washington, D.C.: American Chemical Society; **2000**, 195.
- [22] Chirakul, P.; Hampton, P. D.; Bencze, Z. "A convergent synthesis of hexahomotriazacalix[3]arene" *J. Org. Chem.* **2000**, 65, 8297-8300.
- [23] (a) Thuéry, P.; Nierlich, M.; Vicens, J.; Takemura, H. "Crystal structure of *p*-chloro-*N*-benzylhexahomotriazacalix[3]arene and of the complex of its zwitterionic form with neodymium(III) nitrate" *J. Chem. Soc., Dalton Trans.* **2000**, 42, 279-283. (b) Thuéry, P.; Nierlich, M.; Vicens, J.; Masci, B.; Takemura, H. "Oxa- and Azacalixarenes as Ligands for Uranyl Ions - Evidence for Two Different Complexation Modes" *Eur. J. Inorg. Chem.* **2001**, 637-643. (c) Thuéry, P.; Nierlich, M.; Vicens, J.; Takemura, H. Complexes of ytterbium(III) nitrate and triflate with homoazacalix[*n*]arenes (*n*=3,4)" *Polyhedron.* **2000**, 19, 2673-2678.
- [24] Chiang, C. K.; Fischer, C. R.; Park, Y. W.; Heeger, A. J.; Shirakawa, H.; Louis, E. J.; Gau, S. C.; MacDiarmid, A. G. "Electrical Conductivity in Doped Polyacetylene" *Phys. Rev. Lett.* **1977**, 39, 1098-1101.
- [25] Shirakawa, H.; Louis, E. J.; MacDiarmid, A. G.; Chiang, C. K.; Heeger, A. J. "Synthesis of electrically conducting organic polymers: halogen derivatives of polyacetylene, (CH)_{*x*}" *J. Chem. Soc. Chem. Commun.* **1977**, 578-580.
- [26] Scrosati, B. *Applications of Electroactive Polymers*. London: Chapman & Hall; **1994**.
- [27] Chiang, C. K.; Gau, S. C.; Fincher, C. R.; Park, Y. W.; MacDiarmid, A. G. "Polyacetylene, (CH)_{*x*}: *n*-type and *p*-type doping and compensation" *Appl. Phys. Lett.* **1978**, 33, 18-20.
- [28] Burroughes, J. H.; Bradley, D. D. C.; Brown, A. R.; Marks, R. N.; MacKay, K.;

- Friend, R. H.; Burn, P. L.; Holmes, A. B. "Light-emitting diodes based on conjugated polymers" *Nature* **1990**, *347*, 539-541.
- [29] Hoegl, H. "On Photoelectric Effects in Polymers and Their Sensitization by Dopants" *J. Phys. Chem.* **1965**, *69*, 755-766.
- [30] Schattuck, M. D.; Vahtra, U. "Method for making two-piece hollow devitrified mirror blank" *US Patent*. 3,484,327.
- [31] Schaffert, R. M. IBM. *J. Res. Dev.* **1971**, *15*, 75.
- [32] Meerholz, K.; Volodin, L. B.; Sandalphon, K. B. Peyghambarian, N. "A photorefractive polymer with high optical gain and diffraction efficiency near 100%" *Nature* **1994**, *371*, 497-500.
- [33] Wang, Y.; Kroschwitz, J.; Howe-Grant, M. *4th ed. Kirk-Othmer Encyclopedia of Chemical Technology*, 18. New York: Wiley; **1996**, 837.
- [34] Wang, G.; Qian, S.; Xu, J.; Wang, W.; Liu, X.; Lu, X.; Li, F. "Enhanced photovoltaic response of PVK/C₆₀ composite films" *Physica. Part B.* **2000**, *279*, 116-119.
- [35] Pearson, J. M.; Stolka, M. *Poly(N-vinylcarbazole). Polymer Monographs, Vol. 61*. New York: Gordon and Breach; **1981**.
- [36] Pearson, J. M.; Mark, H. F.; Bikales, N. M.; Overberger, C. G.; Menges, G.; *Encyclopedia of Polymer Science and Engineering*, 17. New York: Wiley; **1989**, 257.
- [37] Biswas, M.; Das, S. K. "Recent progress in carbazole based polymers" *Polymer.* **1982**, *23*, 1713-1726.
- [38] (a) Stolka, M.; Chilton, J. A.; Goosey, M. T. *Special Polymers for Electronics and Optoelectronics*. London: Chapman and Hall; **1995**, 284. (b) Borsenberger, P. M.; Weiss, D. S. *Organic Photoreceptors for Imaging Xerography*. New York: Marcel Dekker; **1998**, 768. (c) Mort, J.; Pfister, G.; Mort, J.; Pfister, G. *Electronic Properties of Polymers*. New York: Wiley; **1982**, 215. (c) Naarmann, H.; Strohmriegl, P.; Kricheldorf, H. R. *Handbook of Polymer Synthesis, Part B*. New York: Marcel Dekker; **1992**, 1353. (d) Strohmriegl, P.; Grazulevicius, J. V.; Nalwa, H. S. *Handbook of Organic and Conductive Molecules and Polymers, 1*. Chichester: Wiley; **1997**, 553. (e) Grazulevicius, J. V.; Strohmriegl, P. Stolka, M. *Handbook of Advanced Electronic and Photonic Materials and Devices, 10*. San Diego: Academic Press; **2001**, 233.

- [39] Bäuerle, P. "Thin Oligothiophene Films. UV/VIS, IR and Fluorescence Studies" *Adv. Mater.* **1993**, *5*, 879-886.
- [40] Skotheim, T.; Reynolds, J.; Elsenbamer, R. *Handbook of Conducting Polymers 2nd Edition*. NY, USA: New York; **1998**.
- [41] Skotheim, T. *Handbook of Conducting Polymers*. NY, USA: New York; **1986**.
- [42] Bredas, J. L.; Street, G. B. "Polarons, bipolarons, and solitons in conducting polymers" *Acc. Chem. Res.* **1985**, *18*, 309-315.
- [43] (a) Garnier, F.; Horowitz, G.; Fichou, D. "Conjugated polymers and oligomers as active materials for electronic devices" *Synth. Met.* **1989**, *28*, C705. (b) Fichou, D.; Horowitz, G.; Nishikitani, Y.; Garnier, F. "Semiconducting conjugated oligomers for molecular electronics" *Synth. Met.* **1989**, *28*, C723. (c) Garnier, F.; Horowitz, G.; Peng, X.; Fichou, D. "An All-Organic Soft Thin Film Transistor With Very High Carrier Mobility" *Adv. Mater.* **1990**, *2*, 592-594. (d) Xu, B.; Fichou, D.; Horowitz, G.; Garnier, F. *Adv. Mater.* **1991**, *3*, 150.
- [44] Mullen, K.; Wegner, G., Ed. *Electronic Materials: The Oligomer Approach*, New York: Wiley-VCH; **1998**.
- [45] Gommers, F. J. "Increase in the nematicidal activity of alpha-terthienyl and related compounds by light" *Nematologica*. **1972**, *18*, 458-462.
- [46] Kagan, J.; Chan, G. *Experimentia*. **1983**, *39*, 402-403.
- [47] Hudson, J. B. "Plant photosensitizers with antiviral properties" *Antiviral Research*. **1989**, *12*, 55-74.
- [48] Rossi, R.; Carpita, A.; Ciofalo, M.; Houben, J. L. *Gazz.* "Synthesis and characterization of 2,2':5',2''-terthiophene derivatives of possible therapeutic use" *Chim. Ital.* **1990**, *120*, 793-803.
- [49] Schoeler, U. Tews, K. H.; Huhn, H. *J. Chem. Phys.* **1974**, *61*, 5009-5014.
- [50] Fichou, D.; Horowitz, G.; Nishikitani Y.; Garnier, F. *Chemtronics*, **1988**, *3*, 176-178.
- [51] Horowitz, G.; Fichou, D.; Garnier, F. "Alpha-sexithienyl : a p- and n-type dopable molecular semiconductor" *Solid State Commun.* **1989**, *70*, 385-388.
- [52] Ito, Y.; Konoike, T.; Harada, T.; Saegusa, T. "Synthesis of 1,4-diketones by oxidative coupling of ketone enolates with copper(II) chloride" *J. Am. Chem. Soc.* **1977**, *99*, 1487-1493.
- [53] Tamao, K.; Kodama, S.; Nakajima, I.; Kumada, M. "Nickel-Phosponine

- Complex-Catalyzed Grignard Coupling-II: Grignard Coupling of Heterocyclic Compounds" *Tetrahedron*. **1982**, 38, 3347-3354.
- [54] Espinet, P.; Echavarren, A. M. *Angew.* "C-C coupling: the mechanisms of the Stille reaction" *Chem. Int. Ed.* **2004**, 43, 4704-4734.
- [55] Suzuki, A.; Diederich, F.; Stang, P. J. "*Metal-catalyzed Cross-coupling Reactions*" Weinheim: Wiley-VCH; **1998**, 49-97.
- [56] Buhleier, E. W.; Wehner, W.; Vögtle, F. "'Cascade"- and "nonskid-chain-like" syntheses of molecular cavity topologies" *Synthesis* **1978**, 155-163.
- [57] Tomalia, D. A.; Baker, H.; Dewald, J. R.; Hall, M.; Kallos, G.; Martin, S.; Roeck, J.; Ryder, J.; Smith, P. "A New Class of Polymers: Starburst-Dendritic Macromolecules" *Polym. J. (Tokyo)* **1985**, 17, 117-132.
- [58] Tomalia, D. A.; Baker, H.; Dewald, J. R.; Hall, M.; Kallos, G.; Martin, S.; Roeck, J.; Ryder, J.; Smith, P. "Dendritic Macromolecules: Synthesis of Starburst Dendrimers" *Macromolecules* **1986**, 19, 2466-2468.
- [59] Newkome, G. R.; Yao, Z.-Q.; Baker, G. R.; Gupta, K. "Cascade Molecules: A [27]-Arborol" *J. Org. Chem.* **1985**, 50, 2003-2005.
- [60] Wörner, C.; Mülhaupt, R. "Polynitrile- and Polyamine-Functional Poly(trimethylene imine) Dendrimers" *Angew. Chem., Int. Ed. Engl.* **1993**, 32, 1306-1308.
- [61] De Brabander-van den Berg, E. M. M.; Meijer, E. W. "Poly(propylene imine) dendrimers" *Angew. Chem., Int. Ed. Engl.* **1993**, 32, 1308-1311.
- [62] Hawker, C. J.; Fréchet, J. M. J. "Preparation of Polymers with Contr. Molecular Architecture: A New Convergent Approach to Dendritic Macromolecules" *J. Am. Chem. Soc.* **1990**, 112, 7638-7647.
- [63] Xu, Z.; Moore, J. S. "Synthesis and Characterization of a High Molecular Weight Stiff Dendrimer" *Angew. Chem., Int. Ed. Engl.* **1993**, 32, 246-248.
- [64] Moore, J. S. "Shape-Persistent Molecular Architectures of Nanoscale Dimension" *Acc. Chem. Res.* **1997**, 30, 402-413.
- [65] Newkome, G. R.; Moorefield, C. N.; Vögtle, F. *Dendritic Molecules: Concepts, Syntheses and Perspectives*. Weinheim, Germany: VCH; **1996**.
- [66] De Gennes, P. G.; Hervet, H. "Statistics of "Starburst" polymers" *J. Phys. Lett.* **1983**, 44, 351-360.
- [67] (a) Tomalia, D. A.; Naylor, A. M.; Goddard, W. A., III. *Angew. Chem., Int. Ed.*

Engl. **1990**, 29, 138-175. (b) Vögtle, F., Schalley, C. A. *Dendrimers IV: Metal Coordination, Self-Assembly, Catalysis*; Topics in Current Chemistry, No. 217. Berlin: Springer-Verlag; **2001**. (c) Vögtle, F. *Dendrimers III: Design, Dimension, Function*; Topics in Current Chemistry, No. 212. Berlin: Springer-Verlag; **2001**. (d) Fréchet, J. M. J., Tomalia, D. A. *Dendrimers and Other Dendritic Polymers*. Chichester, U.K.: John Wiley & Sons; **2001**. (e) Vögtle, F. *Dendrimers II: Architecture, Nanostructure and Supramolecular Chemistry*; Topics in Current Chemistry, No. 210, Berlin: Springer-Verlag; **2000**. (f) Vögtle, F. *Dendrimers*; Topics in Current Chemistry, No. 197, Berlin: Springer-Verlag; **1998**. (g) Newkome, G. R.; Moorefield, C. N.; Vögtle, F. *Dendritic Molecules: Concepts, Synthesis Perspectives*. New York; VCH: **1996**.

- [68] (a) Grayson, S. M.; Fréchet, J. M. J. "Convergent Dendrons and Dendrimers: from Synthesis to Applications" *Chem. Rev.* **2001**, 101, 3819-3868. (b) Hawker, C. J.; Fréchet, J. M. J. "Preparation of Polymers with Contr. Molecular Architecture: A New Convergent Approach to Dendritic Macromolecules" *J. Am. Chem. Soc.* **1990**, 112, 7638-7647. (c) Hawker, C. J.; Fréchet, J. M. J. "Control of Surface Functionality in the Synthesis of Dendritic Macromolecules Using the Convergent-Growth Approach" *Macromolecules*, **1990**, 23, 4726-4729. (d) Wooley, K. L.; Hawker, C. J.; Fréchet, J. M. J. "Polymers with Contr. Molecular Architecture: Control of Surface Functionality in Synthesis of Dendritic Hyperbranched Macromolecules" *J. Chem. Soc., Perkin Trans.1* **1991**, 1059-1075. (e) Miller, T. M.; Neenan, T. X. "Convergent synthesis of monodisperse dendrimers based upon 1,3,5-trisubstituted benzenes" *Chem. Mater.* **1990**, 2, 346-349. (f) Kwock, E. W.; Neenan, T. X.; Miller, T. M. *Chem. Mater.* **1991**, 3, 775.
- [69] Grayson, S. M.; Fréchet, J. M. J. "Convergent Dendrons and Dendrimers: from Synthesis to Applications" *Chem. Rev.* **2001**, 101, 3819-3868.
- [70] (a) Knapen, J. W. J.; van der Made, A. W.; de Wilde, J. C.; van Leeuwen, P. W. N. M.; Wijkens, P.; Grove, D. M.; van Koten, G. "Homogeneous Catalysts Based on Silane Dendrimers Functionalized with Arylnickel(II) Complexes" *Nature* **1994**, 372, 659-663. (b) Chow, H.-F.; Mong, T. K.-K.; Nongrum, M. F.; Wan, C.-W. "The Synthesis and Properties of Novel Dendritic Molecules" *Tetrahedron* **1998**, 54, 8543-8660. (c) Hearshaw, M. A.; Hutton, A. T.; Moss,

- J. R.; Naidoo, K. J. in *Advances in Dendritic Macromolecules*, Vol. 4 (Ed.: Newkome, G. R.). Greenwich: JAI Press; **1999**, pp. 1-60. (d) Seebach, D.; Rheiner, P. B.; Greiveldinger, G.; Butz, T.; Sellner, H. *Top. Curr. Chem.* **1998**, *197*, 125-164.
- [71] Brunner, H.; Altmann, S. *Chem. Ber.* **1994**, *127*, 2285-2296.
- [72] (a) Gitsov, L.; Ivanova, P. T.; Fréchet, J. M. J. *Macromol. Rapid Commun.* **1994**, *15*, 387-393. (b) Oosterom, G. E.; van Haaren, R. J.; Reek, J. N. H.; Kamer, P. C. J.; van Leeuwen, P. W. N. M. *Chem. Commun.* **1999**, 1119. (c) Brunner, H.; Altman, S. "Optically Active Nitrogen Ligands with Dendrimeric Structure" *Chem. Ber.* **1994**, *127*, 2285-2296. (d) Mak, C. C.; Chow, H.-F. "Dendritic Bis(oxazoline)copper(II) Catalyst. 2. Synthesis, Reactivity and Substrate Selectivity" *J. Org. Chem.* **1997**, *62*, 5116-5127. (e) Bhyrappa, P.; Young, J. K.; Moore, J. S.; Suslick, K. S. *J. Mol. Catal. A: Chem.* **1996**, *113*, 109-116. (f) Kimura, M.; Sugihara, Y.; Muto, T.; Hanabusa, K.; Shirai, H.; Kobayashi, N. *Chem. Eur. J.* **1999**, *5*, 3495-3500. (g) Rheiner, P. B.; Seebach, D. *Chem.-Eur. J.* **1999**, *5*, 3221-3236.
- [73] (a) Haruta, M.; Kobayashi, T.; Sano, H.; Yamada, N. "Novel Gold Catalysts for the Oxidation of Carbon Monoxide at a Temperature far Below 0" *Chem. Lett.* **1987**, 405-408. (b) Haruta, M.; Yamada, N.; Kobayashi, T.; Ijima, S. "Gold catalysts prepared by coprecipitation of low-temperature oxidation of hydrogen and of carbon monoxide" *J. Catal.* **1989**, *115*, 301-309. (c) Haruta, M. "Size-and Support-dependency in the Catalysis of Gold" *Catal. Today* **1997**, *36*, 153-166.
- [74] Gopidas, K. R.; Whitesell, J. K.; Fox, M. A. "Nanoparticle-Cored Dendrimers: Synthesis and Characterization" *J. Am. Chem. Soc.* **2003**, *125*, 6491.
- [75] Lee, J.-J.; Ford, W. T.; Moore, J. A.; Li, Y. "Reactivity of Organic-Anions Promoted by a Quaternary Ammonium Ion Dendrimer" *Macromolecules* **1994**, *27*, 4632-4634.
- [76] (a) Hovestad, N.; Eggeling, E. B.; Heidebuechel, H. J.; Jastrzebski, J. T. B. H.; Kragl, U.; Keim, W.; Vogt, D.; Van Koten, G. *Angew. Chem. Int. Ed.* **1999**, *38*, 1655. (b) Knapen, J. W. J.; van der Made, A. W.; de Wilde, J. C.; van Leeuwen, P. W. N. M.; Wijkens, P.; Grove, D. M.; van Koten, G. "Homogeneous catalysts based on silane dendrimers functionalized with arylnickel(II) complexes" *Nature* **1994**, *372*, 659-663. (c) Reetz, M. T.;

- Lohmer, G.; Schwickardi, R. "Synthesis and Catalytic Activity of Dendritic Diphosphane Metal Complexes" *Angew. Chem. Int. Ed.* **1997**, *36*, 1526-1529.
- [77] (a) Zhao, M.; Sun, L.; Crooks, R. M. "Preparation of Cu nanoclusters within dendrimer templates" *J. Am. Chem. Soc.* **1998**, *120*, 4877-4878. (b) Zhao, M.; Crooks, R. M. "Homogeneous Hydrogenation Catalysis with Monodisperse, Dendrimer-Encapsulated Pd and Pt Nanoparticles" *Angew. Chem. Int. Ed.* **1999**, *38*, 364-366. (c) Crooks, R. M.; Zhao, M.; Sun, L.; Chechik, V.; Yeung, L. K. "Dendrimer-Encapsulated Metal Nanoparticles: Synthesis, Characterization, and Applications to Catalysis" *Acc. Chem. Res.* **2001**, *34*, 181-190.
- [78] Balogh, L.; Tomalia, D. A.; "Poly(Amidoamine) Dendrimer-Templated Nanocomposited. I. Synthesis of Zerovalent Copper Nanoclusters" *J. Am. Chem. Soc.* **1998**, *120*, 7355-7356.
- [79] (a) Lor, M.; Thielemans, J.; Viaene, L.; Cotlet, M.; Hofkens, J.; Weil, T.; Hampel, C. Mullen, K.; Verhoeven, J. W.; Van der Auweraer, M.; De Schryver, F. C. "Photoinduced electron transfer in a rigid first generation triphenylamine core dendrimer substituted with a peryleneimide acceptor" *J. Am. Chem. Soc.* **2002**, *124*, 9918-9925. (b) Capitosti, G. J.; Cramer, S. J.; Rajesh, C. S.; Modarelli, D. A. "Intramolecular Photoinduced Electron-Transfer Within Porphyrin-Containing Polyamide Dendrimers" *Org. Lett.* **2001**, *3*, 1645-1648. (c) Sadamoto, R.; Tomioka, N.; Aida, T. "Photoinduced electron transfer reactions through dendrimer architecture" *J. Am. Chem. Soc.* **1996**, *118*, 3978-3979.
- [80] (a) Guldi, D. M.; Swartz, A.; Luo, C.; Gómez, R.; Segura, J.; Martín, N. "Rigid dendritic donor-acceptor ensembles: Control over energy and electron transduction" *J. Am. Chem. Soc.* **2002**, *124*, 10875-10886. (b) Qu, J.; Pschirer, N. G.; Liu, D.; Stefan, A.; De Schryver, F. C.; Müllen, K. *Chem. Eur. J.* **2004**, *10*, 528. (c) For a study in which the branching units are partially oxidized to generate a mixed valence compound, which was involved in an electron-transfer quenching of the excited state of light absorber, see: Belser, P.; von Zelewsky, A.; Frank, M.; Seel, M. Vögtle, F.; De Cola, L.; Bargelletti, F.; Balzani, V. "Supramolecular Ru and/or Os complexes of tris(bipyridine) bridging ligands. Syntheses, absorption spectra, luminescence properties, electrochemical behavior, intercomponent energy and electron transfer" *J. Am.*

- Chem. Soc.* **1993**, *115*, 4076. (d) Choi, M.-S.; Aida, T.; Luo, H.; Araki, Y.; Ito, O. "Fullerene-Terminated Dendritic Multiporphyrin Arrays: "Dendrimer Effects" on Photoinduced Charge Separation" *Angew. Chem., Int. Ed.* **2003**, *42*, 4060-4063.
- [81] Thomas, K. R. J.; Thompson, A. L.; Sivakumar, A. V.; Bardeen, C. J.; Thayumanavan, S. "Energy and Electron Transfer in Bifunctional Non-Conjugated Dendrimers" *J. Am. Chem. Soc.* **2005**, *127*, 373-383.
- [82] Guldi, D. M.; Swartz, A.; Luo, C.; Gómez, R.; Segura, J.; Martín, N. "Rigid Dendritic Donor-Acceptor Ensembles: Control over Energy and Electron Transduction" *J. Am. Chem. Soc.* **2002**, *124*, 10875-10886.
- [83] Percec, V.; Johansson, G.; Ungar, G.; Zhou, J. "Fluorophobic effect induces the self-assembly of semifluorinated tapered monodendrons containing crown ethers into supramolecular columnar dendrimers which exhibit a homeotropic hexagonal columnar liquid crystalline phase" *J. Am. Chem. Soc.* **1996**, *118*, 9855-9866.
- [84] (a) Lehn, J.-M. *Supramolecular Chemistry, Concepts and Perspectives*; Germany: WCH: Weinheim; **1995**. (b) Inoue, Y.; Gokel, G. W. *Cation Binding by Macrocycles, Complexation of Cationic Species by Crown Ether*. New York: Marcel Dekker; **1990**.
- [85] Gutsche, C. D. *Calixarenes, Monographs in Supramolecular Chemistry*. Cambridge, U.K.: Stoddart, J. F., Ed.; Royal Society of Chemistry; **1989**; Vol. 1.
- [86] Recent examples of dual receptor systems: (a) Byriel, K. A.; Gasperov, V.; Gloe, K.; Kennard, C. H. L.; Leong, A. J.; Lindoy, L. F.; Mahinay, M. S.; Pham, H. T.; Tasker, P. A.; Thorp, D.; Turner, P. "Host-guest assembly of ligand systems for metal ion complexation; synergistic solvent extraction of copper(II) ions by N₃O₂-donor macrocycles and carboxylic or phosphinic acids" *J. Chem. Soc., Dalton Trans.* **2003**, 3034-3040 (b) Cafeo, G.; Gattuso, G.; Kohnke, F. H.; Notti, A.; Occhipinti, S.; Pappalardo, S.; Parisi, M. F. "Remarkable boosting of the binding of ion-paired organic salts by binary host systems" *Angew. Chem., Int. Ed.* **2002**, *41*, 2122-2126. (c) Qian, Q.; Wilson, G. S.; Bowman-James, K.; Girault, H. H. "MicroITIES detection of nitrate by facilitated ion transfer" *Anal. Chem.* **2001**, *73*, 497-503.
- [87] Tumcharern, G.; Tuntulani, T.; Coles, S. J.; Hursthouse, M. B.; Kilburn, J. D.

- “A Novel ditopic receptor and reversal of anion binding selectivity in the presence and absence of bound cation” *Org. Lett.* **2003**, *5*, 4971-4974. (b) Tongraung, P.; Chantarasiri, N.; Tuntulani, T. “Calix[4]arenes containing urea and crown/urea moieties: effects of the crown ether unit and Na⁺ towards anion binding ability” *Tetrahedron Lett.* **2003**, *44*, 29-32.
- [88] Some examples are already known of "tripod-aza" receptor molecules combining calix units and tren: (a) Abidi, R.; Oueslati, I.; Amri, H.; Thuery, P.; Nierlich, M.; Asfari, Z.; Vicens, J. “Synthesis, structure and complexing properties of new calix[4](aza)crowns” *Tetrahedron Lett.* **2001**, *42*, 1685-1689. (b) Tuntulani, T.; Poompradub, S.; Thavornyutikarn, P.; Jaiboon, N., Ruangpornvisuti, V.; Chaichait, N.; Asfari, Z.; Vicens, J. “Aza crown ether calix[4]arenes containing cation and anion binding sites: effects of metal ions towards anion binding ability” *Tetrahedron* **2001**, *42*, 1685-1689.
- [89] Chirakul, P.; Hampton, P. D.; Duesler, E. N. “Synthesis and crystal structures of an O-silylated hexahomotriazacalix[3]arenes” *Tetrahedron Lett.* **1998**, *39*, 5473-5476.
- [90] (a) Moshfegh, A. A.; Mazandarani, B.; Nahid, A.; Hakimelahi, G. H. “The synthesis of hetero-halogenated derivatives of phloroglucide analogues” *Helv. Chim. Acta.* **1982**, *65*, 1229. (b) Openshaw, H. T.; Robinson, R. *J. Chem. Soc.* **1946**, 912.
- [91] Vogel, A. I. *A text-book of Quantitative Inorganic Analysis*. Norfolk: Longman; **1975**.
- [92] Vetrogon, V. I.; Lukyanenko, N. G.; Schwing-well, M. J.; Arnaud-Neu, F. “A PC compatible computer program for the calculation of equilibrium constants by the simultaneous processing of different sets of experimental results” *Talanta* **1994**, *41*, 2105-2112.
- [93] X-ray data were collected on a Bruker SMART CCD area detector. The crystal structure was solved by direct methods and refined by full matrix least-squares. All non-hydrogen atoms were refined anisotropically, and hydrogen atoms were refined using the riding model. All calculations were performed using a crystallographic software package, WinGX v1.64.05. Crystal data for **L2**: *Mr*) 1095.3, monoclinic, space group *P21_n*, *a*) 13.297(2) Å, *b*) 19.191(3) Å, *c*) 23.602(5) Å, β) 97.599(1)°, *V*) 5969.82(8)³, *Z* = 4, ρ_{calc} =

1.120 g cm⁻³, $2\theta_{\max} = 57.4^\circ$, Mo K α ($\alpha = 0.71075$), $\mu = 0.71$ cm⁻¹, θ - ω scans, $T = 293(2)$ K, 42, 269 independent reflections, 16,815 observed reflections ($I > 3.0\sigma(I)$), 340 refined parameters, $R1 = 0.092$, $R_w = 0.136$, $\Delta\rho_{\max} = 2.38$ e⁻³, $\Delta\rho_{\min} = -2.26$ e⁻³; CCDC 292414.

- [94] Crystal data for **L3**: C₈₄H₇₅Cl₃N₆O₆•3H₂O, $M_r = 1424.90$, monoclinic, space group $P-1$, $a = 16.1795(3)$ Å, $b = 16.5809(3)$ Å, $c = 16.6482(2)$ Å, $\alpha = 92.624(1)^\circ$, $\beta = 105.880(1)^\circ$, $\gamma = 112.174(1)^\circ$, $V = 3921.97(11)$ Å³, $Z = 2$, $\rho_{\text{calc}} = 1.207$ g cm⁻³, $2\theta_{\max} = 30.54^\circ$, Mo K α ($\lambda = 0.71075$ Å), $\mu = 0.176$ mm⁻¹, θ - ω scans, $T = 293(2)$ K, 28143 independent reflections, 20620 unique reflections ($I > 2.0\sigma(I)$), 924 refined parameters, $R1 = 0.1276$, $R_w = 0.3142$, $\Delta\rho_{\max} = 1.204$ e Å⁻³, $\Delta\rho_{\min} = -0.395$ e Å⁻³; CCDC 673516.
- [95] Kaewtong, C.; Fuangswasdi, S.; Muangsin, N.; Chaichit, N.; Vicens, J.; Pulpoka, B. "Novel C_{3v}-Symmetrical N₇-Hexahomotriazacalix[3]cryptand: A Highly Efficient Receptor for Halide Anions" *Org. Lett.* **2006**, *8*, 1561-1564.
- [96] Lee, D. H.; Lee, K. W.; Hong, J. "An Azophenol-Based Chromogenic Anion Sensor", *Org. Lett.* **2001**, *3*, 5-8.
- [97] (a) Fery-Forgues, S.; Le Bris, M-T.; Guetté, J-P.; Valeur, B. "Ion-responsive fluorescent compounds. 1. effect of cation binding on photophysical properties of a benzoxazinone derivative linked to monoaza-15-crown-5" *J. Phys. Chem.*, **1988**, *92*, 6233-6237. (b) Bouson, J.; Valeur, B. "Ion-responsive fluorescent compounds. 2. cation-steered intramolecular charge transfer in a crowned merocyanine" *J. Phys. Chem.*, **1988**, *93*, 3871-3876.
- [98] (a) Galindo, F.; Becerril, J.; Burguete, M. I.; Luis, S. V.; Vigara, L. "The β -lactone route to α,β -unsaturated δ -lactones. Total syntheses of (\pm)-goniothalamine and (-)-massoialactone" *Tetrahedron Lett.* **2004**, *45*, 1659-1663. (b) Roy, M. B.; Samanta, S.; Chattopadhyay, G.; Ghosh, S. "Exciplex emission and photoinduced energy transfer as a function of cavity dimension in naphthalene-linked aza-crown ethers" *J. Lumin.* **2004**, *106*, 141-152.
- [99] Liu, Y.; Han, B.-H.; Chen, Y. T. "Inclusion Complexation of Acridine Red Dye by Calixarenesulfonates and Cyclodextrins: Opposite Fluorescent Behavior" *J. Org. Chem.* **2000**, *65*, 6227-6230.
- [100] (a) Kim, J. S.; Quang, D. T. "Calixarene-Derived Fluorescent Probes" *Chem.*

- Rev.* **2007**, *107*, 3780-3799. (b) Kim, S. K.; Kim, S. H.; Kim, H. J.; Lee, S. H.; Lee, S. W.; Ko, J.; Bartsch, R. A.; Kim, J. S. "Indium(III)-induced fluorescent excimer formation and extinction in calix[4]arene-fluoroionophores" *Inorg. Chem.* **2005**, *44*, 7866-7875.
- [101] (a) Lee, S. H.; Kim, S. H.; Kim, S. K.; Jung, J. H.; Kim, J. S. "Fluorescence ratiometry of monomer/excimer emissions in a space-through PET system" *J. Org. Chem.* **2005**, *70*, 9288-9295. (b) Choi, J. K.; Kim, S. H.; Yoon, J.; Lee, K.-H.; Bartsch, R. A.; Kim, J. S. "A PCT-Based, pyrene-armed Calix[4]crown fluoroionophore" *J. Org. Chem.* **2006**, *71*, 8011-8015. (c) Kim, J. S.; Kim, H. J.; Kim, H. M.; Kim, S. H.; Lee, J. W.; Kim, S. K.; Cho, B. R. "Metal ion sensing novel calix[4]crown fluoroionophore with a two-photon absorption property" *J. Org. Chem.* **2006**, *71*, 8016-8022.
- [102] (a) Cakir, U.; Cicek, B. "Extraction-ability and -selectivity of tetra-aza-crown ethers for transition metal cations" *Transit. Metal. Chem.* **2004**, *29*, 263-268. (b) Costero, A. M.; Salvador Gil, S.; Sanchis, J.; Peransí S.; Sanz, V.; Williams, J. A. G. "Conformationally regulated fluorescent sensors. Study of the selectivity in Zn²⁺ versus Cd²⁺ sensing" *Tetrahedron* **2004**, *60*, 6327-6334. (c) Liang, X.; Parkinson, J. A.; Parsons, S.; Weishäupl, M.; Sadler, P. J. "Cadmium Cyclam Complexes: Interconversion of *Cis* and *Trans* Configurations and Fixation of CO₂" *Inorg. Chem.* **2002**, *41*, 4539-4547. (d) Nelson, J.; Mckee, V.; Morgan, G.; *Progress in Inorganic Chemistry "Coordination Chemistry of Azacryptands"* **2007**, *47*, 167-316.
- [103] Swager, T. M. *Acc. Chem. Res.* **1998**, *31*, 201. (b) Dimitriev, O. P. *Macromolecules* **2004**, *37*, 3388. (c) Ferguson, G.; Gallagher, J. F.; Lough, A. J.; Notti, An.; Pappalardo, S.; Parisi, M. F. "1,3-Calix[4]arene Crown Ether Conformers with a 3-Thienyl Pendant Functionality at the Lower Rim" *J. Org. Chem.* **1999**, *64*, 5876-5885.
- [104] (a) Richard D. M. *Adv. Mater.* **1998**, *10*, 93. (b) Roncali J. *J. Mater. Chem.* **1999**, *9*, 1875-1893. (c) Janata J.; Mira Josowicz M. *Nature Materials.* **2003**, *2*, 19. (d) Bobacka J.; Ivaska A.; Lewenstam A. *Electroanalysis.* **2003**, *15*, 366.
- [105] (a) Mallouk, T. E.; Gavin, J. A. *Acc. Chem. Res.* **1998**, *31*, 209-217. (b) Crooks, R. M.; Ricco, A.J. "New organic materials suitable for use in chemical sensor arrays" *Acc. Chem. Res.* **1998**, *31*, 219-227.
- [106] (a) Rani, V.; Santhanam *J. Solid. State. Electrochem.* **1998**, *2*, 99. (b) Kawde,

- R.B.; Laxmeshwar, N.B.; Santhanam, K.S.V. *Sens. Actuators B*, **1995**, *23*, 35.
- (c) Choudhury, S.; Saxena, V.; Gupta, S.K.; Yakhmi, J.V. *Thin Solid Films* **2005**, *493*, 267.
- [107] (a) Baba A.; Onishi K.; Knoll W.; Advincula R. "Investigating work function tunable hole-injection/transport layers of electrodeposited polycarbazole network thin films" *J. Phys. Chem. B*. **2004**, *108*, 18949-18955. (b) Taraneekar P.; Fulghum T. M.; Baba A.; Patton D.; Advincula R. "Quantitative Electrochemical and Electrochromic Behavior of Terthiophene and Carbazole Containing Conjugated Polymer Network Film Precursors: EC-QCM and EC-SPR" *Langmuir*. **2007**, *23*, 908-917.
- [108] (a) Kuwabara, Y.; Ogawa, H.; Inada, H.; Nona, N.; Shirota, Y. *Adv. Mater.* **1994**, *6*, 667-672. (b) O'Brien, D. F.; Burrows, P. E.; Forrest, S. R.; Koene, B. E.; Loy, D. E.; Thompson, M. E. "Hole Transporting Materials with High Glass Transition Temperatures for Use in Organic Light-Emitting Devices" *Adv. Mater.* **1998**, *10*, 1108-1112. (c) Koene, B. E.; Loy, D. E.; Thompson, M. E. "Asymmetric, Thermally Stable Hole Transporting Amines for Organic Light Emitting Diodes" *Chem. Mater.* **1998**, *10*, 2235. (d) Thomas, K. R. J.; Lim, J. T.; Tao, Y. T.; Ko, C. W. "Novel Light-emitting Carbazole derivatives: Potential Electroluminescent Materials" *J. Am. Chem. Soc.* **2001**, *123*, 9404-9411. (e) Li, J.; Liu, D.; Li, Y.; Lee, C. S.; Kwong, H. L.; Lee, S. "A high T_g carbazole-based hole-transporting material for organic light-emitting devices" *Chem. Mater.* **2005**, *17*, 1208-1212.
- [109] (a) Liu, B.; Yu, W. L.; Lai, Y. H.; Huang, W. "Blue-Light-Emitting Fluorene-Based Polymers with Tunable Electronic Properties" *Chem. Mater.* **2001**, *13*, 1984-1991. (b) Xia, C.; Advincula, R. C. "Decreased Aggregation Phenomena in Polyfluorenes by Introducing Carbazole Copolymer Units" *Macromolecules* **2001**, *34*, 5854-5859. (c) Stephen, O.; Vial, J.-C. *Synth. Met.* **1999**, *106*, 115.
- [110] Kang, J. F.; Perry, J. D.; Tian, P.; Kilbey, S. M. "Growth and Morphology of Polythiophene on Thiophene-Capped Monolayers: 1. Single-Component Monolayers" *Langmuir*. **2002**, *18*, 10196-10201.
- [111] Tran-Van, F.; Chevrot, C. "Synthesis and electrochemical properties of mixed ionic and electronic modified polycarbazole" *Electrochim. Acta*, **2002**, *47*, 2927-2936.
- [112] (a) Buttry, D. A. In *Electroanalytical Chemistry*. New York: Bard, A. J., Ed.;

- Marcel Dekker; **1991**, Vol. 17, p 1. (b) Taranekar, P.; Baba, A.; Fulghum, T.; Advincula, R. "Conjugated Polymer Network Films from Precursor Polymers: Electrocopolymerization of a Binary Electroactive Monomer Composition" *Macromolecules* **2005**, *38*, 3679-3687.
- [113] Taranekar, P.; Park J.-Y.; Patton D.; Fulghum T.; Ramon G. J.; Advincula R. "Conjugated Polymer Nanoparticles via Intra-molecular Cross-linking of Dendrimeric Precursors" *Adv. Mater.* **2006**, *18*, 2461-2465.
- [114] (a) Zhu S. S.; Swager T. M. "Defining Space Around Conducting Polymers: Reversible Protonic Doping of a Canopied Polypyrrole" *J. Am. Chem. Soc.* **2003**, *125*, 6870-6871. (b) Lee, D.; Swager T. M. "Defining Space around Conducting Polymers: Reversible Protonic Doping of a Canopied Polypyrrole" *J. Am. Chem. Soc.* **2003**, *125*, 6870-6871.
- [115] (a) Miller, L. L.; Mann, K. R. " π -Dimers and π -Stacks in Solution and in Conducting Polymers" *Acc. Chem. Res.* **1996**, *29*, 417-423. (b) Cornil, J.; Beljonne, D.; Calbert, J.-P.; Bre'das, J.-L. "Interchain Interactions in Organic π -Conjugated Materials: Impact on Electronic Structure, Optical Response, and Charge Transport" *Adv. Mater.* **2001**, *13*, 1053-1067.
- [116] Buttry, D. A.; Ward, M. D. "Measurement of Interfacial Processes at Electrode Surfaces with the Electrochemical Quartz Crystal Microbalance" *Chem. Rev.* **1992**, *92*, 1355-1379.
- [117] Muramatsu, H.; Tamiya, E.; Karube, I. "Computation of Equivalent Circuit Parameters of Quartz Cryontact with Liquids and Study of Liquid Properties" *Anal. Chem.* **1988**, *60*, 2142-2146.
- [118] Sannicolo, F.; Brenna, E.; Benincori, T.; Zotti, G.; Zecchin, S.; Schiavon, G.; Pilati, T. "Highly Ordered Poly(cyclopentabithiophenes) Functionalized with Crown-Ether Moieties" *Chem. Mater.* **1998**, *10*, 2167-2176.
- [119] (a) Taranekar, P.; Baba, A.; Park, J. Y.; Fulghum, T. M.; Advincula R. "Dendrimer Precursors for Nanomolar and Picomolar Real-Time SPR/Potentiometric Chemical Nerve Agent Sensing using Electrochemically Cross-linked Ultrathin Films" *Adv. Funct. Mater.* **2006**, *16*, 2000-2007. (b) Kang, X.; Jin, Y.; Cheng, G.; Dong, S. "Surface Plasmon Resonance Studies on the Electrochemical Doping/Dedoping Processes of Anions on Polyaniline-Modified Electrode" *Langmuir.* **2002**, *18*, 10305-10310.

- [120] Neumann, T.; Johansson, M.-L.; Kambhampati, D.; Knoll, W. "Surface-plasmon Fluorescence spectroscopy" *Adv. Funct. Mater.* **2002**, *12*, 575-583.
- [121] (a) Lehn, J.-M. "Toward complex matter : Supramolecular chemistry and self-organization" *Proc. Natl. Acad. Sci. U.S.A.* **2002**, *99*, 4763. (b) Lee, M.; Cho, B.-K.; Zin, W.-C. "Supramolecular structures from rod-coil block copolymers" *Chem. Rev.* **2001**, *101*, 3869-3892. (c) Sarikaya, M.; Tamerler, C.; Jen, A. K.-Y.; Schulten, K.; Baneyx, F. "Molecular biomimetics: nanotechnology through biology" *Nature Mater.* **2003**, *2*, 577-585. (d) Hoeben, F. J. M.; Jonkheijm, P.; Meijer, E. W.; Schenning, A. P. H. J. "About Supramolecular Assemblies of π -Conjugated Systems" *Chem. Rev.* **2005**, *105*, 1491-1546. (e) Cornelissen, J. J. L. M.; Rowan, A. E.; Nolte, R. J. M.; Sommerdijk, N. A. J. M. "Chiral Architectures from Macromolecular Building Blocks" *Chem. Rev.* **2001**, *101*, 4039-4070.
- [122] (a) Newkome, G. R.; Moorefield, C. N.; Vçgtle, F. *Dendrimers and Dendrons: Concepts, Syntheses, Applications*. Weinheim: Wiley-VCH; **2001**. (b) Ossterom, G. E.; Reek, J. N.H.; Kamer, P. C. J.; van Leeuwen, P. W. N.M. *Angew. Chem.* **2001**, *113*, 1878; *Angew. Chem. Int. Ed.* **2001**, *40*, 1828. (c) Astruc, D.; Chardac, F. "Dendritic Catalysts and Dendrimers in Catalysis" *Chem. Rev.* **2001**, *101*, 2991-3031. (d) Grayson, S. M.; FrW-chet, J. M. J. "Convergent Dendrons and Dendrimers: from Synthesis to Applications" *Chem. Rev.* **2001**, *101*, 3819-3868. (e) Stiriba, S. E.; Frey, H.; Haag, R. "Dendritische Polymere for medizinische Anwendungen: auf dem Weg zum Einsatz in Diagnostik und Therapie" *Angew. Chem.* **2002**, *114*, 1385-1390; *Angew. Chem. Int. Ed.* **2002**, *41*, 1329-1334. (f) Aulenta, F.; Hayes, W.; Rannard, S. "Dendrimers: a new class of nanoscopic containers and delivery devices" *Eur. Polym. J.* **2003**, *39*, 1741-1771. (g) Boas, U.; Heegaard, P. M. H. "Dendrimers in drug research" *Chem. Soc. Rev.* **2004**, *33*, 43-63. (h) Svenson, S.; Tomalia, D. A. "Dendrimers in biomedical applications — reflections on the field" *Adv. Drug Delivery Rev.* **2005**, *57*, 2106-2129.
- [123] (a) Kim, Y. H.; Webster, O. W. "Water-Soluble Hyperbranched Polyphenylene: A Unimolecular Micelle" *J. Am. Chem. Soc.* **1990**, *112*, 4592-4593. (b) Newkome, G. R.; Moorefield, C. N.; Baker, G. R.; Johnson, A. L.; Behera, R. K. "Hydrocarbon Cascade Polymers Possessing Micellar Topology:

- Micellanoic Acid Derivatives” *Angew. Chem., Int. Ed. Engl.* **1991**, *30*, 1176-1178. (c) Naylor, A. M.; Goddard, W. A., III; Kiefer, G. E.; Tomalia, D. A. *J. Am. Chem. Soc.* **1998**, *111*, 2339.
- [124] (a) Wang, C.; Wyn-Jones, E.; Sidhu, J.; Tam, K. C. “Supramolecular Complex Induced by the Binding of Sodium Dodecyl Sulfate to PAMAM Dendrimers” *Langmuir*, **2007**, *23*, 1635-1639. (b) Mizutani, H.; Torigoe, K.; Esumi, K. *J. Colloid Interface Sci.* **2002**, *248*, 493. (c) Sidhu, J.; Bloor, D. M.; Couderc-Azouani, S.; Penfold, J.; Holzwarth, J. F.; Wyn-Jones, E. “Interactions of poly(amidoamine) dendrimers with the surfactants SDS, DTAB, and C12EO6: an equilibrium and structural study using a SDS selective electrode, isothermal titration calorimetry, and small angle neutron scattering” *Langmuir* **2004**, *20*, 9320-9328.
- [125] Chun, D.; Wudl, F. Nelson, A. “Supramacromolecular Assembly Driven by Complementary Molecular Recognition” *Macromolecules* **2007**, *40*, 1782-1785.
- [126] Chechik, V.; Zhao, M.; Crooks, R. M. “Self-Assembled Inverted Micelles Prepared from a Dendrimer Template: Phase Transfer of Encapsulated Guests” *J. Am. Chem. Soc.* **1999**, *121*, 4910-4911.
- [127] (a) Polowinski, S. *Prog. Polym. Sci.* **2002**, *27*, 537. (b) Szumilewicz, J. *Macromol. Symp.* **2000**, *161*, 183. (c) Polacco, G.; Cascone, M. G.; Petarca, L.; Maltinti, G.; Cristallini, C.; Barbani, N.; Lazzeri, L. *Polym. Int.* **1996**, *41*, 443.
- [128] Serizawa, T.; Hamada, K.; Akashi, M. “Polymerization within a molecular-scale stereoregular template” *Nature* **2004**, *429*, 52-55.
- [129] (a) Ganeva, D.; Antonietti, M.; Faul, C. F. J.; Sanderson, R. D. “Polymerization of the Organized Phases of Polyelectrolyte-Surfactant Complexes” *Langmuir* **2003**, *19*, 6561-6565. (b) Ganeva, D.; Faul, C. F. J.; Gotz, C.; Sanderson, R. D. “Directed reactions within confined reaction environments: Polyadditions in polyelectrolyte-surfactant complexes” *Macromolecules* **2003**, *36*, 2862-2866.
- [130] (a) Mueller, A.; O'Brien, D. “Supramolecular materials via polymerization of mesophases of hydrated amphiphiles” *Chem. Rev.* **2002**, *102*, 727-757. (b) Summers, M.; Eastoe, J. “Applications of polymerizable surfactants” *Adv. Colloid Interface Sci.* **2003**, *100-102*, 137-152.

- [131] Lee, Y.-S.; Yang, J.-Z.; Sisson, T. M.; Frankel, D. A.; Gleeson, J. T.; Aksay, E.; Keller, S. L.; Gruner, S. M.; O'Brien, D. "Polymerization of Nonlamellar Lipid Assemblies" *J. Am. Chem. Soc.* **1995**, *117*, 5573-5578.
- [132] Dreja, M.; Lennartz, W. "Polymerizable polyelectrolyte-surfactant complexes from monomeric ammonium cations and polystyrenesulfonate" *Macromolecules* **1999**, *32*, 3528-3530.
- [133] (a) Hatano, T.; Takeuchi, M.; Ikeda, A.; Shinkai, S. "Nano-Rod Structure of Poly(ethylenedioxythiophene) and Poly(pyrrole) As Created by Electrochemical Polymerization Using Anionic Porphyrin Aggregates as Template" *Org. Lett.* **2003**, *5*, 1395-1398. (b) Ikegame, M.; Tajima, K.; Aida, T. *Angew. Chem., Int. Ed.* **2003**, *42*, 2154-2157. (c) Li, G.; Bhosale, S.; Wang, T.; Zhang, Y.; Zhu, H.; Fuhrhop, J.-H. *Angew. Chem., Int. Ed.* **2003**, *42*, 3818-3821. (d) Spange, S. *Angew. Chem., Int. Ed.* **2003**, *42*, 4430-4432.
- [134] (a) Witker, D.; Reynolds, J. R. "Soluble Variable Color Carbazole-containing Electrochromic Polymers" *Macromolecules* **2005**, *38*, 7636-7644. (b) Gaupp, C. L.; Reynolds, J. R. "Multichromic Copolymers Based on 3,6-Bis(3,4-Ethylenedioxythiophene)-N-Alkylcarbazole Derivatives" *Macromolecules* **2003**, *36*, 6305-6315.
- [135] (a) Sotzing, G. A.; Reddinger, J. L.; Katritzky, A. R.; Soloducho, J.; Musgrave, R.; Reynolds, J. R. "Multiply Colored Electrochromic Carbazole-Based Polymers" *Chem. Mater.* **1997**, *9*, 1578-1587. (b) Reddinger, J. L.; Sotzing, G. A.; Reynolds, J. R. "Multicolored electrochromic polymers derived from easily oxidized bis[2-(3,4-ethylenedioxy)thienyl]carbazoles" *Chem. Commun.* **1996**, *15*, 1777-1778.
- [136] Taranekar, P.; Fulghum, T.; Patton, D.; Ponnampati, R.; Clyde, G.; Advincula, R. "Investigating Carbazole Jacketed Precursor Dendrimers: Sonochemical Synthesis, Characterization, and Electrochemical Crosslinking Properties" *J. Am. Chem. Soc.* **2007**, *129*, 12537.
- [137] (a) Hartmann, P. C.; Dieudonne, P.; Sanderson, R. D. *J. Colloid Interface Sci.* **2005**, *284*, 289. (b) Popova, M. V.; Tchernyshev, Y.S.; Michel, D. *Langmuir* **2004**, *20*, 632. (c) Shimizu, S.; Pires, P. A. R.; El Seoud, O. A. "H-1 and C-13 nmr study on the aggregation of (2-acylaminoethyl) rimethylammonium chloride surfactants in D₂O" *Langmuir* **2003**, *19*, 9645-9652.
- [138] (a) Fulghum, T.; Karim, S. M. A.; Baba, A.; Taranekar, P.; Nakai, T.; Masuda,

- T.; Advincula, R. C. "Conjugated Poly(phenylacetylene) Films Cross-Linked with Electropolymerized Polycarbazole Precursors" *Macromolecules* **2006**, *39*, 1467-1473. (b) Taranekar, P.; Fan, X.; Advincula, R. "Distinct Surface Morphologies of Electropolymerized Polymethylsiloxane Network Polypyrrole and Comonomer Films" *Langmuir* **2002**, *18*, 7943-7952. (c) Inaoka, S.; Advincula, R. "Synthesis and Oxidative Cross-Linking of Fluorene-Containing Polymers To Form Conjugated Network Polyfluorenes: Poly(fluorene-9,9-diyl-alt-alkan-a,w-diyl)" *Macromolecules* **2002**, *35*, 2426-2428.
- [139] (a) Thunemann, A. F.; Kubowicz, S.; Pietsch, U.; "Ultrathin solid polyelectrolyte-surfactant complex films: Structure and wetting" *Langmuir* **2000**, *16*, 8562-8567. (b) Thunemann, A. F.; Ruppelt, D.; Ito, S.; Mullen, K. "Supramolecular architecture of a functionalized hexabenzocoronene and its complex with polyethyleneimine" *J. Mater. Chem.* **1999**, *9*, 1055-1057.
- [140] (a) Frisch, M. J.; Trucks, G. W.; Schlegel, H. B.; Scuseria, G. E.; Robb, M. A.; Cheeseman, J. R.; Zakrzewski, V. G.; Montgomery, J. A., Jr.; Stratmann, R. E.; Burant, J. C.; Dapprich, S.; Millam, J. M.; Daniels, A. D.; Kudin, K. N.; Strain, M. C.; Farkas, O.; Tomasi, J.; Barone, V.; Cossi, M.; Cammi, R.; Mennucci, B.; Pomelli, C.; Adamo, C.; Clifford, S.; Ochterski, J.; Petersson, G. A.; Ayala, P. Y.; Cui, Q.; Morokuma, K.; Malick, D. K.; Rabuck, A. D.; Raghavachari, K.; Foresman, J. B.; Cioslowski, J.; Ortiz, J. V.; Stefanov, B. B.; Liu, G.; Liashenko, A.; Piskorz, P.; Komaromi, I.; Gomperts, R.; Martin, R. L.; Fox, D. J.; Keith, T.; Al-Laham, M. A.; Peng, C. Y.; Nanayakkara, A.; Gonzalez, C.; Challacombe, M.; Gill, P. M. W.; Johnson, B. G.; Chen, W.; Wong, M. W.; Andres, J. L.; Head-Gordon, M.; Replogle, E. S.; Pople, J. A. *Gaussian 98*, Revision A.7 ed.; Gaussian, Inc: Pittsburgh, PA, 1998. b) MOLEKEL 4.3, P. Flükiger, H.P. Lüthi, S. Portmann, J. Weber, Swiss Center for Scientific Computing, Manno (Switzerland), 2000-2002.
- [141] (a) Ambrose, Nelson "Anodic Oxidation Pathways of Carbazoles" *J. Electrochem. Soc.* **1968**, *115*, 1159-1164. (b) Kakuta, T.; Shirota, Y.; Mikawa, H. "A rechargeable battery using electrochemically doped poly(N-vinylcarbazole)" *J. Chem. Soc., Chem. Commun.* **1985**, 553-554.
- [142] (a) Iraqi, A.; Wataru, I. "Preparation and properties of 2,7-linked N-alkyl-9H-

- carbazole main-chain polymers" *Chem. Mater.* **2004**, *16* (3), 442-448. (b) Iraqi, A.; Pickup, D. F.; Yi, H. "Effects of Methyl Substitution of Poly(9-alkyl-9*H*-carbazole-2,7-diyl)s at the 3,6-Positions on Their Physical Properties" *Chem. Mater.* **2006**, *18* (4), 1007-1015.
- [143] Albertus, P. H.; Schenning, J.; Fransicus, B.; Benneker, G.; Hubertus, P.; Geurts, M.; Liu, X. Y.; Nolte, R. J. M. "Porphyrin Wheels" *J. Am. Chem. Soc.* **1996**, *118*, 8549-8552.
- [144] (a) Lee, E.; Young-Hwan Jeong, Y-H.; Kim, J-K.; Lee, M. "Controlled Self-Assembly of Asymmetric Dumbbell-Shaped Rod Amphiphiles: Transition from Toroids to Planar Nets" *Macromolecules* **2007**, *40*, 8355-8360. (b) Rakhmatullina, E.; Braun, T.; Chami, M.; Malinova, V.; Meier, W. *Langmuir* **2007**, ASAP Article.
- [145] Suksai, C. ; Gómez, S. F.; Chhabra, A.; Liu, J.; Skepper, J. N.; Tuntulani, T.; Otto, S. "Controlling the Morphology of Aggregates of an Amphiphilic Synthetic Receptor through Host-Guest Interactions" *Langmuir* **2006**, *22*, 5994-5997.
- [146] Crooks, R. M.; Zhao, M.; Sun, L.; Chechik, V.; Yeung, L. K. "Dendrimer-Encapsulated Metal Nanoparticles: Synthesis, Characterization, and Applications to Catalysis." *Acc. Chem. Res.* **2001**, *34*, 181-190.
- [147] (a) Fisher, M.; Vogtle, F. "Dendrimers: From Design to Application - A Progress Report" *Angew. Chem., Int. Ed. Engl.* **1999**, *38*, 884-905. (b) Bosman, A. W.; Janssen, H. M.; Meijer, E. W. "About dendrimers: structure, physical properties, and applications" *Chem. Rev.* **1999**, *99*, 1665-1688.
- [148] Cooper, A. I.; Londono, J. D.; Wignall, G.; McClain, J. B.; Samulski, E. T.; Lin, J. S.; Dobrynin, A.; Rubinstein, M.; Burke, A. L. C.; Frechet, J. M. J.; DeSimone, J. M. "Extraction of a hydrophilic compound from water into liquid CO₂ using dendritic surfactants" *Nature* **1997**, *389*, 368-371.
- [149] (a) Crooks, R. M.; Lemon, B. I.; Sun, L.; Yeung, L. K.; Zhao, M. *Top. Curr. Chem* **2001**, *212*, 82-135. (b) Crooks, R. M.; Zhao, M.; Sun, L.; Chechik, V.; Yeung, L. K. "Dendrimer-Encapsulated Metal Nanoparticles: Synthesis, Characterization, and Applications to Catalysis." *Acc. Chem. Res.* **2001**, *34*, 181-190.
- [150] Turkevich, J.; Stevenson, P. C.; Hillier, J. "A study of the nucleation and

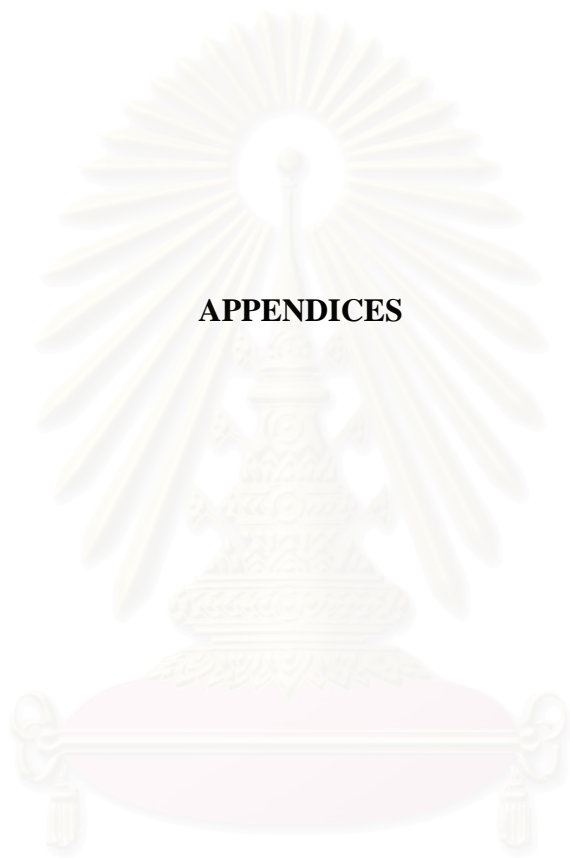
- growth processes in the synthesis of colloidal gold” *Discuss. Faraday Soc.* **1951**, 55-75.
- [150] Selvan, S. T. “Novel nanostructures of gold–polypyrrole composites” *J. Chem. Soc., Chem. Commun.* **1998**, 351-352.
- [151] (a) Pillalamarri, S. K.; Blum, F. D.; Tokuhito, A. T.; Bertino, M. F. “One-Pot Synthesis of Polyaniline-Metal Nanocomposites” *Chem. Mater.* **2005**, *17*, 5941. (b) Tan, Y; Li, Y; Zhu, D. *Synth. Met.* **2003**, *847*, 135.
- [152] Kumar, S. S.; Kumar, C. S.; Mathiyarasu, J.; Phani, K. L. " Stabilized Gold Nanoparticles by Reduction Using 3,4-Ethylenedioxythiophene-polystyrenesulfonate in Aqueous Solutions: Nanocomposite Formation, Stability, and Application in Catalysis” *Langmuir* **2007**, *23*, 3401 -3408.
- [153] (a) Jang, S.-Y.; Sotzing, G. A. “Poly(thiophene)s Prepared via Electrochemical Solid-State Oxidative Cross-Linking; A Comparative Study” *Macromolecules* **2004**, *37*, 4351-4359. (b) Zotti, G.; Marin, R. A.; Gallazzi, M. C. *Chem. Mater.* **1997**, *9*, 2945-2950. (c) Jang, S.-Y.; Sotzing, G. A.; Marquez, M. “Intrinsically Conducting Polymer Networks of Poly(thiophene) via Solid-State Oxidative Cross-Linking of a Poly(norbornylene) Containing Terthiophene Moieties” *Macromolecules* **2002**, *35*, 7293-7300. (d) DiCesare, N.; Belletete, M.; Marrano, C.; Leclerc, M.; Durocher, G. *J. Phys. Chem. A* **1999**, *103*, 795-802.
- [154] Youk, J. H.; Locklin, L.; Xia, C.; Park, M.-K.; Advincula, R. “Preparation of gold nanoparticles from a polyelectrolyte complex solution of terthiophene amphiphiles” *Langmuir* **2001**, *17*, 4681-4683.
- [155] (a) Sarma, T. K.; Chattopadhyay, A. *J. Phys. Chem. A* **2004**, *108*, 7837. (b) Sarma, T. K.; Chowdhury, D.; Paul, A.; Chattopadhyay, A. “Synthesis of Au nanoparticle–conductive polyaniline composite using H₂O₂ as oxidising as well as reducing agent” *Chem. Commun.* **2002**, 1048-1049.
- [156] (a) Garcia-Martinez, J. C.; Crooks, R. M. “Extraction of Au Nanoparticles Having Narrow Size Distributions from within Dendrimer Templates” *J. Am. Chem. Soc.* **2004**, *126*, 16170-16178. (b) Kim, Y.-G.; Garcia-Martinez, J. C.; Crooks, R. M. “Electrochemical properties of monolayer-protected Au and Pd nanoparticles extracted from within dendrimer templates” *Langmuir* **2005**, *21*, 5485-5491.
- [157] (a) Eycken, E. V. D. “Palladium catalyzed synthesis of Ca²⁺ indicators with aryl

- bithiophene and terthiophene fluorophores” *Tetrahedron* **2006**, *62*, 684-690.
- (b) Thomas, K. G.; Kamat, P. V. “Chromophore Functionalized Gold Nanoparticles” *Acc. Chem. Res.* **2003**, *36*, 888-898. (c) Gu, T.; Whitesell, J. K.; Fox, M. A. "Energy transfer from a surface-bound arene to the gold core in ω -fluorenyl-alkane-1-thiolate monolayer-protected gold clusters" *Chem. Mater.* **2003**, *15*, 1358-1366. (d) Aguila, A.; Murray, R. W. “Monolayer-protected clusters with fluorescent dansyl ligands” *Langmuir* **2000**, *16*, 5949-5954.
- [158] Joseph, Y.; Besnard, I.; Rosenberger, M.; Guse, B.; Nothofer, H.-G.; Wessels, J. M.; Wild, U.; Knop-Gericke, A.; Su, D.; Schlogl, R.; Yasuda, A.; Vossmeier, T. “Self-Assembled Gold Nanoparticle/Alkanedithiol Films: Preparation, Electron Microscopy, XPS-Analysis, Charge Transport, and Vapor-Sensing Properties” *J. Phys. Chem. B* **2003**, *107*, 7406-7413.
- [159] (a) Castner, D. G.; Hinds, K.; Grainger, D. W. "X-ray Photoelectron Spectroscopy Sulfur 2p Study of Organic Thiol and Disulfide Interactions with Gold Surfaces" *Langmuir* **1996**, *12*, 5083-5086. (b) Chenakin, S. P.; Heinz, B.; Morgner, H. *Surf. Sci.* **1999**, *421*, 337-352.
- [160] Heister, K.; Zharnikov, M.; Grunze, M.; Johansson, L. S. O. “Adsorption of alkanethiols and biphenylthiols on Au and Ag substrates: A high resolution X-ray photoelectron spectroscopy study” *J. Phys. Chem. B* **2001**, *105*, 4058-4061.
- [161] (a) Lua, Y. *Mater. Lett.* **2007**, *61*, 1039. (b) Maynor, B.W.; Filocamo, S.F.; Grinstaff M.W.; Liu, J. "Direct-Writing of Polymer Nanostructures: Poly(thiophene) Nanowires on Semiconducting and Insulating Surfaces" *J. Am. Chem. Soc.* **2002**, *124*, 522-523. (c) Youk, J.H.; Locklin, J.; Xia, C., Park, M. K. “Preparation of Gold Nanoparticles from a Polyelectrolyte Complex Solution of Terthiophene Amphiphiles.” *Langmuir* **2001**, *17*, 4681-4683.
- [162] (a) Rabani, E.; Egorov, S. A. *Nano Lett.* **2002**, *2*, 69. (b) Saunders, A. E.; Shah, P. S.; Park, E. J.; Lim, K. T.; Johnston, K. P.; Korgel, B. A. “Solvent Density-Dependent Steric Stabilization of Perfluoro-polyether-Coated Nanocrystals in Supercritical Carbon Dioxide” *J. Phys. Chem. B* **2004**, *108*, 15969-15975.
- [163] Albertus, P. H.; Schenning, J.; Fransicus, B.; Benneker, G.; Hubertus, P.; Geurts, M.; Liu, X. Y.; Nolte, R. J. M. *J. Am. Chem. Soc.* **1996**, *118*, 8549-8552.

- [164] Yassar, A.; Moustrou, C.; Youssoufi, H. K.; Samat, A.; Guglielmetti, R.; Garnier, F. “Synthesis and Characterization of Poly(Thiophenes) Functionalized by Photochromic Spiroanthoxazine Groups” *Macromolecules* **1995**, 28, 4548-4553.
- [165] Pan, J.; Zhu, W.; Li, S.; Xu, J.; Tian, H. “Synthesis of Carrier-transporting Dendrimers with Luminescent Core of Perylene Diimides” *Eur. J. Org. Chem.* **2006**, 986.



สถาบันวิทยบริการ
จุฬาลงกรณ์มหาวิทยาลัย



APPENDICES

สถาบันวิทยบริการ
จุฬาลงกรณ์มหาวิทยาลัย

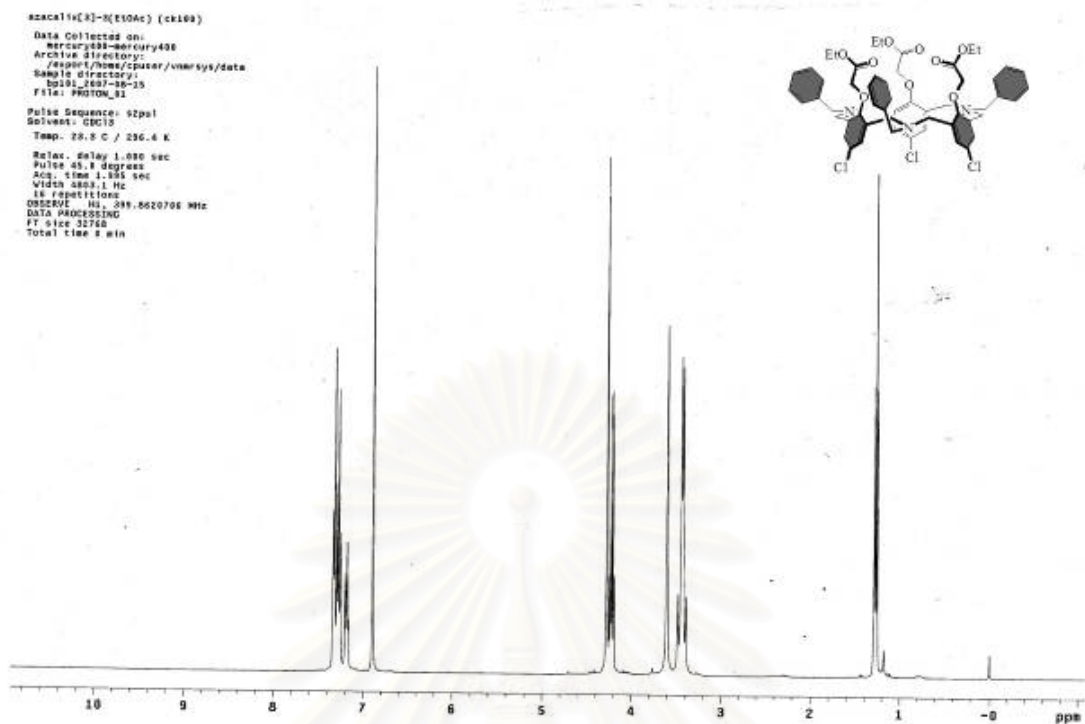


Figure A1. $^1\text{H-NMR}$ spectrum of *N*-benzylhexahomotriaza-*p*-chloro-calix[3]-tri(ethyl acetate) (**2.3a**, cone) in CDCl_3 at 25 °C.

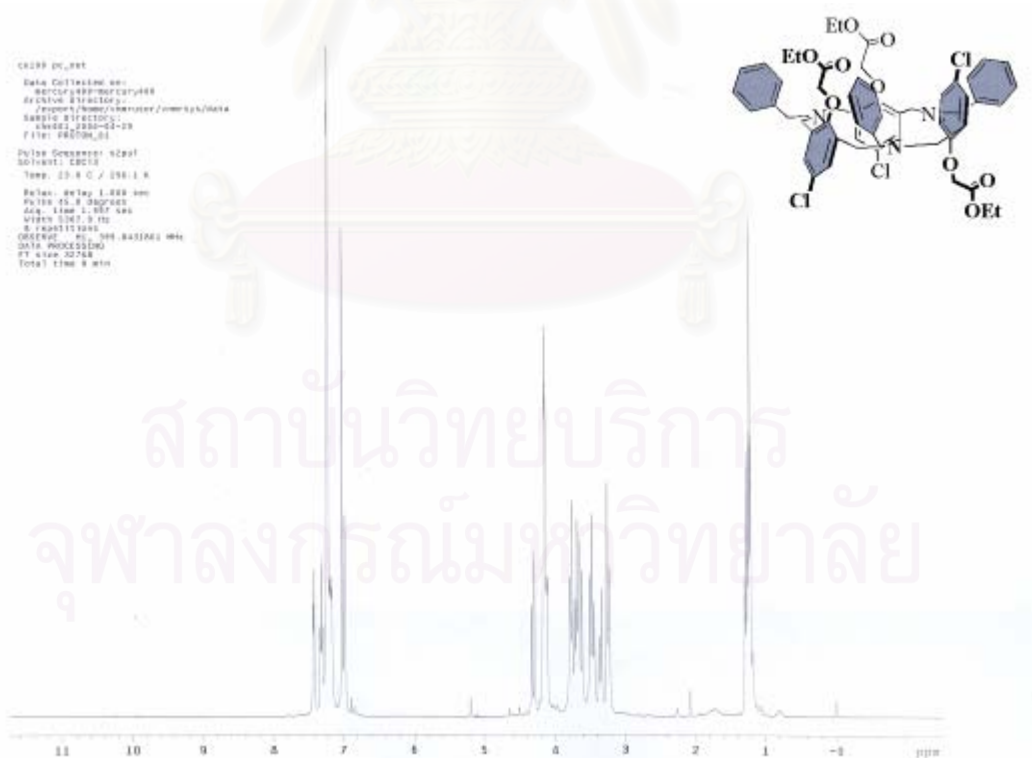


Figure A2. $^1\text{H-NMR}$ spectrum of *N*-benzylhexahomotriaza-*p*-chloro-calix[3]-tri(ethyl acetate) (**2.3b**, partial cone) in CDCl_3 at 25 °C.

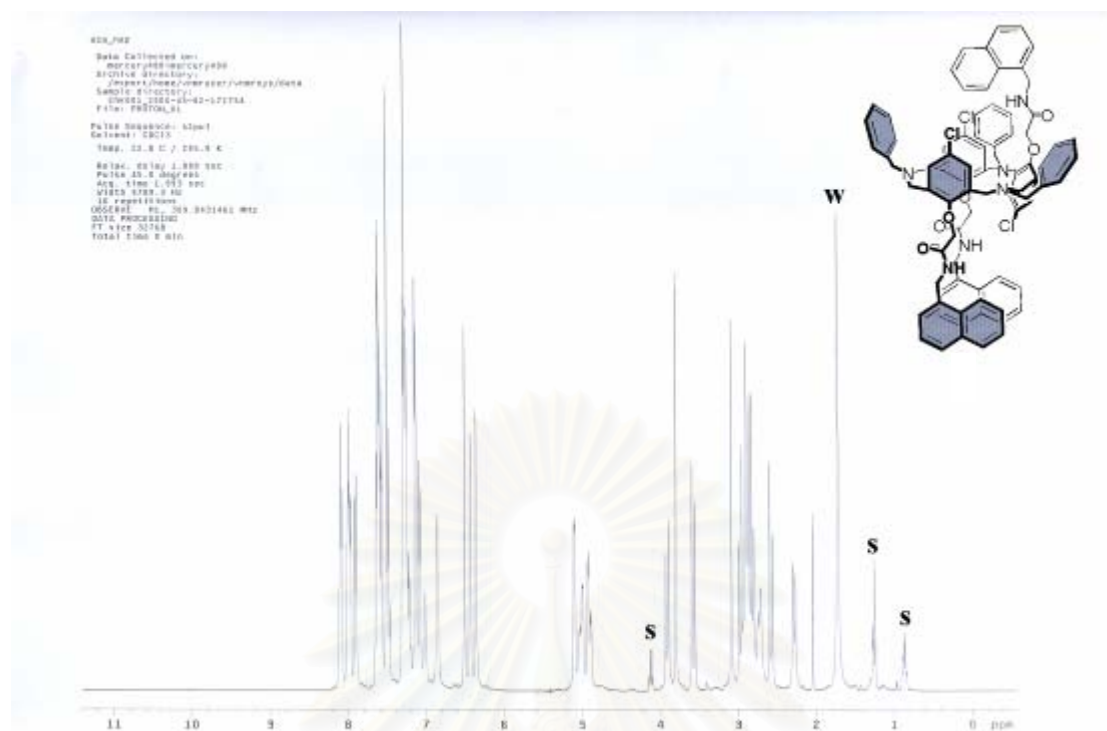


Figure A3. ^1H -NMR spectrum of *N*-benzylhexahomotriaza-*p*-chlorocalix[3]-trinaphthylamide (**L2**) in CDCl_3 at 25 °C. Solvent and water peaks are labeled as “S” and “W”, respectively.

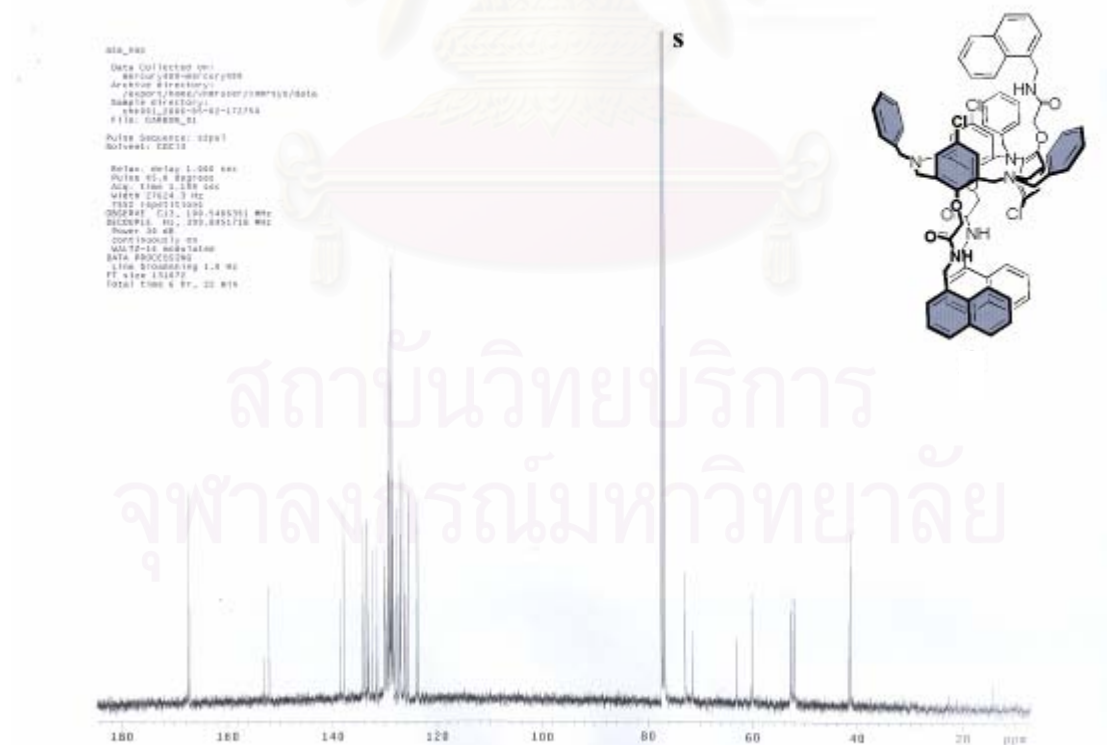


Figure A4. ^{13}C -NMR spectrum of *N*-benzylhexahomo-triaza-*p*-chlorocalix[3]-trinaphthylamide (**L2**) in CDCl_3 at 25 °C.

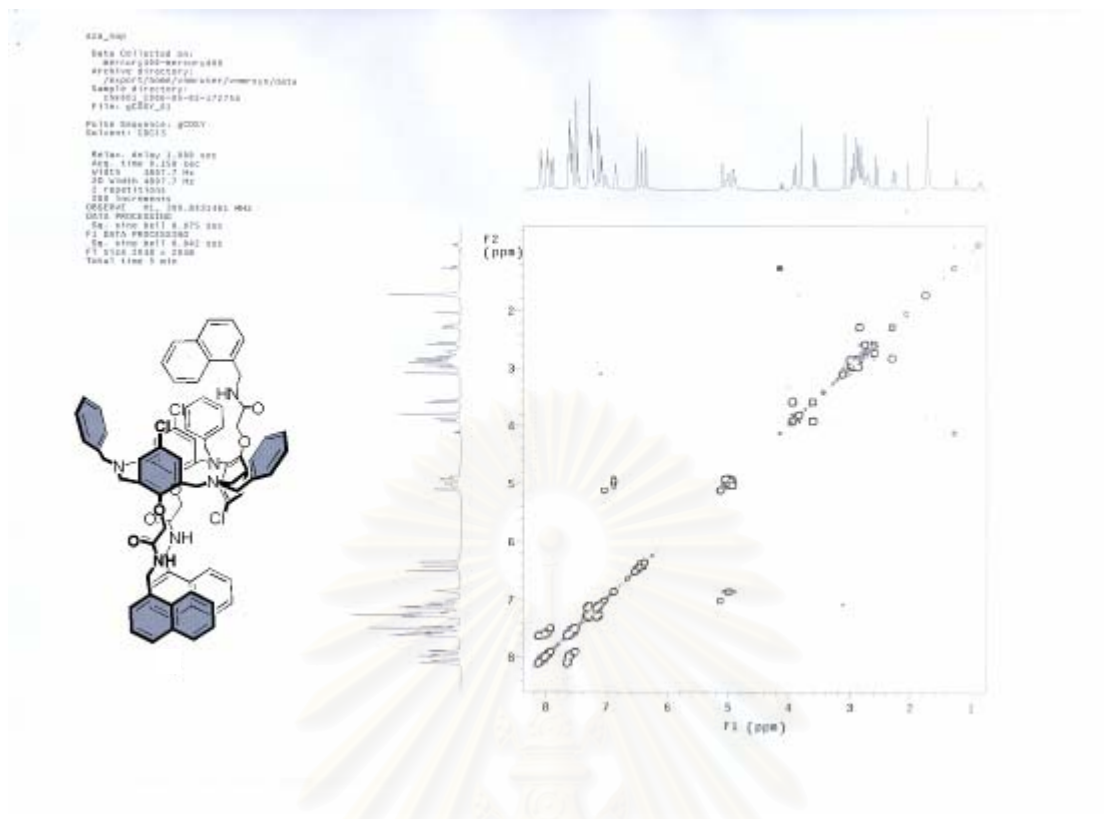


Figure A5. COSY spectrum of *N*-benzylhexahomotriaza-*p*-chlorocalix[3]-trinaphthylamide (**L2**) in CDCl₃ at 25 °C.

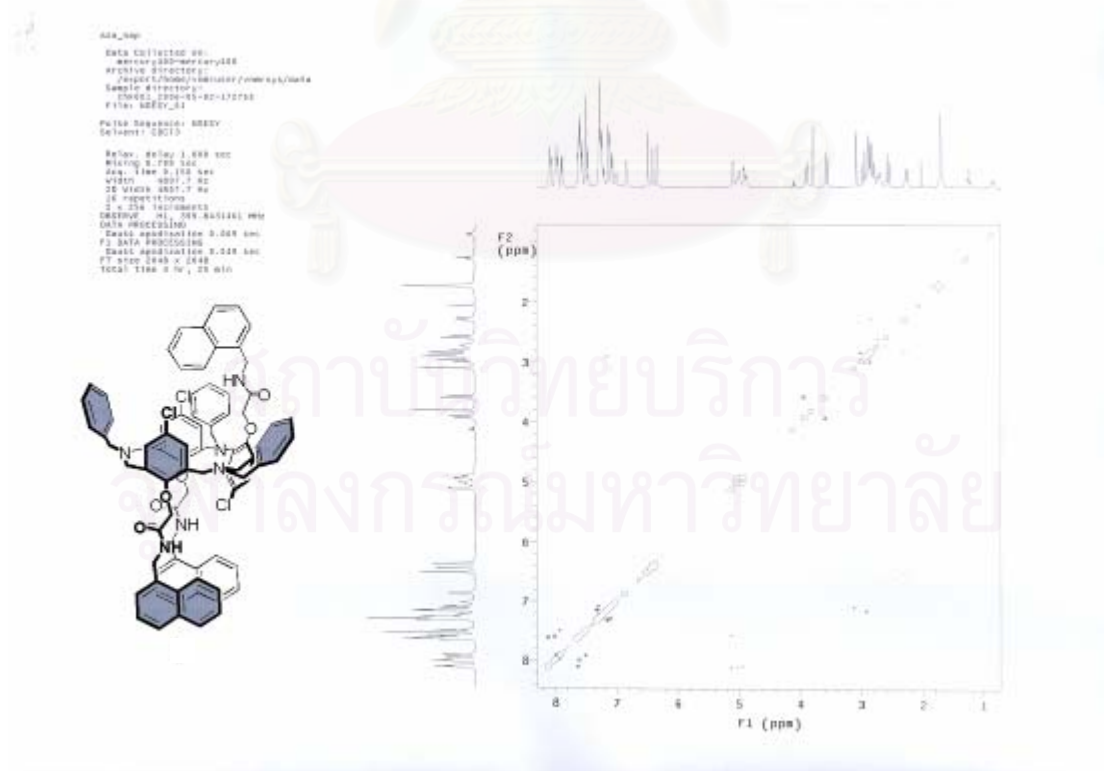


Figure A6. NOESY spectrum of *N*-benzylhexahomotriaza-*p*-chlorocalix[3]-trinaphthylamide (**L2**) in CDCl₃ at 25 °C.

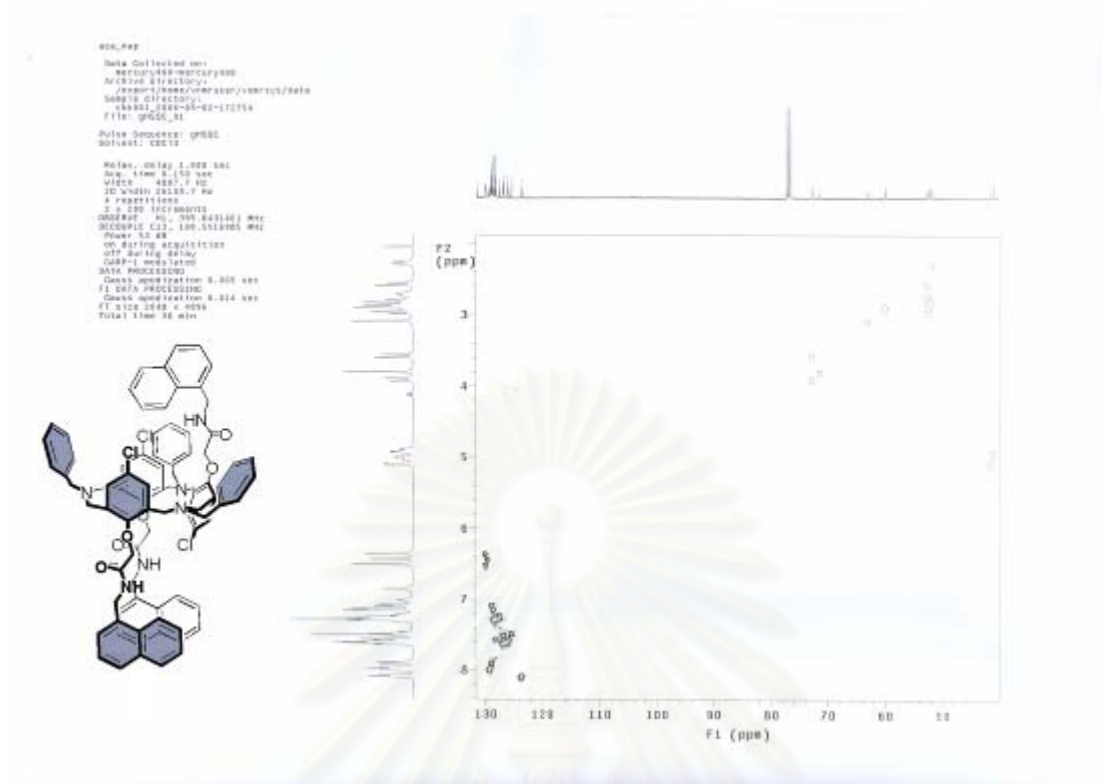


Figure A7. gHSQC spectrum of *N*-benzylhexahomotriaza-*p*-chlorocalix[3]-trinaphthylamide (L2) in CDCl₃ at 25 °C.

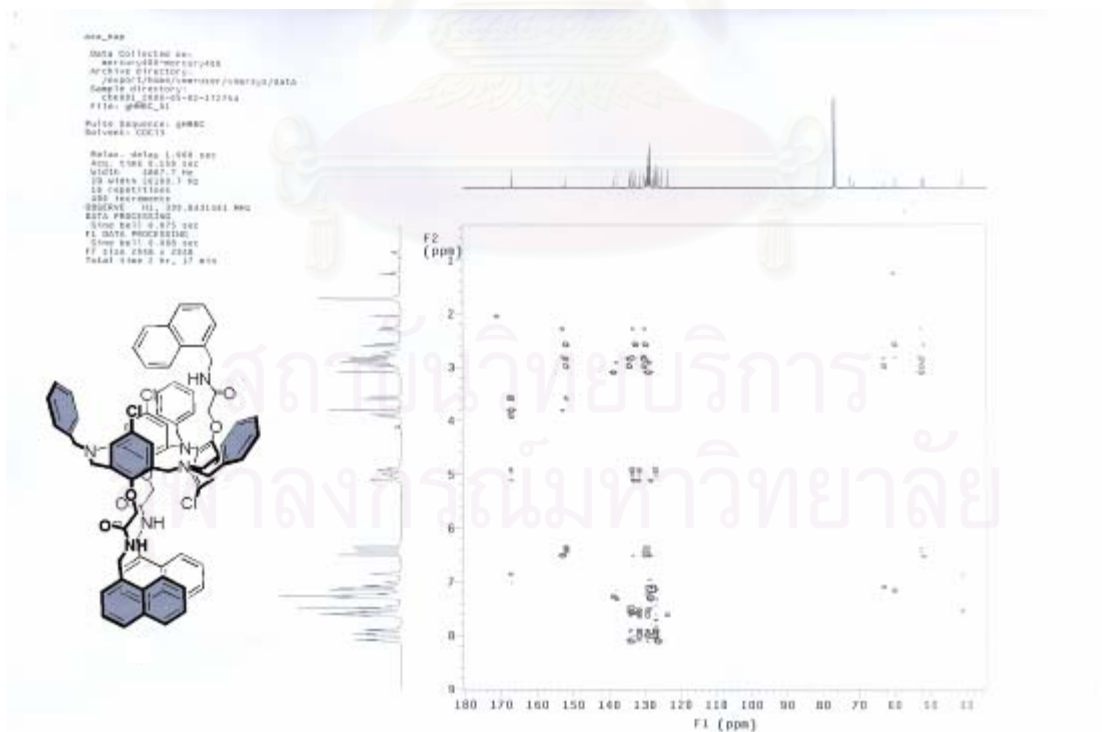


Figure A8. gHMBC spectrum of *N*-benzylhexahomotriaza-*p*-chlorocalix[3]-trinaphthylamide (L2) in CDCl₃ at 25 °C.

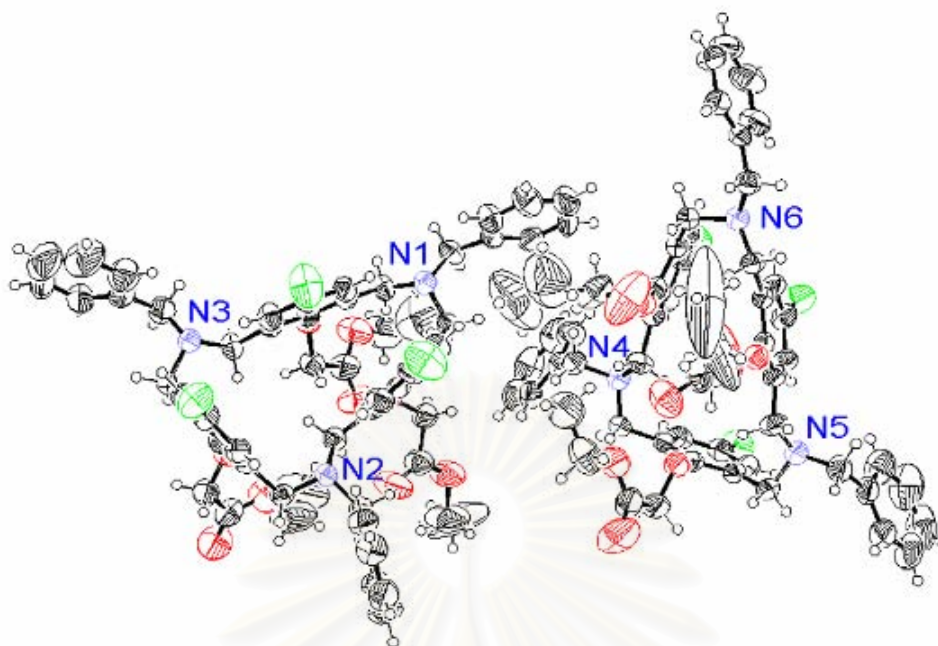


Figure A9. X-ray single crystal structure of *N*-benzylhexahomotriaza-*p*-chlorocalix[3]-tri(ethyl acetate) (**2.3a**)

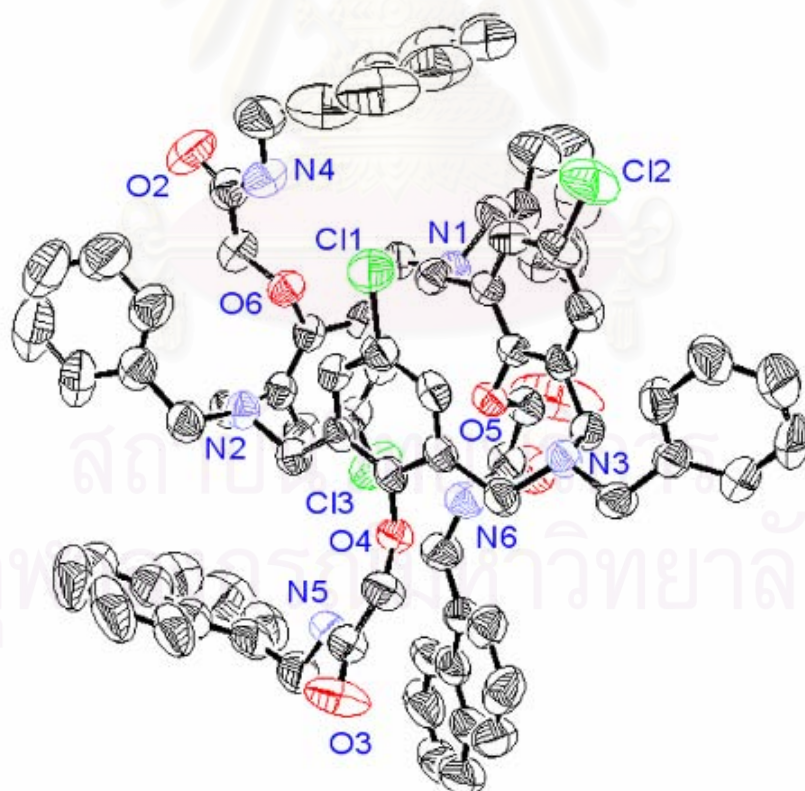


Figure A10. X-ray single crystal structure of *N*-benzylhexahomotriaza-*p*-chlorocalix[3]-trinaphthylamide (**L2**)

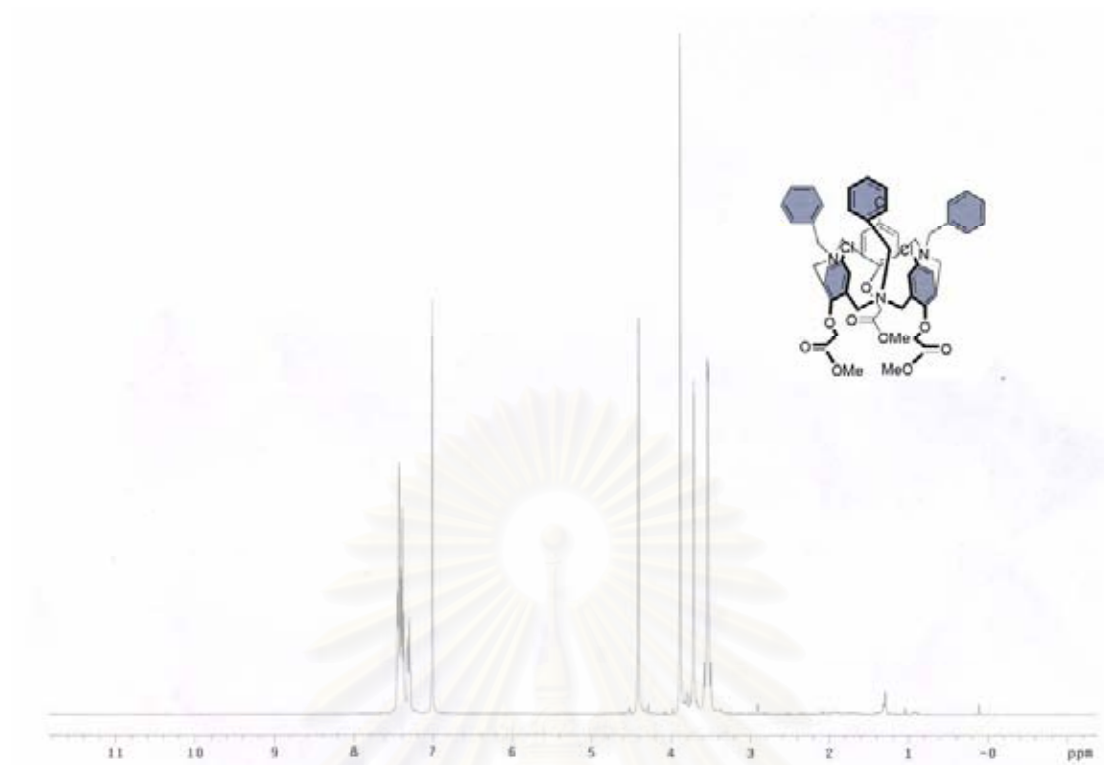


Figure A11. $^1\text{H-NMR}$ spectrum of *N*-benzylhexahomotriaza-*p*-chloro-calix[3]-tri(methyl acetate) (**2.4a**, cone) in CDCl_3 at 25 °C.

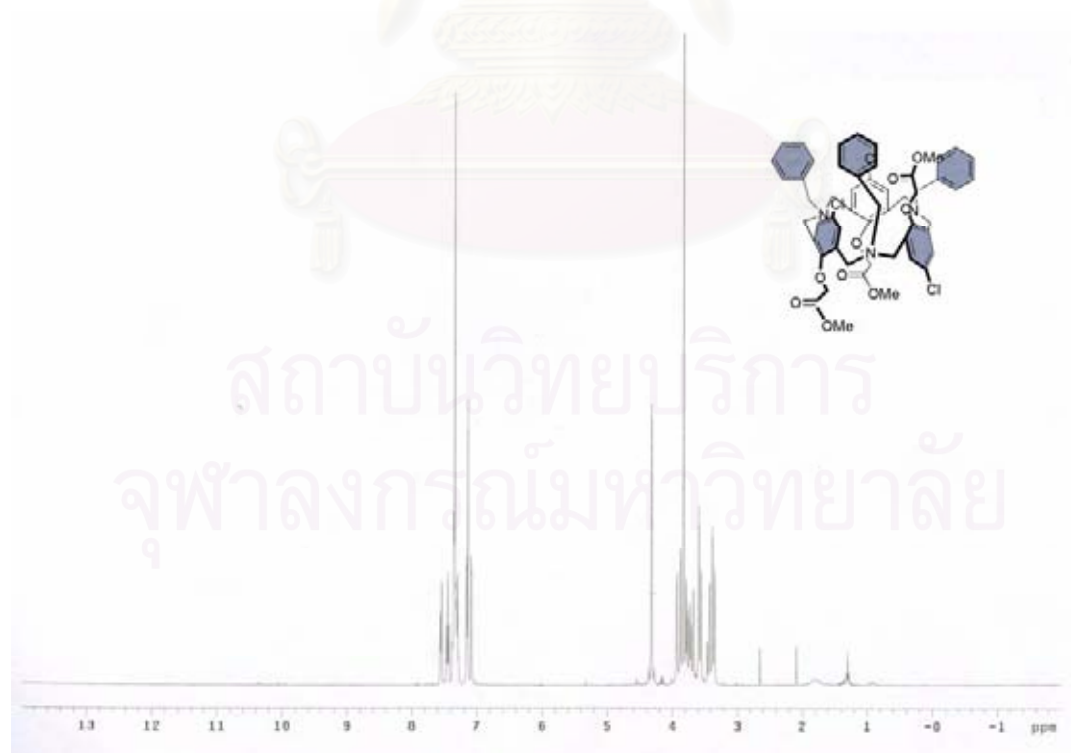


Figure A12. $^1\text{H-NMR}$ spectrum of *N*-benzylhexahomotriaza-*p*-chloro-calix[3]-tri(methyl acetate) (**2.4b**, partial cone) in CDCl_3 at 25 °C.

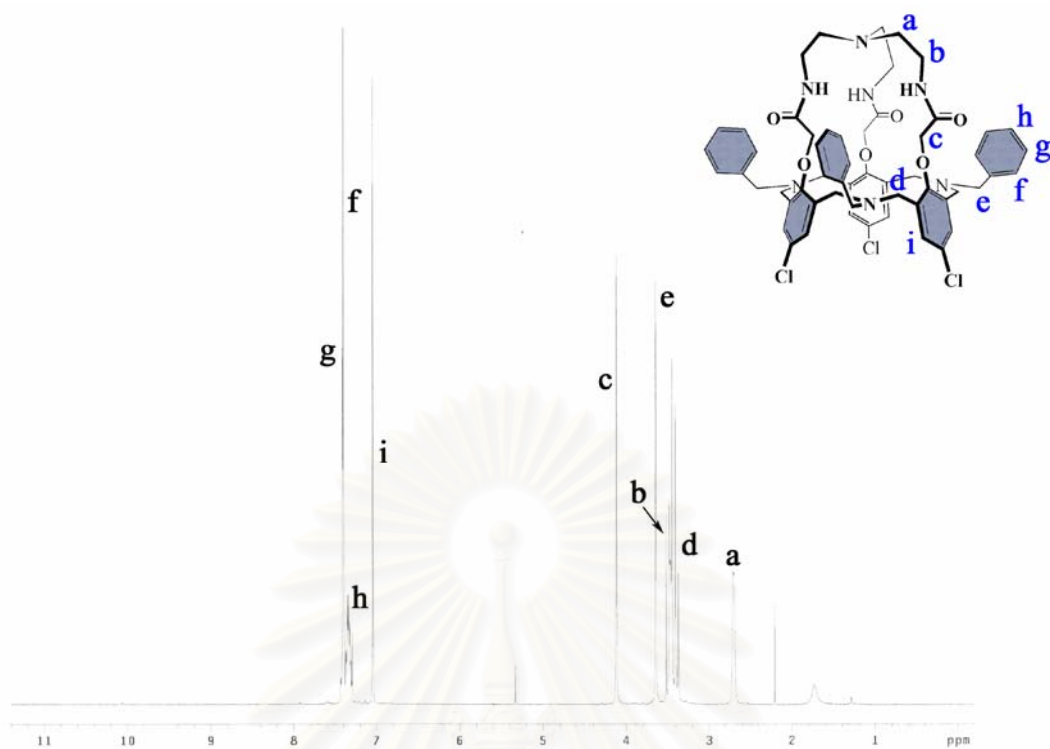


Figure A13. $^1\text{H-NMR}$ spectrum of N_7 -hexahomotriazacalix[3]-cryptand (L3) in CDCl_3 at 25°C .

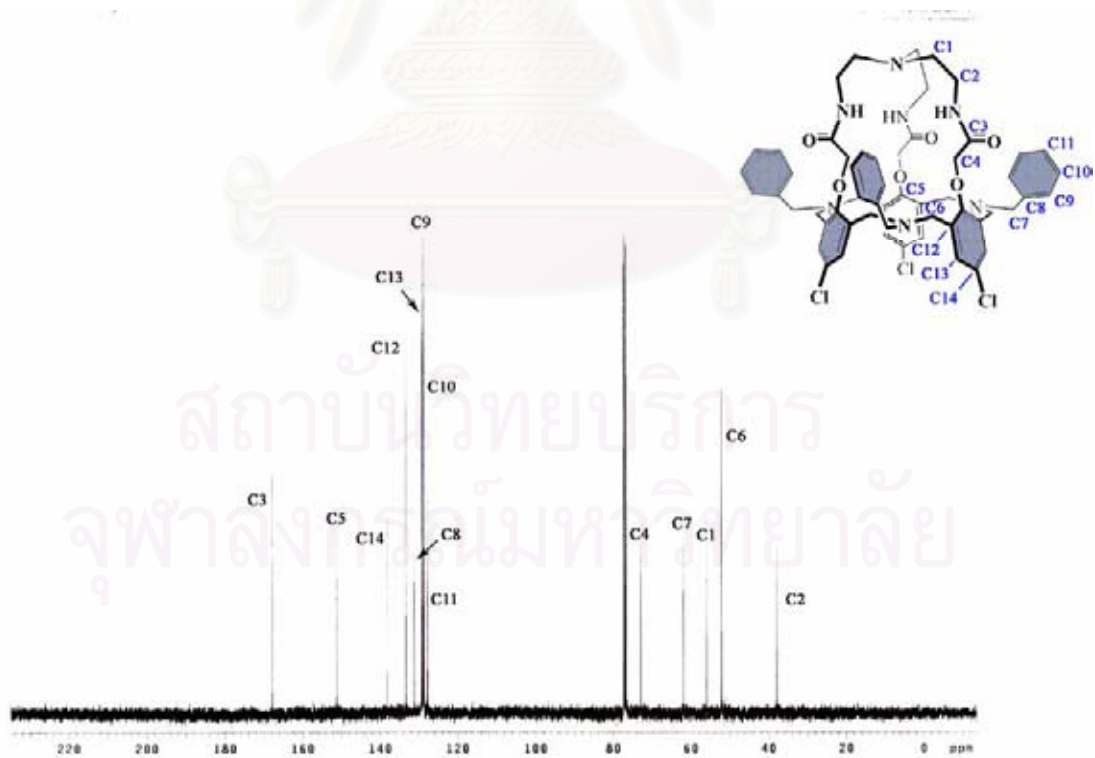


Figure A14. $^{13}\text{C-NMR}$ spectrum of N_7 -hexahomotriazacalix[3]-cryptand (L3) in CDCl_3 at 25°C .

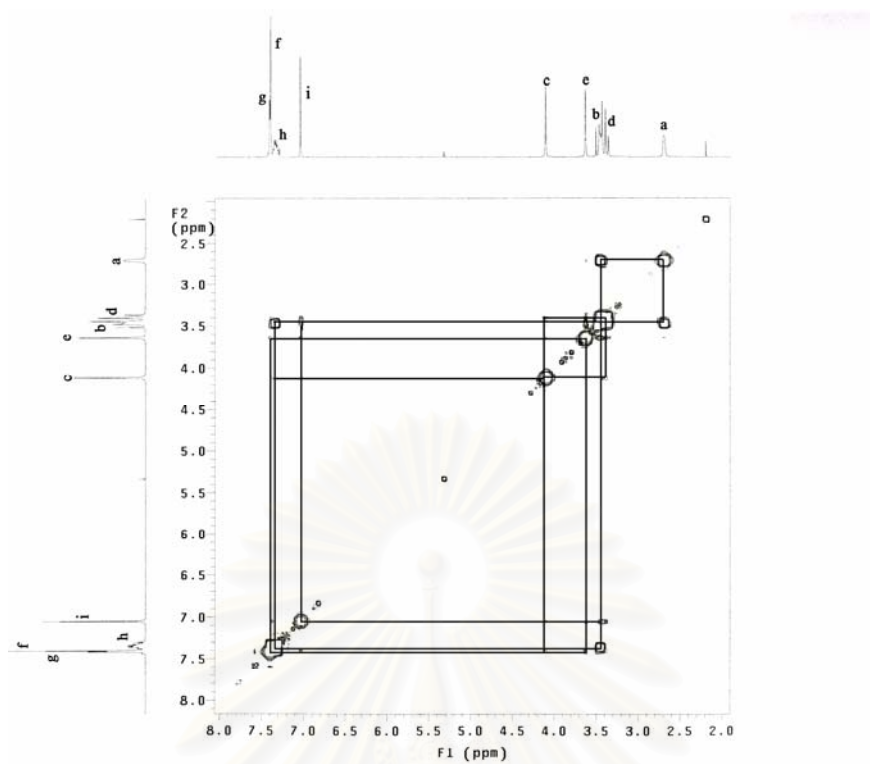


Figure A15. COSY spectrum of N_7 -hexahomotriazacalix[3]-cryptand (**L3**) in $CDCl_3$ at 25 °C.

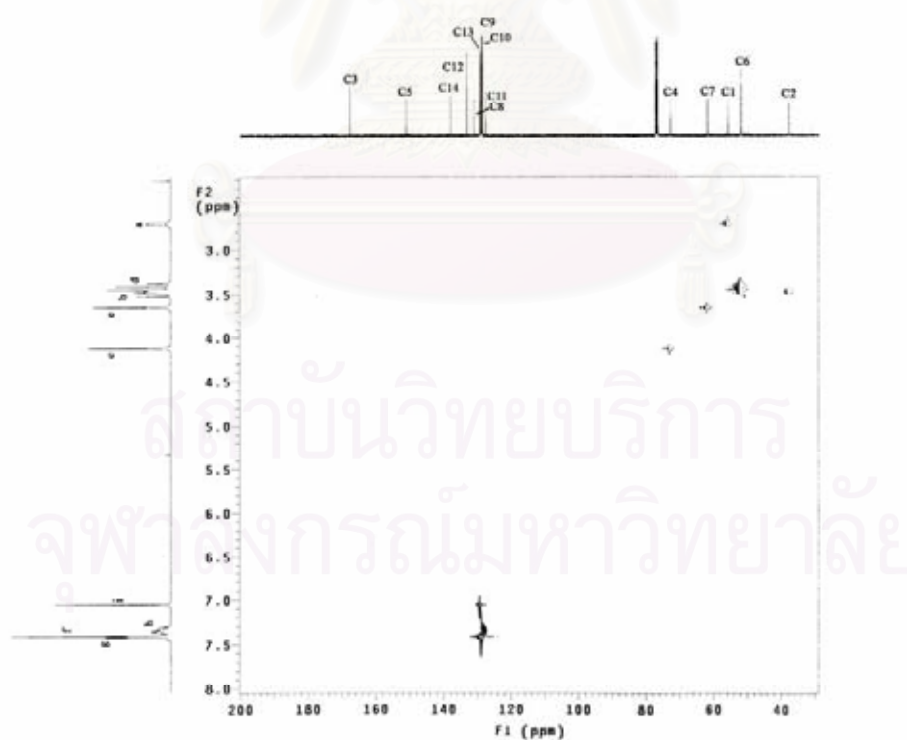


Figure A16. gHSQC spectrum of N_7 -hexahomotriazacalix[3]-cryptand (**L3**) in $CDCl_3$ at 25 °C.

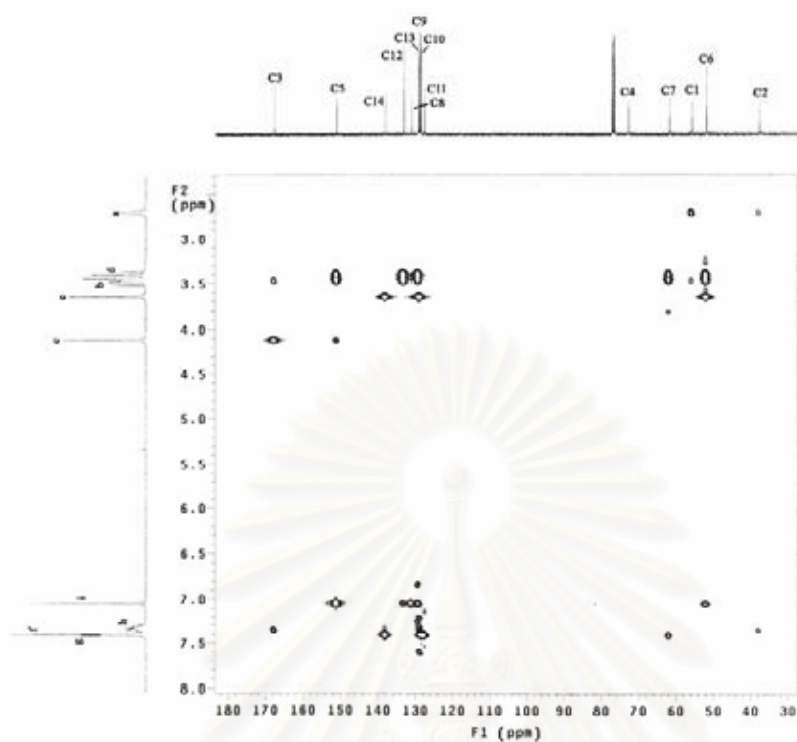


Figure A17. gHMBC spectrum of N₇-hexahomotriazacalix[3]-cryptand (**L3**) in CDCl₃ at 25 °C.

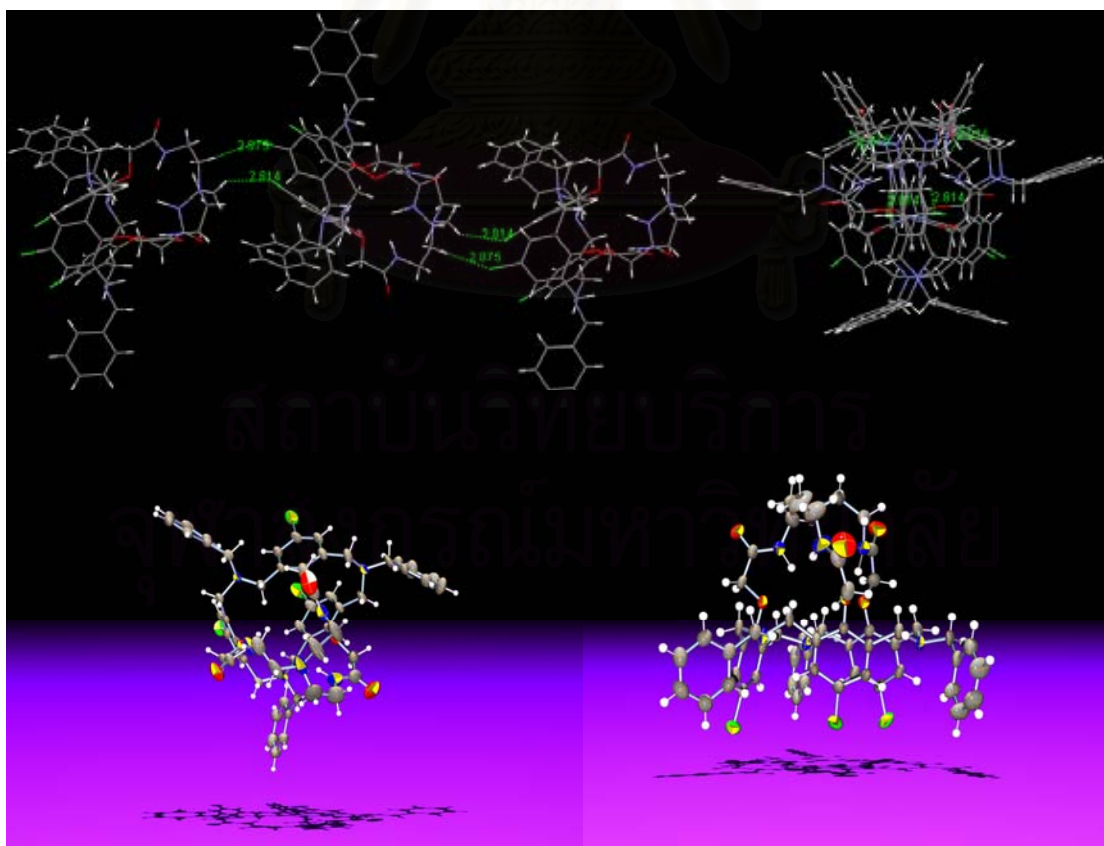


Figure A18. Crystal structure of N₇-hexahomotriazacalix[3]-cryptand (**L1**)

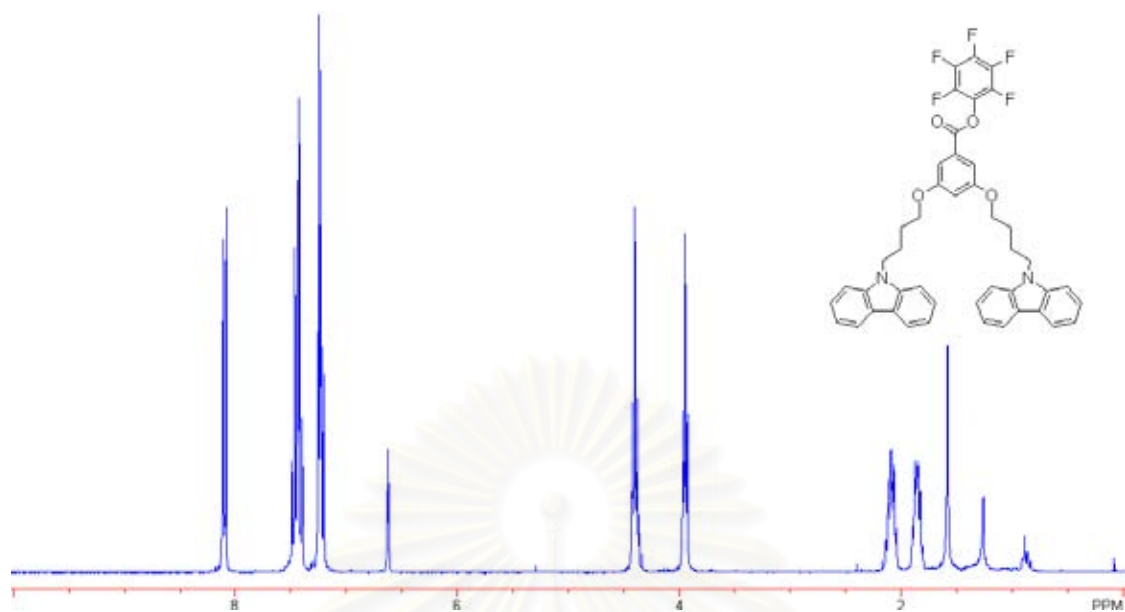


Figure A19. $^1\text{H-NMR}$ spectrum of Perfluorophenyl-3,5-bis(4-(9H-carbazol-9-yl)butoxy)benzoate (**3.8**) in CDCl_3 at 25 °C.

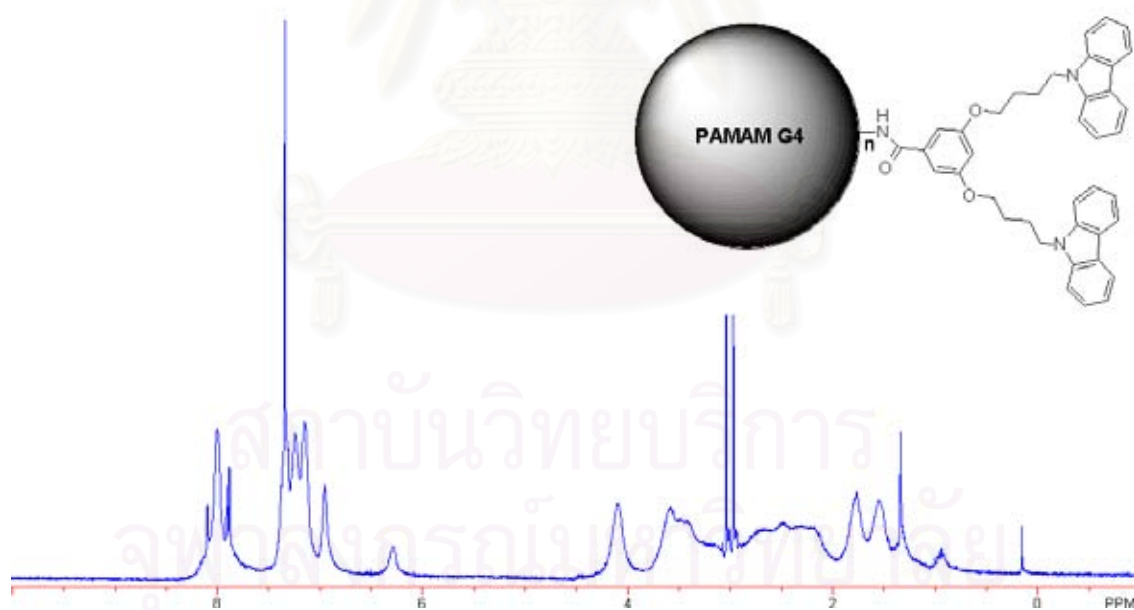


Figure A20. $^1\text{H-NMR}$ spectrum of (3,5-Bis(4-(9H-carbazol-9-yl)butoxy)-benzoyl)-Functionalized Dendrimer, **PC (3.13)** in CDCl_3 at 25 °C.

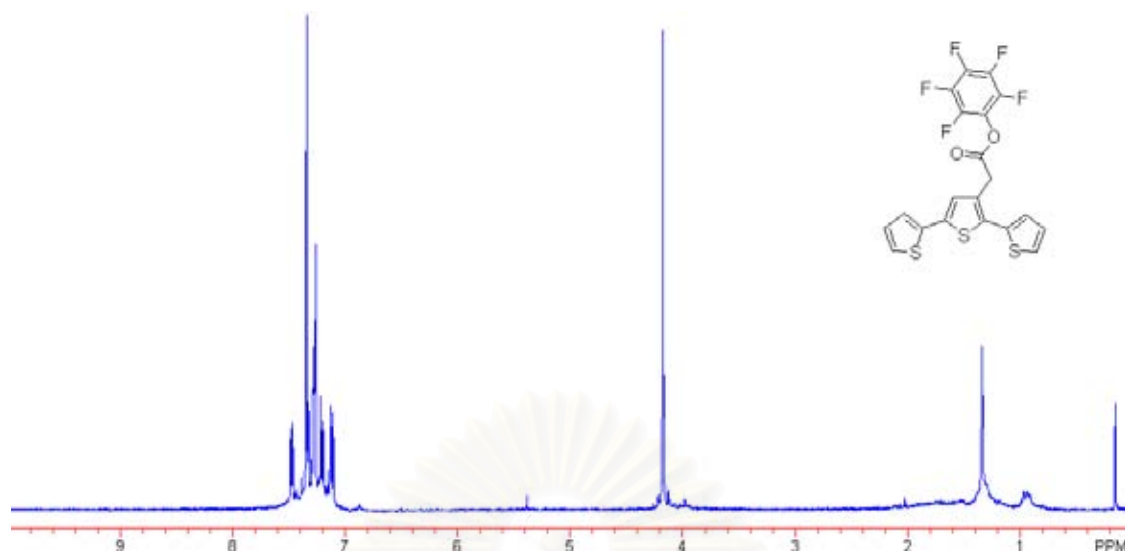


Figure A21. ¹H-NMR spectrum of Perfluorophenyl-2-(2,5-di(thiophen-2-yl)thiophen-3-yl)acetate (**3.12**) in CDCl₃ at 25 °C.

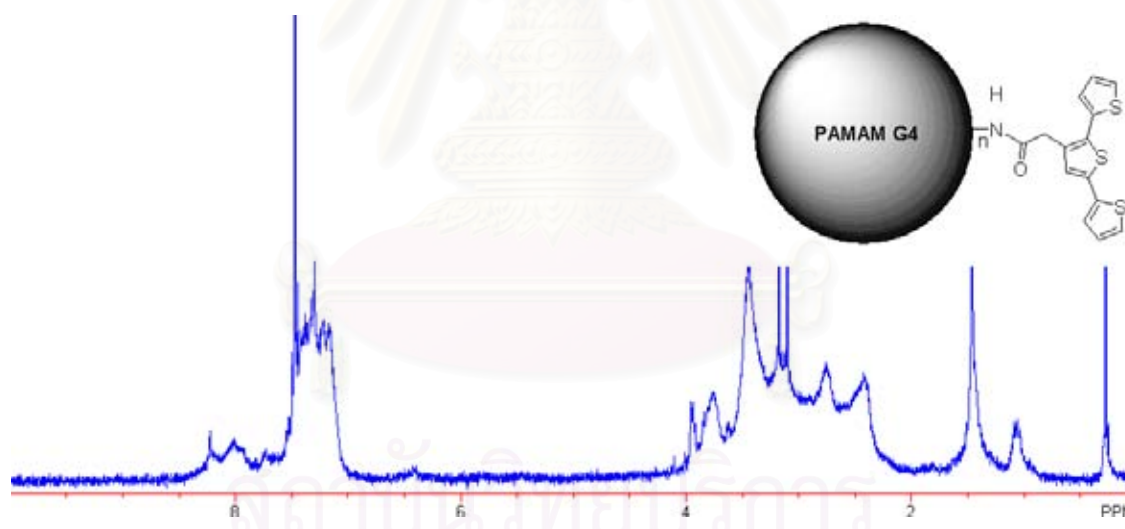


Figure A22. ¹H-NMR spectrum of 2-(2,5-di(thiophen-2-yl)thiophen-3-yl) acetyl-Functionalized Dendrimer, PC (**3.14**) in CDCl₃ at 25 °C.

VITA

Mr. Chatthai Kaewtong was born in March 16, 1981 in Nongbua Lamphu, Thailand. He graduated with high school from Nongbuapittayakarn School, Nongbua Lamphu in 1999. He received his Bachelor's degree of Science in Chemistry from Mahasarakham University in 2002. Since then he has been a postgraduate student studying organic chemistry and become a member of Supramolecular Chemistry Research Unit under the supervision of Associate Professor Buncha Pulpoka. During this period, his financial support is granted by "The Royal Golden Jubilee (RGJ)" from the Thailand Research Fund (TRF). He had an opportunity to do the research under the supervision of Professor Rigoberto Advincula at Department of Chemistry, University of Houston, Houston, Texas, USA during September 2006- August 2007 with the financial support form RGJ and RCA grants. He graduated with a doctorate degree in chemistry in the academic year 2007.

Publications

- 1) "Novel C_{3v} -Symmetrical N_7 -Hexahomotriazacalix[3]cryptand: A Highly Efficient Receptor for Halide Anions" *Organic Letters*. **2006**, 8, 1561-1564.
- 2) "Ultrathin Films of Calixarene-Carbazole Conjugated Polymer Networks (CPN) for Specific Cation Sensing" Accepted for *Chemistry of Materials*. **2008**.
- 3) "Redox Nanoreactor Dendrimer Boxes: *In-Situ* Hybrid Gold Nanoparticles via Terthiophene and Carbazole-PAMAM Dendrimer Oxidation" submitted to *Journal of Materials Chemistry*.
- 4) "Lord of the Nano Rings: Self-Assembly and Electropolymerization of PAMAM-Carbazole Dendron Surfmer Complexes" Accepted for *ACS nano*. **2008**.
- 5) "Conformation Selective Synthesis of *N*-benzylhexahomotriaza-*p*-chlorocalix[3]-trinaphthylamides" Accepted for *Journal of Organic Chemistry*. **2008**.
- 6) "PAMAM-CBz Dendron COMPLEXES: Self-Assembly Properties and Polymerization in Solution and Surfaces" (PMSE Preprints, Proceedings Published **2008** by the American Chemical Society)